Vol. 298, No. 2, November 30, 1994 ISSN 0003-2670

ANALYTICA CHIMICA ACTA

An international journal devoted to all branches of analytical chemistry

ELSEVIER

ANALYTICA CHIMICA ACTA

Scope. *Analytica Chimica Acta* publishes original papers, rapid publication letters and reviews dealing with every aspect of modern analytical chemistry. Reviews are normally written by invitation of the editors, who welcome suggestions for subjects. Letters can be published within **four months** of submission. For information on the Letters section, see inside back cover.

Submission of Papers

Americas

Prof. Harry L. Pardue
Department of Chemistry
1393 BRWN Bldg, Purdue University
West Lafayette, IN 47907–1393
USA

Tel:(+1-317) 494 5320
Fax:(+1-317) 496 1200

Computer Techniques

Prof. J.T. Clerc
Universität Bern
Pharmazeutisches Institut
Baltzerstrasse 5, CH-3012 Bern
Switzerland

Tel:(+41-31) 6314191
Fax:(+41-31) 6314198

Prof. Sarah C. Rutan
Department of Chemistry
Virginia Commonwealth University
P.O. Box 2006
Richmond, VA 23284-2006
USA
Tel:(+1-804) 367 7517
Fax:(+1-804) 367 8599

Other Papers

Prof. Alan Townshend
Department of Chemistry
The University
Hull HU6 7RX
Great Britain

Tel:(+44-482) 465027
Fax:(+44-482) 466410

Prof. Willem E. van der Linden
Laboratory for Chemical Analysis
Department of Chemical Technology
Twente University of Technology
P.O. Box 217, 7500 AE Enschede
The Netherlands
Tel:(+31-53) 892629
Fax:(+31-53) 356024

Prof. Paul Worsfold
Dept. of Environmental Sciences
University of Plymouth
Plymouth PL4 8AA
Great Britain

Tel:(+44-752) 233006
Fax:(+44-752) 233009

Submission of an article is understood to imply that the article is original and unpublished and is not being considered for publication elsewhere. *Anal. Chim. Acta* accepts papers in English only. There are no page charges. Manuscripts should conform in layout and style to the papers published in this issue. See inside back cover for "Information for Authors".

Publication. *Analytica Chimica Acta* appears in 18 volumes in 1995 (Vols. 297–314). *Vibrational Spectroscopy* appears in 2 volumes in 1995 (Vols. 8 and 9). Subscriptions are accepted on a prepaid basis only, unless different terms have been previously agreed upon. It is possible to order a combined subscription (*Anal. Chim. Acta* **and** *Vib. Spectrosc.*).
Our p.p.h. (postage, packing and handling) charge includes surface delivery of all issues, except to subscribers in the U.S.A., Canada, Australia, New Zealand, China, India, Israel, South Africa, Malaysia, Thailand, Singapore, South Korea, Taiwan, Pakistan, Hong Kong, Brazil, Argentina and Mexico, who receive all issues by air delivery (S.A.L.–Surface Air Lifted) at no extra cost. For Japan, air delivery requires 25% additional charge of the normal postage and handling charge; for all other countries airmail and S.A.L. charges are available upon request.

Subscription orders. Subscription prices are available upon request from the publisher. Subscription orders can be entered only by calendar year and should be sent to: Elsevier Science B.V., Journals Department, P.O. Box 211, 1000 AE Amsterdam, The Netherlands. Tel: (+31-20) 5803 642, Telex: 18582, Telefax: (+31-20) 5803598, to which requests for sample copies can also be sent. Claims for issues not received should be made within six months of publication of the issues. If not they cannot be honoured free of charge. Readers in the U.S.A. and Canada can contact the following address: Elsevier Science Inc., Journal Information Center, 655 Avenue of the Americas, New York, NY 10010, U.S.A. Tel: (+1-212) 633 3750, Telefax: (+1-212) 633 3990, for further information, or a free sample copy of this or any other Elsevier Science journal.
Advertisements. Advertisement rates are available from the publisher on request.

US mailing notice – Analytica Chimica Acta (ISSN 0003-2670) is published 3 times a month (total 54 issues) by Elsevier Science B.V. (Molenwerf 1, Postbus 211, 1000 AE Amsterdam). Annual subscription price in the USA US$ 3677.75 (valid in North, Central and South America), including air speed delivery. Second class postage paid at Jamaica, NY 11431. *USA Postmasters*: Send address changes to Anal. Chim. Acta, Publications Expediting, Inc., 200 Meacham Av., Elmont, NY 11003. Airfreight and mailing in the USA by Publication Expediting.

ANALYTICA CHIMICA ACTA

An international journal devoted to all branches of analytical chemistry

(Full texts are incorporated in CJELSEVIER, a file in the Chemical Journals Online database available on STN International; Abstracted, indexed in: Aluminum Abstracts; Anal. Abstr.; Biol. Abstr.; BIOSIS; Chem. Abstr.; Curr. Contents Phys. Chem. Earth Sci.; Engineered Materials Abstracts; Excerpta Medica; Index Med.; Life Sci.; Mass Spectrom. Bull.; Material Business Alerts; Metals Abstracts; Sci. Citation Index)

VOL. 298 NO. 2 CONTENTS NOVEMBER 30, 1994

(Continued overleaf)

Contents (continued)

ELSEVIER

Analytica Chimica Acta 298 (1994) 141–149

ANALYTICA CHIMICA ACTA

Development of enzyme-cartridge flow-injection analysis for industrial process monitoring. Part I. Development and characterization

H. Jürgens [b], R. Kabuß [a], T. Plumbaum [a], B. Weigel [a], G. Kretzmer [a], K. Schügerl [a,*], K. Andres [b], E. Ignatzek [b], F. Giffhorn [c]

[a] *Institute for Technical Chemistry, University of Hannover, Callinstrasse 3, D-30167 Hannover, Germany*

[b] *Eppendorf-Netheler-Hinz GmbH, Hamburg, Germany*

[c] *Institute of Applied Microbiology, University of Saarland, Saarbrücken, Germany*

Received 25 March 1994; revised manuscript received 3 June 1994

Abstract

The preparation of cartridges with five different enzymes: glucose oxidase (GOD), pyranose oxidase (PyOD), alcohol oxidase (AOD), L-amino acid oxidase (L-ASOD) and L-lactate-2-monooxigenase (LMO) immobilized on VA-Epoxy Biosynth carrier were optimized and standardized. The enzyme cartridges were characterized, integrated in flow injection analysis (FIA) systems and the optimal application conditions and salt effects were evaluated.

Keywords: Flow injection; Enzymatic methods; Alcohol oxidase; L-Amino acid oxidase; Glucose oxidase; L-Lactate-2-monooxigenase; Pyranose oxidase; Salt effects

1. Introduction

Flow injection analysis (FIA) became popular in the last 15 years [1]. In biotechnology, FIA is often combined with immobilized enzymes and antibodies [2–4]. However, FIA systems combined with immobilized enzymes are seldom used in industrial practice. In the authors' laboratory FIA systems combined with immobilized enzyme cartridges have been used in the last ten years for process monitoring in biotechnology. For their industrial application it was necessary to develop enzyme cartridges for industrial manufacturing and use with warranted standard quality. Prerequisites were:

- development of simple, inexpensive and well reproducible immobilisation techniques for manufacturing of enzyme cartridges with well-defined and long-standing enzyme activities,
- development of standard methods to control the activities of native and immobilized enzymes
- development of enzyme cartridges with low and invariable pressure drop,
- standardisation of the operation conditions evaluation of the influences of cross sensitivities, and in general, matrix effects on the signal using complex cultivation media,
- evaluation of possible faults and their diagnosis.
- testing of the cartridges for process monitoring under industrial fermentation conditions.

* Corresponding author.

SSDI 0003-2670(94)00264-M

Table 1
Measuring conditions for the activity determination of the enzymes with 0.1 mol/l buffer (mixture of K_2HPO_4 and KH_2PO_4), ABTS (2,2'-azino-di-(3-ethylbenzthiazolin-sulfonic acid-(6)) and pO_2 (LMO) at 25°C

Enzyme	Buffer pH	Substrate conc.	Range (native enzyme), U/ml	Range (immob. enzyme), U/ml
GOD	7	100 g/l Glu	0.02–1.0	0.001–0.083
PyOD	7	100 g/l Glu	0.005–0.25	0.001–0.083
AOD	8	20 g/l EtOH	25–50	0.002–0.083
ASOD	8	2 g/l Met	0.05–0.5	0.002–0.083
LMO	7	25 g/l Lac.	0.1–0.6	0.001–0.083

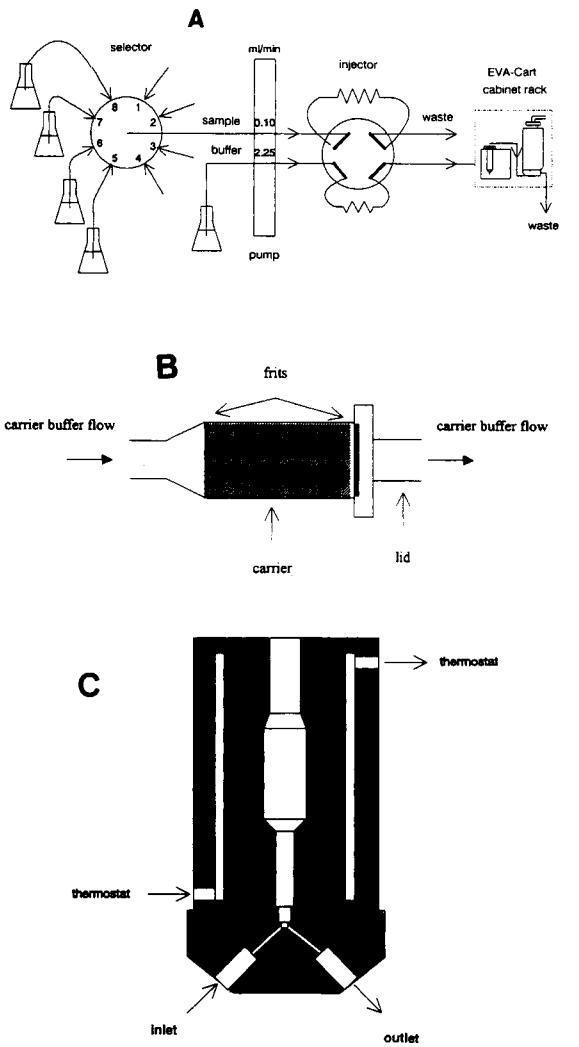

Fig. 1. Experimental setup. (A) Construction of the EVA system with immobilized enzyme and oxygen electrode integrated into the EVA-Cart adapter. (B) Simplified picture of the enzyme cartridge. (C) Geometry of the flow cell for oxygen electrode.

2. Enzyme characterisation and immobilization

2.1. Enzyme characterization

The following enzymes were applied: glucose oxidase (GOD) (*Aspergillus niger*), spec. activity: 288 U/mg lyophilisate. Pyranoseoxidase (PyOD) (*Peniophora gigantea*), spec. activity: 3.7 U/mg protein. Alcohol oxidase (AOD) (*Pichia pastoris*), spec. activity: 33 U/mg protein. L-Amino acid oxidase (L-ASOD) (*Crotus atrox*), spec. activity 0.2–0.5 U/mg lyophilisate. L-Lactate monooxidase (LMO) (*Mycobacterium smegmatis*), spec. activity 15 U/mg lyophilisate.

2.2. Enzyme activity determination

During the reaction of GOD, PyOD, AOD and ASOD with the substrate and oxygen, H_2O_2 is formed. The activities of GOD, PyOD, AOD and ASOD were measured by means of the reaction of H_2O_2 with the redox indicator ABTS (2,2'-azino-di-(3-ethyl-benzthiazolin-sulfonic acid-(6)) catalysed by peroxidase (POD):

$$\text{Substrate} + O_2 \rightarrow \text{product} + H_2O_2 \quad (1)$$

$$\beta\text{-D-glucose} + O_2 \rightarrow \text{D-glucono-}\delta\text{-lacton/gluconicacid} + H_2O_2 \quad (1a)$$

$$\text{Ethanol} + O_2 \rightarrow \text{aldehyde} + H_2O_2 \quad (1b)$$

$$\text{L-aminoacid} + O_2 \rightarrow 2\text{oxoacid} + NH_3 + H_2O_2 + H_2O \quad (1c)$$

$$H_2O_2 + ABTS_{red} \rightarrow H_2O + ABTS_{ox} \quad (2)$$

Table 2
Measuring ranges of the cartridges with immobilized enzymes (M KPB = mol/l mixture of K_2HPO_4 and KH_2PO_4)

Enzyme	Activity (U)	Buffer	Substrate	Measuring range (g/l)
GOD	100	1 M KPB	β-D-Glu	0.01–0.75
	44	1 M KPB		0.05–1.0
	20	1 M KPB		0.05–2.0
	10	1 M KPB		0.10–2.0
	1156	2 M KPB		0.01–0.75
	100	2 M KPB		0.02–0.75
PyOD	8.5	1 M KPB	D-Glu	0.01–0.75
AOD	100	1 M KPB	EtOH	0.01–0.75
	50	1 M KPB		0.05–2.5
	20	1 M KPB		0.10–2.5
ASOD	20	1 M KPB	L-Met	0.02–1.0
LMO	60	1 M KPB	L-Lac.	0.02–1.0
	30	1 M KPB		0.05–2.0
	15	1 M KPB		0.10–5.0

The reagent used consisted of 1.333 g/l ABTS and 1200 U/l POD in potassium phosphate buffer (Table 1). $ABTS_{ox}$ was measured at 436 nm with a Uvicon 940 Kontron Instrument. No H_2O_2 was formed during the reaction of LMO with substrate:

$$\text{L-lactate} + O_2 \rightarrow \text{acetate} + CO_2 + H_2O \quad (3)$$

Therefore the dissolved oxygen with regard to its saturation value (pO_2) was measured with an O_2-sensitive optode (microprocessor controlled optical and portable oxygen sensor, MOPS, TCI, Hannover) or O_2-electrode (Yellow Spring Instruments, YSI).

In Table 1 the conditions for the activity determination are given for the above enzymes.

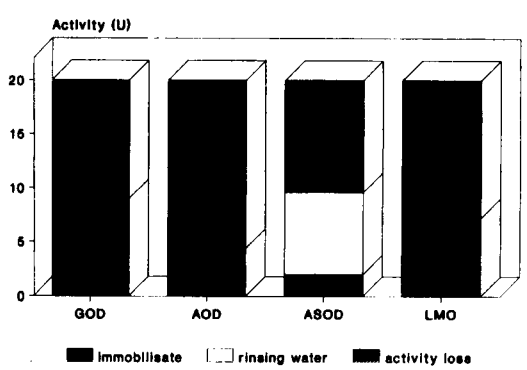

Fig. 2. Enzyme balance of the immobilization of 20 U oxidase cartridges: activities of immobilized enzymes, activities in rinsing water and activity loss (initial activity – activity of immobilisate – activity in rinsing water).

2.3. Enzyme immobilization and encapsulation

The enzymes were immobilized on VA-Epoxy-Biosynth E3- carrier (Riedel de Haen, Seelze). The native enzyme was dissolved in 600 μl potassium phosphate buffer (Table 1) at pH 7–8 (GOD), 8–9 (AOD), 9 (ASOD) and 6–7 (LMO), and the solution was filled into the cartridge, which contained 200 mg carrier. To prevent any loss of enzyme, the preparation vessel was washed with 100 μl buffer, which was transferred into the cartridge as well. The immobilization was performed at room temperature for three days.

These immobilized enzymes were filled in a mini column (Mobicols, Mobitec) of 1 ml volume, provided with polyethylene frits of 6.8 mm in diameter and 35 μm pore diameter at both ends and a Luer lockcup at the upper end, which was placed into a thermostated flow cell (Fig. 1).

In Table 2 the measuring ranges of these cartridges with immobilized enzymes are shown. Enzyme units given in the table represent the amount of native enzyme added initially to the carrier before immobilization.

The immobilization yield was low. The main fraction of the enzyme lost its activity, a small fraction appeared in the rinsing water. Fig. 2 shows the immobilization balances with different enzymes.

It is very important that the pressure drop across the cartridge remains constant during the operation. The fines of the carrier increase the pressure drop by a factor

Table 3
Operation conditions of the FIA system

Parameter	Values
Flow rate of sample solution	0.1 ml/min
Flow rate of buffer solution	2.25 ml/min
Injection volume	30 μl
Temperature of the cartridge	25–30°C
Temperature of the electrode	37°C (EVA-Cart adapter)
	25–30°C (EVA-Dapter adapter)
Sampling frequency	20–30 samples/h
Composition of standard buffer	4.3 g/l K_2HPO_4
	1.9 g/l NaH_2PO_4
	3.0 g/l NaCl
	1.5 g/l ETDA

of 3 to 4. Therefore, a narrow size fraction of the carrier was applied for the immobilization. With such carriers long range invariable pressure drop could be attained.

3. Investigation of the FIA cartridges

3.1. Insertion of the cartridges into the EVA–FIA system

A maximum of 4 enzyme cartridges was integrated in the EVA-Dapter and later in EVA-Cart adapters of the Master Module of the Eppendorf Variable Analysing system (EVA; Eppendorf-Netheler-Hinz, Hamburg), which were operated in series or parallel (Fig. 1). The optimal operation conditions are shown in Table 3.

3.2. Selectivity of the enzyme cartridges

GOD reacts only with glucose, PyOD with different sugars. In Fig. 3a the calibration curves with 44 U GOD and 8.5 U PyOD cartridges are compared. There is a small difference, which has to be investigated.

PyOD reacts with different sugars. In Fig. 3b the calibration curves are shown with glucose and sorbose at different buffer solution flow rates. With glucose higher peak heights are obtained than with sorbose. With decreasing flow rate the peak height increased only with sorbose as substrate, because of the incomplete conversion at high buffer flow rates.

AOD reacts with different alcohols. In Fig. 4 the calibration curves with different alcohols and a 100-U AOD cartridge are shown. The peak heights decreased with increasing chain length and flow rate of the buffer (Fig. 5). Therefore, the enlargements of the conversion are high when low flow rates of the buffer and long chain lengths are used.

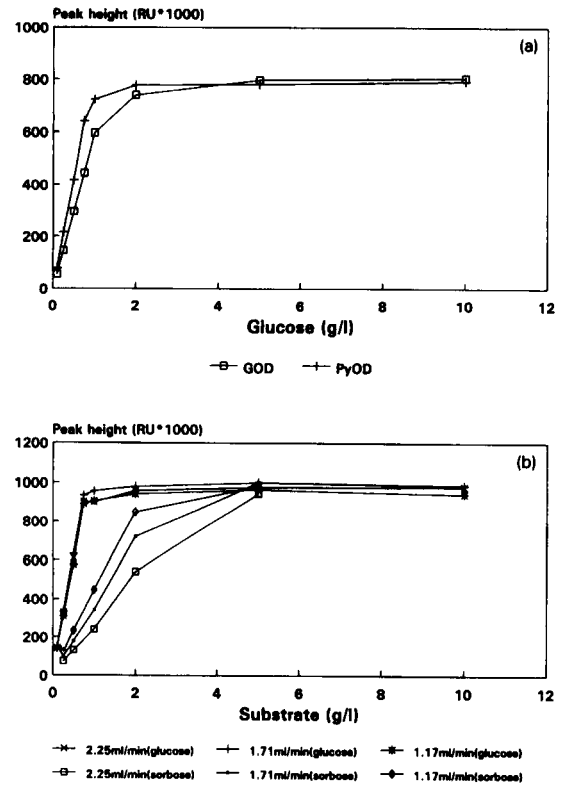

Fig. 3. (a) Calibration curves with 44-U GOD and 8.5-U PyOD cartridges with glucose substrate. (b) Calibration curves of 8.5-U PyOD cartridges with glucose and sorbose substrates at different carrier buffer flow rates.

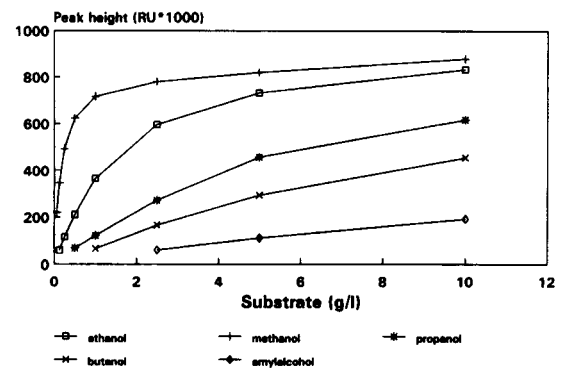

Fig. 4. Calibration curves of 100-U AOD cartridges with methanol, ethanol, propanol, butanol and amyl alcohol.

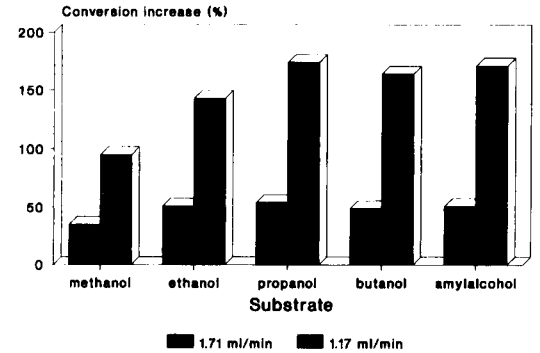

Fig. 5. Substrate conversion increase with 100-U AOD cartridges using 0.063 g/l methanol, 0.5 g/l ethanol, 1.0 g/l propanol, 2.5 g/l butanol and 5.0 g/l amyl alcohol, respectively, at two different carrier buffer flow rates with regard to the standard buffer flow rate (2.25 ml/min).

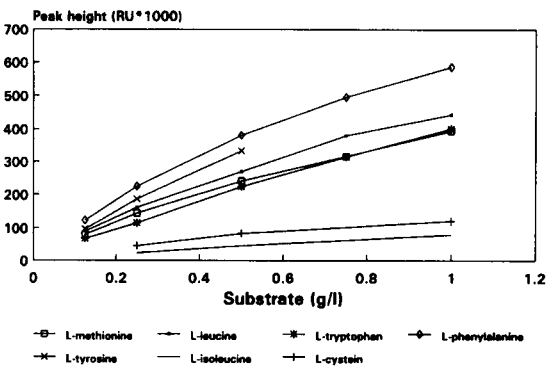

Fig. 6. Calibration curves of the 20-U ASOD cartridge with different amino acids.

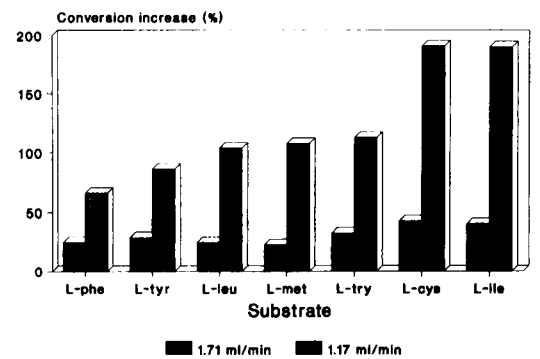

Fig. 7. Substrate conversion increase of 0.125 g/l L-phenlyalanine, L-tyrosine, L-leucine and L-methionine, 0.25 g/l tryptophan, and 1 g/l cysteine and isoleucine with 20-U ASOD cartridge at two different carrier buffer flow rates with regard to the standard buffer flow rate (2.25 ml/min).

ASOD reacts with different amino acids. In Fig. 6 the calibration curves with 7 different amino acids and a 20-U ASOD cartridge are shown. Again the peak height and the conversion increase depend on the flow rate of the buffer solution and the type of substrate (Fig. 7).

3.3. pH and buffer molarity effects on the signal heights

The pH optima of native enzymes are slightly shifted by immobilization in the alkaline range. At high enzyme activities the peak heights are constant in a broad pH range (Table 4).

When using GOD and PyOD, the peak heights increase slightly with the molarity of the buffer solution. The same holds true for KCl solution.

The influence of the buffer molarity on the peak heights of AOD cartridges is rather high: the change from 0.01 mol/l to 0.1 mol/l potassium phosphate buffer causes an increase of 10%, but the change from 0.1 to 1.0 an increase of 44%. AOD is deactivated by the Cl^- ions.

When using ASOD cartridges, the peak heights decrease with increasing buffer molarity. The change from 0.01 to 0.1 mol/l potassium phosphate buffer causes a decrease of the peak height to 72% of the original value, and the increase to 1.0 mol/l a decrease of peak height to 41%. The peak height (with standard buffer) decreases to 10% of its original value after addition of 0.8 mol/l NaCl.

The influence of anions on the activity of LMO has been investigated already [5,6]. Phosphate anions form an enzyme–phosphate complex, which causes a competitive inhibition of the enzyme. In Fig. 8 the influence of the potassium phosphate and imidazolium-chloride (IC) buffer and KCl molarities on the peak heights is shown. The strong decrease with increasing molarity is obvious. In Fig. 9 the influence of 0.1 mol/l anions on the relative peak heights of 30 U LMO cartridge with 1 g/l L-lactate are shown. Nitrate causes the most distinct reduction of the signal of the cartridge. In Table 5 the influence of the pH and potassium phosphate buffer molarity is summarized.

A small amount of surfactant (Triton X-100) raises the enzyme activity and the signal height. In Fig. 10 the influence of Triton X-100 on the peak height of the ASOD cartridge as a function of the L-methionine concentration is shown. This effect is especially high immediately after the immobilisation. After Triton treatment of the cartridge and rinsing with buffer solu-

Table 4
pH and potassium phosphate (KP) buffer molarity effects on the signal heights with immobilized enzymes. The maximum signal height was set to 100%. All other signals refer to this value

Enzyme	Activity (U)	pH optimum	0.001 mol/l KP buffer	0.1 mol/l KP buffer	1.0 mol/l KP buffer
GOD	44	4.5–7.5	68%	70%	100%
PyOD	8.5	4.5–7.5	82%	80%	100%
AOD	100	8.0–9.0	46%	56%	100%
ASOD	20	8.5	100%	72%	41%
LMO	30	6.5–7.0	100%	35%	20%

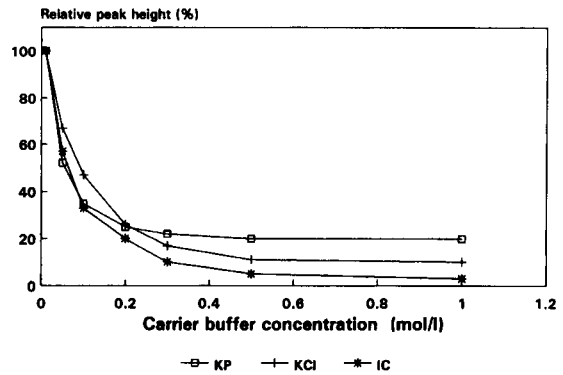

Fig. 8. Variation of the signal peak height with 30-U LMO cartridge, 1 g/l L-lactate as a function of the molarity of different carrier buffer solutions.

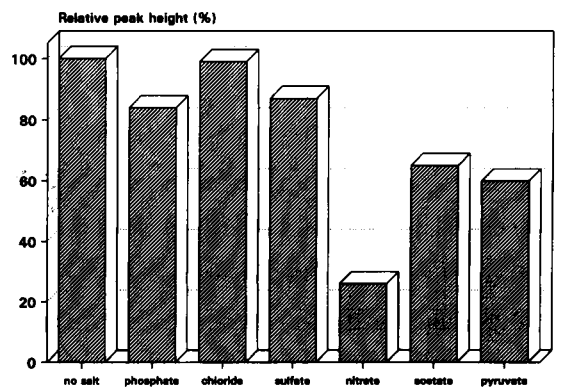

Fig. 9. Relative signal heights with 30-U LMO cartridge and 1 g/l L-lactate in absence and presence of the different salts dissolved in the standard carrier buffer solution.

tion, no change occurs, if Triton is added to the buffer solution again.

After addition of 1.5 g/l EDTA to the buffer solution the two-valence cations are complexed. This hinders the propagation of the microorganisms and increases the lifetime of the buffer without influencing the signal height.

3.4. *Influence of nutrient salts on the enzyme activity and signal height*

For the determination of the influence of salt effects on the signal heights of the cartridges, systematic investigations were carried out with different salts.

No salt effects were found at low salt concentrations (<0.1 mol/l KCl + potassium phosphate) when GOD and PyOD cartridges were used.

The components of the cultivation media influence the activity of the other enzymes and the peak heights of the cartridges. As an example, in Fig. 11a the influence of nutrient salt components of *Saccharomyces cerevisiae* cultivation medium on the relative peak height of the 100-U AOD cartridge signal is presented. These salts were applied in a concentration of 0.1 mol/l. The cartridge was operated with the standard buffer (Table 3) in the presence of 0.5 g/l ethanol (Fig. 11a). When the buffer concentration is reduced to 0.01 mol/l, the relative change of the peak heights were more distinct (Fig. 11b). In this case the ethanol concentration was 0.125 g/l.

The influence of the nutrient salt components of *Escherichia coli* and *Spodoptera frugiperda* cultivation media on the 20-U ASOD cartridge was determined with 0.25 g/l L-MET in 0.01 mol/l potassium phosphate and in standard buffer (Table 3) (Fig. 12). All nutrient salts influence the signal height. At lower buffer capacity the salt effect is higher. The salt effect with the 0.1 mol/l potassium phosphate buffer was comparable with that of the standard buffer [7].

When applying 0.01 mol/l IC buffer, the salt effects are very close to those found with 0.01 mol/l potassium phosphate buffer [7]. In Table 5 the influence of buffer capacity is demonstrated.

The investigations with LMO were carried out with a 30-U cartridge in standard buffer solution, with 1 g/

Table 5
Salt effects on the signal heights of AOD and ASOPD cartridges using 0.01 mol/l potassium phosphate buffer (first line) and a standard buffer (second line). The maximum signal height (without any salt in the sample) was set to 100%, the other values (containing 0.1 mol/l salt) refer to this maximum value

Enzyme	Activity (U)	Sulfate	Chloride	Phosphate	Acetate	Lactate	Pyruvate
AOD	100	93%	88%	93%	64%	–	–
		98%	98%	97%	68%	–	–
ASOD	20	79%	89%	89%	84%	85%	88%
		89%	96%	97%	92%	92%	97%

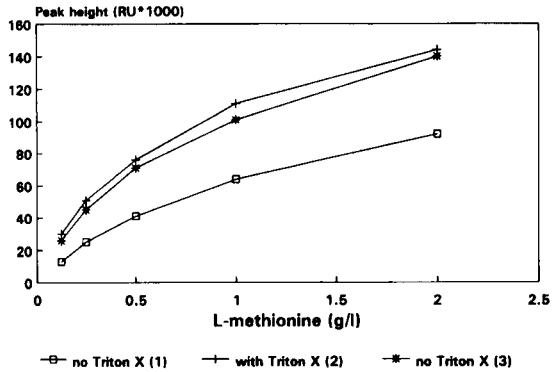

Fig. 10. Calibration curves of a 10-U ASOD cartridge with D,L-methionine (□) initial activity in absence of Triton X-100. (+) Initial activity after Triton was added to the solution. (*) Activity after Triton was removed from the solution.

l L-lactate and with nutrient salt components of *Lactobacillus salivarius* cultivation medium. In Fig. 13 the relative peak heights in the presence of these salts in the sample and in the buffer are shown. The presence of nitrate, pyruvate and acetate cause a considerable decrease of the signal height, especially when the salts are dissolved in the standard buffer solution. In Fig. 14 the effect of the buffer solution molarity at different L-lactate concentrations is shown with respect to that without phosphate. With increasing buffer molarity and L-lactate concentration the relative peak heights increase and the phosphate effect diminishes. With IC buffer similar effects were found.

3.5. *Influence of sodium azide*

In order to avoid the growth of microorganisms in the analyser system, sodium azide is sometimes added to the carrier buffer solution. In Fig. 15 the influence of 1 g/l sodium azide on the enzyme activities are shown in a solution consisting of 0.5 g/l glucose, 0.5 g/l ethanol, 0.25 g/l L-methionine, and 1.0 g/l L-lactate. The cartridges had the following activities: 44 U GOD, 100 U AOD, 20 U ASOD and 30 U LMO. GOD and ASOD cartridge signal peaks are not influenced by the presence of azide, the activity of LMO is considerably reduced and AOD is almost completely deactivated.

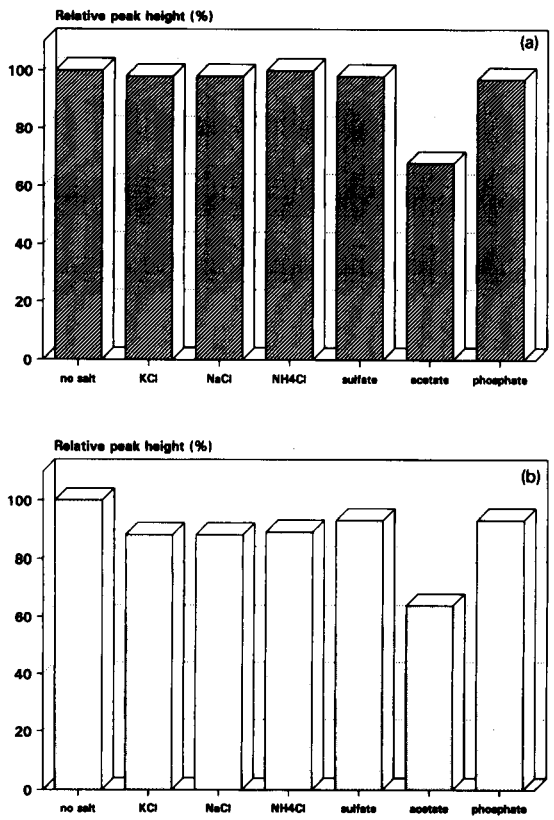

Fig. 11. (a) Relative signal heights with 100-U AOD cartridge with standard carrier buffer and 0.5 g/l ethanol in the absence and presence of 0.1 mol/l salts in the sample. (b) Relative signal peak heights with 100 – U AOD cartridge and 0.01 mol/l potassium phosphate carrier buffer and 0.125 g/l ethanol in absence and presence of 0.1 mol/l salts in the sample.

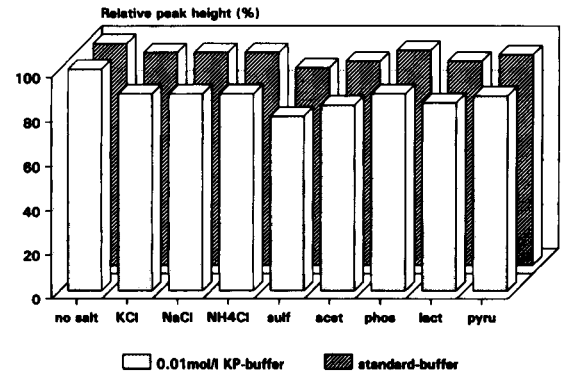

Fig. 12. Relative signal peak heights with 20-U ASOD cartridge, standard and 0.01 mol/l potassium phosphate carrier buffer and 0.25 g/l L-methionine in the absence and presence of 0.1 mol/l salts (sulf = sulfate, acet = acetate, phos = phosphate, lact = lactate, pyru = pyruvate) in the sample.

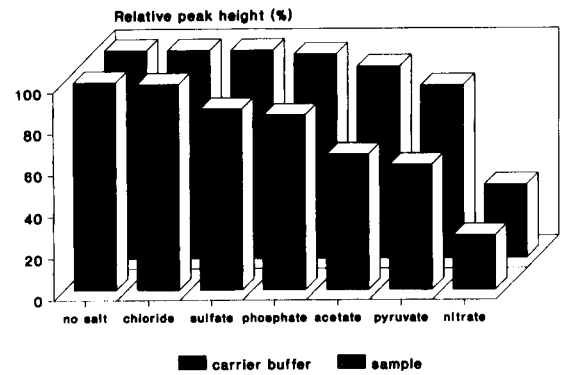

Fig. 13. Relative signal peak heights with 30-U LMO cartridge, 1.0 g/l L-lactate, in the absence and presence of different salts dissolved in the carrier buffer or in the sample solution.

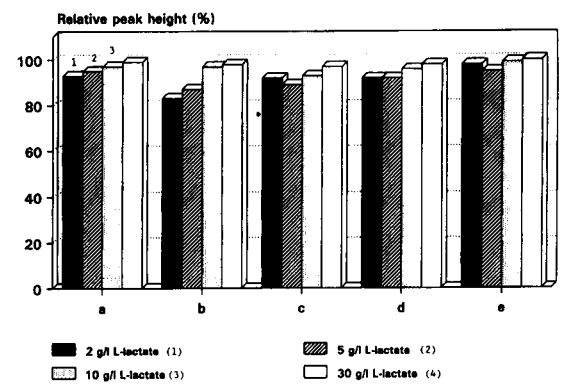

Fig. 14. Relative signal peak heights with 30-U LMO cartridge, 2.0, 5.0, 10.0 and 30.0 g/l L-lactate with the standard carrier buffer (a) or different potassium phospate carrier buffer molarities: (b) 0.01, (c) 0.05, (d) 0.05 and (e) 0.1 mol/l.

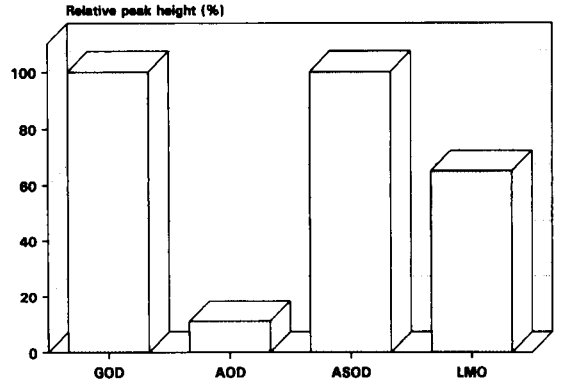

Fig. 15. Relative signal peak heights with 44-U GOD, 100-U AOD, 20-U ASOD and 30-U LMO cartridges, model solution consisting of 0.5 g/l glucose, 0.5 g/l ethanol, 0.25 g/l L-methionine and 1.0 g/l lactate in the absence and presence of 1 g/l azide.

4. Conclusion

When using VA Epoxy Biosynth as a carrier and the standard enzyme immobilization procedure, constant and well reproducible activities were attained. With uniform carrier particle diameters the pressure drop across the cartridges was low and remained constant for many months. These enzyme cartridges were integrated into a commercial FIA system and systematically investigated with regard to the factors which can influence the signal height.

Cultivation media contain salts in different concentrations. GOD and PyOD activities are not influenced by salts at concentrations less than 0.1 mol/l. The activities of the other enzymes are partly strongly affected by nutrient salt components. When using a standard buffer as carrier flow solution, the influence of nutrient salts on the signal height is considerably reduced, but the results can still be influenced. 1 g/l sodium azide solution does not influence GOD and ASOD activities, but strongly reduces the activities of LMO and especially of AOD.

The practical application of these systems for monitoring biotechnological processes are presented in parts II and III [8].

Acknowledgements

The authors gratefully acknowledge the financial support of Eppendorf-Netheler-Hinz, Hamburg.

References

[1] J. Ruzicka and E.H. Hansen, Flow Injection Analysis, Wiley, New York, 2nd edn., 1988.
[2] R.D. Schmid (Ed.), Flow Injection Analysis (FIA) Based on Enzymes or Antibodies, GBF Monographs, Vol. 14, VCH, Weinheim, 1991.
[3] R.D. Schmid and W. Künnecke, J. Biotechnol., 14 (1990) 3.
[4] C. van Dijk (Ed.), Analytical Biotechnology, Elsevier, Amsterdam, 1993.
[5] O. Lockridge, V. Massey and P.A. Sullivan, J. Biol. Chem., 247 (1972) 8097.
[6] M. Mascini, D. Moscone and G. Pallesci, Anal. Chim. Acta, 157 (1984) 45.
[7] H. Jürgens, Entwicklung und Einsatz der Enzymkartuschentechnik in der Fließinjektionsanalyse, Dissertation, University of Hannover, 1993.
[8] H. Jürgens, L. Brandes, R. Joppien, M. Siebold, J. Schubert, X. Wu, G. Kretzmer and K. Schügerl, Anal. Chim. Acta, submitted for publication.

ELSEVIER

Analytica Chimica Acta 298 (1994) 151–157

ANALYTICA CHIMICA ACTA

Functional membranes for flow buffering

Börje Glad, Knut Irgum *

Department of Analytical Chemistry, University of Umeå, S-901 87 Umeå, Sweden

Received 12 October 1993; revised manuscript received 10 June 1994

Abstract

Synthesis of functional membranes applicable to the buffering of pH in flow systems is described. The membranes are interpenetrating polymer networks of 2,3-epoxypropyl methacrylate and ethylene dimethacrylate in a preformed porous polymeric polypropene substrate. The pendant reactive epoxy groups in the membranes are converted into several functional groups with different pK_a values. The functionalized membranes are able to continuously adjust the pH of both acidic and alkaline flowing streams to a value close to the pH of the regenerant buffer.

Keywords: Flow system; Membranes; Flow buffering

1. Introduction

The hydrogen ion activity (pH) is an important parameter in virtually all areas of chemistry, and pH control is therefore often critical. Analytical reactions are examples of this, and it is frequently necessary to carry out the procedures (extractions, chromatography, etc.) within a given pH range to obtain satisfactory results. Problems in this respect are easily solved by the addition of a proper amount of a suitable buffer, and this is often included in standard procedures. There are, however, instances where the problem becomes more complicated, and where addition of a buffer is inconvenient. In analytical flow systems (i.e., liquid chromatography (LC) and flow-injection analysis (FIA)), chemical reactions aimed at optimizing the detection are frequently best carried out at a pH different from that optimal for separation [1,2]. In such reaction schemes the pH of the stream consequently has to be manipulated at some point before the detection device if maximum sensitivity is to be attained. The obvious solution to this problem is to continuously introduce a buffer solution or a proper amount of acid or base before the detection point, and several papers utilizing this approach have been published [3–6].

In 1939 Greissbach [7] pointed out the potential application of ion exchangers for buffering, and one of the first to show this in practice was Teitelbaum [8] in 1958. The concept has also been used for buffering and stabilization of analytes on a solid sorbent [9]. Another modern implementation of the solid buffer concept was presented by Jansen et al. [10] who used an ion exchange column in OH^- form in parallel with the separating column to increase analyte detectability. Davis and Peterson [11], Haginaka and Wakai [12] and Hwang and Dasgupta [13] employed membrane introduction of ammonia or ammonium ion for the same reason, using microporous or ion exchange membranes.

The problem with adding a buffer as solution is that the change in pH is accompanied by sample dilution and/or addition of an extra substance, and there is also

* Corresponding author.

SSDI 0003-2670(94)00277-S

an obvious risk of contamination. To overcome these drawbacks, Haddad [14] used a strong cation exchange membrane to neutralize strongly alkaline solutions prior to injection in an anion chromatographic system. The same type of membrane is also used for suppression of background conductance, i.e., neutralization of the alkaline eluent, in anion chromatography with hydroxide or carbonate eluents [15]. Similar schemes have been used for cation chromatography, where hydroxide ions are introduced using strong anion exchange membranes [16]. These neutralizations are, however, not true buffering reactions but merely eliminations of hydroxide or hydronium ions by a water producing reaction with an immobilized strong acid or base group.

In comparison with other alternatives, membranes seem to be the ideal choice for chemical flow manipulations. In contrast to continuous flow addition, the membrane technique functions without dilution and without the need for additional high performance pumps [17]. Another problem with continuous liquid reagent introduction is the poor mixing that can be encountered, especially if the two streams that are to be merged have different physical or chemical properties [18].

The most widely used form of reactive polymers in analytical flow systems are spherical particles, either porous or solid. Properly used, they perform very efficiently, and suffer only from two real drawbacks: The increase in backpressure caused by a packed reactor can be substantial, especially if high capacity and low band broadening is needed [18]. If the volume of the packed bed is decreased to alleviate the band-broadening problem, the need for frequent regeneration becomes apparent [19]. Packed bed reactors can also affect the system in other, more unpredictable ways, such as, e.g., the drift in retention times observed in column suppressed ion chromatography [19]. However, in spite of these obvious advantages with the membrane approach, ion chromatography is the only major analytical technique that has adopted an ion exchange membrane reactor as part of a standard analytical system. The likely cause for this sluggish development is lack of suitable functional membranes. In this paper we describe the synthesis and use of functionalized reactive membranes that are capable of performing continuous flow buffering of both acidic and alkaline aqueous streams.

2. Experimental

Synthesis of the reactive membrane intermediates used for functionalization into buffering form is described in detail in another paper [20] and will not be repeated here. These precursor membranes are interpenetrating polymer networks (IPNs) produced by photoinitiated radical polymerization of 2,3-epoxypropyl methacrylate (glycidyl methacrylate; GMA) and ethylene dimethacrylate (EDMA) in the pores of a microporous polypropylene tube. The monomer composition was 95% (w/w) GMA and 5% (w/w) EDMA for all membranes used in this work. The porous IPN substrate was Celgard® X-20, a tubular, porous polypropene membrane with an internal diameter of 0.4 mm, a wall thickness of 25 μm, and a porosity of 40% with a nominal pore size of 0.03 μm.

The functionalization reactions performed in this work were all carried out in a PTFE lined reaction bomb (Perkin-Elmer, Überlingen) for 24 h at a temperature of 80°C. No solvents were used, i.e., the reagents were added in neat form in large excess, typically 10 ml per 10 cm of tube to be functionalized. The reagents were 1-(2-aminoethyl)-piperazine, 1,2-ethylene diamine and orthophosphoric acid (85%), all of analytical grade and used as received.

Membrane characteristics were evaluated in an application-resembling experimental setup. The functionalized membranes were glued, using a high viscosity cyanoacrylate adhesive (Mega-firm, Mega

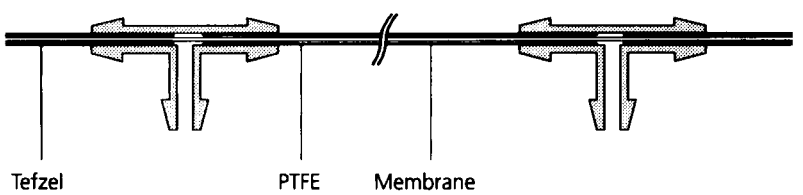

Fig. 1. Membrane reactor configuration.

Metal, Stockholm), to short pieces of Tefzel® tubing and mounted to two barbed polypropylene tee pieces connected by a 50 cm Teflon® tube making up a reactor configuration as shown in Fig. 1. A two-piston reciprocating HPLC pump (LKB 2150, Pharmacia, Uppsala), with a 70 kPa back-pressure regulator coupled in-line (upstream the membrane cell), was used to deliver the analyzed flow at 0.5 ml/min through the hollow fiber lumen. Influent solution in the analyzed channel was 1 mM HNO_3 or 1 mM KOH, with 9 mM KNO_3 added to balance the ionic strength of the buffer outside the membrane. The effluent pH was continuously monitored with a pH meter (Model 632; Metrohm, Herisau) equipped with a combination electrode (Type 6.0211.000; Metrohm) designed for measurement in small sample volumes, which had been mounted in a specially manufactured flow-cell (not shown). The pH electrode was calibrated with commercial standard buffers (Merck, Darmstadt) under flow conditions. The regeneration buffer solution was pumped in the regenerant channel outside the hollow fiber at 3 ml/min, in a flow direction counter-current to the analyzed flow, using a peristaltic pump (P-1, Pharmacia). The regenerant buffers were prepared by dissolving the buffer substance (orthophosphoric acid, triethanolamine, or tris(hydroxymethylamine)) in approximately 90% of the final volume, adding sodium hydroxide or hydrochloric acid to the desired pH, and diluting to the final volume. The buffer substance concentration was 20 mM in all cases.

Titration of the membranes was carried out by converting their ion exchange groups into the acid form by repeated immersions in 0.1 M HNO_3. They were thereafter washed several times with large amounts of deionized water until the electrolytic conductivity was not increased on immersion of the membranes. The washed membranes were then placed in separate plastic capped glass vials with 30 ml aliquots of 1.0 mol/l KCl solution. After equilibration the pH of the solutions was measured with the same combination electrode and pH meter described above, whereafter a 20 μl aliquot of 0.100 mol/l KOH was added. The membranes were allowed to equilibrate for 24 h at room temperature and the procedure was repeated until the entire titration curve was recorded. The vials were continuously agitated with a shaker (IKA-Vibrax-VXR; Janke und Kunkel, Staufen) during all equilibrations.

3. Results and discussion

A detailed description of the synthesis of the reactive membrane intermediates used as basis for the functionalizations in this work is presented in Ref. [20]. These precursor membranes are manufactured by photopolymerization of a reactive monomer and a crosslinker inside the pores of a preformed porous polypropene hollow fiber, forming an interpenetrating polymer network (IPN). Further functionalization of the tubes, which is the scope of this work, was carried out using reactions described in the literature [21,22]. It has been

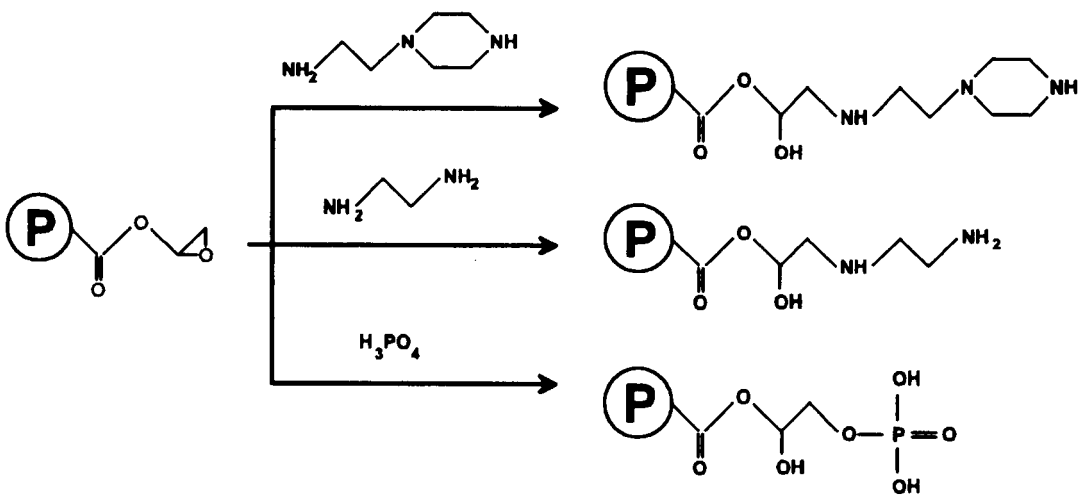

Fig. 2. Functionalization pathways for buffering membranes.

Table 1
Buffering data for the different membranes and buffers

Membrane functionality	Regenerant buffer/pH	Effluent pH with 1 mM HNO_3 as influent	Effluent pH with 1 mM KOH as influent	ΔpH
No membrane	–	3.0	11.0	8.0
1,2-Diaminoethane	Ethanolamine/9.5	9.1	9.7	0.6
1,2-Diaminoethane	Tris/8.2	7.3	8.7	1.4
N-2-Aminoethyl piperazine	Ethanolamine/9.5	8.6	10.5	1.9
N-2-Aminoethyl piperazine	Tris/8.2	6.5	9.0	2.5
Orthophosphoric acid	Phosphate/2.2	2.7	2.8	0.1
Orthophosphoric acid	Phosphate/7.1	5.8	9.3	3.5

The membranes were 0.5 m by 0.4 mm i.d. and the flow was 0.5 ml/min. Regenerant flow was 3 ml/min and the buffer concentration 20 mM. 9 mM KNO_3 was added in the influent solutions for ionic strength balancing.

shown that a large fraction of the epoxy groups in these membranes are accessible for reaction with a proper nucleophilic reagent [20], whereby this work will concentrate on evaluation of the operational performance of the resultant membranes, rather than chemical and morphological studies of the functionalization reactions and products.

It is important for the resulting membrane performance that the functionalization reaction is efficient, and that it proceeds without side reactions [23]. Since the diffusion of the reagent in the membrane phase is slow and the reaction normally encountered is fast, the functionalization will start at the membrane surface and gradually proceed throughout the material. This reaction scheme is known from the functionalization of particulate polymers, and is sometimes used as a means of synthesizing superficially functionalized spheres with an inert core, in order to obtain rapid exchange kinetics [24]. In the functionalization of membrane material, however, low reagent penetration represents a serious problem, since it can leave the least accessible central part of the membrane virtually unaffected by the functionalization reaction [20]. In the extreme case this causes a spatial void of transporting groups. If this scenario is experienced the resulting membrane will show a low transmembrane transport rate since the central part of the membrane, with the lowest concentration of active groups, will be rate-determining.

This problem of low reagent penetration is especially likely to occur with thick membranes and when the reagent is bulky or available only in dilute form. For efficient membrane functionalization the reagents should preferably be used in high concentration and/or in a solvent that has suitable swelling characteristics with respect to the reactive part of the IPN membrane. Another factor promoting good transport characteristics is a high concentration of functional groups, situated on (long) spacer arms which impart good flexibility and provides for facile (bucket-brigade type) interaction between neighbouring groups [25]. In this work we have used neat reagents for all reactions, but efficient functionalizations of similar materials have been reported with dioxane or water as solvents [22].

Three different types of weak acids and bases (ethylenediamine, aminoethylpiperazine and phosphoric acid) were covalently immobilized onto the membrane matrix via reaction with the epoxy groups present in the native IPN membranes (as described in the Experimental section). The functionalization reactions used are outlined in Fig. 2 together with the expected products. The ability of the resulting functionalized membranes to alter the pH of a flowing acidic or alkaline stream is presented in Table 1. All the membranes are able to adjust the pH of the effluent stream to a value close to the pK_a of the respective immobilized functionality, when constantly regenerated by a buffering solution adjusted to this pH. The most powerful buffering action is shown by the phosphate-containing membrane and a remarkable stability in effluent pH over quite a broad range of influent pH values tested is also evident using the membrane reacted with 1,2-ethylenediamine. This indicates that these functionalized membranes are capable of efficiently exchanging ions or to transport ion pairs (see discussion below) from one solution interface to the other.

It would be beneficial to have access to membranes with functionalities and pK_a values other than those

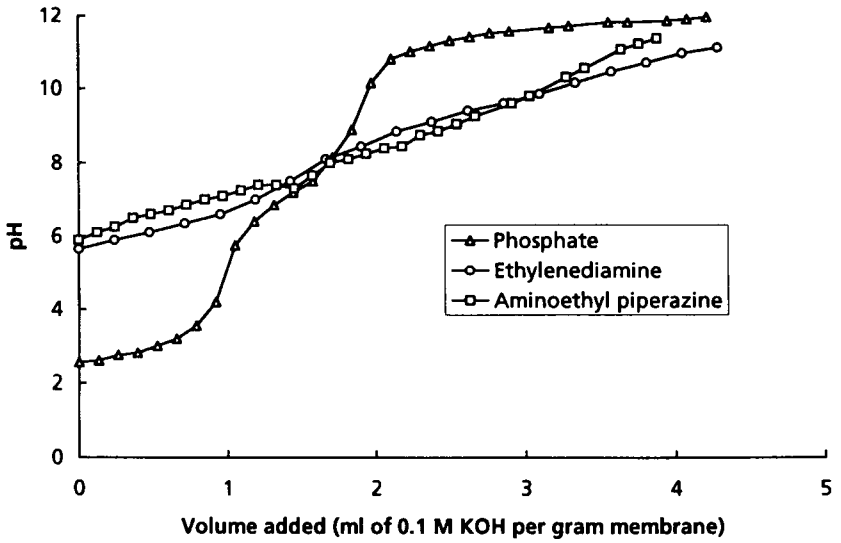

Fig. 3. Titration curves for three different functionalized membranes.

presented here, thus being able to cover the entire aqueous pH scale. Several other functional groups were in fact tested in addition to those reported here, but none of these functioned satisfactorily when used for buffering. Among these unsatisfactory functionalization reagents were dimethylamine, ethanolamine, morpholine, and mercapto and amino carboxylic acids. The reason for their inadequate performance could be a low degree of functionalization or insufficient flexibility of the spacer arm, as discussed elsewhere [20,25]. There are also reasons to suspect that steric hindrance in the proton exchange could hamper the operation of membranes with substituted amino functional groups, i.e., dimethylamine and ethanolamine, as opposed to membranes with primary amino functionalities. No investigations have been undertaken to pursue the exact cause of this, but we believe that the most efficient membranes would be produced by direct polymerization of the functional monomer of interest (see below).

The tubular membranes used in this work could have been replaced by a reactor designed for flat sheet membranes. Narrow bore tubular membranes are, however, generally more efficient because of their higher area to volume ratio. They are also better for providing low dispersion connections to the tubes ordinarily used in analytical flow systems. On the negative side, the hollow fiber membranes can only be synthesized with water-insoluble monomers [20]. This prohibits the customized synthesis of membranes with ionizable or other hydrophilic functionalities using direct polymerization of the functional monomers. The technique of customized polymerization is, however, possible in the synthesis of flat sheets [20], and such direct polymerization of monomers carrying desired functional groups eliminates any "bottle-neck" effects experienced in post-synthesis functionalization. We believe that some of the differences in achieving a high buffering capacity can be ascribed to inefficient functionalization with the bulkier reagents. However, due to unavailability of suitable functional monomers, no directly polymerized membrane has been tested.

As can be seen from the titration curves of the membranes in Fig. 3, the phosphate group shows two distinct pK_a values, the first one around 3 and the second around 7, which is consistent both with literature values [26] and with our buffering experiments. The amine-containing membranes do not exhibit any equally obvious inflection points. Instead, the titration curves are almost linear in the pH-range from 7 to 10. No difference can be seen between the two curves, although the piperazine functionality is expected to have a slightly lower pK_a than the primary and secondary amines present in the ethylenediamine functionalized membrane.

Incorporation of these membranes in an analytical flow system requires some consideration. Care must be taken in choosing the right functionality, not only in terms of the desired pH, but also with respect to the analytes of interest. Since these membranes are all weak

ion exchangers, they are partially ionized at the pH values encountered. Specific interactions with the analytes, like ion pair formation, or even removal of ions by ion exchange, can seriously degrade the performance of the analytical system. Any ions transported into or out of the analytical flow stream must be replaced by an ion of the same charge sign, or accompanied by simultaneous transport of a counterion, in order to retain the electroneutrality. This means that with weak cation exchangers, such as the phosphate membrane, the flux of protons across the membrane is balanced by transport of cations in the opposite direction. In the case of the weak anion exchangers the proton flux is accompanied by the flux of counterions (i.e., transport of an ion pair). The buffer substance used for regulating pH at the regeneration side of the membrane must therefore be chosen carefully if introduction of buffer substance is to be avoided. The ionic form of the buffering substance should have the same charge sign as the charged form of the membrane functionality. If this condition is fulfilled, and if the concentration of ionic groups in the membrane is high, the buffer ion will be effectively excluded from the membrane by Donnan exclusion [27]. This was the reason for choosing phosphate and amine buffers for the regeneration of the respective membranes. The ionic strength of the buffers was adjusted to match that of the analyzed solutions to minimize concentration driven ion exchange. The analyzed solutions were kept at a total ion concentration of 10 mmol/l for two reasons; firstly not to restrict the ion exchange across the membrane by deficiency of exchangeable ions in the analytical stream, and secondly to minimize streaming potentials at the pH electrode in the evaluation setup.

The membranes prepared in this work carry covalently bound weakly acidic or basic groups which are responsible for the "facilitated transport" exhibited by the membranes. If this type of material is operated under normal conditions, i.e., no extreme temperatures, pressures, pH values, etc., the lifetime can be expected to be several months [28,29].

Increase in the capacity of the buffering device without concurrent increase in band broadening could be achieved by introduction of spheres, with high capacity and of the same functionality as the membrane matrix, into the membrane tube, converting the tube into a single bead string reactor (SBSR) in order to promote transport of the reactants to the membrane wall [30–32]. This was, however, not tested in this work.

Acknowledgements

This work was supported by grants from the Swedish Natural Science Research Council. Celgard is a registered trademark of Hoechst Celanese, who kindly put samples of the material at our disposal. Teflon and Tefzel are trademarks of DuPont de Nemours.

References

[1] S.K. Ratanatanawongs and S.R. Crouch, Anal. Chim. Acta, 192 (1987) 277.
[2] L.D. Bowers, in I.S. Krull (Ed.), Reaction Detection in Liquid Chromatography, Marcel Dekker, New York, 1986, pp. 195–226.
[3] K. Gamoh and S. Imamichi, Anal. Chim. Acta, 251 (1991) 255.
[4] S.E. Meek and D.J. Pietrzyk, Anal. Chem., 60 (1988) 1397.
[5] D.R. Luke, G.R. Matzke, J.T. Clarkson and W.M. Awni, Clin. Chem., 33 (1987) 1450.
[6] E.P. Scott, J. Pharm. Sci., 72 (1983) 1089.
[7] R. Greissbach, Angew. Chem., 52 (1939) 215.
[8] C.L. Teitelbaum, J. Org. Chem., 23 (1958) 646.
[9] K. Irgum and M. Lindgren, Anal. Chem., 57 (1985) 1330.
[10] H. Jansen, C.J.M. Vermunt, U.A.Th. Brinkman and R.W. Frei, J. Chromatogr., 366 (1986) 135.
[11] J.C. Davis and D.P. Peterson, Anal. Chem., 57 (1985) 768.
[12] J. Haginaka and J. Wakai, J. Chromatogr., 390 (1987) 421.
[13] H. Hwang and P.K. Dasgupta, Anal. Chem., 58 (1986) 1521.
[14] P.R. Haddad, J. Chromatogr., 482 (1989) 267.
[15] T.S. Stevens, J.C. Davis and H. Small, Anal. Chem., 53 (1981) 1488-92.
[16] P.R. Haddad and R.E. Jackson, Ion Chromatography, Elsevier, Amsterdam, 1990, p. 264.
[17] P.K. Dasgupta, J. Chromatogr. Sci., 27 (1989) 422; and references cited therein.
[18] B. Lillig and H. Engelhardt, in I.S. Krull (Ed.), Reaction Detection in Liquid Chromatography, Marcel Dekker, New York, 1986, pp. 1–61.
[19] H. Small, T.S. Stevens and W.C. Bauman, Anal. Chem., 47 (1975) 1801.
[20] B. Glad, K. Irgum and P Hörstedt, J. Membrane Sci., submitted for publication.
[21] K. Saito, T. Kaga, H. Yamagishi, S. Furusaki, T. Sugo and J. Okamoto, J. Membrane Sci., 43 (1989) 131.
[22] F. Svec, H. Hrudkova, D. Horak and J. Kalal, Angew. Makromol. Chem., 63 (1977) 23.
[23] P. Hodge, in D.C. Sherrington and P. Hodge (Eds.), Syntheses and Separations using Functional Polymers, Wiley, Chichester, 1988, p. 50.

[24] W. Fries, React. Polym., 19 (1993) 97.
[25] A. Guyot, in D.C. Sherrington and P. Hodge (Eds.), Syntheses and Separations using Functional Polymers, Wiley, Chichester, 1988, p. 31.
[26] F. Helfferich, Ion Exchange, McGraw-Hill, New York, 1962, p. 86.
[27] F. Helfferich, Ion Exchange, McGraw-Hill, New York, 1962, p. 134 ff.
[28] L. Bromberg, G. Levine and O. Kedem, J. Membrane Sci., 71 (1992) 41.
[29] A.M. Neplenbroek, D. Bargeman and C.A. Smolders, J. Membrane Sci., 67 (1992) 149.
[30] J.M. Reijn, W.E. van der Linden and H. Poppe, Anal. Chim. Acta, 126 (1981) 1.
[31] J.M. Reijn, H. Poppe and W.E. van der Linden, Anal. Chim. Acta, 145 (1983) 59.
[32] J.M. Reijn, H. Poppe and W.E. van der Linden, Anal. Chem., 56 (1984) 943.

ELSEVIER

Analytica Chimica Acta 298 (1994) 159–165

ANALYTICA CHIMICA ACTA

Study of mass-transfer efficiency in pervaporation processes

I.L. Mattos [1], M.D. Luque de Castro *

Department of Analytical Chemistry, Faculty of Sciences, University of Córdoba, E-14004 Córdoba, Spain

Received 9 March 1994; revised manuscript received 31 May 1994

Abstract

A method for the determination of the mass-transfer efficiency of pervaporation processes through semipermeable membranes is reported. Aliquots of ammonium ion solution were injected sequentially into two parallel manifolds with and without a pervaporation unit, both using the same reaction zone and detector. A channel which transports the Nessler's reagent was merged with the channels from both manifolds and the area of the peak obtained on passage of the reaction product through the photometric detector was used as the analytical signal. The variables influencing the efficiency of the pervaporation process (i.e., flow-rate, temperature, type of membrane, halting of the flow, etc.) were exhaustively checked in order to establish the working conditions for optimal development of the separation process.

Keywords: Spectrophotometry; Flow system; Pervaporation, ammonium

1. Introduction

Non-chromatographic continuous separation processes coupled to unsegmented flow systems started to be significant after the paper by Baadenhuijsen and Seuren-Jacobs in 1979 [1], where gas diffusion coupled to flow injection (FI) was used for the first time. Since then techniques such as gas-diffusion [2,3], dialysis [4], ion-exchange [5], etc. have grown to constitute an interesting alternative for implementing several steps of the preliminary operations in order to accommodate the raw sample to the measuring instrument [6–8]. The development of these techniques in a continuous, unsegmented fashion facilitates the automation of the overall analytical process, reducing the need for human participation, which is one of the primary goals of today's analytical chemistry [6–9].

Pervaporation is a promising separation technique which integrates an evaporation and a gas-diffusion process in a single step. It is easy to implement in a continuous mode, thus allowing great simplification and miniaturization of preliminary operations in such a way that analytical quality and productivity can be clearly improved [7]. Despite its capabilities there are few methods dealing with the use of this technique for analytical purposes [10,11]. An essential step to clarify and demonstrate the real analytical capability of pervaporation is the development of a systematic study of the mass-transfer efficiency achievable by this technique.

The method previously proposed by Novic and Pihlar [3] for determining the separation efficiency in gas-diffusion processes has been applied in the present research for establishing the variables affecting the process, the optimal working conditions to achieve maximum mass-transfer and the absolute amount of diffused species. Ammonia was the species chosen for

* Corresponding author.

[1] Permanent address: Institute of Chemistry, State University of Campinas, Campinas, SP, Brazil (C.P. 6154).

SSDI 0003-2670(94)00273-O

this study and the Nessler's reagent was used for derivatization. The method used for the determination of the mass-transfer through the pervaporation membrane is based on a dual manifold into which identical aliquots of the analyte are injected. One of the aliquots passes through the separation module before the analyte enters into contact with the reagent, while the other aliquot is directly merged with the reagent. Both plugs are transported to a common detector through the same reaction coil and the areas yielded in both experiments are compared.

2. Experimental

2.1. Reagents

All chemicals used were of analytical reagent grade, and the solutions were prepared with distilled/deionized water.

Preparation of the Nessler's reagent: to 4 g of potassium iodide in 40 ml of distilled water is added slowly 4% mercury(II) chloride solution, stirring gently until the appearance of a red precipitate. Then, 100 ml of a 10 M sodium hydroxide solution are added and the solution is diluted to 500 ml with distilled water, finally adding a small amount of mercury(II) chloride solution until permanent turbidity. The solution is allowed to stand overnight, then decanted and stored in a topaz bottle.

Aqueous solutions of 2 M sodium hydroxide (Merck); 1×10^{-3} M sodium acetate/acetic acid (Merck) buffer, pH 4.5; 1×10^{-2} M sodium tetraborate (Panreac) were prepared. A 50 μg ml^{-1} bromocresol green (BCG, Merck) solution was prepared in the borate solution. A 1000 μg ml^{-1} ammonium stock standard solution was prepared from ammonium chloride (Merck).

Cellulose, polyvinylidene fluoride (PVDF) and polytetrafluoroethylene (PTFE) membranes of 5.0 μm pore size and 47-mm diameter purchased by Millipore were also used.

2.2. Instruments and apparatus

A Unicam 8625 spectrophotometer furnished with a Hellma 1000 QS flow-cell (10-mm pathlength) and connected to a Merck-Hitachi D-2500 Chromato-Integrator was used. Two four-channel Gilson Minipuls-2 peristaltic pumps with rate-selectors, two Rheodyne 5041 injection valves, PTFE tubing of 0.5 mm i.d. and a Selecta 382-S recirculating thermostat were also used.

A pervaporation module was custom-built from machined parts [7]. It consisted of the following elements: (a) an upper chamber with an inlet and outlet, through which the acceptor stream is circulated. The acceptor solution collected the gaseous analyte by reaction with a suitable reagent contained in it. (b) A thin membrane support (1 mm) made of PTFE owing to the difficulty to machine it in methacrylate. (c) Spacers of different thickness (2–10 mm) placed below and above the membrane support in order to enlarge the lower and upper chamber, respectively. (d) A lower, donor stream/sample chamber through which the feed stream for evaporation/diffusion was circulated. The whole pervaporation module (membrane support excluded) was made of methacrylate in order to allow continuous checking of it during the experiments. Firm contact between parts was achieved by screwing aluminium supports with four cylinders.

2.3. Manifold and procedure

The dual manifold used to study the mass-transfer efficiency of the pervaporation process is outlined in Fig. 1. The reference aliquot is injected through valve IV_1 into a 1×10^{-3} M sodium acetate/acetic acid car-

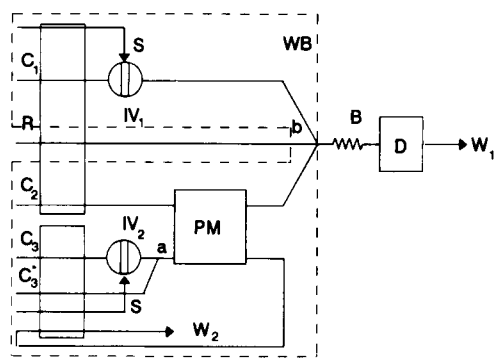

Fig. 1. Flow diagram of the hydrodynamic system employed for the study of the mass-transfer efficiency of pervaporation. C_1, C_2, C_3 and C_3^* are carrier stream buffer solution, pH 4.5, 0.001 M; acceptor and donor streams (0.001 M buffer solution, pH 4.5, and 2 M sodium hydroxide, respectively); R, Nessler's reagent; S, sample; IV_1 and IV_2, reference and investigated sample injection valves respectively; PM, pervaporation module; a and b, merging points; B, coiled reactor; D, detector; W, waste; PP, peristaltic pump; WB, water bath.

rier stream (C_1) and merged at b with the Nessler solution and with the acceptor stream from the pervaporation module. The derivatization reaction is developed in reactor B and the product is monitored on passage through the flow-cell located in the spectrophotometric detector. The area of the FI peak obtained is digitized by the integrator. The investigated aliquot is inserted into a 2 M sodium hydroxide carrier stream (C_3) through IV_2 and then merged with another stream (C_{3*}) of the same composition in order to achieve a homogeneous basic pH along the injected plug. This yields quantitative conversion of the analyte (NH_4^+) into NH_3 when the plug reaches the pervaporation unit. The gas removed from the solution permeates through the porous membrane after passage through the gaseous phase located between the flowing basic solution and the membrane and is accepted by a 1×10^{-3} M sodium acetate/acetic acid carrier stream (C_2). After merging with the reagent R at b, the derivatization, detection and data processing are similar to that described on injection of the reference aliquot.

2.4. Manual procedure

To check the results of the experiments (including the determination of the diffused analyte) a manual procedure was used. The channels merging at b were disconnected and the analyte from the aliquots alternatively injected through IV_1 and IV_2 were collected in volumetric flasks and, after addition of the conditioning buffer and derivatization reagent, the absorbance of the solutions was monitored. The mass-transfer efficiency calculated compared well with the results obtained by the flow method.

3. Results and discussion

Prior to starting the study, the independence of the peak-area measurements from sample dispersion was verified in both sub-manifolds by injecting 50 μl-aliquots of bromocresol green solution of 100 μg ml^{-1} as follows: some aliquots were injected into C_1 through IV_1 using different lengths of B (from 30 to 300 cm). Then, similar aliquots were injected into C_3, passed through the lower chamber of the pervaporation module (PM) and monitored by connecting the detector at the PM outlet (W_2 in Fig. 1), and using the PM with and without glass-beads in its lower part in order to achieve different dispersion conditions. Three different flow-rates (0.5, 1.0 and 3.0 ml min^{-1}) were used in both sets of experiments. The areas were identical in all instances within the limits of the experimental error, as can be seen in Table 1.

Table 1
Study of reproducibility of peak-area measurements

Mixing coil length[a]	Flow-rate (ml min^{-1})		
	0.5	1.0	3.0
300 cm × 0.8 mm i.d.	36.7 ± 0.6[b]	17.8 ± 0.2	6.7 ± 0.2
	37.2 ± 0.8[c]	17.1 ± 0.8	6.5 ± 0.1
100 cm × 0.8 mm i.d.	35.4 ± 0.2	17.6 ± 0.5	6.4 ± 0.2
	36.4 ± 0.1	18.0 ± 0.9	6.4 ± 0.9
30 cm × 3.0 mm i.d.	35.3 ± 0.8	17.4 ± 0.2	6.1 ± 0.7
	37.4 ± 0.2	17.5 ± 0.8	6.4 ± 0.1
60 cm (SBSR) × 0.8 mm i.d.	37.0 ± 0.1	18.7 ± 0.6	6.4 ± 0.2
	38.0 ± 0.5	19.1 ± 0.7	6.2 ± 0.3

[a]Injected sample (50 μl of 100 μg bromocresol green ml^{-1}).
[b]Mean value (area, %) related to the first dilution condition (in this case, $B = 300$ cm).
[c]Mean value (area, %) related to diffusion unit.

3.1. Influence of the experimental variables on the mass-transfer efficiency

All the experiments were carried out by simultaneous functioning of all the streams in Fig. 1. The possibility of inserting a selection valve at b to select either channel C_1 or C_2, depending on the plug to be monitored (injected via IV_1 or IV_2) was rejected in order to avoid changes in the system which could affect the results.

3.2. Influence of the flow-rate

The influence of the flow-rate on the mass-transfer efficiency was checked by changing the acceptor and donor flow-rates as shown in Fig. 2. An increase in efficiency of 390% was observed, for an injected volume of 2 ml, by changing the donor flow-rate from 3.0 to 0.5 ml min^{-1} at a constant acceptor flow-rate of 1.0 ml min^{-1}. This is a logical consequence of the shorter residence-time of the analyte in the lower part of the pervaporation unit. When the donor flow-rate was kept constant at 0.5 ml min^{-1} and the acceptor flow-rate

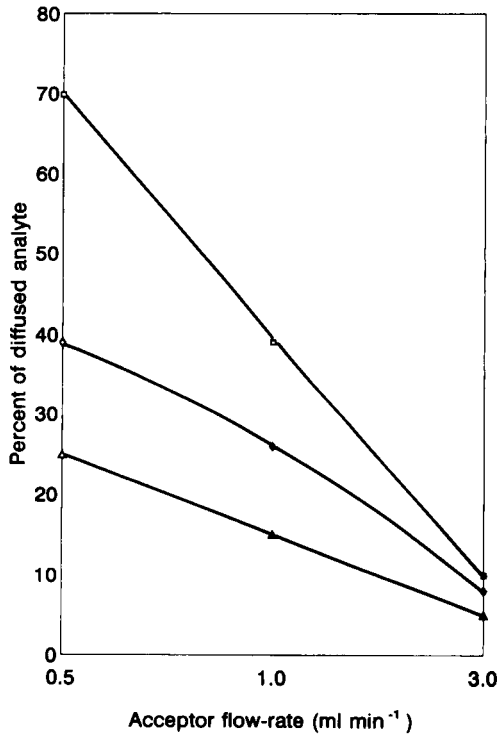

Fig. 2. Influence of the donor and acceptor flow-rates on the mass-transfer efficiency. Injected volume, 2 ml of 100 μg ml^{-1}; 40°C; PTFE membrane, 5 μm pore size. The donor flow-rate values were 0.5 (△), 1.0 (◇) and 3.0 (□) ml min^{-1}.

was changed from 3.0 to 0.5 ml min^{-1}, the efficiency was increased 600% as a consequence of the higher volume into which the analyte was collected, that involved a more dilute collector stream and thus a displacement of the mass-transfer equilibrium towards a higher mass-transfer.

A set of experiments was performed by using continuous aspiration (completely continuous flow analysis [12]) of the ammonium solution through both sub-systems by changing C_1 and C_3 by the sample solution. The concentration of the solution had to be lowered to 5 μg ml^{-1} in order to fit the absorbance yielded by aspiration through the C_1-channel, within the detection range, as no dispersion took place along the system under these conditions. No area measurements were possible in this situation, but constant absorbance monitoring was performed.

An increase of 10% in the mass-transfer efficiency was achieved at an acceptor flow-rate of 1.0 ml min^{-1} as a consequence of a faster passage of the sample through the lower part of the pervaporation module, which resulted in a smaller decrease in the ammonium concentration of the solution in the module and thus a higher passage of NH_3 to the gaseous phase in order to maintain the equilibrium.

A 15% decrease in the signal was observed for a constant donor flow-rate of 0.5 ml min^{-1} by changing the acceptor flow-rate from 0.5 to 3.0 ml min^{-1}. It is worthwhile to note that this decrease does not result in a lower efficiency of the mass-transfer but to higher dilution of the analyte into the acceptor stream, which is not compensated by the type of measurement.

The following working conditions were chosen for further experiments: acceptor and donor stream flow-rates, 1.0 and 0.5 ml min^{-1}, respectively; injected volume 2.0 ml.

3.3. *Influence of the temperature and type of membrane*

The percentage of diffused species was dependent on both the temperature and type of membrane as can be observed in Fig. 3. The zones within the dotted lines in Fig. 1 were thermostated to the required temperatures and the rest of the system was kept at 5°C in order to avoid precipitation of the reaction product (NH_2Hg_2IO) in both the reaction coil and flow-cell, which was favoured by increased temperatures. Cellulose, PVDF and PTFE membranes were tried. An increase of the mass-transfer efficiency of ca. 100% was achieved by changing the temperature from 30 to 60°C for the three types of membranes and a better performance of the PTFE membrane in all instances can be deduced from Fig. 3. The effect of temperature was more significant in the range from 30 to 40°C. A temperature of 40°C was chosen for subsequent experiments.

3.4. *Influence of stopping the flow*

The following experiments were performed with stop times between 60 and 240 s in order to assess the influence of this variable on the separation process: (a) halt the flow of the acceptor stream while keeping the donor flow-rate constant at 0.5 ml min^{-1}; (b) halt the flow of the donor stream while keeping the acceptor flow-rate constant at 1.0 ml min^{-1}; (c) halt simultaneously both the donor and acceptor streams. As was foreseeable, an increase in the ammonia diffusion

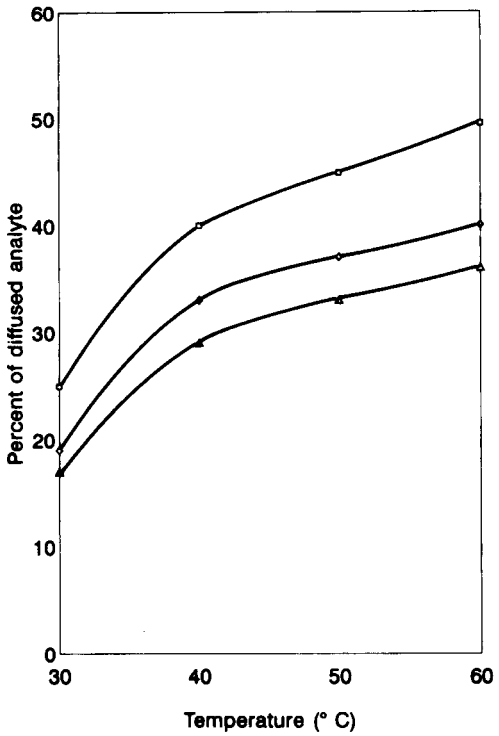

Fig. 3. Influence of temperature and membrane type on the mass-transfer efficiency. Injected volume, 2 ml of 100 μg ml^{-1}; donor and acceptor flow-rates 0.5 and 1.0 ml min^{-1}, respectively. Cellulose (△), PVDF (◇) and PTFE (□) membranes with 5 μm pore size.

through the membrane was obtained in all instances in comparison with the non-stopped (continuous flow) conditions, the increase being more noticeable (92%) when both streams were halted for a stop-time of 240 s than when the donor (35%) or the acceptor (21%) streams were halted. The fact that a lower mass-transfer efficiency was achieved by halting the acceptor stream for 240 s keeping the donor stream at 0.5 ml min^{-1} constant in contrast to the opposite situation was due to complete removal of the injected aliquot from the PM 300 s after injection (Fig. 4).

As the stop-time dramatically influences the sampling frequency, a compromise is advisable depending on both the sensitivity and expeditiousness required.

3.5. *Influence of the collection conditions*

The studies mentioned above were performed by using a slightly acidic acceptor stream in order to favour the mass-transfer of NH_3 through the membrane by removal of the diffused species by conversion to ammonium ions. The C_2 stream was changed from 1×10^{-3} M sodium acetate/acetic acid to 1×10^{-3} M potassium hydrogen carbonate/anhydrous sodium carbonate, keeping the working conditions constant at the following values: acceptor and donor stream flow-rates, 1.0 and 0.5 ml min^{-1}, respectively; injected volume, 2.0 ml. A decrease of the percentage of the diffused analyte from 40 to 26 was observed in the absence of an acid–base reaction of the diffused analyte crossing the membrane.

3.6. *Influence of the injected volume and diffused species concentration*

An increase in the mass-transfer from 16 to 42% was observed when the volume of the injected aliquots was changed from 1 to 2 ml, but higher volumes slightly increased the efficiency of the process (from 42% to 76% for 4 ml; from 76% to 98% for 6 ml). This is a consequence of the volume of the lower part of the pervaporation module (ca. 1.8 ml when packed with glass-beads) which created almost continuous aspira-

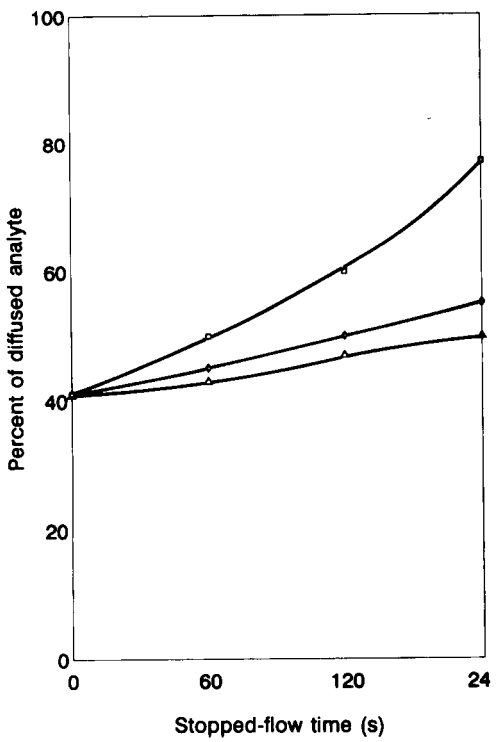

Fig. 4. Influence of halting the flow. Injected volume, 2 ml of 100 μg ml^{-1}; 40°C; PTFE membrane, 5 μm pore size. The flow was stopped in the acceptor (△), donor (◇) and both (□) streams.

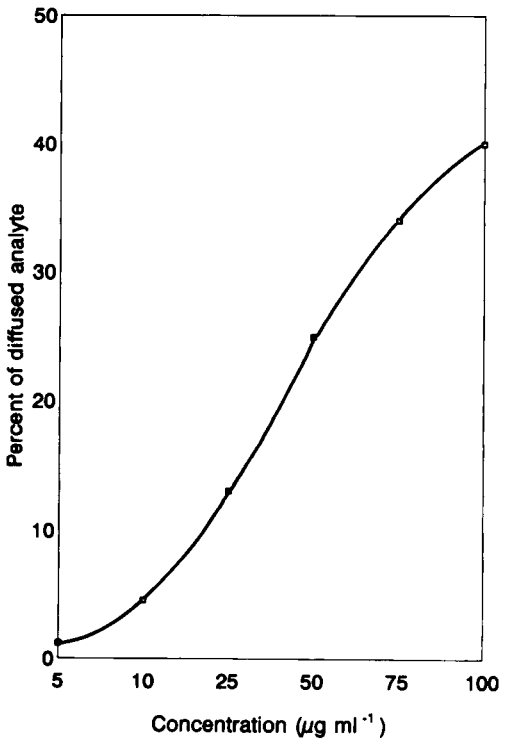

Fig. 5. Influence of the ammonium concentration. Injected volume, 2 ml; 40°C; PTFE membrane, 5 μm pore size; acceptor and donor flow-rates 0.5 and 1.0 ml min^{-1}, respectively.

tion conditions when the injected volume is higher than ca. 2 ml.

The influence of the concentration of the target species on the separation process was checked by changing the concentration of ammonium in the injected solutions from 5 to 100 μg ml^{-1}. A poor efficiency was achieved at low concentrations as the constant gaseous volume between the liquid level and the membrane in the lower part of the chamber must be saturated before the species crosses the membrane. This effect is more pronounced at low concentrations, as shown in Fig. 5. An almost linear relationship (slope 0.4531, correlation coefficient 0.9960) between percentage of diffused species and concentration of this in the sample solution was obtained between 10 and 75 μg ml^{-1}. The lower linear limit can be lowered by removal of the low-part PM spacers, thus decreasing the volume occupied by gaseous phase.

Table 2
Precision of the proposed method and comparison with the manual method.

Method	Efficiency (%)[a]	R.S.D. (%)[b]
FIA	40.1	1.3
Manual	38.9	2.5

[a] Standard solution, 100 μg ml^{-1}.
[b] $n=11$.

3.7. Precision of the method and comparison with the manual method

The following working conditions were used to study the precision of the method: acceptor and donor stream flow-rates, 1.0 and 0.5 ml min^{-1}, respectively (injected volume, 2.0 ml). Eleven different solutions were injected in triplicate in both sub-systems and the results obtained, in terms of R.S.D. percentage, are listed in Table 2, and they compare well with those obtained by using the manual method detailed in the Experimental section.

4. Conclusions

The following can be concluded from the above study.

The method used for the determination of the mass-transfer efficiency of pervaporation is fast, precise and easy to implement in an automated way.

The efficiency of this separation technique is similar or higher than that achieved by other membrane-based separation techniques such as dialysis or gas-diffusion [6]. The advantage of no-contact between sample-matrix and membrane, characteristic of pervaporation, can be crucial when complex samples (e.g., biological fluids, fermentation or industrial samples) are the target systems.

The efficiency of the pervaporation process can be widely manipulated by changing the experimental conditions, thus achieving a wider range of analyte concentration in the acceptor stream.

Very diluted samples would require long stop-time, small gaseous volume of the lower part of the pervaporation module, and sample volumes of ca. 2 ml.

The results reported here could be of interest to enlarge the scope of application of non-chromatographic continuous separations techniques to complex, heterogeneous samples involving immiscible phases, solids in suspension, etc.

Acknowledgements

The Spanish Dirección General de Investigación Científica y Técnica (DGICyT) is gratefully acknowledged for financial support. One of the authors (I.L.M.) wishes to express his gratitude to Dr. G. Oliveira Neto and the Brazilian Conselho National de Desenvolvimento Cientifico y Technològico (CNPq) for funding his stay in Spain.

References

[1] H. Baadenhuijsen and E.H. Seuren-Jacobs, Clin. Chem., 25 (1979) 443.
[2] A. Tanaka, K. Mashiba and T. Deguchi, Anal. Chim. Acta, 214 (1988) 214.
[3] M. Novic and B. Pihlar, Anal. Chim. Acta, 251 (1991) 261.
[4] B. Olsson, H. Lundback and G. Johansson, Anal. Chim. Acta, 167 (1985) 123.
[5] L. Risinger, Anal. Chim. Acta, 179 (1988) 509.
[6] M. Valcárcel and M.D. Luque de Castro, Non-Chromatographic Continuous Separation Techniques, Royal Society of Chemistry, London, 1991.
[7] I.L. Mattos, M.D. Luque de Castro and M. Valcárcel, Anal. Chem., submitted for publication.
[8] M.D. Luque de Castro and M. Valcárcel, Anal. Chim. Acta, 261 (1992) 425.
[9] M. Valcárcel, M.D. Luque de Castro and M.T. Tena, Anal. Proc., 30 (1993) 276.
[10] V. Prinzing, I. Ogbomo, C. Lehn and H.L. Schmidt, Sensors Actuators, B1 (1990) 542.
[11] H. Usthche and G. Histi, J. Membr. Sci., 8 (1981) 105.
[12] M. Goto, Trends Anal. Chem., 2 (1983) 92.

ELSEVIER

Analytica Chimica Acta 298 (1994) 167–173

ANALYTICA CHIMICA ACTA

Determination of copper in water and rice samples by flame atomic absorption spectrometry with flow-injection on-line adsorption preconcentration using a knotted reactor

Hengwu Chen [1], Shukun Xu, Zhaolun Fang *

Flow Injection Analysis Research Center, Institute of Applied Ecology, Academia Sinica, Shenyang 110015, China

Received 28 March 1994; revised manuscript received 16 May 1994

Abstract

A flow-injection on-line adsorption preconcentration flame atomic absorption spectrometric system for the determination of copper was developed. The copper diethyldithiocarbamate chelate was adsorbed on the walls of a PTFE knotted reactor. The sorbed species was eluted by isobutyl methyl ketone at a flow-rate of 4.1 ml min^{-1}. Air segmentation between sample and eluent was employed to avoid mixing of the neighbouring phases under fast elution rates. An enhancement factor of 120 and a detection limit of 0.2 $\mu g\ l^{-1}$ Cu were achieved for a 60 s loading period (sample throughput 46 h^{-1}). The relative standard deviations were 1.7% and 3.6% at the 20 $\mu g\ l^{-1}$ and 2 $\mu g\ l^{-1}$ Cu levels, respectively. Interference from at least 50 $\mu g\ l^{-1}$ Fe(III) was eliminated by adding ascorbic acid. The method has been applied successfully to determine $\mu g\ l^{-1}$ amounts of copper in drinking water and sea water and $\mu g\ g^{-1}$ amounts of copper in rice.

Keywords: Atomic absorption spectrometry; Flow injection; Copper; Rice; Waters; Preconcentration; Knotted reactor

1. Introduction

Since Olsen et al. [1] first coupled flow-injection (FI) on-line ion-exchange preconcentration to flame atomic absorption spectrometry (FAAS) for the determination of trace heavy metals in water samples, various separation methods based on ion-exchange, liquid–liquid extraction, sorbent extraction, precipitation and coprecipitation have been adapted to FI on-line preconcentration for FAAS [2]. Such combined techniques extended the detection limits of FAAS for elements such as copper, lead and cadmium down to $\mu g\ l^{-1}$ or $ng\ l^{-1}$ levels.

A FI on-line preconcentration method using coprecipitation without filtration was first developed by Fang et al. [3] for FAAS determination of trace amounts of lead in biological samples. In the system, Fe(II) was reacted with hexamethyleneammonium hexamethylenedithiocarbamate (HMA-HMDTC) forming a water-insoluble chelate which served as a carrier for the coprecipitation of trace metals. A knotted reactor was used to collect the precipitate.

In a recent study on the on-line preconcentration of cadmium with the knotted reactor, Fang et al. [4] observed that the cadmium–diethyldithiocarbamate (DDC) chelate could also be retained by the reactor without a coprecipitation carrier. It was assumed that the cadmium was retained through adsorption of the metal chelate on the PTFE tube wall. In this paper the

* Corresponding author.

[1] On leave from the Department of Chemistry, Hangzhou University, Hangzhou, China.

SSDI 0003-2670(94)00248-K

technique has been extended to on-line adsorption preconcentration of copper for FAAS analysis of water samples and biological samples. The manifold design was improved to prevent intermixing of sample and eluent, resulting in higher enrichment factors.

2. Experimental

2.1. Apparatus

A model WFX-1D atomic absorption spectrometer (Ruili, Beijing) equipped with a copper hollow cathode lamp and a chart-recorder (Dahua Instrument Co., Shanghai, China) was used at 324.7 nm with a 10 mA lamp current. The flame conditions were 8.5 l min^{-1} air flow-rate and 0.8 l min^{-1} acetylene, which was slightly leaner than that recommended by the manufacturer. This measure was taken to allow introduction of the organic solvent which served as extra fuel. The impact bead was removed from the spray chamber.

An LZ-2000 FI processor (Zhaofa Institute of Laboratory Automation, Shenyang) was used for FI on-line preconcentration. The manifold of the FI-AAS system is shown in Fig. 1. The knotted reactor was made of PTFE tubing with 0.5 mm i.d. [4]. PVC pump tubes were used to propel the sample, reagent, water and air. The organic eluent was delivered by the introduction of water into a displacement bottle.

2.2. Reagents and standard reference materials

Copper standard solution was prepared by step-wise dilution of a stock solution of 100 μg ml^{-1} (Institute of Chemical Metallurgy, Beijing) using 1.0 M hydrochloric acid.

(0.25%, m/v) DDC solution was prepared by dissolution of an appropriate amount of sodium diethyldithiocarbamate (Xinzhong, Shanghai) in pH 9.2 buffer solution (0.02 M ammonia–0.01 M acetic acid).

(10%, m/v) ascorbic acid aqueous solution (North-Eastern Pharmaceutical, Shenyang) and isobutyl methyl ketone (IBMK) (Shanghai Solvent, Shanghai) were also used.

Biological standard reference material GBW 08502 (rice powder) was obtained from The Institute of Environmental Monitoring (Beijing).

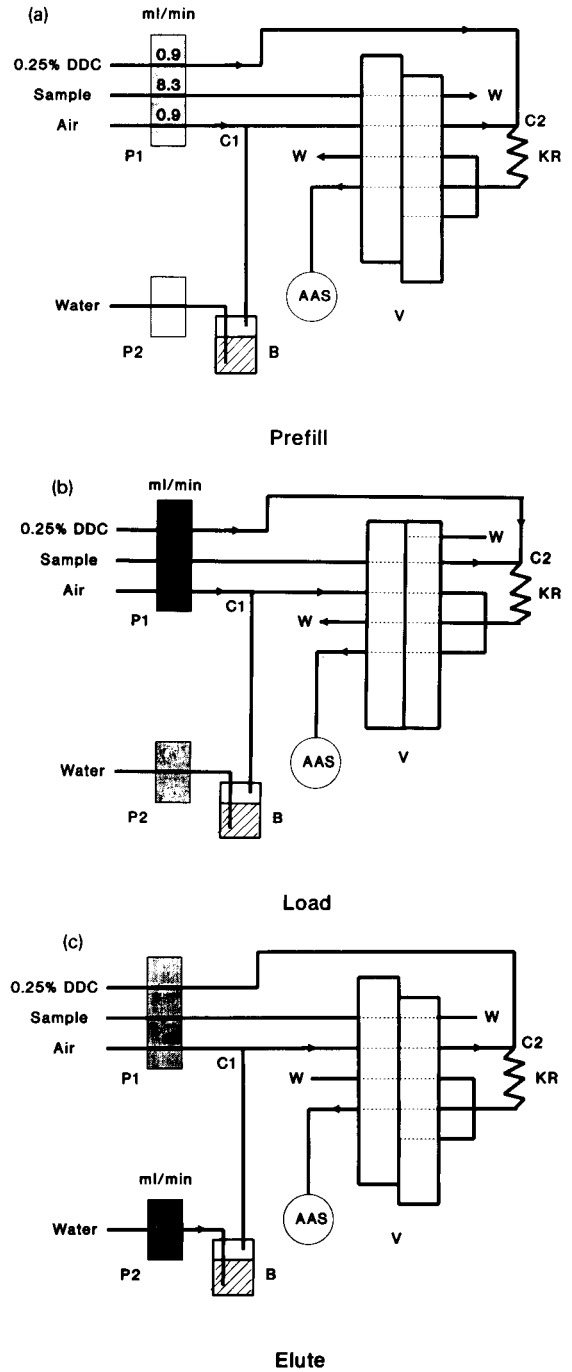

Fig. 1. FI manifold for on-line adsorption preconcentration and FAAS system. AAS, flame atomic absorption spectrometer; B, displacement bottle; C1, confluence point of air and IBMK conduits; C2, confluence point of sample and DDC solution; KR, knotted reactor, 0.5 mm i.d., 200 cm PTFE tubing, 15 knots/50 cm; P1 and P2, peristaltic pumps; V, injection valve; W, waste. a, prefill; b, sample loading; c, elution.

Table 1
FI operation program for on-line adsorption preconcentration and elution

Step	Function	Time (s)	Pump speed (rpm) [a]		Valve position
			Pump 1	Pump 2	
1	Prefill	5	100 (8.3)	0	Injection
2	Loading	60	100 (8.3)	0	Fill
3	Elution	12	0	60 (4.1)	Injection

[a] The flow-rates (ml min^{-1}) are given in parentheses.

All chemicals used were of analytical grade, and deionized water was used throughout.

2.3. Procedure

Water samples were acidified to 0.01 M HNO_3 immediately after collection, and filtered before analysis. For the rice samples, 0.3 g rice powder was accurately weighed into a 50 ml beaker, and 3 ml aqua regia was added. The mixture was gently warmed on a hot plate until the disappearance of fumes. After cooling to room temperature, 0.1 ml of concentrated perchloric acid was added to the residual solution. The solution was then heated at 140°C until disappearance of dense white fumes. After cooling, about 20 ml of 1 M hydrochloric acid was added to the beaker to dissolve the residue. The solution was transferred into a 50 ml volumetric flask and 2.5 ml of 10% ascorbic acid solution was added before diluting to volume with 1 M HCl.

2.4. System operation

The operation sequence of the preconcentration system is shown in Table 1. In the prefill step with the valve position as shown in Fig. 1a, the sample or standard solution was pumped by P1 for 5 s to wash out the previous sample solution remaining in the conduit while the eluent pump P2 was stopped. The valve was turned to the loading position as shown in Fig. 1b, and sample or standard solution was pumped and merged with the DDC reagent before passing through the knotted reactor when the Cu–DDC complexes formed were collected on the walls of the reactor. This preconcentration sequence usually lasted for 60 s. Meanwhile air was pumped into the eluent line (eluent pump stopped), forming an air segment between the IBMK eluent and valve inlet. In the elution step shown in Fig. 1c, sampling pump P1 was stopped, and elution pump P2 activated to deliver IBMK and elute the Cu–DDC complexes collected in the knotted reactor into the spectrometer, preceded by an air segment. 12 s were sufficient for complete elution.

3. Results and discussion

3.1. The function of air segmentation between sample and eluent

IBMK was used by Fang et al. [3] as eluent for on-line preconcentration by coprecipitation of hexamethylenedithiocarbamate metal chelates owing to its high dissolution efficiency. In a recent study on on-line sorption preconcentration through the formation of metal–dithiocarbamate complexes, this solvent again proved to be the best among the eluents studied [4]. In these studies, dispersion of analyte between sample waste and eluent, which followed immediately after, was obstructed owing to the fact that IBMK is slightly miscible with water. In preliminary studies in the present work using the FI manifold described in the above mentioned reports, a normal peak was recorded when the elution flow-rate of IBMK was less than 3.0 ml min^{-1}. However, with a flow-rate of 3.4 ml min^{-1}, a shoulder which was about 8% of the peak height appeared in front of the main peak; while at 5.5 ml min^{-1}, the shoulder increased to 35% peak height as shown in Fig. 2a. These effects decreased the peak heights on which the readouts and enrichment factors were based. Since the shoulder was not corrected using background correction, it could not have been due to the change of flame conditions when the organic solvent entered the flame. Presumably, this phenomenon was due to segmentation of the two immiscible phases at the boundary at increased flow-rates in the knotted reactor. Based on this assumption, it was decided to introduce a small air segment between the sample waste and organic eluent. To achieve this, the manifold was modified as shown in Fig. 1. With this manifold, the air segment, which remained in the PTFE tubing between confluence point C1 and the port of the valve at the end of the sample loading operation sequence,

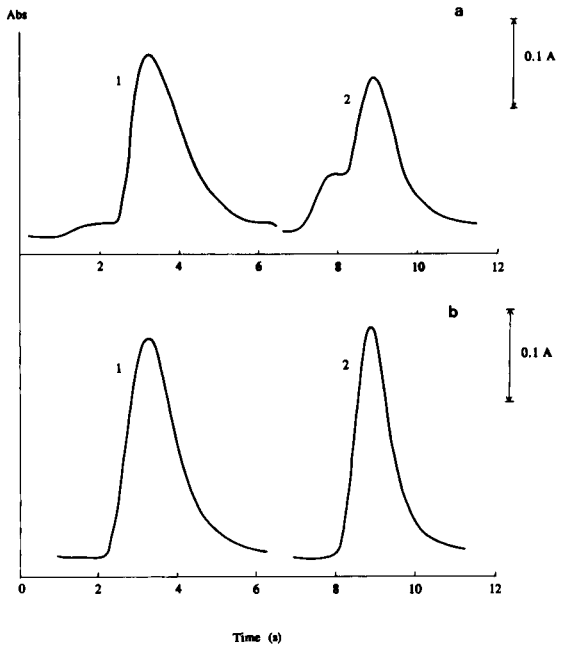

Fig. 2. The effect of air segmentation on the peak shape of 20 $\mu g\, l^{-1}$ Cu. (a) Without air segment; (b) with air segment. (1) Elution flow-rate, 3.4 ml min^{-1}; (2) elution flow-rate, 5.5 ml min^{-1}. Other conditions are as in Fig. 1.

served as a barrier between the two phases when the valve was activated and the IBMK was introduced. Hence, no special sequence for air segment introduction in the FI program was required. The effect of introducing the air segment can be seen in Fig. 2. The peak height increased by at least 20%, while no shoulders were observed at high elution rates.

3.2. *Optimization of the system*

Important experimental parameters including sample acidity and DDC concentration during sample loading, knotted reactor length, sample loading time and elution rate were optimized for the preconcentration system.

Sample acidity, in the range of 0.01–1.0 M HCl, had no significant influence on the preconcentration efficiency with 0.25% DDC under the flow-rate parameters shown in Fig. 1. The effect of DDC concentration was investigated at acidities of 0.1 M and 1.0 M HCl. As expected, without DDC no copper was retained by the reactor, but almost identical copper signals were obtained in the DDC concentration range 0.1–1.0% at both acidities. A sample acidity of 1.0 M HCl and DDC concentration of 0.25% were selected for use with concurrent considerations on selectivity (see also the section on interference study).

In an on-line sorption preconcentration system using a knotted reactor no extra backpressure was developed in the reactor during the preconcentration. This is an outstanding merit compared to on-line coprecipitation systems where back pressure in the knotted reactor increases with reactor length and sample loading time. In the present system, the collection capacity of the reactor could readily be increased by lengthening the reactor. The copper signal increased almost linearly with knotted reactor length to about 100 cm but levelled off gradually to a constant value at about 250 cm. Nevertheless the signal was 20% higher at 200 cm than at 100 cm. Therefore, a 200 cm-length reactor was used in further studies for better sensitivity, since no difficulties were encountered even at a relatively large sample flow-rate of 8.3 ml min^{-1}.

Studies on the effect of preconcentration time on the peak absorbance of 20 $\mu g\, l^{-1}$ Cu(II) showed that the sensitivity increased almost linearly with an increase of loading time up to 180 s. However, long loading periods would lead to lower sample throughputs and concentration efficiencies. A 60 s loading time was chosen as a compromise between sensitivity (enrichment factor) and sample throughput.

The effect of IBMK elution rate on the analyte signal is shown in Fig. 3a. A maximum signal was obtained within the IBMK flow-rate range of 4.1–4.8 ml min^{-1}, which was close to the free uptake rate of the nebulization system (6.5 ml min^{-1}). Fast scanning recordings of the elution peak revealed that the half peak width ($W_{1/2}$) expressed in seconds decreased significantly with an increase of the elution rate up to 4.1 ml min^{-1} IBMK, after which only slight decreases were observed (Fig. 3b). In contrast, the eluent volumes containing the bulk of analyte expressed by $2qW_{1/2}$, where $W_{1/2}$ is the half peak width and q (ml/s) the corresponding IBMK flow-rate, were basically the same below 4.1 ml min^{-1}, and above this value the volume increased linearly with increase in flow-rate (Fig. 3b). This implies that at flow-rates lower than 4.1 ml min^{-1} the signals were governed by the difference between eluent feeding rate and nebulization uptake rate rather than the dissolution kinetics of the sorbed analyte. The results also imply that the flow-rates above this level were too high for achieving dissolution equi-

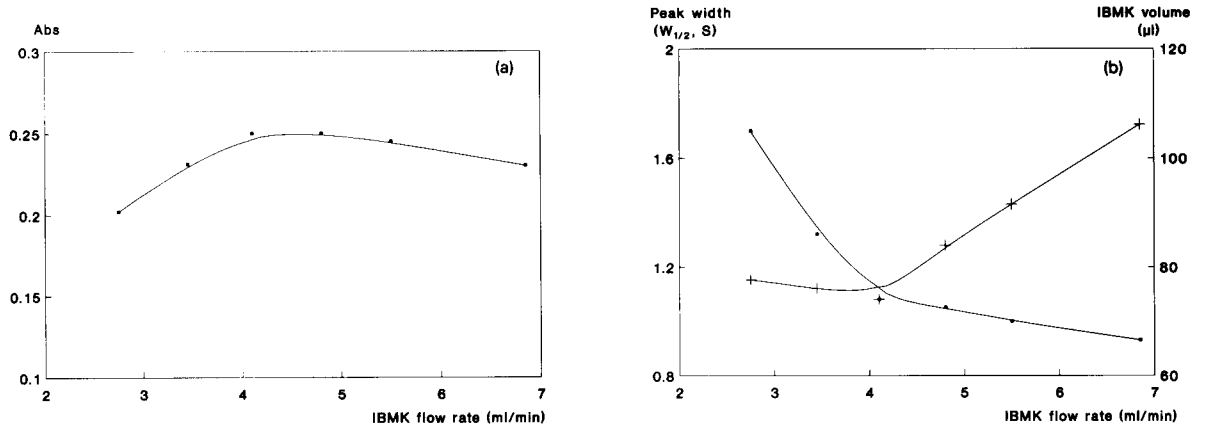

Fig. 3. The effect of elution rate on peak profile. 20 $\mu g\,l^{-1}$ Cu in 1.0 M HCl loaded for 60 s at 8.3 ml min^{-1} using the manifold shown in Fig. 1. (a) Peak height versus elution flow-rate; (b) half peak width ($W_{1/2}$) and IBMK volumes containing the bulk of analyte versus elution flow-rate.

Table 2
Analytical performance of the on-line adsorption preconcentration-FAAS determination of copper for 60 s preconcentration

Enhancement factor	120
Enrichment factor	91
Sample volume (ml)	8.3
Sampling frequency (h^{-1})	46
Concentration efficiency (min^{-1}) [a]	92
R.S.D. (%, $n=11$)	1.7 (20 $\mu g\,l^{-1}$)
	3.6 (2 $\mu g\,l^{-1}$)
Detection limit ($\mu g\,l^{-1}$)	0.2 (3σ)
Range of calib. graph ($\mu g\,l^{-1}$)	0–30
Regression equation [b]	$A=0.0052+0.0093C$
Correlation coefficient	0.999

[a] Including enhancement effect from organic solvent.
[b] A = abs., C = [Cu] in $\mu g/l$, $n=6$.

librium, requiring more eluent for complete elution. However, the unfavourable kinetics were partially compensated because the flow-rates were closer to the free uptake rate of the nebulizer, resulting in a smaller degree of starvation. These effects could be seen from the relatively gradual decrease in copper signal with increasing flow rates above 4.1 ml min^{-1}. The optimum elution rate in the present system is significantly greater than that in the on-line coprecipitation system [3]. This is due to faster elution of a sorbed species in comparison to dissolution of a precipitate.

The analytical performance of the optimized system is shown in Table 2. The detection limit (d.l.) is similar to that obtained using a FI sorbent extraction column preconcentration system [5] with inferior selectivity, and is significantly better than a FI liquid–liquid extraction preconcentration system reported recently (d.l. = 20 $\mu g\,l^{-1}$) [6].

3.3. Interference studies

For analysis of environmental water and biological samples using the present system, the most likely interferences were considered to be iron and zinc. Thus,

Table 3
Interference of foreign ions in determination of 20 $\mu g\,l^{-1}$ Cu(II) in 1.0 M HCl and 0.5% ascorbic acid

Ion	Concentration ($\mu g\,ml^{-1}$)	Copper recovery (%)
Al(III)	10	101
	100	106
Cd(II)	2.0	96
	4.0	81
Co(II)	0.2	101
	0.5	87
	1.0	75
Cr(VI)	10	99
	100	103
Fe(III)	20	101
	50	96
	100	84
Mn(II)	100	100
Ni(II)	0.2	103
	0.5	72
Pb(II)	1.0	103
	4.0	90
	10	52
Zn(II)	100	104

Table 4
Determination of copper in water samples and the recovery of spiked copper

Water	Cu(II) added ($\mu g\ l^{-1}$)	Found ($\mu g\ l^{-1}$)	Recovery (%)
Tap water I	0	0.3	–
	10.0	9.5	92
Tap water II	0	0.9	–
	5.0	6.4	109
Hot tap water I [a]	0	13.1	–
	10.0	23.6	105
Hot tap water II[a]	0	19.5	–
	8.0	28.2	108
Sea water	0	2.2	–
	5.0	6.9	94

[a] First samples collected in the morning from water heaters with copper piping.

different sample acidities and masking reagents were used to study the interfering effects of the Fe(III) and Zn(II). Preliminary studies showed that high sample acidities of about 1 M HCl were sufficiently effective for depression of interferences from zinc, but not from Fe(III). The reduction of Fe(III) to Fe(II), however, by addition of ascorbic acid at such acidities significantly decreased the interference from iron. Since ascorbic acid had no deleterious effects on the preconcentration of the analyte, 1.0 M HCl containing 0.5% ascorbic acid was finally chosen as the reaction medium for preconcentration. It is not necessary to add ascorbic acid to standard solutions for calibration unless small blank values are introduced owing to impurities in the ascorbic acid used. The results of interference studies under these conditions are shown in Table 3. The tolerance of interferences was generally good except for Ni(II) and Co(II). These interferents are not likely to be encountered in unpolluted water samples or biological sample digests at such concentration levels.

3.4. Applications

The method was applied to the determination of copper in tap water and coastal sea water. The results are shown in Table 4. The recoveries of spiked copper were satisfactory.

The accuracy of the method was checked through the determination of the copper content in a rice powder standard reference material (GBW 08502). The copper content was found to be $2.85 \pm 0.10\ \mu g\ g^{-1}$ (mean ± S.D., $n = 3$) which was in good agreement with the certified value of $2.6 \pm 0.3\ \mu g\ g^{-1}$.

4. Conclusions

In the FI on-line adsorption preconcentration system, the introduction of an air segment between sample loading (preconcentration) and elution was found to be beneficial for preventing the intermixing of neighbouring phases at the boundary zone between the aqueous sample solution and organic eluent at high elution flow-rates. The use of high elution rates approaching the free uptake rate of the spectrometer produced high enrichment factors. Interference of iron in the DDC complex sorption can be significantly decreased by addition of ascorbic acid, making it possible to determine copper at the $\mu g\ l^{-1}$ level in tap water and natural waters and at the $\mu g\ g^{-1}$ level in some biological samples.

Acknowledgements

This work was supported by a research grant from the Instrumental Analysis Center of The Shenyang Branch of Academia Sinica. The authors are grateful to Lijing Sun for valuable discussions.

References

[1] S. Olsen, L.C.R. Pessenda, J. Ruzicka and E.H. Hansen, Analyst, 108 (1983) 905.
[2] Zhaolun Fang, Flow Injection Separation and Preconcentration, VCH, Weinheim, 1993.
[3] Z.L. Fang, M. Sperling and B. Welz, J. Anal. At. Spectrom., 6 (1991) 301.
[4] Z.-L. Fang, S.-K. Xu, L.-P. Dong and W.-Q. Li, Talanta, submitted for publication
[5] Z.-L. Fang, T.-Z. Guo and B. Welz, Talanta, 38 (1991) 613.
[6] M.A. Memon, Z.-X. Zhuang and Z.-L. Fang, At. Spectrosc., 14 (1993) 50.

ELSEVIER

Analytica Chimica Acta 298 (1994) 175–182

ANALYTICA CHIMICA ACTA

Determination of enantiomeric purities using CD/CD detection

Allan R. Engle, Neil Purdie *

Chemistry Department, Oklahoma State University, Stillwater, OK 74078-0447, USA

Received 11 April 1994; revised manuscript received 6 June 1994

Abstract

Enantiomeric purities are determined for binary mixtures of D-pseudoephedrine with the L-enantiomer and with the (+)- and (−)-ephedrines in bulk solutions using circular dichroism (CD) detection in the visible range. The molecules are individually derivatized by ligand exchange with tartrate in the first coordination sphere of Cu(II) metal complexes. Chiral–chiral interactions, after substitution, are specific enough to uniquely discriminate among all four enantiomers using spectra for the mixed complexes. A univariate calibration model is used to predict enantiomeric purities for mixtures of the pseudoephedrines, and multivariate models are used for all three binary mixtures. Results for enantiomeric ratios that lie in the mole fraction range 0.95–1.00 are an improvement over current methods. Achiral mesotartrate is the optimum host ligand to use for the analysis of binary mixtures of diastereoisomers.

Keywords: Circular dichroism; Enantiomeric purity; Ephedrines; D-Pseudoephedrine

1. Introduction

Determining enantiomeric purities (EP) of drug substances has taken on greater meaning in light of (i) the awareness of the different pharmacological responses to stereoisomeric pairs, that began with the discovery of the teratogenic effects of *S*-(−)-thalidomide [1,2], (ii) the emphasis on production of enantiomeric drug forms by the new and emerging chiral-technology industries, and (iii) the regulatory requirements imposed upon the pharmaceuticals industry to develop methods for analytical quality control of new drug submissions that are intended to be marketed as enantiomers [2]. There is a desire in the industry for a general method with which to determine EPs routinely. Based on the assumption that both enantiomers of a chiral compound might always be present, the analytical problem is reduced to making two independent experimental measurements without disturbing the composition. Options are either to measure both isomers independently, with or without prior separation, or to measure the total concentration of the mixture and the concentration of just one of the isomers.

Current methods are summarized succinctly in a recent special issue on chiral discriminations [3]. Emphasis is given to chromatographic methods [3–10]. These are broadly divided between methods that employ conventional column materials and achiral solvents, and methods that use the various combinations of chiral and achiral mobile phases together with chiral and achiral stationary phases [5]. A significant prior step in many of the determinations is to prepare diastereoisomers by reacting the chiral mixture with a third chiral species which allows for the physical separation of the enantiomers. When good separations are achieved, retention times are often very long, although

* Corresponding author.

SSDI 0003-2670(94)00263-L

capillary electrophoresis methods have reduced the times enormously [13]. Detection is by single channel absorbance or refractive index measurement, and because of the miniaturization of the sample size, analyses call for the use of laser sources [3,12] and thermal lens detection [13]. If the method of choice is to not separate the enantiomers, then determinations involve two detectors in sequence, one of which is chiroptical, perhaps circular dichroism (CD) but more often polarimetry [10,11]. Depending upon the particular problem, a high level of accuracy in the measurement of EPs is sometimes very difficult to achieve with the present technology [9].

Discriminating between diastereoisomers by their nuclear magnetic resonance (NMR) spectra is a very viable alternative to chromatography [14]. NMR has the added advantage that, being a multichannel detector, a certain level of analytical selectivity is achieved. Another method with inherent selectivity is full spectrum CD detection which has been applied to unseparated bulk samples [15,16]. Compared to chromatography, CD calls for higher analyte concentrations, longer pathlengths, and conventional light sources. As a result detection limits are increased. Enantiomeric purities for SRMs of chiral drug substances have been measured fairly accurately using CD measurements in the UV range [17], either by a combination of CD/absorbance or by CD/CD. In the latter case, spectra are measured for equimolar amounts of the analyte dissolved first in an achiral solvent, and then in a chiral solvent system with which the analyte forms a diastereoisomer. An example might be water and an aqueous solution of a chiral solute such as a cyclodextrin. The ultimate success of the method relies upon the selectivity of the chiral solvent for the analyte and the magnitude of the spectral differences between enantiomers. CD is not immune to background absorbance and, if this is excessive, the S/N ratio for the signal will be lowered to a point where there is insufficient precision with which to measure EP. In these instances prior sample clean-up is required, and is best done using chromatography.

The primary chromophores in drug molecules are aromatic ring and carbonyl functional groups which absorb in the near UV where interferences from matrix absorption are worst. These are avoided if the CD bands can be shifted to the visible range, which was done in a qualitative study of aminoglycoside antibiotics by complexing them to the Cu(II)–L-tartrate metal complex [17]. Chiral interactions between the coordinated tartrate and the aminoglycoside ligands are so specific that high levels of analytical selectivity were achieved. The same metal complex is part of the biuret reagent, which is used routinely in clinical applications to measure total protein [18], and also to assay neomycin sulfate [19]. Both applications use absorbance detection. In this article, multichannel detection and multivariate calibration methods are combined with ligand exchange reactions between tartrates and ephedrines as model systems to evaluate the routine measurement of EPs using induced CD spectral data.

2. Experimental

2.1. Reagents

Derivatizing reagents were prepared using reagent grade $CuSO_4 \cdot 5H_2O$ (Fisher), with NaK–L-tartrate (Fisher), KH–D-tartrate (Sigma), or mesotartaric acid (Sigma). KI (Baker) is added as a stabilizer. Hydrochlorides of the four ephedrine isomers, of at least 99% chemical purity, were obtained from Sigma or Aldrich. All materials were used without purification. No product certifications were provided for the EPs for the ephedrines, so each was presumed to be 100% pure.

2.2. Solution preparations

Reagents were prepared by dissolving 3.81 mmole of tartrate salt in 250 ml deionized water in a 500-ml flask. 5.0 ml of $CuSO_4$ stock solution (0.1910 M), 10 ml NaOH (5.0 M), and 2.5 g KI are added in that order and the mixture made up to volume with de-ionized water. Final reagent concentrations are 1.91 mM in Cu(II), 7.62 mM in tartrate, 0.1 M in NaOH, and 0.03 M in KI. Excess tartrate prevents precipitation of copper hydroxide. Ephedrine stocks were prepared by dissolving known weighed amounts of the hydrochlorides into measured volume aliquots of the Cu(II)–tartrate reagents.

Test solutions for single enantiomers or their binary mixtures were prepared by placing the desired volume aliquots from the ephedrine stock solutions into a 25-ml flask and filling to the mark with the reagent solution. The total $[Cu^{2+}]$, therefore, is always constant at

1.91 mM and in excess over the analyte by at least a factor of 1.2. This ratio assures a tartrate to ephedrine ratio at least 4.8:1, and 1:1 stoichiometry for the ligand exchange. Compositions for the binary mixtures covered the whole mole fraction range.

2.3. Measurements

Spectra were measured using a Jasco 500-A automatic recording spectropolarimeter coupled to an IBM-compatible PC through a Jasco IF-500 II serial interface and data processing software. Instrument parameters were: wavelength range 400–700 nm; sensitivity 100 mdeg/cm; time constant 0.25 s; scan rate 200 nm/min; repeat scans 2; slit width 2 mm; sample pathlengths 1, 2, and, most often, 5 cm. The sensitivity scale was calibrated daily using a 0.025% w/w solution of androsterone in dioxan. The temperature was maintained to be within ± 1°C.

Metal tartrates in aqueous base are stable analytical reagents. Only the D- and L-tartrate reagents have a CD spectrum. These were measured before and after every series of experiments done on the mixed ligand complexes and were added to a single file in which the average was continually updated. Day to day spectral reproducibilities, expressed as standard deviations from the mean values at the major maxima, are excellent, e.g., for Cu(II)–L-tartrate the measured ellipticity at 650 nm is -246.1 ± 0.4 mdeg. As a result, file spectra for the reagents can be recalled and used routinely to measure EP and determinations have effectively been reduced to measuring the CD spectra for the solution of only the mixed ligand complex.

2.4. Calibration/prediction models

In spectroscopy, calibrations and predictions for single analytes are generally made using the univariate Beer's law equation, $A = \varepsilon cd + (\mathrm{er})$, where (er) is an error term added in order to include the combined effects of chemical, sampling, and instrumental errors associated with a one-time measurement. The analogous equation for CD is: $\psi = [\theta]cd + (\mathrm{er})$, where ψ and $[\theta]$ are the measured and molar ellipticities respectively. The goodness of a calibration is measured by the magnitude of the residual variance term expressed as the linear least squares regression for $(\mathrm{er}) = \{\psi - [\theta]cd\}$ for the points in the calibration set. Predictions are made using $c = \{\psi - (\mathrm{er})\}/[\theta]d$. Results are never exact because (er) is not a reproducible quantity.

In multivariate methods several analytes are determined simultaneously using multichannel detection data [20–22]. The data are referred to as independent variables and the analyte concentrations as response variables. Calibrations are made indirectly using independent variables from M wavelengths for N sample mixtures whose response variables, Q, are somehow known. Typically $M > Q$, so that there are more equations than unknowns. For EP determinations, $Q = 2$, and from the extent of the measured CD spectra, vide supra, the maximum value for M in this case is 150. The calibration equation, written in matrix form, is $\boldsymbol{\psi} = \boldsymbol{\Sigma}[\boldsymbol{\Phi}]_j\mathbf{C} + \mathbf{ER}$, for $\mathbf{j} = 1 \ldots N$ samples, given that $\boldsymbol{\psi}$ is the $(M \times N)$ matrix, $\mathbf{C}$ is the $(N \times 2)$ matrix, and the error vector is $\mathbf{ER}$. Partial least squares (PLS) algorithms are the most dependable methods for solving matrix equations of this kind for spectroscopic data [20–22]. By analogy with the univariate model, regression coefficients are found that minimize the residual variance expressed as $\boldsymbol{\sigma}^2 = \boldsymbol{\Sigma}\{\boldsymbol{\psi} - \boldsymbol{\Sigma}[\boldsymbol{\Phi}]_j\mathbf{C}\}^2$ for the subset of N samples selected for the calibration experiment.

Residual variances for multivariate calibrations are reduced significantly over what ever is possible using univariate models. The best calibration (training) set is one that is representative of all conceivable compositions that will ever be encountered in future sample populations. As the bases for the calibration model for each pair of enantiomers, training sets were prepared that used compositional and spectral data for from $N = 18$ to 35 prepared binary mixtures whose mole fractions C, were varied over the full range. Modelling was done using $M = 76$ variables taken at equal intervals over the 400–700 nm range. Sums of the analyte concentrations were not always equal, but values were never allowed to exceed the $[Cu^{2+}]$ in the tartrate reagents.

Multivariate predictions are done using a "pseudo"-inversion of the matrix equations [20–22]. Results, again, are never exact because of the unpredictability of the (er) term for each mixture speciated. Prediction steps are also an integral part of the calibration step, by subdividing the set into random segments for cross-validation. One segment is used to calibrate and the regression coefficients from that segment are used to

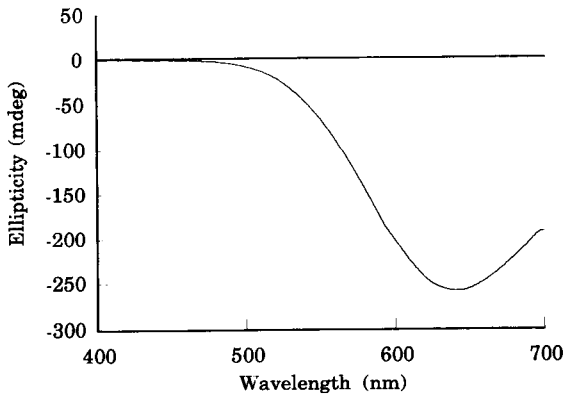

Fig. 1. CD spectrum for a 1.91 mM solution of the Cu(II)–L-tartrate reagent in aqueous base.

predict the response variables for the remainder. The process is repeated until every calibration sample has been kept out just once, and any ($[\psi]c_i$) cross terms that are of insignificant proportion to the model are deleted from the training set. Models are validated statistically in a number of ways using some function of the differences in the observed and predicted values, e.g., root mean square error (RMSE).

The algorithm used for this work was PLS2 which is part of the spectroscopic analysis UNSCRAMBLER II software package that is available from CAMO (Trondheim, Norway).

3. Results and discussion.

3.1. CD spectra for copper–tartrate complexes

The simple CD spectrum for the Cu(II)–L-tartrate reagent is shown in Fig. 1. CD activity is induced by dissymmetric perturbations of the ground and excited state ligand field orbitals by the chiral ligand. While molar absorptivities, ε, for copper tartrate complexes are small numbers, molar ellipticities, θ_c, which are proportional to absorbance differences, $\Delta\varepsilon$, are large, and as a result, analytical limits of detection are lowered significantly. The positive band that begins around 400 nm is attributed to bound and free L-tartrate. The spectrum for Cu(II)–D-tartrate is the mirror image of Fig. 1. Cu(II)–mesotartrate has no CD spectrum.

3.2. Equilibrium expressions and CD spectra for mixed ligand complexes

The Cu(II) ion forms stable complexes [23] and undergoes very rapid ligand exchange into the first coordination sphere [24]. Exchange between a bound ligand L and an analyte ligand L* can be described by:

$$CuL_x + yL^* \Leftrightarrow CuL_{(x-y)}L^* + yL \quad (1)$$

provided CuL_x is in enough of an excess that the stoichiometry of the exchange is one. The measured ellipticity, ψ, is related to the concentrations of the species by:

$$\psi = \{\theta_u d[CuL_x] + \theta_c d[CuL_{(x-y)}L^*]\} \quad (2)$$

where θ_u and θ_c are the molar ellipticities for host and mixed ligand complexes respectively. CD induction is also expected for a chiral L*, even if L is achiral, e.g., mesotartrate, in which case the first term on the right is zero.

Because of differences in the second term of Eq. 2, spectra for equimolar solutions of mixed ligand complexes for the ephedrines with mesotartrate divide into two distinct mirror image pairs, Fig. 2. Interactions between coordinated ligands are specific enough to discriminate between diastereoisomers, but not between enantiomers, in spite of the fact that mesotartrate is achiral. Analytical selectivity from these spectra is increased over the spectra in the UV for the underiva-

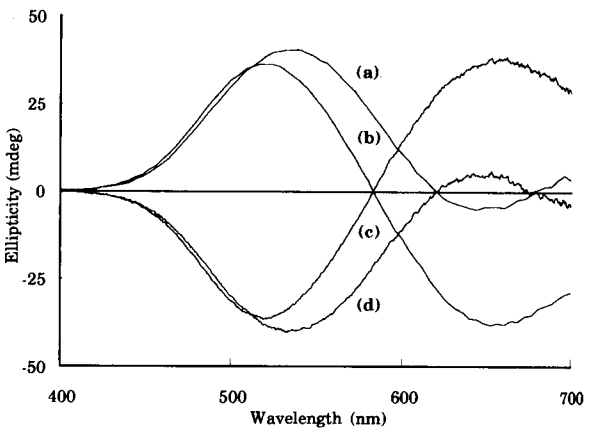

Fig. 2. CD spectra for the mixed Cu(II) complexes with equimolar solutions of: (a) D-pseudoephedrine; (b) (−)-ephedrine; (c) (+)-ephedrine; and (d) L-pseudoephedrine with mesotartrate.

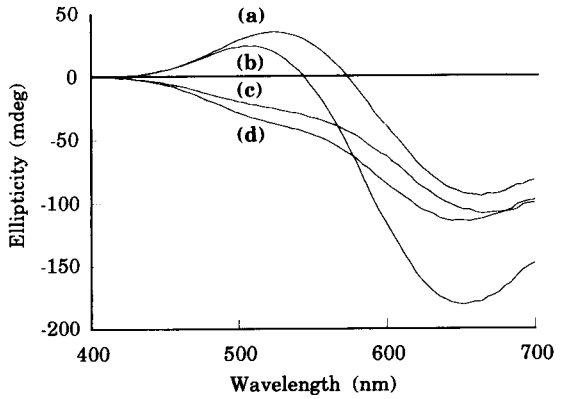

Fig. 3. CD spectra for the mixed Cu(II) complexes with equimolar solutions of: (a) D-pseudoephedrine; (b) (−)-ephedrine; (c) L-pseudoephedrine; and (d) (+)-ephedrine with L-tartrate.

tized molecules, which amount to two equivalent, indistinguishable, mirror image pairs.

Spectra for equimolar solutions of mixed ligand copper complexes with L-tartrate, on the other hand, differ entirely from one another whether they are compared directly, Fig. 3, or expressed as differences from the file spectrum for the host complex, Fig. 4. For D-tartrate, the CD spectra are exact mirror images of those in Figs. 3 and 4.

3.3. *Treatment of data for the analysis of binary mixtures*

For binary mixtures, L* represents both enantiomers. Two exchange equilibria occur that are known to

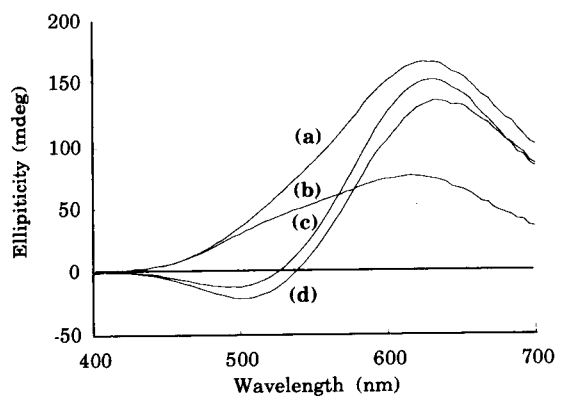

Fig. 4. Difference CD spectra for the mixed Cu(II) complexes with equimolar solutions of: (a) D-pseudoephedrine; (b) (−)-ephedrine; (c) L-pseudoephedrine; and (d) (+)-ephedrine with L-tartrate.

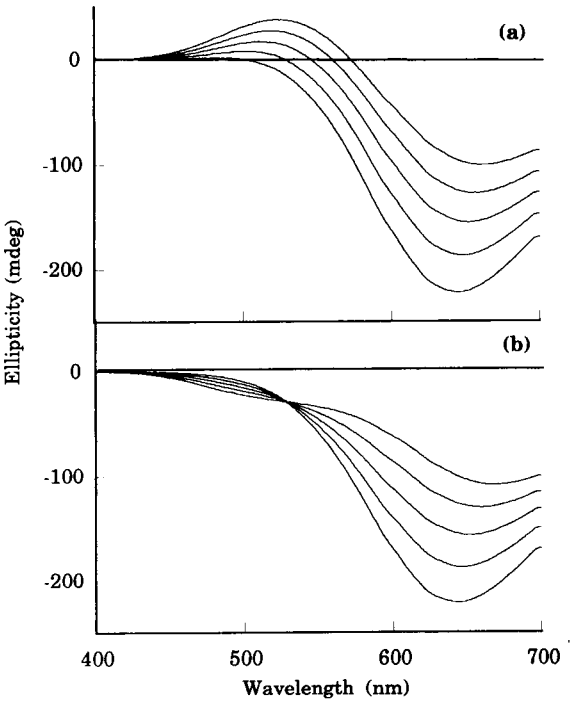

Fig. 5. CD spectra vs. solution concentration for the mixed Cu(II) complexes with (a) D-pseudoephedrine and (b) L-pseudoephedrine. The isosbestic point is at 527 nm with an ellipticity of −24.9 mdeg.

have different formation constants [6]. A mixture that is exactly racemic can be described by:

$$\mathrm{CuL}_x + [\,y/2(+)\mathrm{L}^* + y/2(-)\mathrm{L}^*] \Leftrightarrow \mathrm{CuL}_{(x-y/2)}(+)\mathrm{L}^* + \mathrm{CuL}_{(x-y/2)}(-)\mathrm{L}^* + y\mathrm{L} \quad (3)$$

where L* is the limiting reagent. Ellipticities and concentrations are correlated by:

$$\psi = \{\,\theta_u d[\,\mathrm{CuL}_x] + \theta_{(+)} d[\,\mathrm{CuL}_{(x-y/2)}(+)\mathrm{L}^*] + \theta_{(-)} d[\,\mathrm{CuL}_{(x-y/2)}(-)\mathrm{L}^*]\} \quad (4)$$

To discriminate between enantiomers in a mixture, it is a necessary condition that $\theta_{(+)} \neq \theta_{(-)}$, so even a mixture that is racemic will have a net CD spectrum for the mixed complex. For the non-racemic case $[(+)\mathrm{L}^*] \neq [(-)\mathrm{L}^*] \neq y/2$ in Eq. 4.

Spectra are plotted as a function of [L*] in Figs. 5 and 6. Sign changes occur at higher concentrations when L* is (1*S*,2*S*)-ephedrine, (i.e., D-pseudoephed-

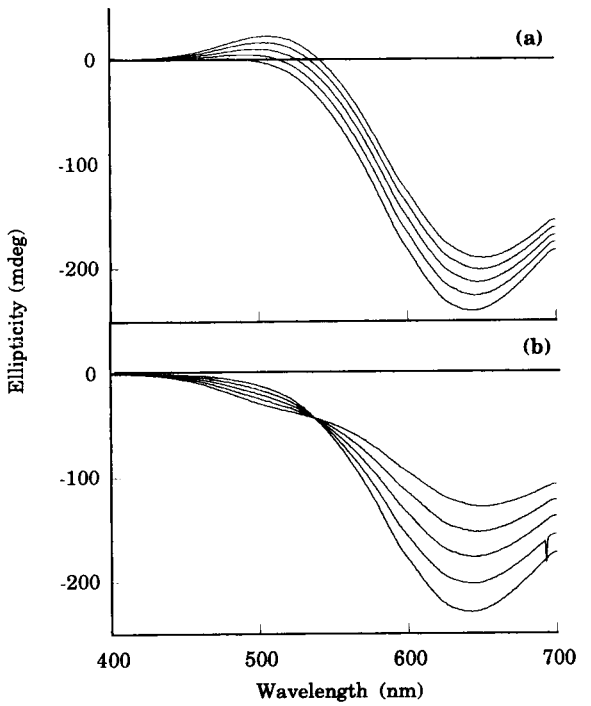

Fig. 6. CD spectra vs. solution concentration for the mixed Cu(II) complexes with (a) (−)-ephedrine and (b) (+)-ephedrine. The isosbestic point is at 538 nm with an ellipticity of −43.7 mdeg.

rine), and (1*R*,2*S*)-(−)-ephedrine. The series of spectra when L* is L-pseudoephedrine and (1*S*,2*R*)-(+)-ephedrine intersect with the spectrum for the host complex at characteristic isosbestic points which differ from each other by about 10 nm. This evidence supports the idea that only two metal complexes are present over the concentration ranges used in the study. The phenomenon of just one enantiomer having an isobestic point is very general because the spectrum for only one of the two can ever intersect the spectrum for the host complex. Relationships are reversed when L is D-tartrate, i.e., isosbestic points are observed at corresponding wavelengths for the (1*S*,2*S*)- and (1*R*,2*S*)-isomers.

3.4. Univariate analysis of binary mixtures using isosbestic point data

Ellipticities at the isosbestic wavelengths normalize to zero when spectra are expressed as differences between the host and mixed complexes. A net CD signal measured at that wavelength for a binary mixture, therefore, must be directly proportional to the concentration of the other enantiomer (Fig. 7a). Data were measured for a series of binary pseudoephedrine solutions in which the concentration of the D-enantiomer was systematically increased. The host complex was Cu(II)–L-tartrate. This information alone is insufficient to measure EP. Either the total analyte concentration must be measured, or the net ellipticity at the isobestic point should be measured for the same mixtures added to the Cu(II)–D-tartrate host (Fig. 7b). This univariate method for measuring EPs gives good predictions for a series of prepared anonymous mixtures of the pseudoephedrines, as long as the mole fraction is less than 0.95 (Table 1). Enantiomer concentrations were calculated using the correlation equations in Fig. 7. Sums for these calculated concentrations show an average positive bias of ~2.0% when compared with the total concentration amounts used to prepare the mixtures. Results are of comparable quality to those obtained by chiral chromatography [9].

3.5. Multivariate analyses of binary mixtures

To improve upon the results in Table 1, and particularly over the mole fraction range 0.95 to 1.0 for binary mixtures, predictions were made using multivariate calibration data determined for three model systems, namely with L-pseudoephedrine, (+)-ephedrine, and (−)-ephedrine. These are representative of problems

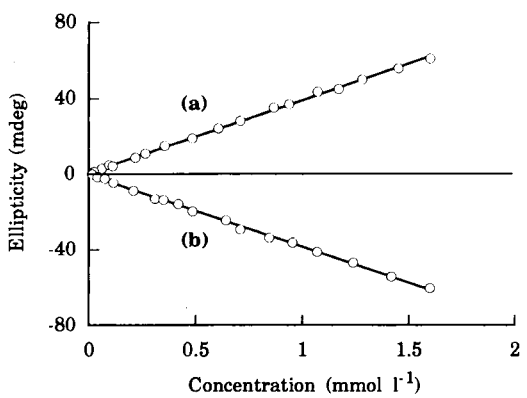

Fig. 7. Correlation curves for ellipticities measured at the isosbestic points vs. (a) [D-pseudoephedrine] for a series of D- and L-pseudoephedrine mixtures with Cu–L-tartrate ($y = 0.709 + 38.2x$) and (b) [L-pseudoephedrine] for a series of D- and L-pseudoephedrine mixtures with Cu–D-tartrate, ($y = -0.417 - 38.0x$) of variable ratios and total concentrations.

Table 1
Calculated enantiomeric purities of prepared binary mixtures using univariate calibration. D-Pseudoephedrine:L-pseudoephedrine (with L-tartrate)

Composition	0.990:0.010	0.950:0.050	0.900:0.100	0.750:0.250	0.500:0.500
Mean ($n=3$)	0.995:0.005	0.945:0.055	0.900:0.100	0.748:0.252	0.500:0.500
C.I. ±	0.006	0.004	0.018	0.006	0.009

that are of pharmaceutical significance. For instance, in the synthesis of D-pseudoephedrine, L-pseudoephedrine might be present as an optical impurity; and during storage, racemization to (+)- and/or (−)-ephedrine might occur, depending upon which of the side-chain chiral carbon centers undergoes inversion. These processes, however, are unlikely to occur to any large degree, in which case the most significant mole fraction range is $X > 0.95$. Best fits to the calibration models were achieved using two components, with which better than 99.8% of the Y-variances were explained. Individual enantiomer concentrations were predicted directly and models were validated by comparing their sums with the total analyte concentrations in the prepared solutions. Deviations are within ±1.0% with no statistical bias. Predicted EP values, expressed as mole fractions, are given in Table 2. Imprecisions are expressed as confidence intervals, CI. There is a substantial improvement over results from the univariate model, and especially in the critical range of $X > 0.95$.

Imprecisions were greatest for *D*-pseudoephedrine and (−)-ephedrine mixtures (see Table 2) which was expected because the spectra for their mixed complexes with L-tartrate are the most similar, Fig. 3. Predicted values are still acceptable when compared with results from other methods [9]. Mixtures of these diastereoisomers were also analyzed using the Cu(II)–mesotartrate reagent and the results are an improvement over those obtained with L-tartrate, which is testimony to the special discriminatory powers of the meso-form towards diastereoisomers.

The only experimental constraint, in either mathematical model, is that the analytical tartrate concentration must be in large excess over the total enantiomer

Table 2
Predicted enantiomeric purities of prepared binary mixtures using PLS2 multivariate regression analysis
(a) D-Pseudoephedrine:L-pseudoephedrine (with L-tartrate)

Composition	0.990:0.010	0.950:0.050	0.900:0.100	0.500:0.500	0.100:0.900	0.050:0.950	0.010:0.990
Mean ($n=3$)	0.992:0.008	0.952:0.048	0.905:0.095	0.505:0.495	0.099:0.901	0.047:0.953	0.007:0.993
C.I. ±	0.006	0.019	0.014	0.010	0.005	0.021	0.001
(b) D-Pseudoephedrine:(+)-ephedrine (with L-tartrate)							
Composition	0.990:0.010	0.950:0.050	0.900:0.100	0.500:0.500	0.100:0.900	0.050:0.950	0.010:0.990
Mean ($n=3$)	0.989:0.011	0.953:0.047	0.904:0.096	0.498:0.502	0.102:0.898	0.055:0.945	0.018:0.982
C.I. ±	0.011	0.005	0.007	0.006	0.009	0.004	0.002
(c) D-Pseudoephedrine:(−)-ephedrine (with L-tartrate)							
Composition	0.990:0.010	0.950:0.050	0.900:0.100	0.500:0.500	0.100:0.900	0.050:0.950	0.010:0.990
Mean ($n=3$)	0.958:0.042	0.918:0.082	0.927:0.073	0.477:0.523	0.064:0.936	0.044:0.956	0.033:0.967
C.I. ±	0.020	0.012	0.126	0.030	0.018	0.013	0.032
(d) D-Pseudoephedrine:(−)-ephedrine (with mesotartrate)							
Composition	0.990:0.010	0.950:0.050	0.900:0.100	0.500:0.500	0.100:0.900	0.050:0.950	0.010:0.990
Mean ($n=3$)	0.992:0.008	0.950:0.050	0.900:0.100	0.503:0.497	0.108:0.892	0.055:0.945	0.013:0.987
C.I. ±	0.012	0.006	0.011	0.003	0.014	0.011	0.019

concentration. Absorption by the reagent is not limiting at the concentration used and could be increased by at least ten-fold without affecting the S/N by too much. The one factor that determines how successful the method might be towards other potential analytes is the extent of the spectral change that accompanies the ligand exchange. These changes can be optimized by altering the ratio of the reagent to analyte concentrations. Copper(II) ion forms very stable complexes where the ligand donor atoms are heteroatoms such N-, S-, and P-, which opens up the method to a wide selection of potential chiral compounds for study. With the excellent reproducibility observed for the reagent solutions, EP calculations are effectively reduced to making one experimental measurement, the CD spectrum for the mixed ligand complex.

4. Conclusions

In its present state of development, the method cannot account for chemical impurities other than one of the other three enantiomers. An achiral impurity that competes with tartrate, e.g., creatinine [16], will reduce the spectral intensity of the host while leaving the basic features intact. Changes due to other chirals that can also displace tartrate are less predictable, but are unlikely to fit any of the three calibration models developed here. The method can be applied immediately to the measurement of EPs in drug forms dissolved in bulk media. With some adaptation, the reagent could be introduced through a post-column reactor in conventional column liquid chromatography, and applied to routine measurements of EP in drug formulations.

Acknowledgements

We are grateful for the collaboration with Drs. Frank Cox and Brian MacDonald and for the financial support of this work from the Analytical Development Laboratories of the Burroughs Wellcome Co., Greensville, NC.

References

[1] Y.F. Shealy, C.E. Opliger and J.A. Montgomery, Chem. Ind., (1965) 1030.
[2] W.H. DeCamp, Chirality, 1 (1989) 2.
[3] A.F. Fell, Trends Anal. Chem., 12 (1993) 125–189.
[4] W.H. Pirkle and J.M. Finn, in J.D. Morrison (Ed.), Asymmetric Synthesis, Vol. 1, Academic Press, New York, 1983.
[5] T.J. Ward and D.W. Armstrong, in M. Zief and L.J. Crane (Eds.), Chromatographic Chiral Separations, Chromatographic Science Series, Vol. 40, Marcel Dekker, New York, 1988.
[6] V.A. Davankov, in J.C. Giddings (Ed.), Advances in Chromatography, Vol. 18, Marcel Dekker, New York, 1980.
[7] W. Boehme, G. Wagner, U. Oehme and U. Priesnitz, Anal. Chem., 54 (1982) 709.
[8] C. Meinard, P. Bruneau and J. Perronnett, J. Chromatogr., 34 (1985) 109.
[9] J. Zukowski, Y. Tang, A. Bethod and D.W. Armstrong, Anal. Chim. Acta, 258 (1992) 83.
[10] A. Mannschreck, Trends Anal. Chem., 12 (1993) 220.
[11] K. Otsuka and S. Terabe, Trends Anal. Chem., 12 (1993) 125.
[12] E.S. Yeung and R.E. Synovec, Anal. Chem., 568 (1986) 1237A.
[13] K.J. Skogerboe and E.S. Yeung, Anal. Chem., 38 (1986) 1014.
[14] D. Parker, Chem. Rev., 91 (1991) 1441.
[15] N. Purdie and K.A. Swallows, Anal. Chem., 61 (1989) 77A.
[16] N. Purdie, K.A. Swallows, L.H. Murphy and R.B. Purdie, Trends Anal. Chem., 9 (1990) 136.
[17] N. Purdie, in N. Purdie and H.G. Brittain (Eds.), Analytical Applications of Circular Dichroism, Elsevier, Amsterdam, 1994.
[18] N.W. Tietz, Fundamentals of Clinical Chemistry, Saunders, Philadelphia, PA, 3rd edn., 1987.
[19] J.K. Agrawal, S.G. Harmalkar and R. Vijayavargiya, Microchem. J., 21 (1976) 202.
[20] H. Martens and T. Naes, Multivariate Calibration, Wiley, New York, 1989.
[21] W.R. Hruschka and K. Norris, Appl. Spectrosc., 36 (1982) 261.
[22] H. Martens, T. Karstang and T. Naes, J. Chemometr., 1 (1987) 201.
[23] A.E. Martell and L.G. Sillen, Stability Constants, Special Publication No. 17, The Chemical Society, London, 1964.
[24] E.F. Caldin, Fast Reactions in Solution, Blackwell, Oxford, 1964.

ELSEVIER

Analytica Chimica Acta 298 (1994) 183–191

ANALYTICA CHIMICA ACTA

Control analysis of a pharmaceutical preparation by near-infrared reflectance spectroscopy. A comparative study of a spinning module and fibre optic probe

M. Blanco [a,*], J. Coello [a], H. Iturriaga [a], S. Maspoch [a], C. de la Pezuela [a], E. Russo [b]

[a] *Departamento de Química, Unidad de Química Analítica, Universidad Autónoma de Barcelona, E-08193 Bellaterra, Barcelona, Spain*

[b] *Istituto di Analisi e Tecnologie Farmaceutiche ed Alimentari, Facultá di Farmacia, Universitá di Genova, Genova, Italy*

Received 4 January 1994; revised manuscript received 7 June 1994

Abstract

The potential of near-infrared diffuse reflectance spectroscopy for quality control of the manufacturing process for a solid pharmaceutical preparation was investigated. The analytical procedure used for this purpose included identification and qualification of the product, as well as quantitation of its active compound. Two spectral recording systems based on a spinning sample cell and fibre optics were used and the results obtained are compared. The identification and qualification of the samples was carried out by reference to a library containing the second derivative spectra for 163 pure components commonly used in the pharmaceutical industry. Both sample holding systems provided satisfactory results in this respect. The active compound in the pharmaceutical was quantified by partial least squares calibration by using two different strategies to select samples for inclusion in the calibration set, viz. flat calibration and sample selection. The accuracy and precision of the results obtained by applying both selection strategies to the spectra recorded with the two systems are compared. Based on the errors of prediction obtained, which were less than 1% in all instances, the fibre optic probe was found to perform comparably to the conventional spinning cuvette. Also, the flat calibration model appears to be more robust than the sample selection model for choosing samples to be included in the calibration set.

Keywords: Infrared spectrometry; Pharmaceutical preparation; Spinning sample cell; Fibre optic probe

1. Introduction

Applications of near infrared diffuse reflectance spectroscopy (NIRRS) were until recently restricted to analyses of foodstuffs owing to the limitations of filter spectrophotometers, which made the technique scarcely appealing for general analytical purposes. However, the inception of high-scan rate instruments allowing highly reproducible recording of full NIR spectra in a very short time, and modern chemometric procedures for processing complex signals, in addition to the little or no sample pretreatment required and the ability to implement remote analyses by using fibre optic modules as radiation conductors, have turned NIRRS into a very interesting analytical technique with a wide scope of application, particularly in the industrial and, especially, pharmaceutical field [1,2].

The dependence of NIRRS signals on both the chemical composition and physical properties of samples makes it fit for three general purposes, viz. qualitative analyses involving global characterization of samples,

* Corresponding author.

SSDI 0003-2670(94)00275-Q

the determination of physical parameters such as the particle size [3,4], and the quantitative determination of major components.

Pharmaceutical applications of NIRRS have so far been focused on the characterization of raw materials and manufactured products prior to dosing [5–9], as well as determinations of the water content [10,11]. Relatively few applications to manufactured products have so far been reported, though [12–16].

NIRRS spectra can be recorded by using both ordinary cuvette or fibre optic probes. The latter minimize sample manipulation by the analyst, boost throughput and allow use in continuous process control. On the other hand, they result in increased background noise and hence diminished signal-to-noise ratios. This has essentially limited the use of fibre optic probes to qualitative analyses (quantitative applications are still largely implemented by using conventional cells instead). However, there are some precedents of the use of fibre optics for quantitative analysis in the resolution of solvent mixtures [17,18].

This paper compares the results obtained in the qualitative and quantitative control analyses of a pharmaceutical preparation by using a conventional spinning cuvette and a fibre optic probe to record NIR spectra.

Qualitative analyses involved the prior compilation of a library containing the spectra for a number of samples meeting the specifications and encompassing the natural variability of the product. From those spectra the average spectrum and standard deviations at all wavelengths were calculated.

The identification process involved comparing the sample spectrum with the average spectrum of each product included in the library by means of correlation coefficient in order to find the closest fit. The sample is identified as the product that presents the highest correlation coefficient whenever this value surpasses a preset threshold. The correlation coefficient offers important advantages in relation to other identification criteria [19] because it is independent of library composition.

Once the sample is identified, the qualification is tested. The qualification involved comparing the spectrum of the sample with the spectra of this product contained in a library. Due to the natural variability in the manufacturing process, the spectra of the samples included in the library are not represented by a single point in the wavelength space, but by a certain volume. Qualification of a sample involved the check if the spectrum of the sample is enclosed or not in this volume. If this is the case, this means that the sample meets all product specifications (particle size, homogeneity, moisture, active compound concentration, etc.) that could affect the NIR spectrum.

The active compound in the pharmaceutical product was quantified by using a multivariate calibration procedure based on partial least squares (PLS) regression [20]. The results obtained by using two procedures for selection of samples to be included in the calibration set are compared.

2. Experimental

2.1. Reagents and samples

The pharmaceutical product used was Mentis®, a commercially available preparation from Laboratorios Menarini S.A. containing a nominal 880 mg/g (300 mg/capsule) of the active compound pirisudanol dimaleate, viz. butanedioic acid 2-(dimethylamino)ethyl[5-hydroxy-4-(hydroxymethyl)-6-methyl-3-pyridinyl]methyl ester. The preparation includes magnesium stearate, talc and colloidal silica intended to improve the stability and mechanical properties of the mixture in dosing and encapsulation. All products were supplied by the manufacturer and used without purification. Fig. 1A shows the NIRRS spectra of pirisudanol dimaleate and Mentis, and Fig. 1B their corresponding first derivatives.

The chemicals used included pro-analysis grade methyl alcohol and 0.25 M EDTA solution.

2.2. Apparatus

The experimental set-up used consisted of a NIR-Systems 6500 near-infrared spectrometer equipped with a reflectance detector, a spinning sample module and an AP6641 ANO4P fibre optic module for qualitative and quantitative analysis. The spinning cell is a rotatory conventional cuvette, a prefixed number of scans is recorded and finally averaged while the holder sample spins, which minimizes problems arising from sample heterogeneity and distribution particle size. The instrument is operated via the bundled software NSAS v. 3.20. A Hewlett-Packard HP8452A diode array spec-

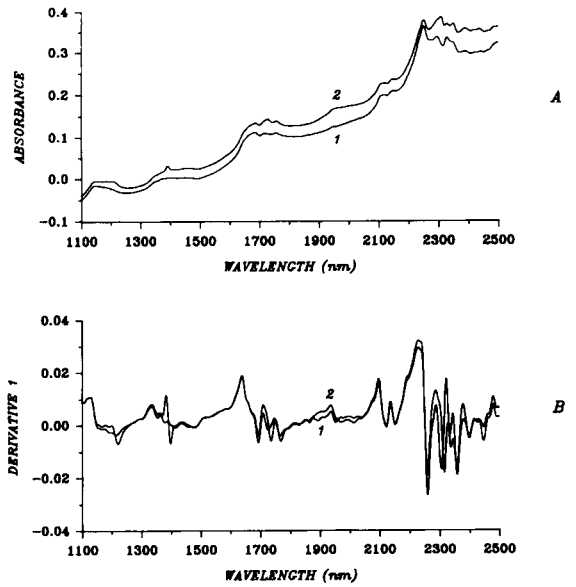

Fig. 1. (A) NIRRS spectra of (1) pirisudanol dimaleate and (2) Mentis. (B) First-derivative NIRRS spectra of (1) pirisudanol dimaleate and (2) Mentis.

trophotometer controlled by an IBM PC-XT computer via an HP-IB interface. The bundled MS-DOS software of the HP89530 UV–visible spectrophotometer includes programs for operating the instrument as well as for acquiring and pretreatment of the spectra. Other instruments used were a Selecta ultrasonic bath and an ABT-4 rotary mixer.

2.3. Software

The computer software used included three different packages. (i) A multicomponent (MC) analysis program developed by the Unidad de Química Analítica of the Universidad Autónoma de Barcelona that allows the concentrations of mixture components to be determined by least squares fitting of the mixed spectrum from those of the individual components. (ii) IQ^2 (Identify, Qualify and Quantify), a series of programs included in the NSAS package that enables qualitative analyses by comparison with a set of spectra included in a library. It also allows mixture components to be quantified by using PLS or multiple linear regression (MLR) multivariate calibration. (iii) UNSCRAMBLER v. 3.54, a commercially available PCR and PLS multivariate calibration package with additional features allowing variable selection and outlier detection. The spectra used by this program were converted into the JCAMP format on transfer from the instrument.

2.4. Determination of pirisudanol in Mentis

UV spectrophotometric procedure

An amount of 1 g of previously ground Mentis was dissolved in 50 ml of distilled water and 4 ml of 0.25 M EDTA in the ultrasonic bath for 10 min, followed by magnetic stirring for 15 min and dilution to 100 ml. The solution was filtered and a 5 ml aliquot was made up to 50 ml with distilled water. A 5 ml aliquot of this solution was made up to 50 ml with methanol and its spectrum recorded between 200 and 350 nm versus methanol (Fig. 2).

The sample spectrum was resolved over the range 270–310 nm by using the MC program and the spectrum for pirisudanol dimaleate as standard.

The method is bias free and presents a variation coefficient of 0.8% for 10 replicates.

NIRRS procedure

In order to expand the concentration range for the calibration set, under- and overdosed samples were prepared by adding a known amount of pirisudanol dimaleate or a mixture of all excipients at the same relative concentration as in the pharmaceutical preparation to a given, also accurately known, amount of product. The mixture was homogenized for 20 min in the rotary mixer. Samples thus prepared were labelled as overdosed samples, while those used as supplied by the manufacturer were labelled as original samples.

Each sample was used to record three spectra, each being the average of 50 scans over the range 1100–2500 nm. Spectra were recorded by using both the spinning module and the fibre optic probe, samples being turned over between spectra.

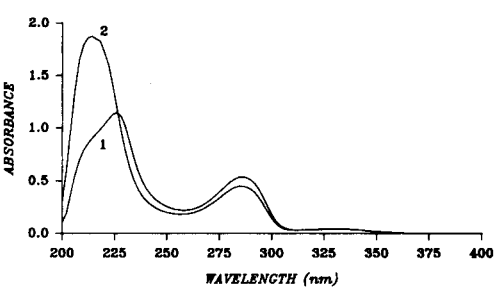

Fig. 2. UV spectrum for 50 mg/l pirisudanol dimaleate (1) and 100.5 mg/l Mentis (2).

The three spectra obtained for each sample were used to compile the library needed to identify and qualify the pharmaceutical preparation. The pirisudanol dimaleate content in the preparation was determined by using the average spectra.

3. Results and discussion

Three stages of quality control in pharmaceutical industry can be identified: (1) identification of raw materials, (2) characterization of manufactured products prior to dosing (intermediate), entailed checking that the unknown sample met the specifications (particle size, homogeneity, ...) and (3) quantification of active compounds.

For a quantitative analytical method to be efficient, it must be able to accurately quantify both central values and accepted limits. Therefore, construction of a robust calibration set requires using a large sample set encompassing the whole working concentration range. Problems arise when the concentrations in available samples are all very close to the nominal content; this allowed us to prepare overdosed samples from the original pharmaceutical preparation. The amounts of pirisudanol or excipient added must be quite small in order to avoid altering any physical property and hence introducing spectral changes not associated with the chemical composition.

3.1. Qualitative analysis

The two-fold dependence of NIRRS signals on the chemical and physical nature of the sample can be turned into an extremely useful tool for qualitative analysis of pure compounds and any type of product of well-defined composition and properties.

Qualitative NIRRS analyses entail compiling a library comprising raw materials and manufactured products of interest in pharmaceutical industry. Each product therefore requires acquiring a set of samples meeting the specifications and encompassing potential variations arising in the manufacturing process. The library can be created using absorbance, first- or second-derivative spectra. The second-derivative spectra are requested in order to facilitate distinction between the spectra of the different products and minimization of scattering due to changes in the physical properties of the samples.

The first step in qualitative analyses is the identification, it involves comparing the sample spectra with those contained in a library in order to find the closest fit. The match can be assessed in terms of correlation or distance. The correlation coefficient (ρ_{jk}) is used to identify the sample because this parameter is independent of library composition and insensitive to concentration variations if the matrix does not absorb.

Every spectrum can be represented by a vector in a p-multidimensional space where p represents the wavelengths. The correlation coefficient is the cosine of the angle between the vectors of the sample spectrum and the average spectrum of each product contained in a library. It is computed according to

$$\rho_{jk} = \frac{\sum_{i=1}^{p} (x_{ij} - \bar{x}_j)(x_{ik} - \bar{x}_k)}{\sqrt{\sum_{i=1}^{p} (x_{ij} - \bar{x}_j)^2} \sqrt{\sum_{i=1}^{p} (x_{ik} - \bar{x}_k)^2}} \quad (1)$$

where the subscripts k and j denote the sample and product reference spectra, respectively, acquired at p wavelengths, x_{ik} and x_{ij} are measured values of the sample and the product reference at wavelength i, and $\bar{x}_j$ is the value of the average spectrum j over all p wavelengths.

This cosine value is called match index and may vary from -1 to $+1$, a value of $+1$ indicates perfect matching between the unknown product and that in the library. However, random noise in the measurements makes such a value unattainable. The software computes the match index between sample spectrum and average spectrum of each product included in the library. The sample is identified as the product that presents the highest correlation coefficient whenever this value surpasses a threshold of 0.95.

Qualification can be regarded as a typical supervised pattern recognition problem. In this case, the similarity can be expressed in distance terms. This parameter is able to detect small chemical or physical deviations from normal processing and to establish the degree of conformity of a batch with the standard quality.

In our case, the qualification is performed by computing the distance at each wavelength between the measured value and the average spectra of the product contained in the library according the Eq. 2. The sample

is qualified positively if the maximum distance computed does not surpass a preset threshold.

The maximum distance (d_{kj}) between the sample spectrum and the average of product in the library, in standard deviation units, for the training set of the jth product:

$$d_{kj} = \max\left(\frac{|x_{kp} - \bar{x}_{jp}|}{s_{jp}}\right)_{\text{over all } p} \quad (2)$$

where the subscripts k and j denote the sample and product reference spectra, x_{kp} is the measured value of the sample at wavelength p, $\bar{x}_{jp}$ is the value of the average spectrum for product reference j at wavelength p, and s_{jp} is the inflated standard deviation calculated from the training set for product j at wavelength p according to

$$s_{jp} = \left(1 + \frac{1}{\sqrt{2(n-1)}}\right)\left(\frac{\sum_{i=1}^{n}(x_{ip} - \bar{x}_p)^2}{n-1}\right)^{1/2} \quad (3)$$

The term in the first bracketed multiplicand is an inflation factor for the standard deviation that helps to account for uncertainty in s when estimated from a small number of samples, n. This term permits the use of the same limit for all products independently of the number of spectra contained in the library.

A sample is qualified by comparing its maximum distance to the reference product with the distance threshold. A default value of 3.0 is usually taken for the threshold since, if the sample belongs to the same population, then there is a probability of 99.7% that the distance will be less than 3 times the standard deviation.

One advantage of this procedure is a high sensitivity to the impurities present in the sample, so much that it often allows recognition of the causes that hinder the qualification [9].

Identification and qualification of Mentis

The library used for this purpose contained 163 products including those of excipients, active compounds, amino acids and vitamins. The number of second-derivative spectra for each product included in the library ranged between 3 and 27.

The number of spectra for each product reference to include in a library can be chosen on the basis of different strategies. One involved using all available samples for each product. The other strategy is to select a subset of samples encompassing potential variations from batch to batch and sample to sample. The last option offers the advantage to provide a reduced library that contains all relevant information. However, it has the disadvantage of requiring a criterion for sample selection.

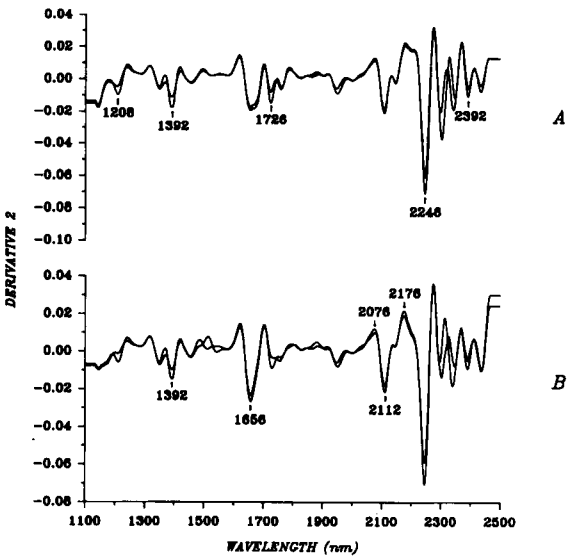

Fig. 3. Wavelengths used by the sample selection subroutine for the spinning module (A) and fibre optic probe (B). The second-derivative spectra of samples 1 and 28 are shown in both cases.

Mentis samples to be used in order to obtain the representative spectra for inclusion in the library were selected by using the sample selection subroutine of NSAS. This uses the absorbance values obtained at five wavelengths chosen by the analyst to select the subset of samples that accounts for a preset percentage of the overall variability (95% in our case). The first sample selected is closest to the average absorbance of all five wavelengths, the second sample is most distant from the mean, the third sample is closest to the mean of the first and second sample, and so on. The idea is to have a boxcar type distribution for the development of an accurate library. This selection procedure was only applied to original samples, thereby assuring that the spectral variability encompassed by the library was consistent with that actually involved in manufacturing the preparation. This strategy was applied to the spectra recorded by using both the spinning module and the fibre optic probe. The five wavelengths used differed for the two recording systems because noise in spectra

obtained with fibre optic probes increases considerably above 2200 nm. Fig. 3 shows the wavelengths chosen for each spectral recording system used.

The number of original samples required for a variability of 95% to be encompassed was 13 in both recording systems, yet the samples were not exactly the same. The concentration range encompassed by the two systems was from 859.0 to 888.9 mg/g.

The identification and qualification of the product was carried out by using second-derivative spectra for all the overdosed samples, and the original samples not included in the library, over the wavelength range 1100–2500 nm for the spinning module and 1100–2200 for the fibre optic probe.

All overdosed and original samples were identified as Mentis with a match index higher than 0.975 when spectra were recorded by using the fibre optic probe. On the other hand, all the samples processed by using the spinning module were identified as Mentis with a match index above 0.982 except that overdosed with the largest amount of active compound (sample No. 28), which was identified as pirisudanol with a match index of 0.965. The second best match index for this sample (0.960) was Mentis, even though the index was not its highest, it also surpassed the preset threshold. This incorrect identification can be ascribed to the fact that the sample was that containing the largest amount of pirisudanol.

Table 1 summarizes the results obtained in the identification of the samples.

As regards the qualification results, it should be noted that, whether spectra were recorded by using the fibre optic probe or the spinning module, all the original samples were qualified as Mentis, with distances between 1.809 and 2.076 for the former and 1.570–2.076 for the latter recording system.

Table 2
Distances obtained for the overdosed samples failed to qualify

Sample	Spinning module	Fiber optic
19[a]	4.178	4.388
20[a]	3.375	3.589
26[a]	5.582	4.369
27[a]	3.336	3.763
28[a]	563.724	6.213

[a]Overdosed samples.

Also, irrespective of the recording system used, five overdosed samples did not surpass the qualification thresholds, even though the distance obtained was occasionally not much greater than the preset value (three times the standard deviation), as can be seen from Table 2. The high distance value obtained for sample No. 28 using the spinning module can be ascribed to the fact that the sample was previously identified as pirisudanol.

The results obtained by using the two sample holding systems were comparable. However, the spinning module as a spectra recording system was found to be more sensitive to low variations in the sample characteristics (homogeneity, particle size, etc.) that affect the NIR spectrum.

3.2. *Quantitative analysis of Mentis samples using PLS*

PLS was used for calibration in the quantitative analysis of Mentis by NIRRS. The overall set of samples (original and overdosed) was divided into two groups; one was used as the calibration set and the other as the external set for determining the predictive value in the analysis of samples not included in the calibration process.

Table 1
Results obtained in the identification of samples

	Samples identified as Mentis	Samples identified as pirisudanol
Spinning module	14 $0.992 < 13$ samples < 0.999 1 sample = 0.982	1 1 sample = 0.965
Fiber optic	15 $0.995 < 10$ samples < 0.999 $0.983 < 4$ samples < 0.989 1 sample = 0.975	0

Samples for the calibration set were chosen on the basis of two different criteria. One involved using the flat calibration model, which essentially entails encompassing regularly the concentration range to be analyzed by using a fairly large number of samples. The other criterion was the sample selection subroutine included in the bundled software of the instrument, which uses the absorbance values obtained at 5 wavelengths chosen by the analyst to select the subset of samples that account for a preset percentage of the overall variability (we chose a variability level of 90%).

The two selection strategies were applied to the spectra recorded by using both the spinning module and the fibre optic probe. The accuracy of the results was determined by applying the Student's *t*-test to paired data, while their precision was calculated by using the *F* criterion on the square of the standard error of prediction (*SEP*), both for the calibration samples (*SEPC*) and those for the external test set (*SEPV*):

$$SEP = \sqrt{\frac{\sum_{i=1}^{n} (C_{LAB} - C_{NIR})^2}{n-1}} \qquad (4)$$

where n is the number of samples in the calibration or external test set.

To visualize the quality of the results, the relative standard error of prediction was computed [21] (*RSEP*) for both the calibration set (*RSEPC*) and the external test set (*RSEPV*) according to

$$RSEP(\%) = \sqrt{\frac{\sum_{i=1}^{n} (C_{LAB} - C_{NIR})^2}{\sum_{i=1}^{n} C_{LAB}^2}} \times 100 \qquad (5)$$

where n is the number of samples in the calibration or external test set.

The PLS model used was constructed by cross-validation and optimized by choosing the spectral mode, possibility of data-scaling, wavelength range and number of factors resulting in the minimal error of prediction.

As has been said before, the diffuse reflectance measurements are influenced by scattering of incident radiation, which in turn depends on such physical properties of the sample as particle size, size distribution, crystalline form, etc. The dependence of NIRRS signals on these factors, of great use for characterizing samples, is a serious constraint to the quantitative determination of a given component in a sample. The problem can be solved by subjecting spectra to a mathematical treatment in order to reduce the effects of scattering before a calibration model is developed.

We found that data-scaling did not affect the quality of the results, and therefore the PLS method was applied to unscaled absorbance, first- and second-derivative spectra. First-derivative spectra provided better results than absorbance spectra, but increasing the spectral order did not further improve the results. This can be ascribed to avoidance of the continuous baseline shift already in the first-derivative spectra.

Even though the PLS method is a full-spectrum method provided the number of samples included in the calibration set is not too large – as was the case in this work – it may be useful to discard irrelevant wavelengths. We tested various wavelength ranges for application of the PLS model and eliminated those having an unusually high residual or providing no information on the pirisudanol content.

Narrowing the wavelength range did not significantly improve the results obtained with the spinning module. However, excluding the high end of the spectra obtained by using the fibre optic probe from the calculations resulted in appreciably higher quantification quality.

The number of factors to be used to quantify the active principle was estimated from a plot of the prediction error as a function of the number of factors.

The best PLS calibrations were obtained with unscaled first-derivative spectra recorded over the ranges 1100–2500 and 1100–2200 nm by using the spinning module and fibre optic probe, respectively.

Table 3 shows the reference values obtained by using the laboratory procedure in the determination of pirisudanol dimaleate in both the original and the overdosed samples as the average of two determinations. The same table also shows the results obtained in the PLS quantitation of pirisudanol in the calibration and external test samples by using the spinning module and the fibre probe.

Table 3
Determination of pirisudanol in Mentis

Sample	Lab. value	Flat calibration		Sample selection	
		Spinning	Fiber	Spinning	Fiber
1[a]	841.7	851.8[b]	850.1[b]	850.0[b]	850.2[b]
2[a]	850.3	852.5[b]	864.3[b]	854.6[b]	863.6[b]
3	859.0	864.4	867.3	861.5	868.5
4[a]	861.7	860.7[b]	865.3[b]	861.5	869.0
5	863.4	864.6[b]	858.5[b]	857.8	861.4
6	866.6	862.1	858.6	860.7	862.6[b]
7	867.0	866.0[b]	867.1[b]	860.4[b]	859.3
8	867.7	875.3[b]	859.3[b]	870.3[b]	862.1[b]
9[a]	868.1	874.4	870.9	873.9	875.7
10	868.1	865.3[b]	870.5[b]	864.6	872.9
11	868.7	862.0[b]	867.5[b]	859.8	870.0[b]
12[a]	877.9	876.8	876.4	875.9	877.2[b]
13	879.4	880.9[b]	885.4[b]	883.5	885.6
14	879.4	883.9[b]	875.5[b]	873.9	873.4[b]
15	880.4	869.5	879.5	866.2	882.0
16	881.6	876.3[b]	879.8[b]	869.1[b]	875.4[b]
17	881.8	884.5[b]	884.1[b]	886.1[b]	885.7[b]
18	881.8	882.6	883.5	883.9	885.6
19[a]	882.5	881.6[b]	891.0[b]	876.3	887.0[b]
20[a]	885.2	881.1[b]	882.9[b]	880.9[b]	885.5[b]
21	885.6	892.2	875.6	888.7	875.7
22	888.6	883.0[b]	884.3[b]	884.8	886.1[b]
23	888.9	891.9[b]	877.5[b]	889.3[b]	874.5
24	889.1	885.8	874.4	876.7	872.9
25	890.9	885.9[b]	878.6[b]	875.6	876.6[b]
26[a]	891.0	893.8	898.3	892.4[b]	897.1[b]
27[a]	891.0	885.0[b]	897.2[b]	884.2	890.7[b]
28[a]	911.4	916.9[b]	910.5[b]	913.6[b]	913.0[b]
RSEPC (%)		0.54	0.77	0.66	0.73
RSEPV (%)		0.63	0.86	0.83	1.00

Lab. value are the results obtained by spectrophotometric method.
[a]Overdosed samples.
[b]Prediction values obtained for samples of calibration set.

Flat calibration

The sample set was divided into two groups consisting of 19 and 9 samples that were used as the calibration and external test set, respectively.

As can be seen in Fig. 4A, the number of factors needed for quantification of the active compound was 3 whichever spectral recording system was used.

Application of the *F* criterion revealed the precision of the results provided by the spinning module to be comparable to those obtained with the fibre optic probe, both for the calibration and for the external set. The accuracy of the results provided by the two recording systems compared was not significantly different, nor was it from that of the laboratory procedure used for contrast.

Sample selection

Samples were divided into two sets by using the same five wavelengths employed in the qualitative analysis to determine which samples of the pharmaceutical preparation were to be included in the spectral library (Fig. 3). The subset of samples making up the calibration set was constructed provided that the samples should account for 90% of the overall variability. Thus, the calibration set consisted of 10 samples for the spinning module and 16 for the fibre optic probe.

A plot of the error of prediction as a function of the number of factors used to develop the model revealed the minimum number of factors required for quantitation to be 2 for the spinning module and 3 for the fibre optic probe (Fig. 4B).

The precision of the results provided by the spinning module was comparable to that of the results obtained with the fibre optic probe for both the calibration and the external test set.

Application of the *t*-test showed the accuracy of the results obtained for the external test set using the fibre optic probe to be comparable to the results provided by the laboratory procedure. However, the results obtained with the spinning module were not comparable to the

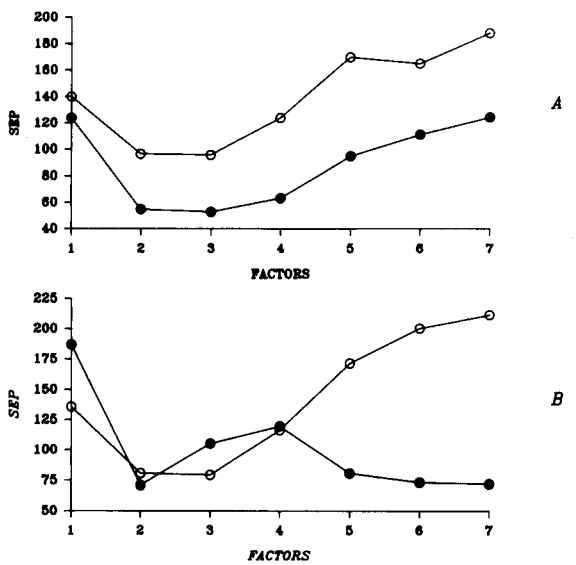

Fig. 4. Plot of SEP against the number of factors used for (A) flat calibration and (B) sample selection. (●) Spinning module. (○) Fibre optic probe.

laboratory method. This can be explained by the small number of samples included in this calibration set that give a less robust calibration model.

For the same recording system the precision of the results obtained with the two selection strategies was also comparable.

4. Conclusions

The joint use of the NIRRS technique and chemometric methods enables qualitative and quantitative non-destructive analyses of pharmaceutical preparations without sample pretreatment in a very short time. This makes this combined approach a powerful tool for quality control analysis.

The results presented in this article show the suitability of fibre optic probes for qualitative and quantitative analyses, where they perform comparably well to conventional spinning modules. In fact, the qualitative identification and qualification results obtained by using these two sample delivery systems were quite good.

Quantitation was accomplished by using PLS and two different strategies to select the samples for inclusion in the calibration set. The flat calibration model was found to provide more robust calibration.

Finally, the errors of prediction obtained in the quantitation of pirisudanol using the spinning module and the fibre optic probe were fully acceptable and comparable to those afforded by other analytical techniques.

Acknowledgements

The authors are grateful to the Spanish DGYCyT for financial support granted for the realization of this work as a part of Project PB90-0722, and Laboratorios Menarini S.A. for complementary supply of the pharmaceutical samples assayed.

References

[1] E.W. Ciurczak, Appl. Spectrosc. Rev., 23 (1978) 147.
[2] E.W. Ciurczak and J.K. Drennenn, Spectroscopy, 7 (1992) 12.
[3] E.W. Ciurczak, P. Torlini and P.M. Demkowicz, Spectroscopy, 1 (1986) 36.
[4] K.I. Hildrum, T. Isaksson, T. Naes and A. Tandberg (Eds.), Near Infra-red Spectroscopy (Bridging The Gap between Data Analysis and Nir Applications), Ellis Horwood, Chichester, 1992, p. 401.
[5] E.W. Ciurczak and T.A. Maldacker, Spectroscopy, 1 (1986) 36.
[6] H.L. Mark and D. Tunnell, Anal. Chem., 57 (1985) 1449.
[7] P.A. Salamin, Y. Cornelis and H. Bartels, Chemom. Intell. Lab. Syst., 3 (1988) 329.
[8] P. Corti, L. Savini, E. Dreassi, G. Ceramelli, L. Montecchi and S. Lonardi, Pharm. Acta Helv., 67 (1992) 57.
[9] W. Plugge and C. Van Der Vlies, J. Pharm. Biomed. Anal., 10 (1992) 797.
[10] J.E. Sinsheimer and N.M. Poswalk, J. Pharm. Sci., 57 (1986) 2007.
[11] R.J. Warren, J.E. Zarembo, C.W. Chong and M.J. Robinson, J. Pharm. Sci., 59 (1970) 109.
[12] R. Lodder and G. Hieftje, Appl. Spectrosc., 42 (1988) 556.
[13] J. Drennen and R. Lodder, J. Pharm. Sci., 79 (1990) 622.
[14] R. Jensen, E. Peuchant, I. Castagne, A.M. Boirac and G. Roux, Spectroscopy, 6 (1988) 63.
[15] A.F. Zappala and A. Post, J. Pharm. Sci., 66 (1977) 292.
[16] E.W. Ciurczak and R.P. Torlini, Spectroscopy, 2 (1987) 41.
[17] H. Martens, T. Naes and H.R. Bjorsvik, The Wave Guide, 1 (1988) 4.
[18] Application Note, Guided Wave Inc., No. A3-987.
[19] J.T. Clerc, E. Pretsch and M. Zürcher, Mikrochim. Acta, II (1986) 217.
[20] H. Martens and T. Naes, Multivariate Calibration, Wiley, New York, 1991.
[21] M. Otto and W. Wegscheider, Anal. Chem., 57 (1985) 63.

ELSEVIER

Analytica Chimica Acta 298 (1994) 193–201

ANALYTICA CHIMICA ACTA

Second-order globalisation for the determination of activation parameters in kinetics

Pascal Bugnon [a], Jean-Claude Chottard [b], Jean-Luc Jestin [a,b], Bernhard Jung [c], Gabor Laurenczy [a], Marcel Maeder [d,*], André E. Merbach [a], Andreas D. Zuberbühler [c]

[a] *Institut de Chimie Minérale et Analytique, Place du Château 3, Université de Lausanne-BCH, CH-1015 Lausanne, Switzerland*

[b] *Université René Descartes, URA 400 CNRS, 75270 Paris Cedex 06, France*

[c] *Institute of Inorganic Chemistry, Spitalstrasse 51, University of Basel, CH-4056 Basel, Switzerland*

[d] *Department of Chemistry, University of Newcastle, Callaghan,NSW 2308, Australia*

Received 3 May 1994

Abstract

First order global analysis consists of linking common parameters across series of measurements, e.g., reaction kinetics measured at different wavelengths where the rate constants are the same for all kinetic traces at individual wavelengths. This approach is taken a step further in second order globalisation. A series of measurements is linked together by a new superimposed model which encompasses the individual measurements. The mathematics for the non-linear least-squares fit of the global parameters is presented. Two modes are possible depending on whether the linear parameters (absorption spectra) are constant or changing across the series. Factor analysis is incorporated for multivariate measurements. The procedures are exemplified with applications of activation analysis in chemical kinetics. Global analysis of complete temperature and pressure dependences results directly in the activation parameters of interest, i.e., activation enthalpies, entropies and volumes. Due to a significant decrease in the number of parameters to be fitted, the robustness is considerably improved.

Keywords: Kinetic methods; Activation parameters; Second-order globalisation

1. Introduction

Determination of activation parameters is an important tool in the investigation of reaction mechanisms. Actual values of rate constants frequently carry no or little information about the molecular mechanism of the reaction. Variation of temperature and pressure can provide crucial additional information about the energetics and the volume changes during the molecular reaction [1–3].

Classically, the determination of activation parameters requires a two step process. (a) Rate constants are determined individually at a range of temperatures/pressures, and (b) Eyring or Arrhenius type of plots result in the activation parameters as slopes and intercepts of straight lines fits, with all the points having the same weight. We propose in this contribution a new approach for the analysis of temperature/pressure dependences. Instead of individual determination of rate constants and subsequent linear plots, the complete set of measurements at a range of temperatures/pressures is treated as a unit. The activation parameters are directly fitted to the complete set of measurements. We

* Corresponding author.

SSDI 0003-2670(94)00255-K

propose to call this procedure second order globalisation.

The term global analysis has been coined for the analysis of multivariate fluorescence decay surfaces [4–6]. Instead of selecting an optimal wavelength for the observation of a kinetic fluorescence decay, the analysis is performed simultaneously at many wavelengths, linking the common parameters, i.e., the decay lifetimes. Naturally, the same principle applies for absorption measurements. Global analysis has a multitude of advantages, the most important ones are: (a) there is a direct link or interaction between the model which is to be determined or confirmed and the parameters defined by the model. In this contribution, the model is given by the Eyring relationship between temperature/pressure and the rate of a reaction. The fitted parameters are the activation enthalpy and entropy or the activation volume. In the classical procedure rate constants are fitted to individual measurements and only in a secondary step their dependences are analysed to yield the parameters of interest; (b) the number of parameters to be fitted is substantially reduced in second order global analysis. For the example of a simple first or second order reaction, investigated at 10 temperatures/pressures, 10 rate constants have to be fitted to the individual measurements which in turn allow the determination of the two activation parameters. We have to deal with a total of 12 parameters of a very different kind. Second order global analysis requires the fitting of 2 parameters only; (c) As a result of the smaller number of parameters, parameter correlation is much less severe and the error surface is transformed form an ill-defined flat to a well-defined quadratic behaviour [7,8]; (d) The choice of the correct model to quantify the observations is usually better supported. Classically, the consistency of the individually determined parameters indicates the appropriateness of the model. However, individual parameters can be poorly defined and then suffer from large uncertainties, particularly at the extremes of the temperature/pressure range. As a consequence model discrimination can be poor and statistically relevant inconsistencies can then only be detected with grossly wrong models [6,9].

Computational methods have been developed to deal with first order global analysis of multivariate absorption data [10]. Crucial steps are data reduction by factor analysis and the appropriate handling of linear and non-linear parameters. The recognised advantage of global analysis of series of measurements will be further exploited in the proposed second order globalisation. Second order global analysis consists not merely in linking common parameters across several series of measurements (rate constants at different wavelengths), but rather in redefining the problem using a new set of global parameters (activation parameters). In this contribution the mathematics of second order global fitting is developed, it is a natural extension of the established techniques for first order global analysis of multivariate absorption data [10].

First we will outline the mathematics required for second order globalisation and later describe results of applications of the method to activation studies of fairly complex kinetic reaction schemes.

2. Mathematics of second order global analysis, non-linear least-squares fitting

For several reasons the Newton-Gauss-Levenberg/Marquardt (NGL/M) algorithm is today's standard method for non-linear least squares fitting. Simplex and gradient methods are conceptually simpler, however, they are usually outperformed by methods which take full advantage of the information contained in the actual residuals rather than relying solely on the sum of their squares [10–12].

The following description is based on absorption measurements. Preferably, the measurements are made at many wavelengths, using a diode array spectrophotometer. This is not crucial, however, and the same principles hold for single wavelength investigations. Furthermore, other types of measurements such as fluorescence, NMR, conductivity, etc. can readily be adapted.

Instead of a complete introduction into non-linear least-squares fitting of multiwavelength absorption data, we refer to a recent publication [10]. We will adopt the notation used in [10] and keep the explanations to a minimum, concentrating on the amendments required for second order global analysis.

The raw data for each measurement at an individual temperature/pressure consist of a matrix $\mathbf{Y}_i$ where the rows are the absorption spectra measured as a function of the reaction time. According to Beer-Lambert's law $\mathbf{Y}_i$ can be decomposed into the product of a concentration matrix $\mathbf{C}_i$ times a matrix of molar absorptivities

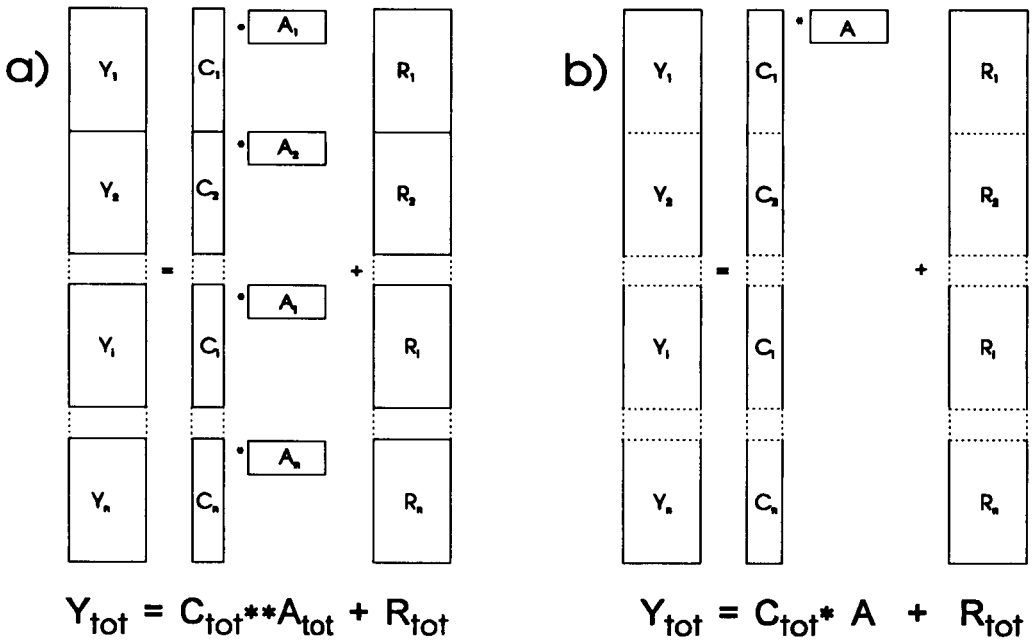

Scheme 1.

$\mathbf{A}_i$. The columns of $\mathbf{C}_i$ are the concentration profiles of the coloured species in function of the reaction time, the rows of $\mathbf{A}_i$ are their corresponding absorption spectra. In the case of single wavelength measurements the matrices $\mathbf{Y}_i$ and $\mathbf{A}_i$ are reduced to column vectors. Note that the spectra $\mathbf{A}_i$ are generally temperature/pressure dependent. Under special circumstances it might be necessary to assume temperature/pressure independent spectra, however, vide infra. Due to noise and related imperfections of any real measurement, the decomposition does not represent $\mathbf{Y}_i$ perfectly, the matrix $\mathbf{R}_i$ of residuals being the difference.

$$\mathbf{Y}_i = \mathbf{C}_i * \mathbf{A}_i + \mathbf{R}_i \quad (1)$$

The dimensions of the matrices are: $\mathbf{Y}_i$ $(M(i) \times W$, $M(i)$ = number of spectra recorded for measurement i, W = number of wavelengths, W is constant throughout the whole series), $\mathbf{C}_i$ $(M(i) \times N$, N = number of absorbing species), $\mathbf{A}_i$ $(N \times W)$, and $\mathbf{R}_i$ $(M(i) \times W)$.

For second order global analysis, the individual $\mathbf{Y}_i$'s are vertically concatenated to form a matrix $\mathbf{Y}_{tot}$ of dimension $\sum M(i) \times W$, similarly the $\mathbf{C}_i$'s and $\mathbf{R}_i$'s are concatenated to form the matrices $\mathbf{C}_{tot}$ $(\sum M(i) \times N)$ and $\mathbf{R}_{tot}$ $(\sum M(i) \times W)$. $\mathbf{A}_{tot}$ is a collection of the individual $\mathbf{A}_i$'s.

$$\mathbf{Y}_{tot} = \mathbf{C}_{tot} ** \mathbf{A}_{tot} + \mathbf{R}_{tot} \quad (2)$$

The corresponding concatenated Eq. 2 is not a proper matrix product and we use the $**$ notation which is not to be confused with the Fortran exponentiation. Refer to Scheme 1a for a graphical representation.

Actual changes in the absorption spectra of the different components in function of temperature/pressure can be negligibly small and/or the contribution of some species might be irrelevant for certain experimental data sets. In these cases it will be advantageous or even necessary to fix the spectra for the complete series, thus substantially reducing the number of linear parameters. A slightly different mode of calculation is then required. $\mathbf{Y}_{tot}$, $\mathbf{C}_{tot}$, and $\mathbf{R}_{tot}$ are defined as above, only $\mathbf{A}_{tot}$ is replaced by one single matrix $\mathbf{A}$ and Eq. 2 is replaced by

$$\mathbf{Y}_{tot} = \mathbf{C}_{tot} * \mathbf{A} + \mathbf{R}_{tot} \quad (3)$$

$\mathbf{C}_{tot} * \mathbf{A}$ is now the proper matrix product, refer to Scheme 1b for a graphical representation.

The theory of the NGL/M algorithm is well established. The crucial steps are (a) the calculation of the residuals as a function of the parameters and (b) the calculation of the Jacobian matrix which consists of the derivatives of the residuals with respect to the parameters [10–12].

2.1. Calculation of the residuals

The matrix $\mathbf{R}_{tot}$ is defined as a function of the non-linear activation parameters which define $\mathbf{C}_{tot}$, and of the molar absorptivities $\mathbf{A}_{tot}$ which are linear parameters. Each individual $\mathbf{C}_i$ is calculated as a function of the rate constants at temperature/pressure (i) which in turn are defined by the activation parameters. For simple reaction schemes the $\mathbf{C}_i$ can be calculated explicitly, otherwise numerical integration of the differential equations is required. The linear parameters can effectively be eliminated from the iterative fitting process by replacing the individual $\mathbf{A}_i$ with their least-squares estimates $\hat{\mathbf{A}}_i$. These are calculated as

$$\hat{\mathbf{A}}_i = \mathbf{C}_i^{+} * \mathbf{Y}_i = (\mathbf{C}_i^t * \mathbf{C}_i)^{-1} * \mathbf{C}_i^t * \mathbf{Y}_i \quad (4)$$

where $\mathbf{C}_i^{+}$ is the pseudo inverse of $\mathbf{C}_i$ which can be calculated via the normal equations as indicated in Eq. 4 or by any other, numerically better method [13]. The $\hat{\mathbf{A}}_i$ are collected in the matrix $\hat{\mathbf{A}}_{tot}$ and the residuals then are calculated as

$$\mathbf{R}_{tot} = \mathbf{Y}_{tot} - \mathbf{C}_{tot} ** \hat{\mathbf{A}}_{tot} \quad (5)$$

For calculations with temperature/pressure independent absorption spectra the linear least-squares estimate $\hat{\mathbf{A}}$ is calculated in a similar way as

$$\hat{\mathbf{A}} = \mathbf{C}_{tot}^{+} * \mathbf{Y}_{tot} \quad (6)$$

and the residuals as

$$\mathbf{R}_{tot} = \mathbf{Y}_{tot} - \mathbf{C}_{tot} * \hat{\mathbf{A}} \quad (7)$$

For both modes, the sum of squares is computed as

$$sq = \sum_{i=1}^{\Sigma M(i)} \sum_{j=1}^{W} \mathbf{R}_{tot}(i,j)^2 \quad (8)$$

2.2. Calculation of the Jacobian

Irrespective of the mode, the derivatives, which form the Jacobian matrix $\mathbf{J}$

$$\mathbf{J} = \frac{\partial \mathbf{R}_{tot}}{\partial \mathbf{par}} \quad (9)$$

are approximated numerically

$$\frac{\partial \mathbf{R}_{tot}}{\partial \mathbf{par(i)}} \cong [\mathbf{R}_{tot}(\mathbf{par(1)},...,\mathbf{par(i)},...,\mathbf{par(n)}) - \mathbf{R}_{tot}(\mathbf{par(1)},...,\mathbf{par(i)} + \Delta\mathbf{par(i)},..., \mathbf{par(n)})]/\Delta\mathbf{par(i)} \quad (10)$$

The use of analytical instead of numerical derivatives would be possible for certain rate laws, e.g., a set of exponentials, it has, however, not been implemented in the present program.

According to the NGL/M algorithm the parameter vector **par** is iteratively improved from an initial starting set of guessed activation parameters. A shift vector $\Delta\mathbf{par}$ is calculated as

$$\Delta\mathbf{par} = (\mathbf{J}^t * \mathbf{J} + mp * \mathbf{I})^{-1} * \mathbf{J}^t * \mathbf{R}_{tot} \quad (11)$$

where mp is the Marquardt/Levenberg parameter and $\mathbf{I}$ is the identity matrix of the appropriate size.

2.3. Factor analysis

The shapes of the matrices in Scheme 1 imply $W > 1$ or, in other words, measurements have been done at several wavelengths, preferably using a diode-array detector. This is mathematically not a prerequisite for the proposed second order globalisation. For $W = 1$ we are dealing with classical one-wavelength kinetics and all the above formulae apply directly. If, however, W is large (e.g., $W = 512$ for an average diode-array), we heavily recommend data reduction by factor analysis. This effectively reduces the number of wavelengths from the original number (e.g., 512) to the number of absorbing species in the system (typically 5). Thus the sizes of the matrices $\mathbf{Y}_{tot}$, $\hat{\mathbf{A}}_{tot}$ or $\hat{\mathbf{A}}$, $\mathbf{R}_{tot}$ and $\mathbf{J}$ are reduced by a factor of typically 100, reducing the memory requirement by almost the same factor. Without data reduction by factor analysis the memory requirements for the large matrices $\mathbf{Y}_{tot}$ and $\mathbf{R}_{tot}$ and particularly $\mathbf{J}$ will in fact be beyond the limits of even well equipped personal computers. The reduction is also accelerating the iterative refinement by a smaller but still substantial factor.

In the case of variable temperature/pressure dependent spectra, the matrices $\mathbf{Y}_i$ are singular value decomposed individually

$$\mathbf{Y}_i = \mathbf{U}_i * \mathbf{S}_i * \mathbf{V}_i \quad (12)$$

The matrices $\mathbf{U_i}$, $\mathbf{S_i}$, and $\mathbf{V_i}$ are reduced to the correct number of columns respectively rows, $\mathbf{U_i}$ $(M(i)\times N)$, $\mathbf{S_i}$ $(N\times N)$, and $\mathbf{V_i}$ $(N\times W)$, where N is the number of absorbing species. Refer to [14] for the statistical considerations on the number of components or factors required to represent the $\mathbf{Y_i}$ accurately. In our experience the actual number N of eigenvectors used to reduce $\mathbf{Y_i}$ is not crucial, it does not harm to use a 'couple of extra ones'.

The Eq. 1 are multiplied from the right with the respective $\mathbf{V_i^t}$.

$$\mathbf{Y_i}*\mathbf{V_i^t}=\mathbf{C_i}*\hat{\mathbf{A}}_\mathbf{i}*\mathbf{V_i^t}+\mathbf{R_i}*\mathbf{V_i^t} \tag{13}$$

In this way we represent the spectral information in the new basis defined by the $\mathbf{V_i}$. The resulting reduced matrices

$$\mathbf{Y_i'}=\mathbf{Y_i}*\mathbf{V_i^t},$$

$$\hat{\mathbf{A}}_\mathbf{i}'=\hat{\mathbf{A}}_\mathbf{i}*\mathbf{V_i^t} \tag{14}$$

and

$$\mathbf{R_i'}=\mathbf{R_i}*\mathbf{V_i^t}$$

replace their originals $\mathbf{Y_i}$, $\hat{\mathbf{A}}_\mathbf{i}$, and $\mathbf{R_i}$ in the appropriate equations. The new dimensions are $\mathbf{Y_i'}$ $(M(i)\times N)$, $\mathbf{A_i'}$ $(N\times N)$, $\mathbf{R_i'}$ $(M(i)\times N)$ and similarly and $\mathbf{Y'_{tot}}$, $\hat{\mathbf{A}}'_{\mathbf{tot}}$, and $\mathbf{R'_{tot}}$ are reduced in the same way.

For calculations with temperature/pressure independent spectra, singular value decomposition has to be performed on $\mathbf{Y_{tot}}$.

$$\mathbf{Y_{tot}}=\mathbf{U_{tot}}*\mathbf{S_{tot}}*\mathbf{V_{tot}} \tag{15}$$

Retaining the correct number of eigenvectors and eigenvalues, and multiplying Eq. 3 from the right with $\mathbf{V_{tot}^t}$ yields

$$\mathbf{Y_{tot}}*\mathbf{V_{tot}^t}=\mathbf{C_{tot}}*\hat{\mathbf{A}}*\mathbf{V_{tot}^t}+\mathbf{R_{tot}}*\mathbf{V_{tot}^t} \tag{16}$$

which can be rewritten analogously as

$$\mathbf{Y'_{tot}}=\mathbf{C_{tot}}*\hat{\mathbf{A}}'+\mathbf{R'_{tot}} \tag{17}$$

with the dimensions $\mathbf{Y'_{tot}}(\Sigma M(i)\times N)$, $\hat{\mathbf{A}}'(N\times N)$, and $\mathbf{R'_{tot}}(\Sigma M(i)\times N)$.

Singular value decomposition of $\mathbf{Y_{tot}}$ might be impossible on a personal computer due to memory limitations. This was the case with the analysis of the TMPA series described below where the dimensions of $\mathbf{Y_{tot}}$ were 500×508. Instead of the normal procedure, the sum $\mathbf{Y_{sum}}$ (50×508) of all matrices $\mathbf{Y_i}$ was singular value decomposed. This yields a matrix $\mathbf{V_{sum}}$ which theoretically spans the same space as the proper $\mathbf{V_{tot}}$ calculated by Eq. 15. In practise the two matrices are slightly different due to different weighting. $\mathbf{V_{sum}}$ replaces $\mathbf{V_{tot}}$ in Eq. 16.

Computer programs have been written in the languages GAUSS (Aptech Systems, Maple Valley, WA) and MATLAB (MathWorks, Natick, MA) and all calculations have been done on IBM clone computers with 386/387 or 486 processors.

3. Temperature dependence of reactions

In the transition state theory, the relationship between the rate constant, k, for a reaction and the change in Gibb's free energy between the reactants and the transition state, $\Delta G^{\neq}$, is given by Eyring's equation, where $k(T)$ is the rate constant at temperature T, k_B the Boltzman constant, h the Planck constant, and R the gas constant.

$$k(T)=\frac{k_BT}{h}\exp\left(\frac{-\Delta G^{\neq}}{RT}\right) \tag{18}$$

This equation leads to

$$k(T)=\frac{k_BT}{h}\exp\left(\frac{-\Delta H^{\neq}}{RT}+\frac{\Delta S^{\neq}}{R}\right) \tag{19}$$

where $\Delta H^{\neq}$ and $\Delta S^{\neq}$ are the enthalpy and the entropy of activation. Note that the equations might have to be modified if assumptions such as temperature independence of the activation parameters are not met [3]. The necessary changes are implemented straightforwardly.

In order to test the second order global analysis with temperature dependent data two experimental series have been investigated. The first example is the reversible binding of molecular oxygen by a copper dioxygen carrier model complex (BPQA = bis[(2-pyridyl)methyl]-[(2-quinolyl)methyl]amine) [15]:

$$2\mathrm{Cu(BPQA)}^{+}+\mathrm{O_2}\rightleftharpoons \tag{20}$$

$$[\mathrm{Cu(BPQA)}]_2(\mathrm{O_2})^{2+}\ k_f,\ k_b$$

This example demonstrated the advantage of allowing variable, temperature dependent absorption spectra. The overall reaction is very fast and due to the dead time of the mixing process the first measured absorption spectra always contained some product. Therefore the

Table 1
Kinetic parameters with standard errors for the reaction of $Cu(BPQF)^+$ with O_2 and the hydrolysis of the Pt(II) complex

	Second order determination[a]	Classical determination[a]
BPQA [15]		
$\Delta H_f^{\neq}$ (kJ mol^{-1})	-8.67 ± 0.01	-8 ± 1
$\Delta S_f^{\neq}$ (J mol^{-1} K^{-1})	-163 ± 0.01	-160 ± 2
$\Delta H_r^{\neq}$ (kJ mol^{-1})	64.17 ± 0.08	61 ± 1
$\Delta S_r^{\neq}$ (J mol^{-1} K^{-1})	34.0 ± 0.3	21 ± 4
Pt(II) aquation [17]		
$k_{0,f}$ (s^{-1})	$(1.858 \pm 0.009) \times 10^{-4}$	$(1.54 \pm 0.05) \times 10^{-4}$
$k_{0,r}$ (M^{-1} s^{-1})	$(1.378 \pm 0.007) \times 10^{-1}$	$(1.64 \pm 0.03) \times 10^{-1}$
$\Delta V_f^{\neq a}$ (cm^3 mol^{-1})	-9.6 ± 0.1	-9.4 ± 0.7
$\Delta V_r^{\neq a}$ (cm^3 mol^{-1})	-5.3 ± 0.1	-4.0 ± 0.4

[a] The errors quoted are the calculated standard deviations, but it is clear that due to possible non-random errors, activation energies and volumes of activation can only be determined to within much larger limits.

calculated spectra of the starting material ($Cu(BPQA)^+$) showed an apparent temperature dependence. Interestingly, the rate is faster at lower temperatures as activation enthalpy and entropy are negative. Further, the spectrum of the product displayed a small but significant temperature dependence. Global analysis performed with temperature independent spectra, yields a significantly worse fit ($\sigma_{abs} = 0.0053$ compared to $\sigma_{abs} = 0.0012$ for the appropriate fit), the resulting spectra are close to the averages of the temperature dependent series, but more importantly the resulting activation parameters ($\Delta H_f^{\neq} = -12.3$ kJ mol^{-1}, $\Delta S_f^{\neq} = -180$ J mol^{-1} K^{-1}, $\Delta H_r^{\neq} = 55.0$ kJ mol^{-1}, and $\Delta S_r^{\neq} = -4$ kJ mol^{-1} K^{-1}) are significantly different from the published values. Refer to Table 1 for the result of the second order global analysis and the published values calculated in the classical way.

Classical analysis consisted in the fitting of two rate constants to the measurements at each temperature (20 parameters) followed by linear plots of $\ln(k/T)$ vs. $1/T$ to yield the 4 activation parameters, a total of 24 parameters had to be determined. In the second order global fit all 4 activation parameters were fitted directly to the complete series of measurements. The results of both analyses are given in Table 1.

The second example of temperature dependent kinetics was much more demanding. It is the study of the reaction of mononuclear $[(TMPA)Cu(AN)]^+$ (TMPA = tris[2-pyridyl)methyl]amine, AN = acetonitrile] with molecular oxygen to give in a two step reaction the *trans*-μ-1,2-peroxo-bridged dicopper(II) couple [15,16]:

$$[(TMPA)Cu(AN)]^+ + O_2 \underset{k_{-1}}{\overset{k_1}{\rightleftharpoons}} [(TMPA)Cu(O_2)]^+ + AN \quad (21)$$

$$[(TMPA)Cu(AN)]^+ + [(TMPA)Cu(O_2)]^+ \underset{k_{-2}}{\overset{k_2}{\rightleftharpoons}} [\{(TMPA)Cu\}_2(O_2)]^{2+} + AN \quad (22)$$

Second order global analysis requires the fit of the series of measurements with $\Delta H^{\neq}$ and $\Delta S^{\neq}$ values for each of the 4 rate constants which adds up to 8 parameters. In this example the analysis had to be performed with fixed, temperature independent spectra. At high temperatures, the intermediate $[(TMPA)Cu(O_2)]^+$ occurs at very low concentrations only, its formation is not directly observed and the calculation of $\hat{\mathbf{A}}_i$ results in a singularity (Eq. 4). Analysis with fixed spectra circumvents this problem as all components are formed in observable concentrations somewhere in the temperature range.

To test the robustness of global analysis absorption data were recalculated based on published [15,16] activation parameters ($\Delta H_1^{\neq} = 32$ kJ mol^{-1}, $\Delta S_1^{\neq} = 14$ J mol^{-1} K^{-1}, $\Delta H_{-1}^{\neq} = 66$ kJ mol^{-1}, $\Delta S_{-1}^{\neq} = 137$ J

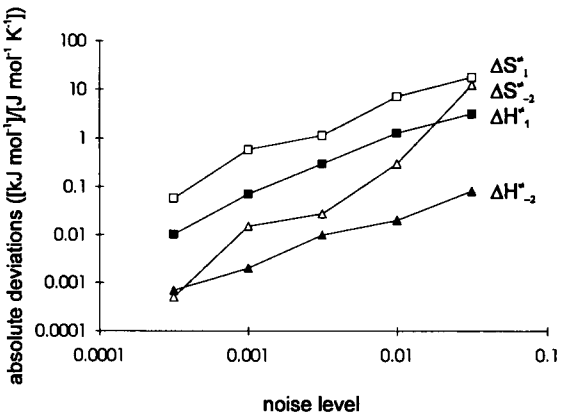

Fig. 1. Plot of the absolute differences between fitted and true parameters as a function of added noise for second order global analysis of the reaction schemes 21 and 22. See text for details.

mol^{-1} K^{-1}, $\Delta H_2^{\neq} = 14$ kJ mol^{-1}, $\Delta S_2^{\neq} = -78$ J mol^{-1} K^{-1}, $\Delta H_{-2}^{\neq} = 61$ kJ mol^{-1}, $\Delta S_{-2}^{\neq} = 19$ J mol^{-1} K^{-1}) and absorption spectra. Different levels of normally distributed noise were added with standard deviations ranging from 0.0003 to 0.03 absorption units which amounts from 0.1% to 10% of the average absorption reading of approximately 0.3. For each noise level four fits were calculated starting with randomised initial values for all eight parameters. The average of the absolute differences between the resulting and the respective true parameters was calculated and plotted in Fig. 1 as a function of the added noise. The units of the ordinate are kJ mol^{-1} for the $\Delta H^{\neq}$ values and J mol^{-1} K^{-1} for the $\Delta S^{\neq}$ values. A double logarithmic plot was used to cover the wide range of values. Further, in order to reduce the complexity of the figure only the activation parameters for k_1 and k_{-2} are displayed. They are the worst and best defined parameters and thus cover the extremes. As expected, the log–log plot displays a near linear relationship for all parameters, including the ones not displayed on the graph. More importantly the resulting differences are well below acceptable levels for the well defined parameters, even at the highest noise level. And only at these levels the differences exceed the published uncertainties for the relatively poorly defined activation entropies $\Delta S_1^{\neq}$ and $\Delta S_{-2}^{\neq}$. This may be partly due to the prior factor analysis which reduces the contribution of noise [14] but it is also due to the improved robustness of the global approach. No doubt experimental data with the TMPA complex could also be treated this way if there were not the combination of very fast reactions (which precludes overall fixed spectra, cf., above) with extreme shift in the stability of the intermediate (which precludes to use individual spectra for each temperature).

4. Pressure dependence of reactions

The interpretation of the effect of pressure on the rate of chemical reactions is now a well accepted way of elucidating reaction mechanisms. During recent years, a large number of variable pressure kinetic studies of solvent exchange and complex formation reactions have been reported [2]. The activation volumes for solvent exchange reactions give the most direct information on their mechanisms. It also becomes clear from available data on a given metal ion that simple substitution reactions take place via the same mechanism in aqueous solution as does water exchange.

Expressing the Eyring equation (Eq. 18) in a logarithmic form, and deriving this new expression with respect to pressure at constant temperature, we obtain Eq. 23, where $\Delta V^{\neq}$ is the activation volume, the difference between the partial molar volumes of the transition states and the reactants.

$$\left(\frac{\partial \Delta G^{\neq}}{\partial P}\right)_T = -RT\left(\frac{\partial \ln k}{\partial P}\right) = \Delta V^{\neq} \qquad (23)$$

$\Delta V^{\neq}$ may be positive or negative, depending if the reaction is slowed down or accelerated with pressure. Integrating Eq. 23 in function of pressure, and assuming that $\Delta V^{\neq}$ is constant with pressure, Eq. 24 is obtained, where k_0 is the rate constant at zero pressure.

$$\ln k = \ln k_0 - \frac{\Delta V^{\neq}}{RT} P \qquad (24)$$

For a complex reaction mechanism, the pressure dependence of each individual rate constant is defined by the same formula and individual k_0 and $\Delta V^{\neq}$. In the global fitting of pressure dependences the parameters are the collection of k_0's and $\Delta V^{\neq}$'s.

To test the second order methodology we examined the aquation of a racemic mixture of a square planar complex of platinum(II), {exo-2-amino-2-aminomethyl-7-oxa-bicyclo[2.2.1]heptane} dichloro platinum, studied by Jestin et al. [17].

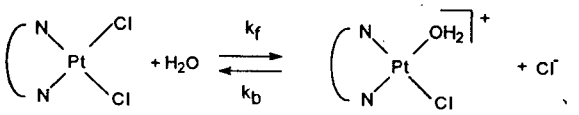

The kinetics of the reaction was investigated as a function of the metal concentration, the chloride concentration, and the pressure. A double-beam Perkin-Elmer Lambda 19 spectrophotometer was used, equipped with a dual beam high-pressure optical cell which was designed and built in Lausanne. (It consists of a double-beam stainless steel (AISI 630) pressure tight barrel, with, for each beam, one sapphire window imbedded at one end, and a closing beryllium-copper assembly at the other end, in which a second sapphire window is enclosed. The sample and the reference are contained each in a 2 cm "pill box Le Noble" quartz cell, immersed in the pressure vessel. A 100-Ω platinum resistance is located inside the vessel, at ambient pressure. A capillary connector transmits the applied pressure through the side wall. The cell is thermostated by circulation of a fluid in a helical groove carved in the outer surface of the barrel, covered by a stainless steel (AISI 630) lagging.) The variable pressure work was carried out up to 201 MPa at 311 K, a temperature at which the time required for the preparation of samples, their introduction into the pressure vessel, and thermostatting at the desired temperature limited the loss of the starting material. The samples of the above complex (Rhône-Poulenc) were dissolved in a solution with a total acid concentration of 6.6×10^{-3} M where various proportions of perchloric and hydrochloric acid were used to vary the initial chloride concentration. All solutions were prepared in doubly distilled water and degassed prior to the measurements. Eight series of spectral data were obtained at five different pressures. For each measurement 20 spectra were measured at 0.4 nm intervals between 240 and 356.4 nm (291 wavelengths). The measurements were stopped before the start of the second aquation.

Singular value decomposition of the individual spectral measurements shows that only two differently absorbing species are present during the reaction, as expected. Unfortunately a global factor analysis is impossible because of baseline displacements due to oil traces diffusing into the high-pressure cell. Furthermore absorption spectra are expected to change within the series due to the spectral pressure dependence. The eigenvector representation reduced the amount of spectral data to be handled in the numerical analysis from 160×291 to 160×2.

The result of the second order global analysis is summarised in Table 1. Plots of the matrix of residuals $\mathbf{R}_{tot}$ do not show any suspicious patterns or peaks, the residual noise is within the expected limits. Moreover, the computed absorption spectra revealed to be as expected.

In Table 1, a comparison between a classical [17] and the second order global analysis is summarised. Classically, a two step process was required: (a) rate constants were determined at each pressure at two different wavelengths from two series performed with different concentrations of Pt(II) complex and chloride. This combination of two sets of concentrations considered at two wavelengths, are necessary to extract the rate constants characterising the equilibrium with sufficient precision. (b) The activation parameters are then calculated using Eq. 24.

Second order global analysis yielded acceptably similar values for the activation parameters. However, it is worth noting that their standard errors are substantially smaller. Ignoring the absolute values of these errors, one can conclude that globally calculated parameters are much better defined.

5. Conclusions

Globalisation of the analysis of series of measurements has well recognised advantages [4–10]. Instead of fitting intermediate parameters to individual measurements which in a secondary process are further analysed to yield the parameters of interest, these are directly refined in second order global analysis. The outcome is usually a significant reduction of the total number of parameters to be fitted which consequently results in much better defined minima. First order global analysis consists of linking common parameters throughout a series of measurements. To illustrate the procedure we consider the determination of reaction kinetics measured at many wavelengths using a diode-array spectrophotometer. The non-global option consists in fitting a set of rate constants to the individual kinetic traces at each wavelength, subsequent averaging yields final rate constants. In first order global analysis the complete measurement is analysed globally, all measurements at the different wavelengths are fitted

with one set of rate constants. In second order global analysis, the concept is carried one step further. The analysis is redefined, using a new model which encompasses the complete series of measurements done under different conditions such as temperature or pressure. The fitted parameters are no longer rate constants but directly the activation parameters. Subsequent applications are envisaged and we are presently developing the software for second order global analysis of concentration or pH dependences to yield kinetically determined equilibrium constants.

In this contribution we developed the detailed mathematics for second order global fitting. We tested and illustrated the method with examples of activation analysis in kinetics. Our experiences can be summarised in the following points. (a) Second order global analysis improved the robustness of the fitting procedure, this is illustrated in Fig. 1 which shows reliable fitting even at noise levels well above those of modern instruments. The highest differences between the real and calculated parameters are the activation entropies which are notoriously ill defined as they are heavily extrapolated intercepts in Eyring plots. (b) Determining the correct chemical model for the reaction under investigation is enhanced by globalisation of the analysis. It is quite common that individual measurements are fitted in a satisfactory way by a model which only proves to be incorrect as it does not fit the data measured under different conditions. It is of course not surprising that similar observations have already been made with respect to first order globalisation. (c) In the examples we investigated, the total sum of squares (Eq. 8) was slightly larger than the total of the sum of squares over all individual measurements in classical analysis. The increase is to be expected as a smaller number of parameters is used to fit the data and furthermore, the differences between the rate constants and the fitted line in the Eyring plots in not taken into consideration. Of course, if the activation parameters determined classically are used to define rate constants at individual temperatures and the residuals are calculated using these rates, the total sum of squares is larger.

Acknowledgements

The Swiss National Foundation and the University of Newcastle are greatly thanked for support including grants delivered to J.-L. Jestin and M. Maeder to stay at the universities of Lausanne and Basel. We thank Rhône-Poulenc for platinum complex.

References

[1] J.H. Esparson, Chemical Kinetics and Reaction Mechanisms, McGraw-Hill, New York, 1981.
[2] R. van Eldik (Ed.), Inorganic High Pressure Chemistry, Elsevier, Amsterdam, 1986.
[3] R.G. Wilkins, Kinetics and Mechanism of Reactions of Transition Metal Complexes, VCH, Weinheim, 2nd edn., 1991.
[4] J.R. Knutson, J.M. Beechem and L. Brand, Chem. Phys. Lett., 102 (1983) 501.
[5] J.M. Beechem, M. Ameloot and L. Brand, Anal. Instrum., 14 (1989) 379.
[6] L.D. Janssens, N. Boens, M. Ameloot and F.C. De Schryver, J. Phys. Chem., 94 (1990) 3564.
[7] J.M. Beechem and E. Haas, Biophys. J., 55 (1989) 122.
[8] J.M. Beechem, Chem. Phys. Lipids, 50 (1989) 237.
[9] H. Gampp, D. Haspra, M. Maeder and A.D. Zuberbühler, Inorg. Chem., 23 (1984) 3724.
[10] M. Maeder and A.D. Zuberbühler, Anal. Chem., 62 (1990) 2220.
[11] P. Gans, Coord. Chem. Rev, 19 (1976) 99.
[12] P.R. Bevington, Data Reduction and Error Analysis in the Physical Sciences, McGraw-Hill, New York, 1969.
[13] G.H. Golub and F. Van Loan, Matrix Computations, 2nd edn., John Hopkins University Press, Baltimore, MD, 1989.
[14] E.R. Malinowski and D.G. Howery, Factor Analysis in Chemistry, Wiley, New York, 2nd edn., 1991.
[15] K.D. Karlin, N. Wei, B. Jung, S. Kaderli, P. Niklaus and A.D. Zuberbühler, J. Am. Chem. Soc., 115 (1993) 9506.
[16] K.D. Karlin, N. Wei, B. Jung, S. Kaderli and A.D. Zuberbühler, J. Am. Chem. Soc., 113 (1991) 5868.
[17] J.-L. Jestin, J.-C. Chottard, U. Frey, G. Laurenczy and A.E. Merbach, Inorg. Chem., in press.

ELSEVIER

Analytica Chimica Acta 298 (1994) 203–207

ANALYTICA CHIMICA ACTA

NEUTIT: a computer program for evaluating equivalence volumes and ionization constants in polar non-aqueous or partially aqueous media

A.G. Gonzalez *, M.A. Herrador, A.G. Asuero

Department of Analytical Chemistry, University of Seville, E-41012 Seville, Spain

Received 25 November 1993; revised manuscript received 31 May 1994

Abstract

A modified version of the EUTIT program, called NEUTIT, which accounts for potentiometric titrations in polar non-aqueous or partially aqueous media is developed. The program was applied to the titration data of several substances in three mixed solvents. The output of the program gives consistent and unbiased estimations of equivalence volumes and acidity constants. Good agreement between acidity constants evaluated from NEUTIT and the reported literature values is found in all cases. The program utilizes all titration data pairs which may be acquired from an automatic titrator unit.

Keywords: Titrimetry; Potentiometry; Computer program; NEUTIT program

1. Introduction

Non-aqueous acid base titrations have become of considerable importance in chemical analysis [1,2]. They find a great number of applications in organic and pharmaceutical analysis and have been accepted by the majority of modern pharmacopoeias as an official analytical method. On the other hand, acid–base titrations of protolytes in non-aqueous or partially aqueous solvents provides a means for evaluating ionization constants of substances at the standard state of the medium considered [3–7].

The proton dissociation constant data of a protolyte are of great interest in several pharmaceutical and analytical respects. The effect of changing the solvent composition on the proton dissociation constant of a protolyte is very useful for inferring changes in the pattern of ion–solvent interactions in binary solvents. In the field of computerized treatments, several programs such as GRAN, CALIBT, TITRATE or ESAB are of interest [8]. Within this realm, Budevsky et al. [9] have proposed a straightforward method for determining acids and bases in non-aqueous media in which no preliminary pH calibration is needed (NABTIT program). We have recently published in this journal [10] an improved computerized version of the Hofstee's method [11] which provides equivalence volumes and ionization constants from potentiometric acid–base titrations (EUTIT program).

The present paper deals with the modification of these algorithms for its application to potentiometric titrations in polar partially aqueous media. Taking into account that the outline of the method is detailed in the referred work, in order to avoid any repetition, we will discuss the innovations only.

* Corresponding author.

SSDI 0003-2670(94)00272-N

2. Theoretical background

When a weak monoprotic acid, HA, is titrated with a strong base in a non-aqueous or partially aqueous solvent (which permits the titrant to be fully dissociated and where the ion pair formation is negligible), Eqs. 1–6 of our previous paper [10] hold true when the following alterations are made:

(i) the ionic product of water K_w must be changed into the corresponding value for the mixed solvent, K_{solv};

(ii) H refers to the concentration of lyonium ions (solvated protons);

(iii) The ionization constant of HA, K_a must be referred to the mixed solvent standard state.

The hydrogen ion concentration, H, in partially aqueous media of constant ionic strength in a thermostated system can be measured potentiometrically using a glass electrode once the reversibility of the electrode assembly has been checked in the studied medium

$$E = E^0 + k \log H \quad (1)$$

E^0 being the formal potential of the galvanic cell and k the theoretical value of Nernstian slope. The solvent ion product may be evaluated by means of potential measurements in the titration of a strong acid with a strong base [12–14].

$$pK_{solv} = (E^0_a - E^0_b)/k \quad (2)$$

where $E^0{}_a$ and $E^0{}_b$ are obtained as the intercepts of the plots of the response of the galvanic cell vs. the lyonium or lyate concentrations in the acid and alkaline range, respectively.

The logarithm of the value of the concentration of solvated protons in a titration experiment may be obtained from the potential readout by using

$$-\log H = (E^0_a - E)/k \quad (3)$$

Once the potential measurements are converted into H one can calculate from the titration data pairs V, H the corresponding x and y variables according to Eqs. 3–4 of our previous work [10].

Accordingly, the following steps must be accomplished in order to evaluate the equivalence volume and ionization constant of an HA acid in mixed polar media:

(1) Titration of a strong acid with a strong base in the studied solvent. The potential (E) and the added volume of titrant (V) are recorded. From these titration data, the limiting values $E^0{}_a$ and $E^0{}_b$ are calculated and consequently, K_{solv} [12–14]. These computations are performed by the subroutine MIXPUT discussed below.

(2) Titration of the acidic solute AH with a strong base in the same solvent. Now the titration data to be recorded are also E and V (potential instead of pH readings). The E values are converted into H values from Eq. 3. From the titration data pairs H and V, NEUTIT computes the equivalence volume and the ionization constant (still without activity corrections)

(3) Activity corrections according to the ionic strength and dielectric permittivity of a medium by using the subroutine CORR.

3. Computational details

The NEUTIT program is implemented in Microsoft QuickBasic 4.5 for use with an IBM compatible PC, XT or At. In order to avoid slow computations it is advisable to use at least an 80286 processor. NEUTIT consists of the following principal procedures:

MIXPUT

This procedure reads the preliminary titration data E and V for the titration of the strong acid with the strong base from an ASCII file, in addition to the initial volume of sample and concentration of titrant. From these data the limiting values $E^0{}_a$ and $E^0{}_b$ as well as K_{solv} are calculated [12–14] and stored.

After this computation, the analyte titration data E and V (as well as the initial sample volume, titrant concentration, and standard errors in E and V, $\sigma(E)$ and $\sigma(V)$) are read from an ASCII file. The standard deviation in $-\log H$ is calculated from $\sigma(E)$ according to

$$\sigma(-\log H) = \sigma(E)/k$$

From these data, the values of x, y, $\sigma(x)$ and $\sigma(y)$ are obtained (Eqs. 3–6 of Ref. [10], remembering that K_w has been changed into K_{solv}) and stored in the file DATA.INP. The equivalence volume V_e and ionization constant K_a are involved in the linear relationship (see Eq. 1 of Ref. [10])

$$y = V_e K_a - K_a x$$

which for convenience we arrange as

$$y = a_1 + a_2 x$$

GUESS

This subroutine computes starting values for a_1 and a_2 from the file DATA.INP by using conventional linear regression.

ITERA

In this subroutine the iterative weighted least square procedure is applied [10]. The convergence criterion is that K digits of each parameter are not changed in the iteration, that is, $|(a_{j,n+1}/a_{j,n}) - 1| < 10^{-K}j$ being 1 or 2, and n being the iteration number. The number of stable digits for convergence is typed from keyboard. This convergence criterion also leads to a minimization of the regression variance and consequently, to a proper correlation coefficient (closer to 1) according to the goodness of the data [20].

ERRORS

Once the optimum values of parameters and weighting factors have been obtained, this procedure computes the elements of the variance–covariance of coefficients, that is, the variances of a_1 and a_2 and its covariance, namely $\sigma^2(a_1)$, $\sigma^2(a_2)$ and $\mathrm{cov}(a_1,a_2)$.

Accordingly, the values of V_e and K_a and their standard errors are computed as follows

$$V_e = \frac{a_1}{a_2}$$

$$\sigma^2(V_e) = \frac{\sigma^2(a_1)}{a_2^2} + \frac{a_1^2\sigma^2(a_2)}{a_2^4} - \frac{2a_1\mathrm{cov}(a_1,a_2)}{a_2^3}$$

$$K_a = -a_2$$

$$\sigma^2(K_a) = \sigma^2(a_2)$$

Significant figures of estimates are established from the first decimal place associated to the error given by the corresponding standard deviation.

CORR

This subroutine performs activity corrections for providing us with suitable thermodynamic pK values. The activity coefficients involved in the computations are evaluated from the values of absolute temperature, T, ionic strength, I, and permittivity, D, of the aqueous solution according to the following equation [13–15]

$$-\log f = (1.825 \times 10^6 (DT)^{-3/2} I^{1/2}) / (1 + 251.45 (DT)^{-1/2} I^{1/2})$$

here f is the activity coefficient for an univalent ion in the studied medium.

OUTPUT

The estimated values of equivalence volume and acidity constant with their standard errors are printed together with tables with various kinds of information.

In order to illustrate how the NEUTIT program works with polar non-aqueous or partially aqueous titrations we have selected some mixed solvent systems such as dioxane–water, methanol–water and dimethylformamide–water for performing the titrations.

4. Experimental

4.1. Reagents

Methanol, *N,N*-dimethylformamide and 1.4-dioxane (Merck, analytical-reagent grade) were stored over molecular sieve 4A for at least one week. The solvents were shown to be free from acidic impurities by titration with tetrabutylammonium hydroxyde in benzene–methanol (Carlo Erba). 2-, 3- and 4-nitrobenzoic acid (2NB, 3NB and 4NB, respectively), tris(hydroxymethyl)aminomethane–hydrochloride (Tris–HCl), sulphanilic acid (SA) (Merck), Methyl Yellow (MY) (Carlo Erba), Bromocresol Green (BCG) (Riedel), 9-fluorene carboxylic acid (FCA) (Aldrich, 97%), concentrated hydrochloric acid, sodium hydroxide and potassium chloride (Merck) were used as received.

p-Aminoazobenzene (PAB) was synthesized by diazotization of aniline and Orange II (OR), *p*-(2-hydroxy-1-naphthylazo)benzene sulfonic acid sodium salt was obtained by coupling β-naphthol with diazotized sulphanilic acid [16]. The crude products were recrystallized from ethanol. The purity of the dyes was checked by thin-layer chromatography as described by Vytras et al. [17]. No coloured impurities were found on the chromatogram.

Glass distilled deionized water (conductivity lower than 1 $\mu\Omega^{-1}\,\mathrm{cm}^{-1}$) was used throughout. It was boiled to remove carbon dioxide and stored under nitrogen before use.

4.2. Measurements

Measurement of $-\log H$ and electromotive force were made with the use of a Beckman combined glass/

Table 1
Titrations in 50% (v/v) methanol–water mixtures with 0.1025 M sodium hydroxide in the same medium

Initial $V=25$ ml, $T=298$ K, $I=0.1$	
Analyte titrated	Results from NEUTIT
Tris–HCl, 0.005 M	$V_e=1.215\pm0.002$ ml $pK_a=8.07\pm0.01$ Purity found = 99.6%
SA, 0.008 M	$V_e=1.933\pm0.008$ ml $pK_a=2.78\pm0.01$ Purity found = 99.1%
2NB, 0.005 M	$V_e=1.204\pm0.005$ ml $pK_a=3.20\pm0.01$ Purity found = 98.7%
3NB, 0.005 M	$V_e=1.210\pm0.002$ ml $pK_a=4.04\pm0.01$ Purity found = 99.2%
4NB, 0.005 M	$V_e=1.208\pm0.006$ ml $pK_a=4.12\pm0.01$ Purity found = 99.0%

Ag/AgCl electrode with the outer chamber filled with 1 M KCl saturated with AgCl. Titrations were carried out in titration vessels thermostated at 25.0 ± 0.1°C. The ionic strength was fixed at 0.1 with a background of KCl.

E^0_a and E^0_b values were obtained from titrations of 25.0-ml aliquots of 0.0800 M hydrochloric acid with 0.1 M sodium hydroxide solution in the mixed solvent studied under a protective stream of nitrogen. Aliquots of 0.050 ml were added stepwise and the electromotive force was reproducible within ±0.6 mV.

The substances to be assayed were dosified by titration of 25.0-ml aliquots of the corresponding analyte sample solutions whose concentration varies within the range 0.005–0.008 M in the 50% (v/v) organic cosolvent–water mixture with 0.1 M sodium hydroxide in the same mixture under a protective stream of nitrogen.

Table 2
Titrations in 50% (v/v) dioxane–water mixtures with 0.0998 M sodium hydroxide in the same medium

Initial $V=25$ ml, $T=298$ K, $I=0.1$	
Analyte titrated	Results from NEUTIT
FCA, 0.005 M	$V_e=1.204\pm0.005$ ml $pK_a=6.17\pm0.01$ Purity found = 96.1%
BCG, 0.006 M (2nd dissociation step)	$V_e=2.987\pm0.006$ ml $pK_a=6.84\pm0.01$ Purity found = 99.3%

5. Results and discussion

In order to illustrate the procedure we have assayed a number of acidic substances in three mixed solvents: 2NB, 3NB, 4NB, SA and Tris–HCl were assayed in a 50% (v/v) methanol–water mixture, BCG and FCA in a 50% (v/v) dioxane–water mixture and PAB, MY and OR in a 50% (v/v) *N,N*-dimethylformamide–water mixture.

From the E^0_a and E^0_b values obtained from the titration of hydrochloric acid with sodium hydroxide, ion product constants for the three mixed solvents were obtained. The results were: 13.61, 15.26 and 14.54 for the 50% (v/v) methanol–water, dioxane –water and *N,N*-dimethylformamide–water mixtures, respectively. By applying the NEUTIT program, the ionization constant of each compound, its purity and the equivalence volume were obtained. The activity corrections were taken into account by using the permittivity values of the mixed solvents considered (the permittivity values of each 50% (v/v) mixture are 59.80 (methanol–water), 35.22 (dioxane–water) and 65.95 (*N,N*-dimethylformamide–water).

All these results are collected in Tables 1, 2 and 3. We have selected the cited substances to be titrated for the sake of comparison with the pK_a values reported in

Table 3
Titrations in 50% (v/v) *N,N*-dimethylformamide–water mixtures with 0.1009 M sodium hydroxide in the same medium

Initial $V=25$ ml, $T=298$ K, $I=0.1$	
Analyte titrated	Results from EUTIT
PAB, 0.007 M	$V_e=1.712\pm0.005$ ml $pK_a=1.78\pm0.02$ Purity found = 98.7%
MY, 0.005 M	$V_e=1.230\pm0.004$ ml $pK_a=1.56\pm0.01$ Purity found = 99.3%
OR, 0.005 M	$V_e=1.215\pm0.005$ ml $pK_a=11.70\pm0.01$ Purity found = 98.1%

Table 4
Thermodynamic pK_a values of the titrated substances compared with the reported values

Analyte titrated	pK_a this work	pK_a reported
Tris–HCl	8.07	7.99 [9]
SA	2.78	2.80 [9]
2NB	3.20	3.17 [18]
3NB	4.04	4.03 [18]
4NB	4.12	4.10 [18]
FCA	6.17	6.13 [7]
BCG	6.84	6.80 [7]
PAB	1.78	1.79 [6]
MY	1.56	1.57 [6]
OR	11.70	11.67 [19]

the literature. Accordingly, the corrected and reported pK_a values are presented in Table 4. As can be observed good agreement is shown between calculated and reported values.

6. Conclusion

The NEUTIT program permits to evaluate titration curves of acids of various strengths in polar non-aqueous or partially aqueous solvents by using all the titration points which may be acquired by means a titrator unit.

Acknowledgements

Financial support from the Dirección General de Investigación Científica y Técnica de España through Project PB 92-0678 is gratefully acknowledged.

References

[1] A.G. Gonzalez, M.A. Herrador and A.G. Asuero, Microchem. J., 44 (1991) 243.
[2] J.T. Rubino and W.S. Berryhill, J. Pharm. Sci., 75 (1986) 182.
[3] A.G. Gonzalez, M.C. Mochon, J.L. Gomez-Ariza and A.G. Perez, Anal. Chim. Acta, 224 (1989) 109.
[4] A.G. Gonzalez, D. Rosales, J.L. Gomez-Ariza and J.F. Sanz, Anal. Chim. Acta, 228 (1990) 301.
[5] A.G. Gonzalez, D. Rosales, J.L. Gomez-Ariza and J.F. Sanz, J. Phys. Org. Chem., 4 (1991) 87.
[6] A.G. Gonzalez, M.A. Herrador and A.G. Asuero, Anal. Chim. Acta, 246 (1991) 429.
[7] A.G. Gonzalez and F. Pablos, Anal. Chim. Acta, 251 (1991) 321.
[8] M. Meloun, J. Havel and E. Högfeldt, Computation of Solution Equilibria, Ellis Horwood, Chichester, 1988.
[9] O. Budevsky, T. Zikolova and J. Tencheva, Talanta, 35 (1988) 899.
[10] A.G. Gonzalez and A.G. Asuero, Anal. Chim. Acta, 257 (1992) 29.
[11] L. Perhrsson, F. Ingman and A. Johansson, Talanta, 23 (1976) 769.
[12] P. Zikolov, A. Astrug and O. Budevsky, Talanta, 22 (1975) 511.
[13] M. Galus, S. Glab, G. Grekulak and A. Hulanicki, Talanta, 26 (1979) 169.
[14] S. Glab and A. Hulanicki, Talanta, 28 (1981) 183.
[15] G. Velinov, P. Zikolov, T. Tcharakova and O. Budevsky, Talanta, 21 (1974) 163.
[16] A.I. Vogel, A Textbook of Practical Organic Chemistry, Longmans, New York, 3rd edn., 1965.
[17] K. Vytras, J. Kalous and J. Cerna-Frybortova, Talanta, 37 (1990) 1025.
[18] M.S.K. Niazi, Bull. Chem. Soc. Jpn., 62 (1989) 1253.
[19] A.G. Gonzalez, Ph.D. Thesis, University of Seville, 1986.
[20] A.G. González, M.A. Herrador and A.G. Asuero, Int. J. Pharm., 108 (1994) 149.

ELSEVIER

Analytica Chimica Acta 298 (1994) 209–217

ANALYTICA CHIMICA ACTA

Concomitant separation of strontium and samarium–neodymium for isotopic analysis in silicate samples, based on specific extraction chromatography

Christian Pin *, Danielle Briot, Chantal Bassin, Franck Poitrasson

Département de Géologie, U.R.A. 10 CNRS, Université Blaise Pascal, 5 rue Kessler, 63038 Clermont-Ferrand, France

Received 9 March 1994; revised manuscript received 7 June 1994

Abstract

A separation scheme for strontium and light rare earth elements and its application to the isotopic analysis of strontium and neodymium in silicate rocks are presented. This method benefits from the selectivity and high capacity of two newly introduced extraction chromatographic materials, referred to as Sr.Spec and TRU.Spec, respectively. These afford a straightforward separation of Sr and Sm + Nd with high yield, good purity and satisfactory blank levels, on very small (0.25 ml) columns using small volumes of solutions of a single mineral acid, HNO_3. The validity of the method is illustrated by the measurement of $^{87}Sr/^{86}Sr$ and $^{143}Nd/^{144}Nd$ ratios in twelve international standard reference materials.

Keywords: Chromatography; Extraction; Samarium; Strontium; Neodymium

1. Introduction

The measurement of isotopic composition and the determination of elemental abundances by the isotope dilution technique are commonly performed by thermal ionization mass spectrometry (ID-TIMS). This requires good chemical separation prior to mass spectrometric analysis. Since the pioneering work of Aldrich et al. [1], ion-exchange resins have proven to be the most useful tools for isolating the elements of interest in isotope geochemistry. Although good separations can be obtained, conventional ion-exchange techniques rarely offer high elemental selectivity. Among the elements extensively used in geochemistry, only Pb in 0.5–1 M HBr medium [2] and Th in ca. 7 M HNO_3 [3] can be separated from most other elements by using very small columns of strongly basic anion exchange resin. In general, separation schemes are based on slight differences in distribution coefficients, and relatively large ion-exchange columns and elution volumes are required.

Recently, a new generation of extraction chromatographic materials has been developed at Argonne National Laboratory (USA) [4]. These were originally designed for separating radioactive nuclides from nuclear waste solutions [5,6] but their high capacity and specificity make them appealing for environmental [7] and geological samples.

In previous work, we evaluated the suitability of a simple method based on small extraction chromatographic columns for the isolation of Sr from geological samples prior to isotopic analyses [8]. Here, we present a separation scheme for Sr and light rare earth elements (LREE), and its application to the isotopic analysis of

* Corresponding author.

SSDI 0003-2670(94)00274-P

strontium and neodymium in silicate rocks. The validity of the method is illustrated by the measurement of $^{87}Sr/^{86}Sr$ and $^{143}Nd/^{144}Nd$ ratios in twelve international standard reference materials.

2. Experimental

2.1. Reagents and materials

Deionised water was further purified with a Milli-Q (Millipore) system. All acids (HF, HNO_3, HCl) were analytical reagent grade, purified by sub-boiling distillation in silica glass or PTFE stills. Oxalic acid (Suprapur grade, Merck) was used as received.

Two recently introduced extraction chromatographic materials, referred to as Sr.Spec and TRU.Spec respectively, were obtained from EIChroM (Darien, IL). In both cases, fine grained (50–100 μm particle size) materials (sps grade) were selected for column work because they lead to narrower elution bands. The Sr.Spec resin consists of a solution of the crown ether di-*tert.*-butylcyclohexano-18-Crown-6 (DtBuCH18-C6) in 1-octanol loaded on the inert support Amberchrom CG-71ms [7,9]. This material allows the extraction of Sr from nitric acid solutions. Only Pb and, to a lesser extent, Ba are also retained [10]. The TRU.Spec (for TRansUranic) "resin" is comprised of a solution of octyl(phenyl)-*N*,*N*-diisobutylcarbamoylmethylphosphine oxide (CMPO) dissolved in tributyl phosphate (TBP) and supported on the same inert substrate as Sr.Spec, i.e., Amberchrom CG-71ms [11]. Besides transuranic elements, thorium, uranium and bismuth are retained [11]. Interestingly, CMPO is also a lanthanide extractant [11] and we investigated whether this property could be used for the separation of the geochemically important elements Nd and Sm.

Polypropylene columns (5 cm×5 mm i.d.) with a 30-μm polyethylene frit at the bottom (Muromachi) were used for separation work. A 165 mg (scheme 1) or 83 mg (scheme 2) portion of Sr.Spec sps or TRU.Spec sps was slurried in a few ml of 0.05 M HNO_3 and transferred to the columns, resulting in ca. 0.5 ml or 0.25 ml beds, respectively. Preconditioning was made with 2 or 1 ml of 3 M or 2 M HNO_3, depending on the separation scheme used.

The Sr.Spec and TRU.Spec columns were operated in a coupled arrangement during loading to effect the simultaneous uptake of Sr and LREE from the sample (Fig. 1A). The columns were then decoupled and subjected to separate elution schemes for recovery of these analytes (Fig. 1B).

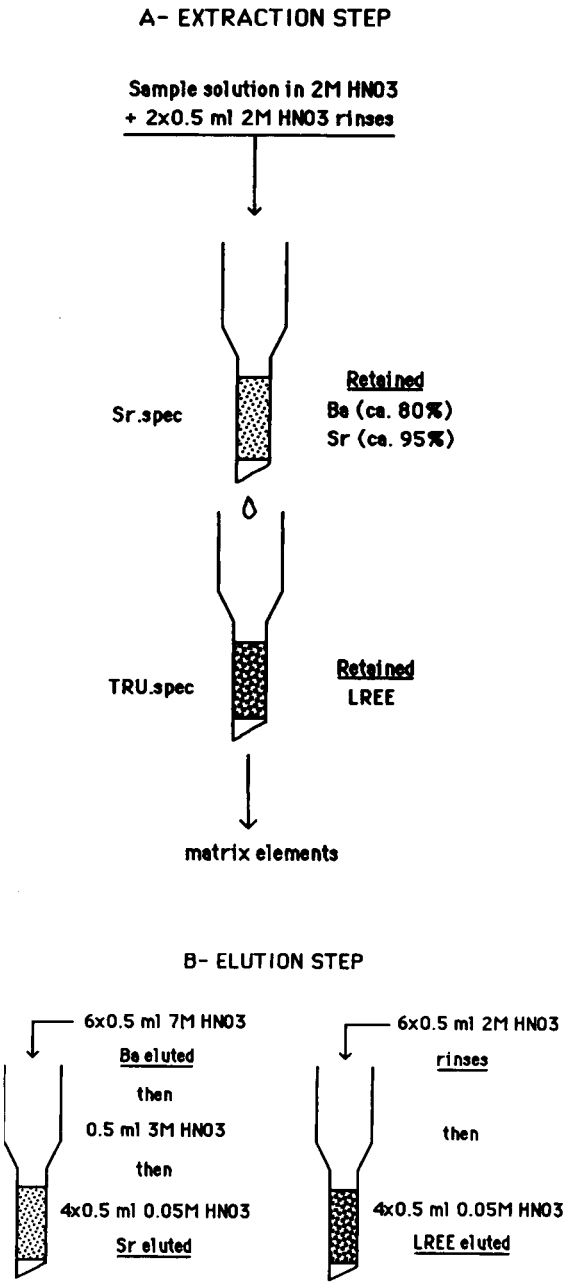

Fig. 1. Column arrangement for concomitant separation of Sr and LREE using Sr.Spec and TRU.Spec extraction chromatographic materials. (A) Loading of sample and extraction step. (B) Elution step.

2.2. Instrumentation

The experimental measurements were performed with an ICP atomic emission spectrometer (Jobin-Yvon 70 II, Longjumeau) using a polychromator for major and minor (including Sr and Ba) element measurements, and a high resolution monochromator for lanthanide detection. Additional data were obtained by ICP mass spectrometry (VG PlasmaQuad II+) at CNRS Service Central d'Analyse (Vernaison). An automated VG 54E thermal ionization mass spectrometer in the double collection mode was used for Sr and Nd isotope composition measurements. Blanks were determined by isotope dilution using ^{84}Sr and ^{145}Nd enriched tracers obtained from Oak Ridge National Laboratory, with a manual Cameca TSN 206S mass spectrometer equipped with a secondary electron multiplier.

2.3. Analytical procedure

Sample decomposition

ca. 100 mg samples of finely powdered rock were dissolved using a mixture of HF and HNO_3, but the exact method used differed depending on the mineralogy of the rocks to be analyzed. For standards of basaltic composition, dissolution was performed on a hot-plate (ca. 70°C, overnight) in closed 15 ml polyfluoroalkoxy (PFA) vials (Savillex, Minnetonka, MN) with 0.5 ml of 14 M HNO_3 and 1 ml of 29 M HF. Granitic standards were dissolved in high pressure PTFE bombs (190°C, 5 days) in order to ensure complete opening of refractory minerals which may contain a large proportion of the REE of the sample. Then, excess HF and volatile SiF_4 were removed by evaporation of the sample to dryness. The residue was taken up in 1 ml of 14 M HNO_3, evaporated to dryness and treated overnight with 5 ml of 6 M HCl at ca. 90°C. This resulted in a clear solution. After evaporation to dryness, the residue was converted to the nitrate form by evaporation with 14 M HNO_3, and finally dissolved in 1.5 or 3 ml of 3 M or 2 M nitric acid, depending on the separation scheme used.

Chemical separation

After loading the sample onto the coupled columns with 2 ml of 2 M HNO_3 and rinsing twice with 0.5 ml of the same acid, the columns were decoupled (Fig. 1). The Sr.Spec column was washed with six 0.5 ml portions of 7 M HNO_3 then 0.5 ml 3 M HNO_3 to elute Ba. Strontium was stripped with four 0.5 ml portions of 0.05 M HNO_3. The TRU.Spec column was washed with six 0.5 ml portions of 2 M HNO_3 before elution of the LREE with four 0.5 ml aliquots of 0.05 M HNO_3.

The Sr fraction was collected in a pre-cleaned disposable polystyrene pot with a conical bottom, evaporated to dryness and was ready for mass spectrometry. The fraction containing the LREE was also evaporated. Before TIMS analyses, it is necessary to isolate Nd from the adjacent lanthanides, especially Sm which has isobaric interferences with Nd at m/z 144, 148 and 150. To do this, we used a well established extraction chromatographic method involving di(2-ethylhexyl)phosphoric acid and dilute HCl [12,13]. A polystyrene–divinylbenzene copolymer (Bio-Beads S-X8; Bio-Rad, Richmond, CA) was used as the stationary-phase support [14].

Thermal ionization mass spectrometry

The Sr fraction was dissolved in a few μl of dilute HNO_3, and an amount corresponding to ca. 2 μg of Sr was loaded with a drop of 3 M H_3PO_4 onto a previously outgassed flat Ta filament. For samples with small Sr concentrations (AC-E, GH), a more sensitive technique involving tungsten filaments covered with a tantalum gel as an ion emitter [15,16] was used. Data acquisition was performed on ion beam intensities between 2 and 4×10^{-11} A. The Nd fraction was loaded onto one of the side filaments of a triple Ta–Re–Ta assembly, and analysed as the metal species with ionic currents of $2–4 \times 10^{-11}$ A.

3. Results and discussion

Two column sizes were tested during this study. First, a column containing 165 mg (corresponding to ca. 0.5 ml resin bed) of TRU.Spec sps was placed in series with a column (Fig. 1A) containing the same quantity of Sr.Spec sps [8] for the sequential separation of Sr and LREE from ca. 0.1 g silicate rock samples. Next, this procedure was scaled down to 83 mg (ca. 0.25 ml) of each extraction chromatographic material for treating samples of the same size. In each case, an in-house rock standard of trachy-andesitic

composition [8] was used to study the elution behaviour of the elements of interest and matrix constituents.

Scheme 1 (coupled 0.5 ml columns)

In the initial trials involving sequential isolation of Sr and lanthanides, the sample (ca. 100 mg) was loaded in 3 ml of 3 M HNO_3–0.05 M $H_2C_2O_4$. This load solution has been shown to be a medium suitable for Sr separation on Sr.Spec [7,8]. ICP-AES analyses of collected fractions showed that most major and trace elements were removed from the columns by 4 rinses, 0.5 ml each, with the same mixture. Among the major rock constituents, only K on Sr.Spec and Fe on TRU.Spec showed noticeable extraction. The heavy rare earths, as exemplified by yttrium, were not significantly ($<15\%$) retained. During loading, the TRU.Spec resin acquired a yellow colour, presumably due to iron, which disappeared with the pure acid rinses. The columns were then decoupled (Fig. 1B). As described previously [8], the Sr.Spec column was washed with 8.5 ml of 3 M HNO_3 to get rid of barium (the most strongly retained element beside Sr and Pb). Then, Sr was eluted with 4 ml of 0.05 M HNO_3. The TRU.Spec column was washed twice with 5 ml of 2 M HNO_3. All remaining elements, mostly Fe and minor amounts of the heavy rare earths, eluted at this time, together with ca. 20% of La. The other rare earths (Ce–Pr–Nd–Sm + Eu and Gd) were stripped with three 1 ml aliquots of 0.05 M HNO_3. Recoveries measured by ICP-AES were ca. 95% for Ce, Pr, Nd and Sm.

Scheme 2 (coupled 0.25 ml columns)

The aim of these experiments was to scale down the procedure and to try to improve the separation of some critical element pairs. Indeed, published distribution ratios [10] suggested that a better separation of Sr from Ba on Sr.Spec could be obtained in more concentrated HNO_3. Moreover, the capacity factor k' (defined as the number of free column volumes to peak maximum) for Fe^{3+} is ca. 2 in 2 M HNO_3 instead of ca. 10 in 3 M HNO_3 [11]. This indicates that the extraction of iron by TRU.Spec would decrease significantly in less concentrated acid. Since oxalic acid contributed significantly to the Sr blank [8] and was not found to be necessary, this was omitted.

Ca. 0.25 ml columns of Sr.Spec and TRU.Spec (corresponding to 83 mg of each resins) were placed in series and preconditioned with two 0.5 ml portions of 2 M HNO_3. The sample (ca. 100 mg) was loaded on top of the first (Sr.Spec) column in three 0.5 ml aliquots of 2 M HNO_3, allowed to drain down to the second (TRU.Spec) column and rinsed twice with 0.5 ml of 2 M HNO_3 (Fig. 1A). Then, the columns were decoupled (Fig. 1B). Analysis of the fractions collected showed that all of the major elements were quantitatively eluted at this stage. Only ca. 2% of Fe was retained on the TRU.Spec column, but this was washed off by two additional 0.5 ml aliquots of 2 M HNO_3 (Fig. 2).

After decoupling, the Sr.Spec column was washed with six 0.5 ml portions of 7 M HNO_3 then with 0.5 ml of 3 M HNO_3 to elute Ba. The use of 7 M HNO_3 resulted in a much narrower Ba peak (Fig. 2) compared to that obtained with 3 M acid [8]. Elution of Sr was performed with four 0.5 ml aliquots of 0.05 M HNO_3, with ca. 95% recovery.

The TRU.Spec column was washed with 8 portions of 2 M HNO_3, each 0.5 ml, to displace any remaining unwanted cations (mainly residual iron). The end of Y and heavy lanthanide elution occurred at this stage. Of the light rare earths, only La began to elute. The eluent was switched to 0.05 M HNO_3. Four 0.5 ml aliquots stripped 94–97% of Ce–Pr–Nd–Sm (Fig. 2). 60% of the lanthanum, 85% of the europium and 40% of the gadolinium loaded were found in this fraction together with less than 0.5% of the zirconium present in the sample. On the basis of available data [11], Zr should be strongly retained on TRU.Spec from 2 M nitric acid. This was not observed in our case. Zr eluted during the loading and rinsing steps, presumably as a fluoride complex formed during the sample dissolution with HF–HNO_3.

Twelve international silicate Reference Materials were analysed (as supplied) in triplicate following the methods outlined above. For the first batch of analyses (referred to as 0 in Table 1), scheme 1 was used, while the second and third batches (referred to as I and II in Table 1) were performed following the scaled-down procedure (scheme 2). The geostandards analysed encompass a range of major element composition and highly variable concentrations of minor elements which could adversely affect the quality of mass spectrometric measurements, e.g., Ca, Ba and Rb for strontium, Ba for neodymium. The results are listed in Table 1. In every case, stable and long-lasting ion beams were obtained, and within-run precisions were similar to

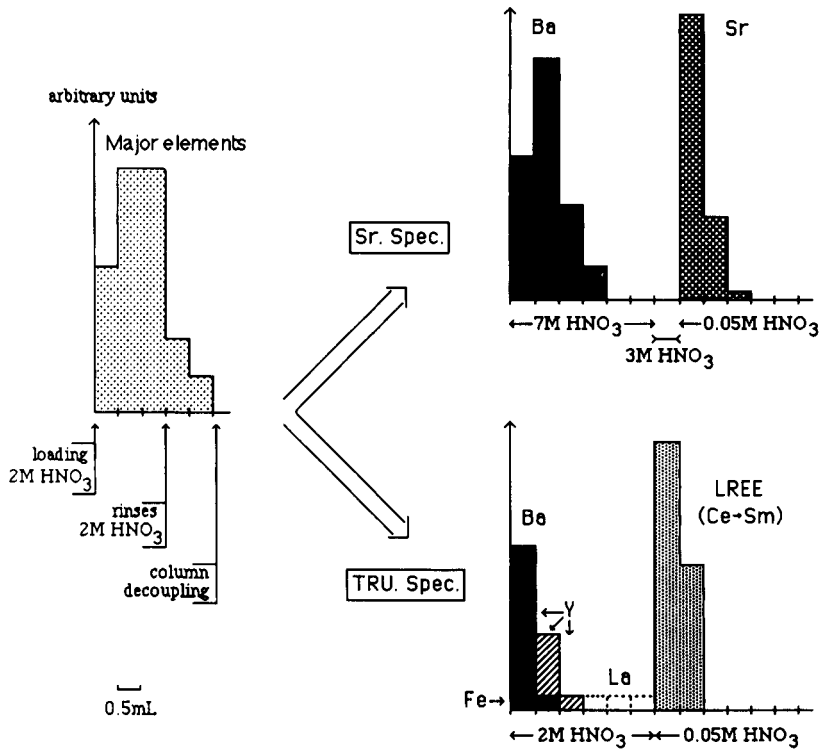

Fig. 2. Typical elution profiles for columns containing 83 mg (0.25 ml) of Sr.Spec and TRU.Spec materials.

those obtained when processing pure salts of the elements. The reproducibility of the method can be evaluated from the three replicate analyses. These were performed on different powder aliquots, and at least some of the observed scatter might reflect heterogeneous sub-sampling at the 100 mg level. Bearing in mind the external reproducibility of our mass spectrometer during the one year period of the analyses expressed by the standard deviation of 8 measurements of $^{87}Sr/^{86}Sr$ in the NIST SRM 987 strontium carbonate ($\sigma = 2 \times 10^{-5}$) and 10 analyses of $^{143}Nd/^{144}Nd$ of the La Jolla neodymium standard ($\sigma = 15 \times 10^{-6}$), most of the differences observed are barely outside analytical uncertainty. However, data for AC-E and GH show significant scatter of $^{87}Sr/^{86}Sr$. These variations occur in rocks with large Rb/Sr ratios, which developed with time high $^{87}Sr/^{86}Sr$ through radioactive decay of ^{87}Rb. Therefore, differences in Sr isotope composition might reflect powder heterogeneity for the Rb/Sr ratio at the sub-sampling level, as shown elsewhere for the NIST K-feldspar standard [17].

Because of the limited amount of isotopic data available on geological Standard Reference Materials (SRM), the accuracy of our results is rather difficult to assess. However, the $^{87}Sr/^{86}Sr$ and $^{143}Nd/^{144}Nd$ ratios measured in this study are in reasonably good agreement with values reported by other laboratories (Table 1) for two basaltic SRMs from the U.S. Geological Survey (BHVO-1) and the Geological Survey of Japan (JB-1a).

Several requirements must be met when considering a separation method for use prior to TIMS measurements:

(i) the method should isolate the element of interest in a high degree of purity, enabling good ionization efficiency and stable emissions to be obtained;

(ii) the chemical yields should be as high as possible, enabling small or/and depleted samples to be analysed;

(iii) the procedural blanks should be negligible with regard to the quantities analyzed;

(iv) the method should preferably use small quantities of a limited number of simple reagents easy to purify and to eliminate;

(v) the method should be straightforward, i.e., simple, rapid, robust.

Table 1
Sr and Nd isotopic results for international silicate reference materials, after separation of the analytes on Sr.Spec and TRU.Spec columns

Reference material	Sr (μg/g)	Nd (μg/g)		$^{87}Sr/^{86}Sr$	$^{87}Sr/^{86}Sr$ litt.	$^{143}Nd/^{144}Nd$	$^{143}Nd/^{144}Nd$ litt.
			0			0.512863 (7)	
AC-E	3	92	I	0.87921 (3)		0.512880 (6)	
			II	0.87722 (3)		0.512855 (8)	
			0	0.70393 (2)		0.512794 (6)	
AGV-1	662	33	I	0.70394 (2)		0.512789 (6)	
			II	0.70391 (2)		0.512795 (6)	
			0	0.70377 (3)		0.512886 (5)	
BE-N	1370	70	I	0.70377 (2)		0.512886 (6)	
			II	0.70377 (2)		0.512871 (10)	
			0	0.70341 (3)	0.70347 ± 4 (ref. [22])	0.512969 (6)	0.512996 ± 12 (ref. [23])
BHVO-1	403	25.2	I	0.70342 (2)	0.70339 ± 4 (ref. [21])	0.512993 (8)	0.51301 ± 2 (ref. [21,22])
			II	0.70341 (2)		0.512971 (11)	0.512991 ± 14 (ref. [24])
			0	0.70309 (5)		0.513084 (8)	
BIR-1	108	2.5	I	0.70307 (2)		0.513069 (8)	
			II	0.70305 (2)		0.513088 (15)	
			0	0.70791 (2)		0.512439 (6)	
DR-N	400	23	I	0.70796 (2)		0.512435 (9)	
			II	0.70793 (2)		0.512433 (12)	
			0	0.70968 (4)		0.512208 (6)	
G2	478	55	I	0.70973 (2)		0.512192 (12)	
			II	0.70973 (1)		0.512203 (7)	
			0			0.512442 (6)	
GH	4.8	29	I	1.70336 (2)		0.512393 (7)	
			II	1.70069 (3)		0.512349 (8)	
			0	0.70406 (2)	0.704083 ± 16 (ref. [19])	0.512793 (7)	0.512784 ± 11 (ref. [19])
JB1a	443	24	I	0.70408 (2)		0.512770 (7)	0.512780 ± 9 (ref. [20])
			II	0.70407 (2)		0.512793 (7)	
			0	0.70415 (6)		0.512782 (5)	
RGM-1	108	19	I	0.70413 (2)		0.512813 (7)	
			II	0.70410 (2)		0.512782 (8)	
			0	0.70371 (4)		0.512915 (5)	
STM-1	18.6	79	I	0.70367 (2)		0.512904 (9)	
			II	0.70368 (2)		0.512910 (11)	
			0	0.70694 (2)		0.512522 (5)	
W2	194	14	I	0.70695 (2)		0.512513 (8)	
			II	0.70695 (2)		0.512519 (11)	

Values in parentheses: uncertainties on the last digits are based on within-run statistics and given at the 95% confidence level. During the period of the analyses, measurements of the NIST SRM 987 strontium carbonate gave $^{87}Sr/^{86}Sr = 0.71021$ (S.D. = 0.00002, $n = 8$) and the La Jolla neodymium isotopic standard gave $^{143}Nd/^{144}Nd = 0.511850$ (S.D. = 0.000015, $n = 10$).

In order to assess the degree of purity of the elements separated from basaltic (BHV0-1; BIR-1), granitic (G2) and intermediate (AGV-1) samples, ICP-MS semi-quantitative analyses of Sr and LREE separated following our procedure (scheme 2) were done. Sr separates were found to contain only negligible Ca (twice the blank level of the instrument), and the separation from Ba and Rb was excellent with decontamination factors (defined [18] as the ratio of impurity recovery to Sr recovery) comprised between 1 and

Table 2
Blanks and memory effect data given in nanograms measured for two Sr.Spec columns A and B

	Column A	Column B
Sr-blank after 1 wash-resettling with 5 ml 0.05 M HNO_3[a]	57	58
Sr-blank after 4 wash-resettling with 8 ml 0.05 M HNO_3[a]	12	13
Sr-blank after 12 wash-resettling with 8 ml 0.05 M HNO_3[a]	6.9	7.2
Memory effect after elution of 50 $\mu g\ g^{-1}$ Sr and wash-resettling with 5 ml 0.05 M HNO_3	82	54
Same after 3×2 ml wash with 0.1 M H_2SO_4 and resettling with 5 ml 0.05 M HNO_3	5.6	4.4
Same after 3 washes with 7 ml 0.1 M H_2SO_4 and resettling with 5 ml 0.05 HNO_3	1.4	1.0
Previously used resin after one year soaking in 0.05 M HNO_3	2.5	2.4
Same as before with additional wash with 2 ml of 0.1 M H_2SO_4	0.62	0.63
Same as before with 3×5ml 0.1 M H_2SO_4 washes and resettling in 0.05 M HNO_3	0.34	0.36

[a]See Ref. [8] for details.

4×10^{-4}. Likewise, semi-quantitative analyses of LREE separates revealed only Zr in minor quantities (less than one part in 10^3 of the quantity initially present in the sample) corresponding to a decontamination factor of Nd with regard to Zr of about 4×10^{-3}. Ba was very low in every case, and possibly due to contamination. As anticipated from the good quality of mass spectrometer runs, these results show that the selectivity and the capacity of both Sr.Spec and TRU.Spec materials are good enough to afford the extraction of sufficiently pure Sr and LREE in a single pass on very small columns. In common silicate rocks, the few co-extracted elements (Ba and Pb on Sr.Spec, Bi, Th and U on TRU.Spec) occur only at trace levels, and do not interfere significantly with the separation of the elements of interest. Barium can be stripped from the column before Sr breakthrough, while the other elements are retained when elution of Sr and the LREE is performed with 0.05 M HNO_3.

Column yields measured for Sr and Ce–Pr–Nd–Sm are >90%, showing that only minor amounts of these elements escape extraction or undergo early breakthrough. Both Sr and the LREE are stripped from the columns with a small volume of very dilute nitric acid which can be eliminated readily by evaporation.

Blanks and memory effects deserve special attention when dealing with isotopic work, where subtle differences (a few parts in 10^5) are often sought. Blanks measured on two Sr.Spec columns containing new resin were comprised between 30 and 150 pg, and were only marginally higher than reagent plus evaporation blanks carried out at the same time which ranged from 30 to 60 pg (Table 2). In most analytical situations, involving the separation of several micrograms of Sr, such blanks would be negligible.

Although more than 95% of the Sr extracted is readily stripped with 0.05 M HNO_3, we found in our previous study [8] that a totally quantitative recovery was not obtained, even after several cycles of washing–resettling or washing the resin with warm 0.05 M HNO_3. Blanks measured on previously used resin ranged from 80 ng to 7 ng, corresponding to memory effects ranging from 0.1 to 1‰ of the amount of Sr previously "seen" by the column. These high values are a significant limitation for isotope geochemistry applications in which samples with widely varying concentrations (from 1 to >1000 $\mu g/g$) and $^{87}Sr/^{86}Sr$ (from 0.702 to >2) are analysed, and preclude re-using the columns. Subsequent measurements showed that very prolonged soaking of the resin in 0.05 M HNO_3 during one year decreased blank levels to ca. 2.5 ng (Table 2). In a further attempt to reduce the memory of previously used Sr.Spec, we used dilute sulfuric acid, which was suggested to remove lead, an element very strongly retained by Sr.Spec [7]. Indeed, successive washings with 0.1 M H_2SO_4 improved the stripping of residual Sr and reduced the blank to values below the ng level (Table 2). This suggests that the Sr.Spec resin could be re-used only after a thorough treatment and a careful check.

Nd blanks on TRU.Spec have been determined by isotope dilution TIMS. Three measurements for new resin contained in new polypropylene columns gave results around 150 pg while reagent plus evaporation and loading blank was $\leq$10 pg (Table 3). Five additional blanks conducted on new resin contained in used

Table 3
Blanks and memory effect data for Nd on TRU.Spec SPS columns

New resin in new polypropylene columns				
145 pg	163 pg	167 pg		
New resin in already used polypropylene columns				
260 pg	590 pg	260 pg	80 pg	280 pg
Reagent + evaporation blanks including loading blank				
≤ 10 pg				
Memory effect				
1.33 ng (after AC-E I)	1.48 ng (after G2 II)	1.68 ng (after RGM II)		

polypropylene columns gave much more scattered results, ranging from 80 pg to 590 pg (Table 3). This suggests that soaking at room temperature in dilute HNO_3 was not sufficient for perfect cleaning of the plastic columns. Also, the lowest measured value implies that the contribution of the TRU.Spec material itself is probably less than 100 pg. In order to evaluate the extent of memory effects, Nd blanks have also been measured on already used resin (83 mg material), after a single wash with 5 ml of 0.05 M HNO_3. The results are closely grouped at ca. 1.5 ng, despite the fact that the amount of analyte previously loaded on the columns varied largely (from 2 to 15 μg, assuming a quantitative yield of the dissolution steps). These data show that, as for Sr.Spec, a significant quantity of the extracted element remains tightly bound to the TRU.Spec material during elution with 0.05 M HNO_3. Although Nd concentrations and $^{143}Nd/^{144}Nd$ ratios show a more limited spread in geological samples compared to Sr, this memory effect cannot be neglected. Considering the small amount or resin used, it is therefore advisable to discard the TRU.Spec material after every sample.

4. Conclusions

The newly introduced specific extraction chromatographic materials Sr.Spec and TRU.Spec show very promising properties for applications in isotope geochemistry. These afford a straightforward separation of Sr and Sm + Nd with high yield, good purity and satisfactory blank levels, by using small amounts of solutions of a single mineral acid. The only significant drawback recognised as yet compared to conventional ion-exchange resins is the fact that these materials are prone to memory effects, requiring the use of new resin whenever low blank levels are necessary. This disadvantage is to a large extent compensated for by the considerable miniaturisation made possible, which alleviates the need for large quantities of reagents and long separation time.

Acknowledgements

We would like to thank Ph. Telouk and J.L. Imbert (SCA CNRS, Vernaison) for generous access to ICP-MS facilities, and S. Rajkovich (EichroM Ind.) for information on extraction chromatographic materials.

References

[1] L.T. Aldrich, J.B. Doak and G.L. Davis, Am. J. Sci., 251 (1953) 377.
[2] T. Andersen and A.B. Knutsen, Acta Chem. Scand., 16 (1962) 849.
[3] T. Danon, J. Inorg. Nucl. Chem., 5 (1958) 237.
[4] M.L. Dietz and E.P. Horwitz, LC·GC, 11 (1993) 424.
[5] E.P. Horwitz, D.G. Kalina, H. Diamond and F. Vandegrift, Solvent Extr. Ion Exch., 3 (1985) 75.
[6] E.P. Horwitz, M.L. Dietz and R. Chiarizia, J. Radioanal. Nucl. Chem., Art., 161 (1992) 575.
[7] E.P. Horwitz, M.L. Dietz and D.E. Fisher, Anal. Chem., 63 (1991) 522.
[8] C. Pin and C. Bassin, Anal. Chim. Acta, 269 (1992) 249.
[9] E.P. Horwitz, R. Chiarizia and M.L. Dietz, Solvent Extr. Ion Exch., 10 (1992) 313.
[10] R. Chiarizia, E.P. Horwitz and M.L. Dietz, Solvent Extr. Ion Exch., 10 (1992) 337.
[11] E.P. Horwitz, R. Chiarizia, M.L. Dietz, H. Diamond and D.M. Nelson, Anal. Chim. Acta, 281 (1993) 361.
[12] J.W. Winchester, J. Chromatogr., 10 (1963) 502.
[13] R. Sochaska and S. Siekierski, J. Chromatogr., 16 (1964) 376.
[14] A.S. Cohen, R.K. O'Nions, R. Siegenthaler and W.L. Griffin, Contrib. Mineral. Petrol., 98 (1988) 303.
[15] J.L. Birck, Chem. Geol., 56 (1986) 73.

[16] L. Briqueu, personal communication.
[17] K.A. Foland and J.C. Allen, Contrib. Mineral. Petrol., 109 (1991) 195.
[18] D. De Soete, R. Gijbels and J. Hoste, Neutron Activation Analysis, Wiley-Interscience, London, 1972, p. 351.
[19] H. Kagami, H. Yokose and H. Honma, Geochem. J., 23 (1989) 209.
[20] Y. Arakawa, Geochem. J., 26 (1992) 105.
[21] C.Y. Chen, F.A. Frey and M.O. Garcia, Contrib. Mineral. Petrol., 105 (1990) 197.
[22] C.Y. Chen, F.A. Frey, M.O. Garcia, G.B. Dalrymple and S.R. Hart, Contrib. Mineral. Petrol., 106 (1991) 183.
[23] R. Maas and M.T. McCulloch, Geochim. Cosmochim. Acta, 55 (1991) 1915.
[24] A. von Quadt, Contrib. Mineral. Petrol., 110 (1992) 57.

ELSEVIER

Analytica Chimica Acta 298 (1994) 219–223

ANALYTICA CHIMICA ACTA

Solid-phase microextraction using pencil lead as sorbent for analysis of organic pollutants in water

Hai Bin Wan, Hua Chi, Ming Keong Wong *, Chup Yew Mok

Department of Chemistry, National University of Singapore, Lower Kent Ridge Road, Singapore 0511, Singapore

Received 1 March 1994; revised manuscript received 16 May 1994

Abstract

Most solid-phase microextraction methods are based on poly(dimethylsiloxane)-coated silica fibers. In the present study, pencil lead was used as an alternative sorbent for solid-phase microextraction. Its application to three organic pollutants with different polarity in water was investigated. The detection limit for determination by gas chromatography with electron capture detector was 0.005 ng ml^{-1} for lindane, 0.05 ng ml^{-1} for methyl parathion and 1 ng ml^{-1} for 2-chlorophenol. The presence of dissolved humic substances (10 mg l^{-1}) in water did not affect the extraction of the three analytes.

Keywords: Chromatography; Solid-phase microextraction; Extraction; Pencil lead; Organic pollutants; Waters

1. Introduction

Solid-phase microextraction (SPME) is a fast, simple and sensitive technique, which does not require the use of organic solvents. In SPME, sorbent coated silica fibers are used to extract analytes from aqueous or gaseous samples. After extraction, the fibers are directly transferred into the injection port of a gas chromatograph via a modified syringe, after which the analytes are thermally desorbed and subsequently analyzed. The sampling technique was first described by Belard and Pawliszyn in 1989 [1], and since then the technique has been applied to the analysis of benzene and its substituted derivatives in water at trace level [2,3], aromatic compounds in ground water [4], halogenated volatiles in water [5] and in foods [6], selected PCBs [7,8], polyaromatic hydrocarbons [8], and caffeine in beverages [9]. Very recently, the technique was used to determine phenols in water [10], in which the extraction of the polar compounds was achieved by using a relatively polar sorbent coated on silica fibers. Extensive studies on the dynamics of adsorption and optimization of SPME have also been conducted by Louch et al. [11], Arthur et al. [12] and Buchholz and Pawliszyn [13].

Most of the previous SPME methods were based on relatively non-polar poly(dimethylsiloxane)-coated silica fibers. In one case, poly(acrylate)-coated silica fibers were used for polar compounds. In the conventional solid-phase extraction procedures, graphitized carbon black, a very popular sorbent, is used for the extraction of relatively polar compounds [14–16]. Fibers coated with or made of graphitized carbon black also seem to be a good alternative sorbent for SPME. Since this kind of fibers was not available, we turned to other materials with similar properties. Pencil lead, which is made mainly of graphite, seemed to be a very convenient choice. A study on the application of pencil

* Corresponding author.

SSDI 0003-2670(94)00270-V

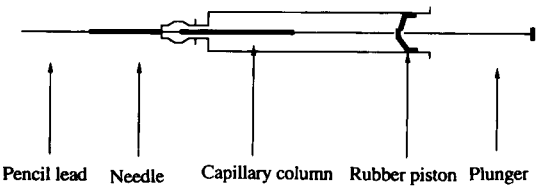

Fig. 1. Syringe assembly used in SPME. When the plunger is pulled back, the pencil lead is drawn inside the needle to protect it from breakage when the septum of a GC injector is pierced.

lead to SPME was therefore carried out with three organic pollutants of different polarity. In this study, several kinds of pencil lead were tested primarily to choose a suitable material. A more detailed investigation aimed at optimizing the conditions for extraction and GC analysis was subsequently carried out with the selected pencil lead.

2. Experimental

2.1. Materials

The modified syringe assembly used in SPME is shown in Fig. 1. A pencil lead (60×0.3 mm) and a plunger from a 10-μl GC syringe were glued together into a capillary column segment (4 cm×0.53 mm i.d.) by a commonly used super glue. The rod was inserted into a 3-ml single use medical syringe with a hypodermic needle (gauge 21). The rubber piston taken from the plunger of the medical syringe was glued to the tube wall of the syringe. It can prevent the leaking of carrier gas through the syringe when the needle is inserted into the GC injector and can also hold the plunger in the right position to protect the pencil lead from breakage. When the plunger is retracted, the lead is drawn into the needle. This protects the lead when the syringe needle is used to pierce the septum of a sample vial or GC injector. The plunger can then be pushed down to expose the lead to the sample solution during the extraction or to the GC carrier gas during thermal desorption. The pencil lead selected was a HB type spare lead (60×0.5 mm; brand name Pacer; made in Japan). It was rinsed with acetonitrile to remove the coating material and then ground thinner to fit the syringe needle using a piece of sand paper (P600A). The lead was rinsed with dichloromethane and then conditioned at 290°C for 5 h before use.

The analytical standards 2-chlorophenol, lindane and methyl parathion from ChemService (West Chester, PA) were dissolved in methanol at 1 mg ml^{-1} as stock solutions. They were used to prepare standard solutions for GC analysis and to spike water samples. A mixture of humic acid, obtained from Kasei (Tokyo), was used to study the effect of humic substances in water on the extraction efficiency. Water samples containing the humic acid equivalent to ca. 10 mg l^{-1} of dissolved humic substances was prepared following the procedures described by Johnson et al. [17]. Distilled water was used to prepare the spiked solutions. The pH of the solutions were adjusted to 5 or 2 with a 0.1 M HCl.

2.2. Methods

The GC analysis was carried out on an Hewlett-Packard 5890A gas chromatograph equipped with a flame ionization detector (FID) and an electron capture detector (ECD). The column used was a HP 17 Megabore column (Hewlett-Packard), 10 m×0.53 mm i.d., 2.0-μm film thickness. The flow rate of the carrier gas was set at 7 ml min^{-1}. A split/splitless injector was used in the splitless mode. The injector temperature was maintained at 170°C for 2-chlorophenol and 200°C for lindane and methyl parathion. The desorption time was 8 min. The oven temperature program was as follows: 40°C (for chlorophenol) or 55°C (for lindane and methyl parathion) for 8 min; increase to 250°C at a rate of 20°C min^{-1}; final holding time 10 min.

Suitable conditions for thermal desorption were selected by using a two-level orthogonal array design. This is a kind of fractional factorial design which uses orthogonal arrays to arrange experiments. Compared to conventional factorial design, it is more convenient for arranging the experiment and for data analysis. Details on this method have been described elsewhere [18,19]. Three relevant variables were examined: the injector temperature, desorption time, and initial oven temperature. To fully use the capacity of the design, the effect of solution pH was also examined. Eight experiment runs were accordingly carried out. The important variables were identified by analysis of variance technique and further optimized by a sequential simplex method. The selection of the levels for each variable was based on the conditions used in previously reported SPME methods. The details on the assignment

Table 1
Assignment of the variables and the arrangement of the experiment runs using an OA_8 (2^7) matrix

Trial	Column[a]						
	1	2	3	4	5	6	7
1	170	5		40			2
2	170	5		55			5
3	170	7		40			5
4	170	7		55			2
5	190	5		40			5
6	190	5		55			2
7	190	7		40			2
8	190	7		55			5

[a](1) Injector temperature (°C); (2) desorption time (min); (3) interaction between the injector temperature and the desorption time; (4) initial oven temperature (°C); (5) interaction between injector temperature and the initial oven temperature; (6) interaction between desorption time and the initial oven temperature; (7) assigned to the solution pH.

of the variables and the levels are given in Table 1.

Under the optimum GC conditions, the effects of the extraction time, the dissolved humic substances, and the properties of the analytes were investigated. The detection limits were determined by comparing the signal-to-noise ratio (S/N) of the lowest detectable concentration to a S/N of 3. For example, if a 2 ng ml^{-1} solution gave a S/N of 6, the detection limit was calculated to be 1 ng ml^{-1}.

3. Results and discussion

The thermal desorption was affected mainly by four factors: the injector temperature, desorption time, initial oven temperature, and the properties of the analytes. Higher injector temperature can reduce the desorption time and thus shorten the time for GC analysis. However, higher injector temperature is likely to cause thermal decomposition of some thermal labile analytes. Too high a injector temperature may also affect the cryofocusing of the analytes in the inlet part of the GC column. A relatively low initial oven temperature is good for reconcentration of the analytes in the inlet part of the GC column. On the other hand, a lower initial oven temperature will require a longer time for the instrument to cool down from the previous run. The thermal desorption conditions also depend on the properties of the analytes. A more volatile compound will require a lower injector temperature, shorter desorption time and lower initial oven temperature.

According to the analysis of variance results from the designed experiment, the peak area counts of methyl parathion increased by 23% when the injector temperature was increased from 170°C to 190°C, and the change of the desorption time from 5 min to 7 min caused the peak area to increase by 28%. The two variables had no effect on lindane, which is more volatile than methyl parathion, within the experimental space. When the initial oven temperature was increased from 40 to 55°C, the peak area and height of the two analytes did not change significantly. The desorption conditions for lindane and methyl parathion were therefore primarily set as follows: injector temperature, 190°C; desorption time, 7 min; initial oven temperature, 55°C. More accurate optimum injector temperature and desorption time located by a sequential simplex method were 200°C for the injector temperature and 8 min for the desorption time. The experimental results also showed that the solution pH had no significant effects on the extraction of lindane and methyl parathion within the range of pH 2 to 5. As a lower solution pH is good for the extraction of phenols [10], the pH of all the spiked solutions was adjusted to pH 2 in later experiments.

For 2-chlorophenol, which is more volatile than lindane and methyl parathion, the thermal desorption conditions were adjusted by trial and error starting from those for lindane and methyl parathion. The injector temperature was 170°C, the desorption time was 8 min, and the initial oven temperature 40°C.

In SPME of analytes with relatively high boiling points, carryover could be a problem. It may interfere with the analysis of following samples. In the present study, carryover was investigated at three temperatures (150, 170 and 200°C). The results are given in Table 2. They are for three successive blank desorptions following the exposure to a solution containing lindane (2 ng ml^{-1}) and methyl parathion (10 ng ml^{-1}). As shown in Table 2, the carryover is very serious at 150°C. At 200°C, however, the amount of the analytes remained on the sorbent after the initial desorption was less than 5%. The effect of carryover on the analysis of following samples can be minimized by keeping the sorbent in the injection port for another 8 min after the initial desorption.

Table 2
Carryover of lindane and methyl parathion on the pencil lead during the desorption

Compound	Temperature (°C)	%Carryover[a]		
		Blank 1	Blank 2	Blank 3
Lindane	150	16.4	8.3	5.5
	170	9.9	4.2	2.0
	200	3.1	0.1	<0.05
Methyl parathion	150	35.0	18.6	11.1
	170	22.0	10.0	5.0
	200	1.0	0.1	<0.05

[a]Expressed as percent area of initial desorption peak.

Fig. 2 shows the adsorption vs. time profiles for lindane and methyl parathion in the mixture. The extraction was near equilibrium when the extraction time was longer than 20 min. An extraction time of 30 min should be sufficient to extract maximum amounts of analytes from water. The time required for the extraction to reach equilibrium depends on how the solution is stirred. The extraction time can be shortened by increasing the stirring rate. In the present study, the stirring rate was maintained constant for each extraction. A GC run will normally take 30–40 min. The extraction can be carried out while the gas chromatograph is analyzing the previously extracted sample. In this case, the extraction actually causes no delay in the analysis.

The detection limit of SPME depends on the amount of the analytes adsorbed by the sorbent and the sensitivity of the GC detectors. The amount extracted depends on the affinity of the analytes to the sorbent and the concentration of the analytes. An equation describing these relationships has been given by Buchholz and Pawliszyn [10]. In the present study, we used the equivalent sample volume (ESV) to estimate the extraction ability of the sorbent. An ESV value of 2 means that the amount of the analyte extracted by the sorbent is equivalent to the amount contained in 2 ml of the solution extracted. ESV depends on the affinity of the analytes to the sorbent and is not affected by the analyte concentration within the linear range. The ESV for the three analytes were determined to be 0.70 ml for lindane, 0.16 ml for methyl parathion, and 0.14 ml for 2-chlorophenol. These data indicate that the amount of the analytes introduced to the chromatograph by one SPME is equivalent to introducing 0.14–0.7 ml of water sample to the GC system. Lindane has a relatively high water solubility (7 mg l^{-1}) among the organochlorine insecticides. Therefore, the ESV value for other organochlorine insecticides, such as dieldrin and DDT, should be higher than 0.7 ml. The detection limit was found to be 0.005 ng ml^{-1} for lindane, 0.05 ng ml^{-1} for methyl parathion, and 1 ng ml^{-1} for 2-chlorophenol.

The linear relationship between the concentration of the analytes and the GC peak area was studied using spiked solutions. The linear range was 10–100 ng ml^{-1} for 2-chlorophenol, 1–100 ng ml^{-1} for methyl parathion, and 1–20 ng ml^{-1} for lindane when an electron capture detector was used. When the concentration of lindane was increased from 20 to 100 ng ml^{-1}, the peak area only doubled. When flame ionization detection was used, a linear relationship was obtained within the range of 20–100 ng ml^{-1}. Concentrations higher than 100 ng ml^{-1} were not studied.

It has been reported that humic substances dissolved in water can reduce the efficiency of solid-phase extraction either by the association with the analytes or by saturation of the sorbent [15–17]. In the present study, the effects of dissolved humic substances were investigated. The results were given in Table 3. The results indicate that the extraction was not affected by humic acid with a concentration equivalent to 10 mg l^{-1} of dissolved humic substances.

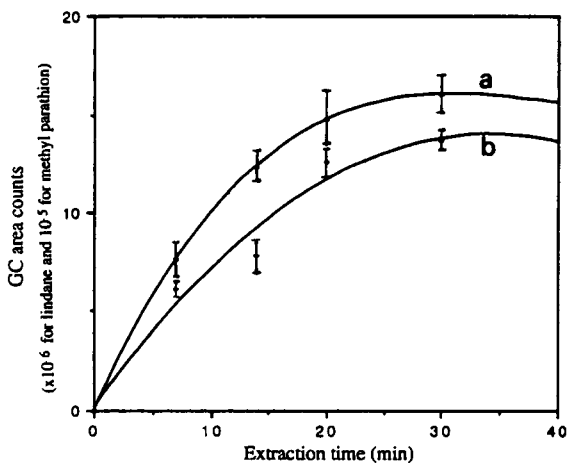

Fig. 2. Adsorption time profiles: (a) Lindane at 2 ng/ml; (b) methyl parathion at 10 ng/ml. (Mean of two replicate determinations for each point.)

Table 3
Effects of dissolved humic substances on SPME

Humic substances (mg l^{-1})	Amount extracted[a] (ng)		
	Chlorophenol	Lindane	Methyl parathion
0	6.8 ± 0.2	25.5 ± 2.2	7.6 ± 1.4
10	7.1 ± 0.8	28.7 ± 2.2	8.1 ± 0.8

[a]Mean of two replicated extractions of solutions containing the 3 analytes at 50 ng ml^{-1}.

Fig. 3 shows the chromatograms of water samples spiked by the three analytes. The sorbent did not produce peaks affecting the analysis during the desorption at 200–210°C. When the temperature was increased to 240°C, however, the sorbent gave two tailing peaks. The two peaks could not be removed by prolonging the conditioning time, but can be considerably reduced by lowering the injector temperature. The pencil lead used contained a kind of polymer to increase the strength of the material. It is possible that the bleeding peaks were caused by the thermal decomposition of the polymer during the thermal desorption. For this reason, the desorption temperature should not be higher than 210°C.

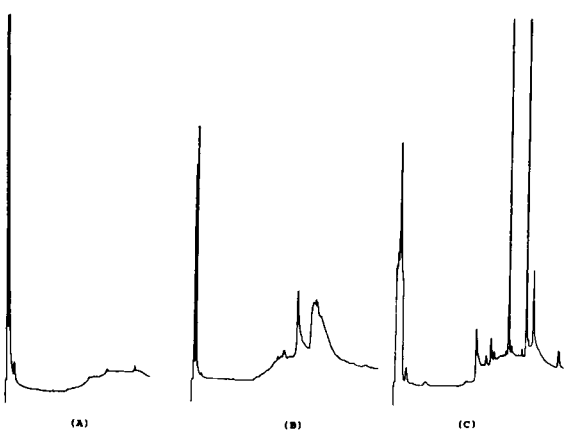

Fig. 3. Chromatograms of water samples extracted by solid-phase microextraction. (A) distilled water, desorption temperature 200°C; (B) distilled water, desorption temperature 240°C; (C) water spiked with 2-chlorophenol (retention time = 11.1 min, 50 ng ml^{-1}), lindane (retention time = 17.8 min, 0.5 ng ml^{-1}), and methyl parathion (retention time = 18.7 min, 10 ng ml^{-1}), desorption temperature 200°C.

Acknowledgements

WHB thanks the National University of Singapore for the award of a research scholarship.

References

[1] R.P. Belard and J.B. Pawliszyn, Pollut. Res. J. Can., 23 (1989) 179.
[2] D.W. Potter and J.B. Pawliszyn, J. Chromatogr., 625 (1992) 247.
[3] C.L. Arthur, K. Buchholz, J. Berg and J.B. Pawliszyn, Anal. Chem., 64 (1992) 1968.
[4] C.L. Arthur, L.M. Killam, S. Motlagh, D.W. Potter and J.P. Pawliszyn, Environ. Sci. Technol., 26 (1992) 979.
[5] C.L. Arthur, L. Killam, K. Bucholz, J. Berg and J. Pawliszyn, High Resolut. Chromatogr., 15 (1992) 741.
[6] B.D. Page and G. Lacroix, J. Chromatogr., 648 (1993) 199.
[7] C. Arthur and J. Pawliszyn, Anal. Chem., 62 (1990) 2145.
[8] D.W. Potter and J. Pawliszyn, Environ. Sci. Technol., 28 (1994) 298.
[9] S.B. Hawthorne, D.J. Miller, J. Pawliszyn and C.L. Arthur, J. Chromatogr., 603 (1992) 185.
[10] K.D. Buchholz and J. Pawliszyn, Environ. Sci. Technol., 27 (1993) 2844.
[11] D. Louch, S. Motlagh and J. Pawliszyn, Anal. Chem., 64 (1992) 1187.
[12] C.L. Arthur, L.M. Killam, K.D. Buchholz and J. Pawliszyn, Anal. Chem., 64 (1992) 1960.
[13] K.D. Buchholz and J. Pawliszyn, Anal. Chem., 66 (1994) 160.
[14] A. Di Corcia, M. Marchetti and R. Samperi, Anal. Chem., 58 (1986) 2048.
[15] A. Di Corcia and R. Samperi, Anal. Chem., 65 (1993) 907.
[16] I. Lisca, E.R. Brouwer, H. Lingeman and U.A.Th. Brinkman, Chromatographia, 37 (1993) 13.
[17] W.E. Johnson, N.J. Fendinger and J.R. Plimmer, Anal. Chem., 63 (1991) 1510.
[18] P.J. Oles, J. AOAC Int., 76 (1993) 615.
[19] H.B. Wan, W.G. Lan, M.K. Wong and C.Y. Mok, Anal. Chim. Acta, 289 (1994) 371.

ELSEVIER

Analytica Chimica Acta 298 (1994) 225–232

ANALYTICA CHIMICA ACTA

Sorption of metal ions on a weak acid cation-exchange resin containing carboxylic groups

Maria Pesavento *, Raffaela Biesuz, José Louis Cortina

Dipartimento di Chimica Generale, Università degli Studi di Pavia, viale Taramelli, n. 12, 27100 Pavia, Italy

Received 28 January 1994; revised manuscript received 24 May 1994

Abstract

The sorption properties of a commercial resin containing a carboxylic active group, Amberlite® CG-50, for magnesium, calcium, copper and zinc were investigated on the basis of the Donnan model. It is assumed that the main driving force for the sorption of divalent metal ions is the complexation by the carboxylic groups inside the resin. Under typical batch conditions (large excess of ligand) only the 1:2 complexes are formed for all metal ions considered, whereas in aqueous solution only 1:1 complexes are reported for calcium and magnesium and the monomeric analogues of the active group of Amberlite® CG-50. The intrinsic complexation constants obtained from the batch experiments agree well with those in aqueous solution. The same holds for the intrinsic complexation constant evaluated from chromatographic experiments. This confirms some previous results obtained with a chelating resin containing an iminodiacetic group, Chelex 100. The values of the complexation constants for the carboxylic groups found with Chelex 100 are in agreement with those found with Amberlite® CG-50.

Keywords: Ion exchange; Metal ions

1. Introduction

The protonation and ion-exchange properties of chelating resins can be predicted from the protonation and complexation constants in aqueous solution of the corresponding hydrosoluble active groups on the basis of the Donnan model [1–3].

In this work, the sorption of divalent metal ions on a weak acid cation-exchange resin containing carboxylic groups was examined. It is widely believed that the sorption of metal ions on such a resin takes place through simple ion exchange. However, it is well known that substances carrying carboxylic groups, e.g., acetic acid, are able to complex a number of divalent metal ions in aqueous solution. The aim of this paper is to show that this complexation takes place also inside the resin and that it is the main driving force for the sorption of divalent metal ions. Hence it can be predicted from the complexing properties of, say, acetic acid in aqueous solution according to the Donnan model. Suppose that the sorption takes place through the equilibrium

$$\mathrm{M} + n\overline{\mathrm{H}_x\mathrm{L}} \leftrightarrow \overline{\mathrm{MH}_{(nx-q)}\mathrm{L}_n} + q\mathrm{H} \qquad (1)$$

where the overbars refer to the resin phase (charges are omitted). Its equilibrium coefficient, β_{nex}, called the exchange coefficient, is related to the thermody-

* Corresponding author.

SSDI 0003-2670(94)00271-M

namic complexation constant β_{ni} by the following relationship [3]:

$$\beta_{nex} = \beta_{ni} \frac{\gamma_M \bar{\gamma}^n_{H_xL}}{\bar{\gamma}_{MH_{(nx-q)}L_n} \gamma^q_H} \frac{a_B^{(z-q)}}{\bar{a}_B^{(z-q)}}$$

$$= \beta_{ni} \frac{\gamma_M \bar{\gamma}^n_{H_xL}}{\bar{\gamma}_{MH_{(nx-q)}L_n} \gamma^q_H} \frac{\bar{a}_C^{(z-q)}}{a_C^{(z-q)}} \quad (2)$$

where γ_Y is the activity coefficient and a_Y is the activity of species Y (in mol kg^{-1}), z is the charge of the metal ion M and B and C are the anion and the cation constituting the ionic medium of the aqueous phase, assumed to be monovalent for the sake of simplicity. The relationship in Eq. 2 between the exchange coefficient and the intrinsic complexation constant has been demonstrated for a number of so-called "loaded resins", in which the active group is a sulfonated azo dye permanently sorbed on a strong base anion-exchange resin by ion exchange [1,2], and for the commercially available Chelex 100 [3], which contains iminodiacetic groups covalently linked to the organic framework. In all these systems the sorption of metal ions on the resin takes place through complexation according to Eq. 1, so that the fraction of sorbed metal ion, f, can be evaluated from the following relationship:

$$f = \frac{\left[\overline{MH_{(nx-q)}L_n}\right] w}{[M]V + \left[\overline{MH_{(nx-q)}L_n}\right] w}$$

$$= \frac{1}{1 + \dfrac{\beta_{nex}\left[\overline{H_xL}\right]^n w}{[H]^q V}} \quad (3)$$

where w is the total amount of water in the resin (grams) and V is the total amount of solvent in the solution (grams).

The Donnan model allows one to evaluate the exchange coefficient β_{nex} by Eq. 2, and so to predict quantitatively the distribution equilibria of metal ions between a chelating resin and an aqueous solution of given acidity and composition. Of course, this point is of interest from a practical point of view. For instance, the selectivity of a chelating resin at given acidity and ionic composition of the aqueous solution can be predicted, and the sorption or elution conditions can be evaluated.

Table 1
Protonation and complexation constants of acetic acid

	$\log \beta_{1i}$	$\log \beta_{2i}$
H^+	4.55[4]	–
Mg(II)	−4.04[5]	–
Ca(II)	−4.02[5]	–
Cu(II)	−2.66[4]	−7.90[4]
Zn(II)	−3.27[4]	−8.29[4]

Acetic acid can be assumed to be a reasonable monomeric model for the active group of the resin Amberlite® CG-50. In Table 1 its protonation and complexation constants in aqueous solution with copper, zinc, calcium and magnesium are shown [4,5]. Both complexes with 1:1 and 1:2 metal to ligand molar composition have been observed in aqueous solution. The complexation constants reported in Table 1 are

$$\beta_{1i} = \frac{[ML][H]}{[M][HL]}$$

$$\beta_{2i} = \frac{[ML_2][H]^2}{[M][HL]^2} \quad (4)$$

In this study the sorption of copper, zinc, calcium and magnesium on the resin Amberlite® CG-50 was investigated. The fraction of sorbed metal ion was experimentally determined and analysed according to Eq. 3. The stoichiometry and the exchange coefficients were compared with those pertinent to the complexation reaction in aqueous solution by Eq. 2. Of course, these values can be used for predicting the distribution of a metal ion between the resin and the aqueous solution. This procedure was used to examine data obtained by a batch procedure and also by column experiments.

2. Experimental

A PHM 84 Research pH meter (Radiometer, Copenhagen) with ABU 80 autoburette (Radiometer) and a combined Orion glass electrode (91-02) were used for the acid–base titrations. A small nitrogen overpressure was applied in the vessel, which was

thermostated at 25 ± 0.3°C. The potentiometric cell for the determination of pH was standardized with respect to H^+ concentration by a previously described procedure [6]. A Perkin-Elmer 1100 B flame atomic absorption spectrometer was used for metal ions determinations. All chemicals were of analytical-reagent grade. Amberlite® CG-50, 100–200 mesh (Aldrich, Steinheim, catalogue N. 21,635-6), delivered in the H^+ form, was used as received. Its water content was determined by drying a known amount of resin at 80°C until a constant weight was reached. The water content was checked once a week. An average value of 93.38 ± 0.84% of dry resin was found over a period of 10 months.

The amount of water and the amount of counter ion in the resin phase, at different degrees of deprotonation were determined as described previously [3].

The acid–base titration curves were obtained by adding a sodium hydroxide solution of known concentration to a volume of 0.1 mol kg^{-1} $NaNO_3$ containing a known excess of acid and a weighed amount of resin as described elsewhere [3]. The final pH was recorded after 1–2 h of equilibration when a steady value of the potential was reached (0.1 mV drift in 10 min).

The sorption isotherms of the metal ions on the resin were determined by a batch procedure as described previously [3].

The elution curves were obtained using a Pyrex column of 11 mm i.d., equipped with a silanized glass-wool plug and a removable stopcock. A 2-g amount of dry Amberlite® CG-50 gives a total bed volume $V_m + V_s = 6.5$ ml. Before each experiment the column was conditioned with a solution of the same ionic composition and acidity of the eluent. A 0.2-ml volume of solution containing the metal ion were introduced at the top of the column and eluted at a flow-rate of 2 ml min^{-1}. Fractions of 3–10 ml were collected and analysed separately for the metal ion content by a standard AAS procedure.

3. Results and discussion

3.1. Characterization of the Amberlite® CG-50 resin

The amount of water sorbed by the resin from sodium nitrate solution at different concentrations and at different degrees of deprotonation are reported in Table 2. It depends mainly on the degree of deprotonation $\alpha = [\overline{L}]/([\overline{L}] + [\overline{HL}])$, the effect of the concentration of the ionic medium being of minor importance.

Table 2
Water content of Amberlite® CG-50 as a function of the degree of deprotonation

	α	q = g H_2O/ g dry resin
$NaNO_3$, 0.1 mol kg^{-1}	0.016	0.90
	0.496	2.13
	0.888	2.49
$NaNO_3$, 1 mol kg^{-1}	0.046	0.84
	0.491	1.99
	0.884	2.18

Amount of dry resin in H^+ form: 0.50 g. Volume of $NaNO_3$ solution: 25 ml.

The total capacity Q of the resin, i.e., the total number of active groups per gram of dry resin, was determined by titration.

A typical acid–base titration curve is reported in Fig. 1, curve 1. One equivalence point is detected in the pH range 3.5–11 examined, corresponding to the neutralization of the carboxylic active group of the resin. No other protonation is detected at more acidic pH values, down to pH 2. The total capacity calcu-

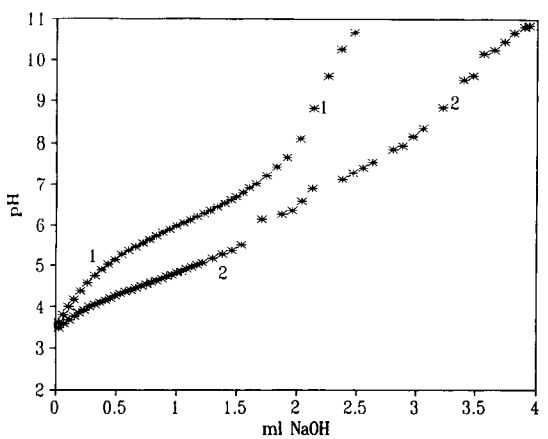

Fig. 1. Titration curve of Amberlite® CG-50 in 1 mol kg^{-1} $NaNO_3$. $T = 25°C$, $V_0 = 34.3$ ml. $N_{NaOH} = 0.192$ mol kg^{-1} $[H_0] = 0$. Amount of dry resin: 0.0402 g. Curve 1: Amberlite CG-50. Curve 2: Amberlite CG-50 and 0.200 mmol of copper(II).

lated from it is $Q = 10.35 \pm 0.38$ mmol/g of dry resin.

The equilibrium coefficient of the proton exchange reaction

$$\overline{L} + H \leftrightarrow \overline{HL} \quad (5)$$

can be evaluated at each point of the acid-base titration curves, on the basis of the equations

$$K_a = \frac{[\overline{HL}]}{[H][\overline{L}]} \quad (6)$$

$$[\overline{L}] = ([H]V - [H_0]V_0 + V_{Tit}N_{Tit})/w \quad (7)$$

$$\overline{C}_L = [\overline{HL}] + [\overline{L}] = Q \cdot (\text{g of dry resin})/w \quad (8)$$

where [H] is the concentration of H^+ measured with the potentiometric cell, $[H_0]$ is the concentration of the excess of proton initially present, V_0 is the amount of solvent (grams) before starting the titration, V_{Tit} is the amount of the titrant added (grams) and N_{Tit} is the titre of the titrant. As the density of the solution is very near 1 g/ml, the values in grams virtually coincide with those in milliliters. The protonation coefficients strongly depend on the ionic composition of the solution phase and on the degree of deprotonation, as shown in Fig. 2.

The intrinsic protonation constant K_{ai} can be evaluated from the protonation coefficient according to the following relationship obtained from the Donnan model [3]:

$$K_a = K_{ai}\frac{\gamma_H \overline{\gamma}_L a_B}{\overline{\gamma}_{HL}\overline{a}_B} = K_{ai}\frac{\gamma_H \overline{\gamma}_L \overline{a}_C}{\overline{\gamma}_{HL} a_C} \quad (9)$$

The ratio of the activity coefficients inside the resin is assumed to be 1, for the sake of simplicity and according to previous findings [1].

The concentration of counter ion in the resin is evaluated as the summation of that which neutralizes the deprotonated groups, $[\overline{C}]_\alpha$, and that which enters by diffusion, $[\overline{C}]_d$ [3]:

$$[\overline{C}]_\alpha = Q\alpha/q \quad (10)$$

$$[C][B] = ([\overline{C}]_\alpha + [\overline{C}]_d)[\overline{C}]_d \quad (11)$$

where q indicates the grams of water per g of dry resin in the H^+ form.

Eq. 11 is obtained from the Donnan equilibrium relative to the salt constituting the ionic medium, CB. The values of K_{ai} obtained at each titration point are reported in Fig. 2. They are independent of the ionic composition of the aqueous phase, but increase with the degree of deprotonation.

It is interesting that the intrinsic protonation constant obtained by extrapolation at $\alpha = 0$ (log K_{ai} = 4.8) is in good agreement with the protonation constant of acetic acid in aqueous solution (Table 1). This can be attributed to the well known polymeric effect [7], for which the protonation constant increases when the number of negative charges near the protonation site increases, owing to the deprotonation. This effect was never found for the other resins examined by us [1–3], but the concentration of the active groups inside Amberlite® CG-50 is much higher than those in the other previously examined systems. This could make the nearest neighbours interact with the protonation site more than in resins with lower capacity. Similar results were previously obtained by Chatterjee and Marinsky [8] for the resin Amberlite IRC-50 manufactured by Rohm & Haas, while in an investigation 10 years later [9] on a resin having a similar composition purchased from Malinckrodt intrinsic protonation constants independent of the degree of deprotonation were obtained. Thus the authors attributed the effect to macroporosity present in the first Amberlite IRC-50 investigated,

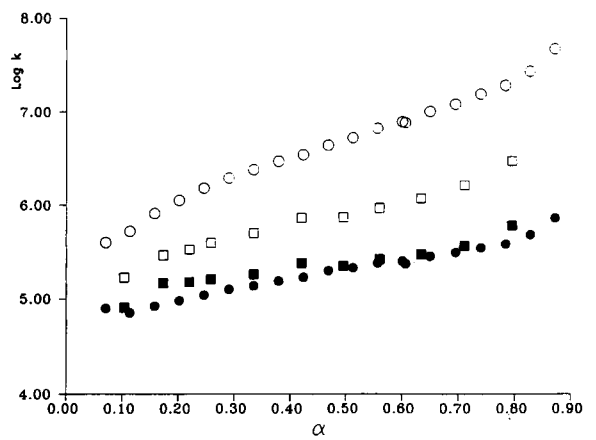

Fig. 2. Protonation coefficient log K_{a1} and intrinsic protonation constant log K_{a1i} of Amberlite® CG-50 at different values of the degree of deprotonation α. (□) log K_{a1} vs. α in 0.13 mol kg^{-1} $NaNO_3$; (○) log K_{a1} vs. α in 1.01 mol kg^{-1} $NaNO_3$; (■) log K_{a1i} vs. α in 0.13 mol kg^{-1} $NaNO_3$; (●) log K_{a1i} vs. α in 1.01 mol kg^{-1} $NaNO_3$.

which caused an incorrect evaluation of the water present in the resin phase.

3.2. Sorption of metal ions on Amberlite® CG-50

Some sorption isotherms of copper(II), zinc(II), calcium(II) and magnesium(II) are shown in Fig. 3. They were obtained in 0.1 mol kg^{-1} sodium nitrate under typical batch conditions (volume of solution phase and amount of resin) and using an excess of active groups in order to mimic the usual situation in practical applications. As expected from the complexation constant values reported in Table 1, they are very close to each other. The sorption takes place at acidities at which the carboxylic groups are still completely protonated. This means that the counter ion can enter into the resin only by diffusion, so that $a_C = \bar{a}_C$. As a consequence, according to Eq. 2, it is

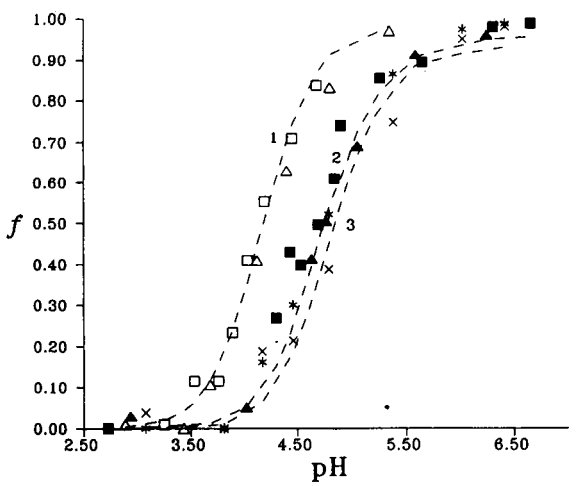

Fig. 3. Sorption isotherms of copper(II), zinc(II), calcium(II) and magnesium(II) on Amberlite® CG-50 in $NaNO_3$ solution of different concentrations. $T = 25°C$. (□) Copper(II), 0.112 mmol. $NaNO_3$, 0.1 mol kg^{-1}. $V = 30.0$ ml. 0.0942 g of dry resin. (△) Copper(II), 0.112 mmol. $NaNO_3$, 1.0 mol kg^{-1}. $V = 30.0$ ml. 0.0942 g of dry resin. (■) Zinc(II), 0.094 mmol. $NaNO_3$, 0.01 mol kg^{-1}. $V = 25.0$ ml. 0.3781 g of dry resin. (▲) Zinc(II), 0.094 mmol. $NaNO_3$, 1.0 mol kg^{-1}. $V = 25.0$ mol. 0.3781 g of dry resin. (*) Calcium(II), 0.250 mmol. $NaNO_3$, 0.01 mol kg^{-1}. $V = 25$ ml. 0.3781 g of dry resin. (×) Magnesium(II), 0.082 mmol. $NaNO_3$, 0.01 mol kg^{-1}. $V = 25$ ml. 0.3781 g of dry resin. Dotted curves are the isotherms calculated with the found values of β_{2ex}: (1) copper(II); (2) zinc(II) and calcium(II); (3) magnesium(II).

Table 3
Exchange coefficients of bivalent metal ions obtained from the sorption isotherms on Amberlite® CG-50 at 25°C under the condition of excess of active groups for magnesium(II), calcium(II), copper(II) and zinc(II) at different concentrations of sodium nitrate (Conditions as in Fig. 3)

	$NaNO_3$ (mol kg^{-1})	$\log \beta_{2ex}\bar{\gamma}^2_{HL}/\bar{\gamma}_{ML_2}$
Mg(II)	0.01	−9.83 (0.39)
Ca(II)	0.01	−9.58 (0.22)
Cu(II)	0.11	−7.74 (0.12)
	1.00	−7.81 (0.06)
Zn(II)	0.01	−8.56 (0.13)
	1.00	−8.39 (0.51)

expected that the exchange coefficient is independent both of the degree of sorption f and the ionic composition of the aqueous phase. Moreover, it has been found that under the condition of an excess of active groups considered here the stoichiometric coefficients of Eq. 1, n and q, are always equal to 2. Thus the sorption reaction of metal ions on Amberlite® CG-50 is

$$M + 2\overline{HL} \leftrightarrow \overline{ML_2} + 2H \quad (12)$$

Since $z = q$, the concentration of the counter ion in the aqueous phase should not have any influence on the values of the exchange coefficient. This is shown in Table 3, where the values of $\log \beta_{2ex}\bar{\gamma}^2_{HL}/\bar{\gamma}_{ML_2}$ obtained experimentally at different concentrations of sodium nitrate are reported. As expected, the same values are found for different concentrations of sodium nitrate. Moreover, $\log \beta_{2ex}\bar{\gamma}^2_{HL}/\bar{\gamma}_{ML_2}$ for copper(II) and zinc(II) are near to the respective complexation constants in aqueous solution reported in Table 1. This indicates that the activity coefficients of the species inside the resin are near to 1, which can probably be attributed to the fact that both the free active group and the complex are fixed to the framework of the resin.

The formation of the 1:2 metal to ligand complexes for calcium(II) and magnesium(II) was never observed before in solution, but is evidently promoted by the high concentration of active groups inside the resin.

An attempt to sorb copper(II) through the formation of the 1:1 metal to ligand complex was per-

formed by lowering the ratio of metal ion to active groups to values near to 1. In Fig. 1 also a titration curve for Amberlite® CG-50 in the presence of copper is reported, at a metal to ligand ratio of 0.5. By comparing this titration curve with that of the resin alone it can be seen that only one proton per sorbed metal ion is exchanged.

The exchange coefficient of copper(II) was calculated from the titration curve. Note that the resin is completely protonated at pH lower than 4.3, at which a large fraction of copper(II) is sorbed on the resin. As a consequence, the activity of the counter ion is the same in the resin and in the solution phase and the protonation and the exchange coefficients are independent of the concentration of the counter ion, both in the resin and in the aqueous phase, regardless of the fact that in this case $z - q = 1$ (see Eq. 2). Thus at pH lower than 4.3 they must be constant, independently of f or pH. For this reason the exchange coefficient could be evaluated by SUPERQUAD [10], a computer program widely used for the calculation of complexation constants in homogeneous phases by potentiometric titration. A value of log $\beta_{1ex} = -2.75$ (0.01) was obtained in the pH range 3.8–4.3. As $a_C = \overline{a_C}$, it corresponds also to the intrinsic complexation constant, and is in good agreement with the constant reported in Table 1 for the complexation of copper(II) with acetic acid in aqueous solution.

3.3. Evaluation of the exchange coefficients of divalent metal ions on Amberlite® CG-50 by a chromatographic procedure

In a previous investigation [11] it was shown that the exchange coefficients of metal ions on anion-exchange resins containing sulphonated azo dyes as chelating groups can be evaluated from the position of the maximum of the elution peaks of metal ions (V_E) obtained by the column technique. In fact, it is widely recognized [12] that the maximum of the elution curve V_E does not depend on the kinetics but only on the distribution coefficient K_D through the relationship

$$V_E = V_m + K_D V_s \qquad (13)$$

where V_m and V_s are the volume of the mobile and stationary phase, respectively. It has been shown [12] that Eq. 13 holds also in the case of the distribution of metal ions on chelating resins, and moreover that K_D can be evaluated from the exchange coefficient β_{nex} according to

$$K_D = \frac{\beta_{nex}[\overline{H_xL}]^n w}{[H]^q V_s} \qquad (14)$$

In this investigation the same relationships were applied to the elution of some bivalent metal ions

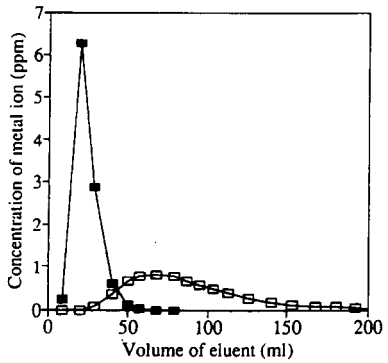

Fig. 4. Elution curves of copper(II) and zinc(II) from a column of Amberlite® CG-50 (2 g of dry resin). Eluent: 0.1 mol kg^{-1} NaCl, pH 3.38. (□) Copper(II), 1×10^{-3} mmol. (■) Zinc(II), 1.53×10^{-3} mmol.

Table 4
Elution of copper(II), zinc(II), calcium(II) and magnesium(II) from a column containing 2 g of dry Amberlite® CG-50

	pH	V_E (ml)	K_D	log β_{1ex}	log β_{2ex}
Cu(II)	3.10	17.5	3.9	–	−7.37
	3.38	70.0	17.5	–	−7.28
	3.73	24.0	61.8	–	−7.43
Zn(II)	3.38	20	4.5	−3.43	–
	3.73	50	12.3	−3.68	–
	4.10	110	28.0	−3.37	–
Ca(II)	3.74	21	4.8	−3.77	–
	4.10	45	11.0	−3.77	–
	4.40	130	33.2	−3.59	–
Mg(II)	3.74	15	3.2	−3.95	–
	4.10	30	7.1	−3.96	–
	4.40	55	13.6	−3.98	–

$V_m + V_s = 6.5$ ml. Eluting solution: 0.1 M NaCl. Elution rate: 1.8 ml/min. T = 20°C (room temperature), HETP = 0.75 cm, mmol of copper(II): 1.0×10^{-3}; mmol of zinc(II): 1.5×10^{-3}; mmol of calcium(II): 2.0×10^{-3}; mmol of magnesium(II): 8.2×10^{-3}.

from a column containing Amberlite® CG-50. As an example the elution curves for copper(II) and zinc(II) obtained at pH 3.38 in 0.1 M NaCl are reported in Fig. 4. In Table 4 the elution volumes on the same column at different pH values for the four metal ions considered are given, together with the values of K_D evaluated with Eq. 13.

The analysis of K_D as a function of pH was performed with Eq. 14 by assuming that the active groups are present in large excess. It was found that one proton is exchanged per sorbed metal ion ($q = 1$), which means that the 1:1 complex is formed in the column. Only in the case of copper(II) are two protons exchanged per sorbed metal ion, indicating that a 1:2 complex is formed in the column; the same is observed in batch under the condition of ligand excess. In Table 4 the values of the exchange coefficients evaluated from the distribution coefficients by Eq. 14 are shown. At the considered acidities the active groups are completely protonated, so that the activity of the counter ion is the same inside and outside the resin. Thus the exchange coefficients must be equal to the complexation constants in aqueous solution, as is seen by comparing the log β_{nex} values reported in Table 4 with the constants in Table 1. The fact that in the chromatographic procedure the 1:1 complex seems to be formed rather than the 1:2 complex is probably due to kinetic reasons.

3.4. Comparison between the sorption of divalent metal ions on Amberlite® CG-50 and on Chelex 100

It has been found previously [3] that calcium is sorbed by the resin Chelex 100, containing iminodiacetic chelating groups, at pH values considerably lower than those which can be predicted from the complexation by iminodiacetate. The sorption reaction has been found to be

$$Ca + 2\overline{H_2L} \leftrightarrow \overline{Ca(HL)_2} + 2H \qquad (15)$$

with an exchange coefficient log $\beta_{22exL} = -5.1$.

It is reasonable to assume that the complexation takes place through two carboxylic groups from two different iminodiacetates and that the residual proton is linked to the aminic nitrogen, which is not involved in the complexation. Since the intrinsic protonation constant of imminodiacetate in Chelex 100 was found to be log $K_{a2i} = 3.0$, the intrinsic formation constant can be evaluated:

$$\log K_2 = \frac{[\overline{Ca(HL)_2}]}{[\overline{Ca}][\overline{HL}]^2} = 0.9$$

which is near to the corresponding value found with Amberlite® CG-50 (log $K_2 = \log \beta_{2i} + 2 \log K_{ai} = 0.5$). No comparison can be made with the formation constant in aqueous solution, because the 1:2 complex was never observed before in the case of calcium. The formation of the $M(HL)_2$ complex inside Chelex 100 explains why the resin is much less selective towards bivalent metal ions than the corresponding model monomers in aqueous solution, being able to sorb calcium and magnesium at an acidity very near to that of other heavy metal ions. Of course, this can be a problem in certain separations, for instance from sea water where alkaline earth metal ions are present at high concentrations.

The similarity of the intrinsic formation constant obtained for the two different resins indicates that the sorption mechanism is the same, involving in both instances a complexation of the metal ion by two carboxylic groups.

4. Conclusions

The sorption of bivalent metal ions on the weak acid cation-exchange resin Amberlite® CG-50 can be described in terms of complex formation by the carboxylic groups which are present inside the resin. This is demonstrated by the fact that the exchange coefficient can be correctly predicted from the complexation constant in aqueous solution with acetic acid, having a structure similar to that of the active group, according to the Donnan model.

If the active groups are present in large excess, the 1:2 metal to ligand complex is predominantly formed in batch experiments, even in the case of those metal ions, such as calcium and magnesium, for which this kind of complex has never been observed in aqueous solution. However, complexes of this structure with two carboxylic group acting as donors towards calcium(II) have also been found to be formed inside the resin Chelex 100. It must be

kept in mind that the concentration of donor groups is very high in the resin phase, and this of course promotes the formation of the 1:2 metal to ligand complexes. In the case of other bivalent metal ions, such as copper(II), zinc(II) and cadmium(II), the formation of 1:2 complexes has been observed also in aqueous solution. Here predictions about sorption equilibria based on the Donnan model are in good agreement with the experimental findings.

The model is convenient because it is based on the knowledge of the complexation constants in aqueous solution, which are in many instances either well known or easily obtainable.

Good agreement between the distribution coefficients obtained experimentally by chromatographic experiments and those predicted from the Donnan model was also found.

Acknowledgement

The financial support of the Italian Ministry of University and Scientific and Technological Research (MURST; 40%) is gratefully acknowledged.

References

[1] M. Pesavento, A. Profumo and R. Biesuz, Talanta, 35 (1988) 431.
[2] M. Pesavento and R. Biesuz, Reactive Polymers, 14 (1991) 239.
[3] M. Pesavento, R. Biesuz, A. Profumo and M. Gallorini, Anal. Chem., 65 (1993) 2522.
[4] R.S. Kolat and J.E. Powell, Inorg. Chem., 1 (1962) 293.
[5] R.K. Cannon and A. Kibrick, J. Am. Chem. Soc., 60 (1938) 2314.
[6] M. Pesavento, C. Riolo, T. Soldi and R. Garzia, Ann. Chim. (Rome), 72 (1982) 217.
[7] I. Michaeli and A. Katchalsky, J. Poymer Sci., 23 (1957) 683.
[8] A. Chatterjee and J.A. Marinsky, J. Phys. Chem., 67 (1963) 41.
[9] J.A. Marinsky, T. Miyajima, E. Högfeldt and M. Muhammed, Reactive Polymers, 11 (1989) 279.
[10] P. Gans, A. Sabbatini and A. Vacca, J. Chem. Soc., Dalton Trans., (1985) 1195.
[11] M. Pesavento et al., in press.
[12] H. Small, in Ion Chromatography, Plenum Press, New York, 1989, p. 16.

ELSEVIER

Analytica Chimica Acta 298 (1994) 233–244

ANALYTICA CHIMICA ACTA

Polarographic and cathodic stripping voltammetric determination of tipredane

M. Valnice B. Zanoni, Josino C. Moreira, Ravinder K. Hindocha, Arnold G. Fogg *

Chemistry Department, Loughborough University of Technology, Loughborough, Leicestershire, LE11 3TU, UK

Received 8 December 1993; revised manuscript received 29 April 1994

Abstract

The electroreduction of tipredane has been investigated by direct current and differential pulse polarography and by cyclic voltammetry at a hanging mercury drop electrode. In Britton–Robinson (B–R) buffer, pH 2.0–5.0, the drug is reduced in a single well-defined step: this reduction process has been shown to involve a preceding protonation step. At pH 12 also there is only a single step, this time involving reduction of the unprotonated species followed by a chemical step involving dimerisation. At intermediate pH values both peaks are present, peak 1 being at a less negative potential; studies of the mechanisms here are complicated by adsorption processes. Tipredane can be determined by differential pulse polarography at a pH of 7.0 or pH 2.0 using the first reduction peak over the concentration range 1.0×10^{-5} to 8.0×10^{-5} M or 1.0×10^{-6} to 8.0×10^{-5} M, respectively. In B–R buffer at pH 4.5 two cathodic stripping peaks are obtained. The first peak, not present in the polarograms, is due to the accumulation and subsequent reduction of a mercury salt from tipredane. The second peak, which corresponds with the first polarographic peak, is recommended for use in the determination of tipredane by cathodic stripping voltammetry in the range 1×10^{-8}–5×10^{-7} M with preconcentration for 2–3 min at 0 V. The detection limit was calculated to be 5×10^{-10} M. The relative standard deviation determined from seven determinations at the 1×10^{-7} M level was 1.3%.

Keywords: Cyclic voltammetry; Polarography; Tipredane

1. Introduction

Tipredane, (11β, 17α)-17(ethylthio)-9-fluoro-11-hydroxy-17-(methylindo) -androsta-1,4-dien-3-one) (**1**), is a sulphur-containing steroid developed for topical treatment of human dermatoses [1]. Tipredane has been shown to possess moderate to potent anti-inflammatory activity and to be an anti-allergic agent [1–3].

Relatively few studies related to the determination of tipredane in formulations or biological fluids have been described. Methods using liquid chromatogra-

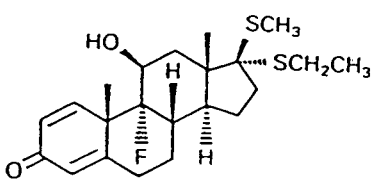

I

* Corresponding author.

SSDI 0003-2670(94)00217-A

phy with UV detection, and supercritical fluid chromatography and mass spectrometry have been published [3–5]. Polarographic methods of determining ketosteroids other than tipredane, are found in the literature [6–10]. Tipredane contains an alpha, beta-unsaturated keto group, which should be easily reduced.

In the present work the electroreduction of tipredane in aqueous methanol solutions has been studied, and a differential pulse polarographic method of determining the drug has been developed. In addition, a cathodic stripping voltammetric method has been developed for determining tipredane at lower levels.

2. Experimental

2.1. Apparatus

All voltammetric measurements were made using a Metrohm Voltammetric Scanner E612 and a Voltammetric Detector E611 with a Houston Instruments 2000 *X–Y* recorder. A Metrohm 663 VA Stand was used in the HMDE mode for cyclic voltammetry and cathodic stripping voltammetry, and in the DME mode for polarographic measurements. The three-electrode system was completed by means of a glassy carbon auxiliary electrode and a silver chloride reference electrode. All potentials are given relative to this Ag/AgCl (3 M KCl) electrode.

2.2. Reagents

Tipredane standard stock solutions (1×10^{-3} M) were prepared by dissolving the pure substance (kindly supplied by Fisons, Loughborough) in methanol. All solutions were freshly prepared daily and more dilute solutions were prepared from the stock solutions as required.

The supporting electrolyte was Britton–Robinson (B–R) buffer prepared by adding to a solution 0.04 M in orthophosphoric acid, 0.04 M in acetic acid and 0.04 M in boric acid an appropriate amount of 0.2 M sodium hydroxide solution. All chemicals were analytical-reagent grade. Water was obtained from a Liqui-Pure system.

2.3. Procedures

The general procedure adopted for obtaining polarograms and cyclic voltammograms was as follows. An aliquot (20 ml) of B–R buffer–methanol (1 + 1, v/v) solution was placed in a clean, dry voltammetric cell and the required volume of standard tipredane solution was added by means of a micropipette. The solution was purged for 15 min before recording polarograms and cyclic voltammograms. The differential pulse mode was used with 50 mV pulse amplitude, 1 s drop time and a scan rate of 3 mV/s, unless otherwise indicated.

For cathodic stripping voltammetry an aliquot of 20 ml of (aqueous) B–R buffer was placed in the cell and the required volume of standard tipredane was added by means of a micropipette. The stirrer was switched on, and the solution was purged for 15 min. Then an accumulation potential was applied to the working electrode while the solution was stirred continuously. Stirring was discontinued and after 15 s, a negative-going differential pulse scan was initiated and the resulting voltammogram was recorded. A pulse amplitude of 50 mV and scan rate of 5 mV/s was utilized.

3. Results and discussion

3.1. Preliminary polarographic observations

At the higher concentrations in the range used for polarography (6×10^{-6} to 1×10^{-4} M) tipredane is insoluble in aqueous solution, and for this reason polarography was carried out in a Britton–Robinson buffer–methanol (1 + 1, v/v) mixture. Repetitive polarograms remained unchanged for at least 8 h after the polarographed solutions were prepared in the pH range 1.0–9.0. However, in very alkaline solutions (pH > 10.0), the wave heights decreased with time: for example, no polarographic waves were observed 4 h after the first polarogram was recorded in 0.2 M sodium hydroxide solution owing to degradation of the tipredane.

3.2. Influence of pH

Sampled direct current (dc_t) polarograms or differential pulse (dp) polarograms of 5×10^{-5} M

tipredane recorded in 0.04 M BR buffer–methanol (1 + 1, v/v) at pH 2.0–11.0 exhibited a single reduction step in acidic medium and two well-defined steps in neutral and alkaline solutions, as shown for the dp polarograms in Fig. 1.

pH had the same effect, in terms of change of half-wave and peak potentials and of the trend in the size of limiting and peak currents, on the current–voltage curves recorded for 5×10^{-5} M tipredane solutions using both dc and dp polarography. The change in the dp peak potential with pH is shown in Fig. 2A. The peak potential of the first wave shifts towards more negative values as the pH increases in the range 2.0–8.0, indicating that hydrogen ions are involved in the electrode reaction. The slopes of $E_{1/2}$ vs. pH and E_p vs. pH plots were 66.7 and 56.9 mV per pH unit, respectively. In contrast, the E_p or $E_{1/2}$ values for the second peak at pH > 6.0 were approximately constant. Fig. 2B shows the influence of pH on peak current. The peak current for the first reduction step is constant in the range pH 3.0–8.0 and then decreases gradually above pH 9.0. However, tipredane exhibits an abnormally large current at pH < 2.0, as observed previously for other corticosteroids with similar structures [6]. The second reduction step, which appears above pH 6.0, has a peak height somewhat smaller than that for the first reduction step, but the two steps approach a similar small height at higher pH values.

3.3. Characteristics of the polarographic waves

The reversibility of the electrode reaction was examined using 5×10^{-5} M tipredane at different pH values by applying Tome's criterion [11]. In general the values of $E_{3/4} - E_{1/4}$ obtained were different, as the pH varied (Table 1). For very acidic solutions (pH 2.0) and alkaline solutions (pH > 10.0) the $E_{3/4} - E_{1/4}$ values are approximately 59.4 and 52.5 mV; respectively. For the intermediate pH values the $E_{3/4} - E_{1/4}$ values decrease from pH 2.5 down to 41.5 mV at pH 5.0, but increase again at pH > 5.0. Concomitantly, new waves are observed in neutral and alkaline medium, with values of ~ 23.5 mV for $E_{3/4} - E_{1/4}$. This behaviour was confirmed by the peak half-widths ($w_{1/2}$) measured for the dp polarograms. Values of $w_{1/2}$ of approximately 90 mV were found with very acidic and very alkaline solutions. Smaller values were found for the range 4.0 < pH < 8.0. Values of $w_{1/2}$ of ~ 31.5 mV were obtained for the second wave from dp polarograms. At pH 12.0 only one wave, as before, was observed (Fig. 3).

Taking into account the apparent dependence of the degree of reversibility on pH, therefore, some of the analytical criteria for characterising the mechanism [12–15] were examined using differential pulse polarography. Two distinct values of pH were investigated at a concentration of 5×10^{-5} M and drop

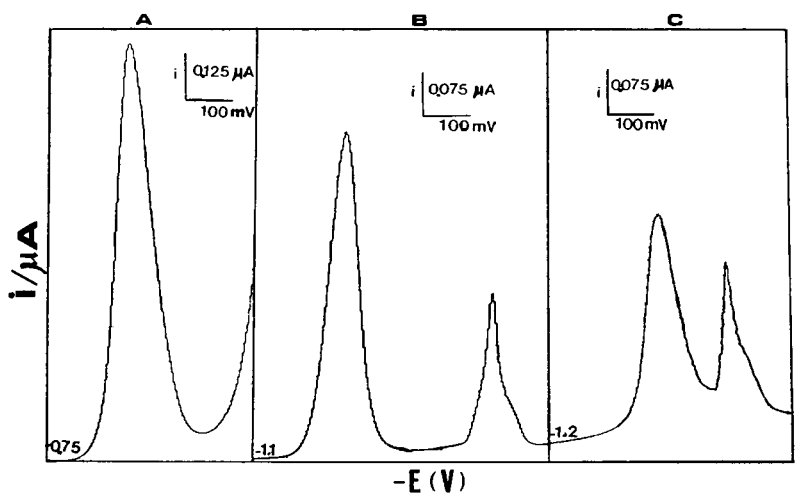

Fig. 1. Differential pulse polarograms of 5×10^{-5} M of tipredane in Britton–Robinson buffer containing 50% methanol pH 2.0 (A), pH 7.0 (B), and pH 10.0 (C). Drop time, 1 s; scan rate, 3 mV/s; and pulse amplitude, 50 mV.

time (t_d) of 0.4 s. In alkaline solution (pH 12.0), only one wave was seen, at −1.5 V. Comparing two recordings at ΔE (pulse amplitude) = +50 mV and ΔE = −50 mV, it is seen that the absolute value of i_p for the cathodic peak is greater than that for the anodic peak ($i_{pa}/i_{pc} = 0.75$), see Fig. 3. Although, the analysis of $E_{3/4} - E_{1/4}$ and $w_{1/2}$ point to a reversible system, these results show that the system is not a simple reversible system [12]. However, this behaviour is usual for irreversible systems (E_i) and for systems with a chemical reaction subsequent to reversible electron transfer (EC) processes. A second analytical criterion, the $\Delta(i_p(t = 2\ s)/i_p(t = 0.4\ s))$ ratios, involving obtaining two recordings at two different pulse amplitudes, were calculated. The ratio tends to 2.51 at +50 mV and 1.91 at −50 mV, which is coincident with that expected for E_i and EC mechanisms [12,13]. At small ΔE values the αn values estimated from W measurements can be used as a third criterion to distinguish between E_i and EC [12]. The αn values corresponding to $\Delta E \pm 10$ mV (for $\alpha n = W/90$) were 0.96 (+10 mV) and 1.06 (−10 mV), which are consistent with the EC mechanism.

Analysis of the shape of the differential pulse polarogram and the dependence of E_p on the concentration, with the aim of distinguishing between a first or pseudo-first order mechanism and a second order mechanism was also carried out. At $t = 0.4$ s and small pulse amplitude (ΔE = +10 mV) the half-width of the peak was 95 mV, but the peak is unsymmetrical. If $E^+_{p/2}$ is used to denote the anodic half peak potential and $E^-_{p/2}$ to denote the cathodic half peak potential, then values of $E^+_{p/2} - E_p = 40$ mV and $E_p - E^-_{p/2} = 55$ mV are indicative that dimerization processes are involved. A plot of E_p vs. log C gave a linear relationship between 5×10^{-6} M–5×10^{-5} M (equation: $-E_p(\text{mV}) = -1.439 + 25.64 \log C$). The slope agrees reasonably well with the theoretical value of 20 mV for a reversible electrode reduction followed by dimerization.

The same analytical criterion was applied to acidic solutions from differential pulse polarograms obtained at pH 2.0. The ratio of $\Delta(i_p(t = 2\ s)/i_p(t = 0.4\ s))$ was 2.7 for ΔE = −50 mV and 0.96 for ΔE = +50 mV. The αn values estimated from W measurements are 0.87 (ΔE = +10 mV) and 0.70 (ΔE = −10 mV). These findings are consistent with a mechanism involving a chemical reaction preceding a reversible electron transfer [9].

At concentrations of 5×10^{-5} M, the slope of the graph between the logarithms of the peak current and drop time varied for pH 2.0, 7.0 or 12.0; these were of 0.52, 0.60 and 0.13, respectively. Although a linear relationship for tipredane was obtained in the range 1×10^{-6}–8×10^{-5} M at pH 2.0 (equation: $i_p(\text{nA}) = 0.0232 + 0.323C$) and 1×10^{-5}–8.0×10^{-5} M at pH 7.0 (Fig. 4), the peak current is not proportional to concentration at higher concentrations. This behaviour may be related to the occurrence of adsorption phenomena at higher concentrations [11]. These results are confirmed by dc_t polarography. The calibration curves are marked by a negative deviation at concentrations higher than 8 ×

Table 1
Sampled dc polarographic data for the reduction of 5×10^{-5} M tipredane in B–R buffer containing 50% methanol

pH [a]	pH [b]	First peak			Second peak		
		$-E_{1/2}$ (V)	i_l (μA)	$E_{3/4} - E_{1/4}$ (mV)	$-E_{1/2}$ (V)	i_l (μA)	$E_{3/4} - E_{1/4}$ (mV)
2.0	2.2	0.919	0.368	59.4	–	–	–
3.0	3.9	1.024	0.230	47.2	–	–	–
4.0	4.7	1.082	0.165	43.0	–	–	–
5.0	5.5	1.119	0.164	41.5	–	–	–
6.0	6.9	1.199	0.143	43.3	1.543	0.079	23.6
7.0	7.8	1.268	0.116	45.4	1.544	0.069	23.5
8.0	8.6	1.307	0.106	47.2	1.547	0.080	23.6
9.0	9.4	1.348	0.130	51.2	1.549	0.077	23.6
10.0	10.4	1.380	0.128	52.5	1.525	0.079	23.4

[a] Value corresponding to the Britton Robinson buffer used.
[b] Measured value corresponding to the mixed aqueous methanolic solution.

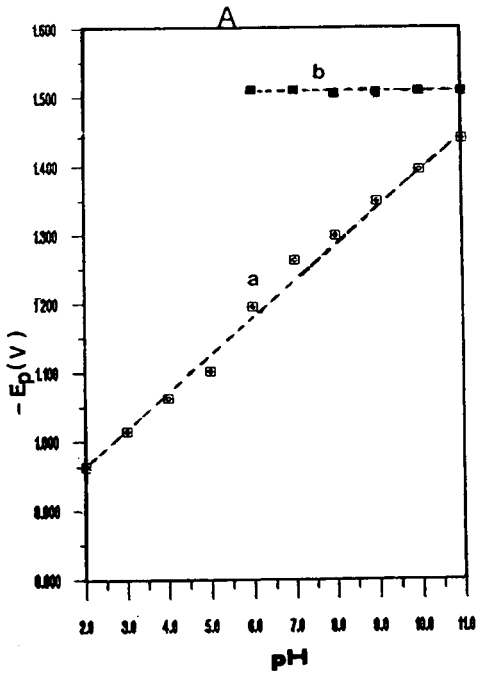

Fig. 2. Dependence of the peak potential (A) and peak current (B) obtained with a 5×10^{-5} M tipredane solution on the pH of the BR buffer + methanol (1 + 1) medium. (a) First peak; (b) second peak.

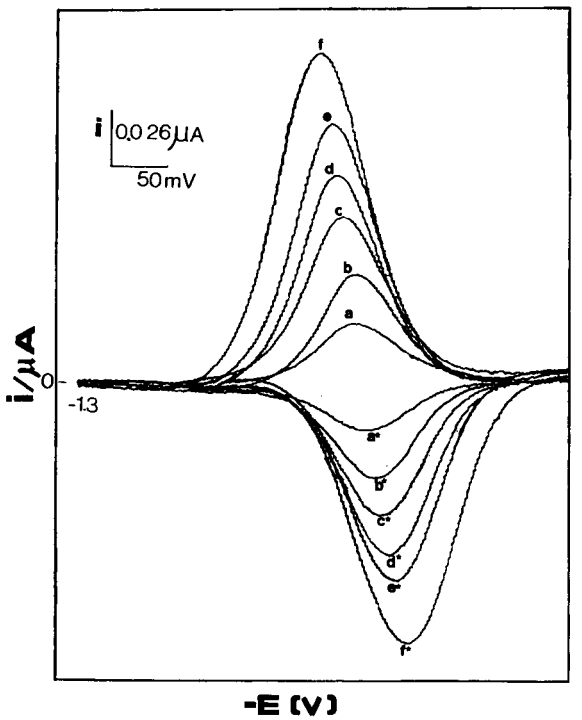

Fig. 3. Differential pulse polarograms of 5×10^{-5} M tipredane in B–R buffer pH 12.0 + methanol (1 + 1). Drop time, 0.4 s; scan rate, 5 mV/s; E_i, −1.3 V; pulse amplitude (ΔE): ±10, ±20, ±30, ±40, ±50, ±70 mV; a to f negative pulses; a′ to f′ positive pulses.

10^{-5} M, and the polarograms are slightly distorted at higher concentrations.

The second wave observed at $7.0 < pH < 11.0$ also displays apparent abnormalities in its dc_t waveform when the tipredane concentration is increased above $\sim 7\times10^{-5}$ M. The wave starts to rise normally, at about half height flattens abruptly for a few hundredths of a volt, and then begins to rise again. Also, dp polarograms split into two peaks at lower drop times ($t_d = 0.4$ s). This effect is clearly indicative of the presence of strong adsorption or other surface phenomena [16] coupled with the second reduction process.

Taking into account the stability of the polarographic signal of the drug at pH 2.0 and 7.0 and their linear relationships obtained for tipredane concentrations below 8.0×10^{-5} M (Fig. 4), both pH values can be used for analytical purposes. In addition, pH 2.0 could be chosen for analytical determinations of

Table 2
Voltammetric data for the reduction of 7.0×10^{-5} M tipredane in B–R buffer pH 7.0 containing 50% methanol

Scan rate v (V/s)	Peak A			Peak A*			Peak B		
	$-E_p$ (V)	i_p (μA)	$i_p \cdot Cv^{1/2}$ (μA/s$^{1/2}$)	$-E_p$ (V)	i_p (μA)	$i_p \cdot Cv^{1/2}$ (μA/s$^{1/2}$)	$-E_p$ (V)	i_p (μA)	$i_p \cdot Cv^{1/2}$ (μA/s$^{1/2}$)
0.01	1.278	0.123	1.76	1.351	0.189	2.70	1.534	0.276	3.94
0.02	1.291	0.241	2.44	1.358	0.261	2.64	1.545	0.386	3.90
0.03	1.299	0.349	2.89	1.358	0.330	2.72	1.551	0.496	4.10
0.04	1.303	0.413	2.95	1.362	0.374	2.68	1.559	0.606	4.34
0.05	1.311	0.492	3.14	1.366	0.418	2.67	1.561	0.685	4.44
0.06	1.315	0.561	3.28	1.366	0.453	2.68	1.563	0.756	4.41
0.07	1.319	0.640	3.46	1.370	0.482	2.64	1.564	0.811	4.38
0.10	1.328	0.839	3.80	–	–	–	1.568	0.886	4.01
0.20	1.354	1.264	4.05	–	–	–	1.579	0.827	2.65
0.30	1.370	1.559	4.10	–	–	–	1.583	0.720	1.88

tipredane at smaller concentrations since higher peak currents are observed.

3.4. Cyclic voltammetry

The shape of the cyclic voltammetric curves obtained for tipredane at the hanging mercury drop electrode was strongly influenced by adsorption effects. However, reproducible voltammograms were obtained as long as the mercury drop was renewed between each potential sweep.

The first reduction step is pH dependent, as verified previously by differential pulse polarography. Fig. 5 shows a typical cyclic voltammogram of 7×10^{-5} M of tipredane in BR buffer pH 7.0 and 2.0 (methanol 1 + 1). The respective voltammetric parameters for pH 7.0 can be seen in Tables 2 and 3. No anodic peak resulting from re-oxidation of the reduction product of the first peak was observed at any scan rate, suggesting the presence of an irreversible chemical reaction following the charge transfer. No cathodic peak is seen in the second scan if the drop is not renewed, suggesting possible poisoning of the electrode and/or chemical reaction between the product and starting material. At slower scan rates the wave was split into two peaks (A and A*) (Fig. 6), which could be evidence for the presence of strong adsorption on the mercury surface or a sequence in which the product of charge transfer undergoes a slow chemical reaction yielding an electrochemically active species (ECE process). However, at $v = 50$ mV/s when during a forward scan the potential was held between the first (A) and this new peak (A*) for a few seconds (enough time for the chemical reaction to proceed), the peak A* was removed completely from the voltammogram. This suggests that the peak observed (A*) cannot be attributed to the reduction of the chemical reaction product diagnosed previously.

The effect of the scan rate on the peak current and

Table 3
Voltammetric data for the reduction of various amounts of tipredane in BR buffer pH 7.0 containing 50% methanol ($v = 0.05$ V/s)

Conc. (mM)	Peak A			Peak A*			Peak B		
	$-E_p$ (V)	i_p (μA)	$i_p \cdot Cv^{1/2}$ (μA/s$^{1/2}$)	$-E_p$ (V)	i_p (μA)	$i_p \cdot Cv^{1/2}$ (μA/s$^{1/2}$)	$-E_p$ (V)	i_p (μA)	$i_p \cdot Cv^{1/2}$ (μA/s$^{1/2}$)
0.052	1.303	0.472	4.06	–	–	–	1.561	0.803	6.89
0.061	1.304	0.465	3.39	1.376	0.323	2.35	1.559	0.717	5.25
0.070	1.303	0.504	3.21	1.366	0.394	2.52	1.561	0.724	4.62
0.078	1.307	0.528	3.02	1.354	0.488	2.70	1.555	0.709	4.06
0.095	1.311	0.555	2.61	1.350	0.555	2.61	1.559	0.720	3.38
0.113	1.307	0.567	2.24	1.339	0.626	2.47	1.543	0.650	2.57

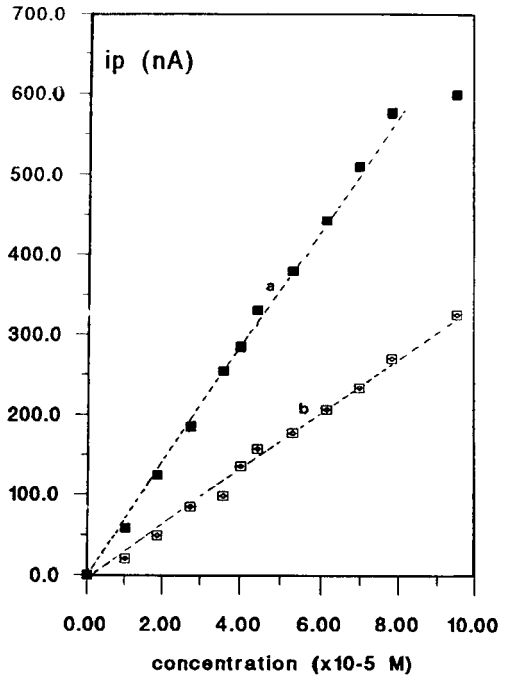

Fig. 4. Calibration graphs obtained from differential pulse polarograms of tipredane in BR buffer pH 7.0 + methanol (1 + 1). Drop time, 1 s; pulse amplitude, 50 mV. (a) First peak; (b) second peak.

other voltammetric parameters are shown in Table 2. When the height of the first two peaks (A and A*) are compared, it is possible to see that the value of i_pII/i_pI decreases with increasing scan rate. The

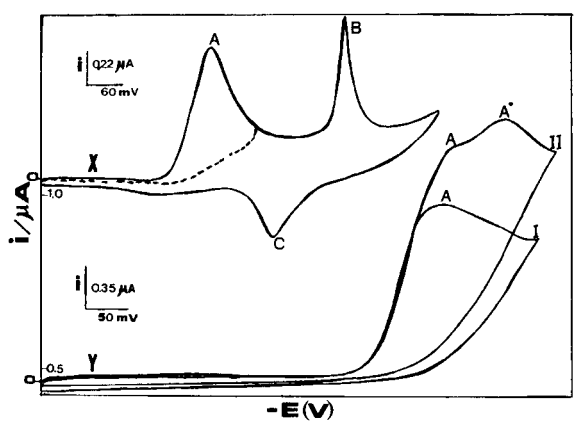

Fig. 5. Cyclic voltammograms of (X) 7×10^{-5} M tipredane in B–R buffer pH 7.0 + methanol (1 + 1). Scan rate, 0.1 V/s; (Y) 7×10^{-5} M tipredane in B–R buffer pH 2.0 + methanol (1 + 1) (line I) and 1×10^{-4} M tipredane (line II).

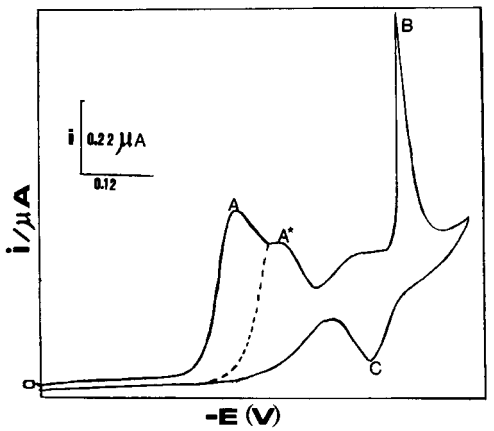

Fig. 6. Cyclic voltammograms of 7×10^{-5} M tipredane in B–R buffer pH 7.0 + methanol (1 + 1). Scan rate 0.05 V/s.

peak A is proportional to v and the peak A* is proportional to $v_{1/2}$. It is indicative of an electrodic process involving strong adsorption of the reaction product [17], which produce a pre-peak on the voltammetric timescale.

The effect of tipredane concentration on the occurrence of peak A* confirms this hypothesis. At a scan rate of 100 mV/s, a similar split of the first peak (A) can be seen by increasing the concentration, as shown for pH 2.0 in curve Y of Fig. 5 (line II). The same effect is seen at pH 7.0 and the corresponding values of current and the current function ($i_p/Cv^{1/2}$) from voltammograms are shown in Table 3. The second peak increases linearly with increasing concentration, but the first one remains nearly constant. These results can be explained by assuming that strong adsorption phenomena are present in the reduction mechanism [17]. At low concentrations, the surface of the electrode is unsaturated and virtually only one adsorption controlled peak is observed. At higher concentrations the diffusional controlled peak is observed concomitantly. A similar effect is responsible for the split of the original peak depending on the scan rate of the potential.

The second reduction peak observed only above pH 6.0 is always very sharp (see Figs. 5 (line X) and 6). Its relative intensity is larger than the one recorded in the polarographic timescale. The effects of scan rate and tipredane concentration are indicated in Tables 1 and 2. The current function decreases at high scan rates and high tipredane concentrations.

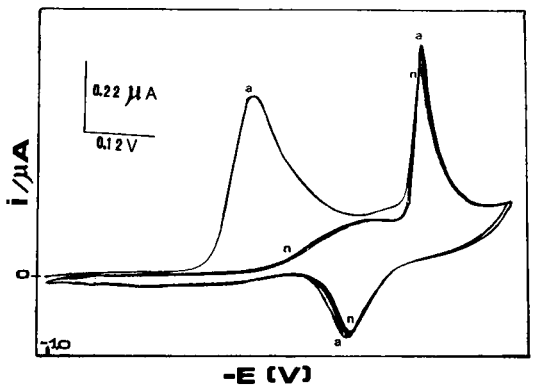

Fig. 7. Cyclic voltammograms of 7×10^{-5} M tipredane in B–R buffer pH 7.0 + methanol. Scan rate 0.05 V/s. Curve a: first scan. Curve n: successive scans at the same mercury drop.

An anodic peak (C) resulting from the re-oxidation of the species formed in the peak (B) was observed in the anodic scan (see Figs. 5 and 6), but the anodic peak potential is far from the cathodic peak and does not characterize a reversible system. Additionally, if the potential sweep is repeated at the same mercury drop, the first peak (A) disappears completely, as shown in curve *n* of Fig. 7. In contrast, the height of the second peak decreases slowly, indicating that either the product formed remains on the electrode surface preventing other reduction or the substrate is consumed by chemical reaction between product and starting material. The abnormal shape of the peak has been observed previously on covered surfaces [16,18,19] and is attributed to the deblocking process requirement when a compact film is formed before electrolysis.

3.5. Reduction of tipredane

Taking into consideration the polarographic results obtained for low concentrations of tipredane, where adsorption effects are minimised, the reduction mechanism can be attributed to the one electron reduction of the $\Delta^{1,4}$-3 keto group in the molecule. Preliminary results can be explained by a scheme from a general mechanism for related steroids proposed previously by De Boer et al. [8,9]:

$$S + H^+ \rightleftharpoons SH^+ \quad (1)$$

$$SH^+ + e^- \rightleftharpoons {}^{\cdot}SH \quad (2)$$

$${}^{\cdot}SH + SH^+ \rightarrow \text{product} \quad (3)$$

$$S + e^- \rightarrow S^{\cdot-} \quad (4)$$

$$S^{\cdot-} + H^+ \rightarrow {}^{\cdot}SH \quad (5)$$

$${}^{\cdot}SH + S \rightarrow H\text{–}S\text{–}S^{\cdot} \quad (6)$$

$$H\text{–}S\text{–}S^{\cdot} + e^- \rightleftharpoons \text{product} \quad (7)$$

In acidic media, only a one-electron wave related to the reduction of a protonated steroid molecule (S) was observed, (Eqs. 1 and 2). The E_p and $E_{1/2}$ values from dp and dc polarography depend on the pH. From dc_t polarographic slopes of 66.9 mV per pH unit are similar to those observed previously [6], which is indicative that one hydrogen ion is involved in the first reduction step. Cyclic voltammetric results show evidence that a fast chemical reaction consumes the electron transfer product and possibly involves the original species.

From the literature [8–10], a proposal of a reduction mechanism involving dimerization by the final coupling of a protonated radical and the substrate can be suggested (Eq. 2). The strong adsorption effect verified at the hanging mercury drop electrode (HMDE) and in polarograms recorded in high concentration could be indicative that these reactions seem to proceed via the mercury surface resulting in a passivation of the electrode [20].

In neutral and alkaline solution the electrode process is more complex owing to the occurrence of a second reduction step, which can be attributed to the reduction of the steroid molecule before protonation (S) (Eq. 4). Between $6.0 < pH < 11.0$ the E_p and $E_{1/2}$ are not pH dependent, which confirms this hypothesis. The occurrence of several parallel reactions that consume the anion radical formed is proposed by De Boer et al. [8,9]. Taking into account the cyclic voltammetric results, the coupling via a protonated anion radical and substrate molecule forming an electroactive species (H–S–S$^{\cdot}$) seems preponderant in the tipredane reduction mechanism. The unusual shape of the second peak observed in the cyclic voltammogram for tipredane reduction at $pH > 6.0$ seems to show that the reduction of the non-protonated steroid (Eqs. 4–7) probably occurs on the mercury electrode surface previously coated by product formed in the first reduction step (Eq. 1–3).

Evidence of product dimerization was evident at pH 12.0 by DPP, when surface effects are not ob-

served and only the reduction of the non-protonated steroid can be observed.

From the polarographic behaviour of tipredane in aqueous solution, it is clear that the first reduction step can be used for a convenient determination of the drug at levels of 1×10^{-6}–8×10^{-5} M by differential pulse polarography. Results below, however, show that even lower levels of the drug can be determined by means of cathodic stripping voltammetry.

3.6. Cathodic stripping voltammetry

In B–R buffer–methanol (1 + 1) solutions the drug is not appreciably adsorbed onto the surface of a hanging mercury drop electrode. Tipredane, however, can be determined at nanomolar concentration levels by adsorptive stripping voltammetry if the methanol addition to the buffer is eliminated.

The influence of pH was studied in solutions of tipredane in 0.04 M B–R buffer in the pH range 2.0–10.0. Accumulation studies were carried out in stirred solutions, and determination was made using differential pulse cathodic stripping voltammetry. Instrumental parameters used were: accumulation time, 120 s; accumulation potential, 0 V vs. Ag–AgCl; pulse amplitude, −50 mV; pulse interval, 1 s; and sweep rate, 5 mV/s. A pH of 4.5 provided the best analytical signal and therefore was used in all further studies.

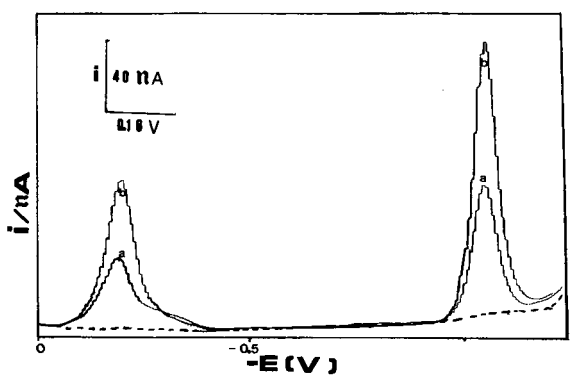

Fig. 8. Differential pulse cathodic stripping voltammograms of tipredane in B–R buffer pH 4.5. Accumulation potential, 0.0 V; accumulation time, 120 s. Concentration 1×10^{-7} M (curve a) and 2×10^{-7} M (curve b).

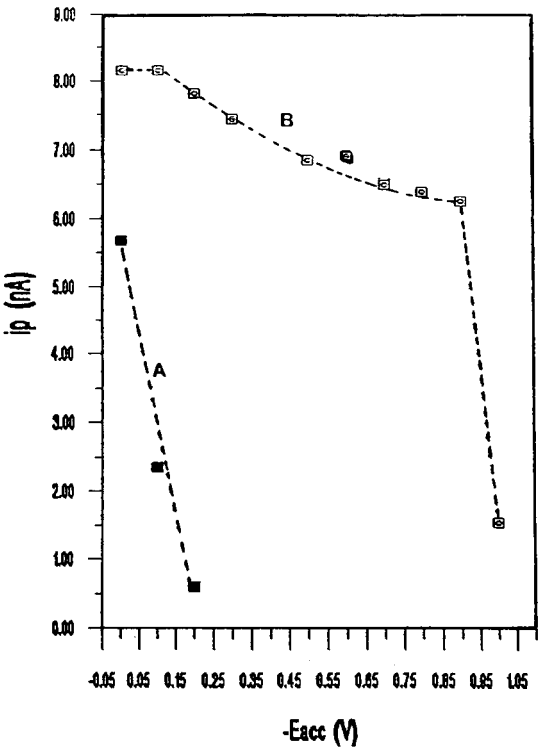

Fig. 9. Effect of accumulation potential on the peak currents obtained for differential pulse cathodic stripping voltammograms of 1×10^{-8} M tipredane in B–R buffer, pH 4.5. Accumulation time, 120 s. (A) First peak; (B) second peak.

In contrast to the differential pulse polarographic results, the stripping voltammograms exhibited an extra peak at −0.26 V (Fig. 8), in addition to the reduction peak at −1.02 V. Similar results were obtained using either a 0.04 M solution of B–R buffer or a 0.1 M acetate buffer at pH 4.5. The reproducibility of the height of the first peak is not as good as that of the second peak. The influence of accumulation potential on the peak stripping currents is shown in Fig. 9. The height of the second peak does not change significantly between 0 and −0.90 V. The first peak, on the other hand is very large when an accumulation potential of +0.1 V is used, but it shows a decrease of 58% in height with an accumulation potential of −0.1 V compared with that for 0 V, and is practically eliminated at −0.2 V.

The nature of this first peak was investigated further using cyclic voltammetry without accumula-

tion before scanning (see Fig. 10). Clearly with no accumulation the peak does not appear when scanning from 0 V (line X of Fig. 10A), and is very small when scanning from +0.05 V (line Y), whereas when scanning from +0.1 V (line Z) the peak is present and is very large. When scanning anodically from −0.5 V (Fig. 10B) without accumulation to +0.2 V before reversing the scan, an anodic peak (peak 1a) appears at about +0.1 V just before the main oxidation of the mercury, and the first cathodic peak (1c) appears during the subsequent cathodic scan. The first peak then could be due to the reduction of a mercury tipredane complex formed by oxidation of mercury in the presence of tipredane at more positive potentials, or to the reduction of an oxidation product of tipredane which might be produced at the more positive potentials. The latter possibility was eliminated by carrying out cyclic voltammetry of tipredane at a platinum electrode. Only the cathodic peak at −1.0 V was obtained: the first cathodic and the anodic peaks were absent.

Various instrumental parameters directly affect the cathodic stripping voltammetric response. The peak current depends on the pulse amplitude, varying linearly between 20 and 80 mV (following the equation $y = 0.01 + 0.192x$; $r = 0.986$, where y = peak current (μA) and x = pulse amplitude (mV)). A value of 50 mV was chosen for further study. The biggest drop surface (size 3) was selected. Although the signal increases by 40% when the stirring speed is varied from 1 to 3 during the accumulation the peak current is constant at higher stirring rates. Therefore a stirring rate of 3 was selected.

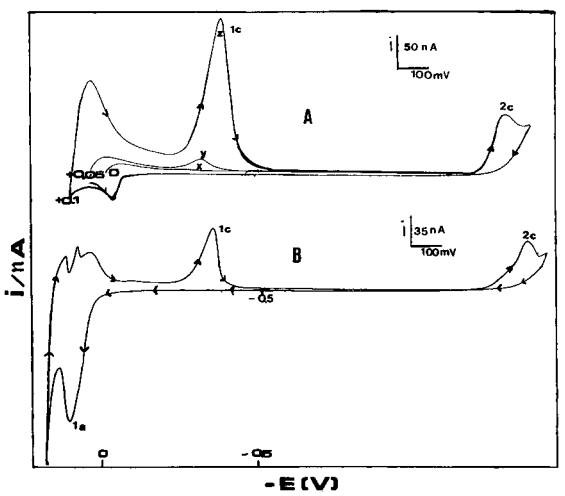

Fig. 10. Cyclic voltammetry without accumulation of 7×10^{-5} M tipredane in Britton–Robinson buffer pH 4.5; (A) potential scan started from 0 V (x), +0.05 V (y) and +0.1 V (z). Scan rate = 0.1 V s^{-1}; (B) cathodic and anodic voltammograms. Potential scan started from −0.5 V. Scan rate = 50 mV s^{-1}.

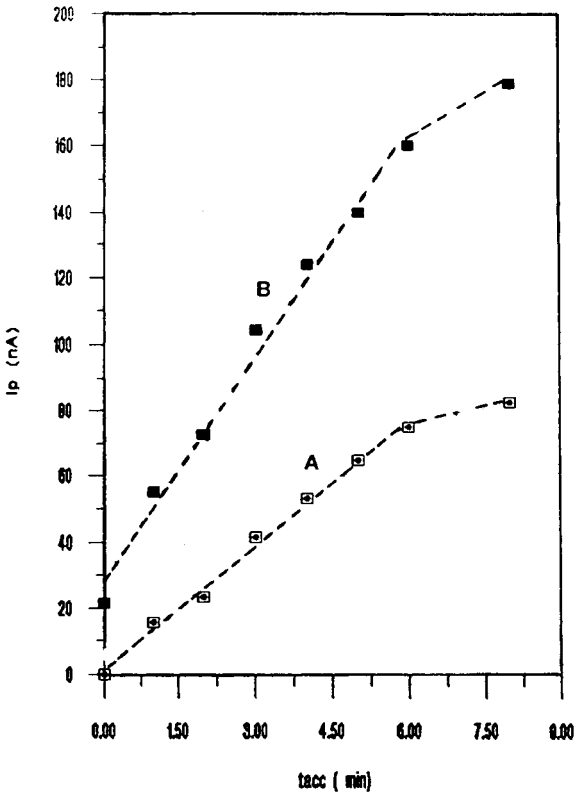

Fig. 11. Effect of accumulation time on the peak currents obtained for differential pulse cathodic stripping voltammograms of 1×10^{-7} M tipredane in B–R buffer, pH 4.5. $E_{acc} = 0$ V. (A) First peak, (B) second peak.

The variation of peak current with pre-concentration time for a 1×10^{-7} M tipredane solution at accumulation potential 0 V is shown in Fig. 11. The height of the first peak (A) increased rectilinearly with accumulation time between 0–6 min, but the peak height was always lower than that of the second peak. Also, the second peak remains linear up to 6 min, which suggests that saturation of the electrode surface only occurs at longer accumulation times. Hence, the second peak was chosen as the better one for analytical purposes.

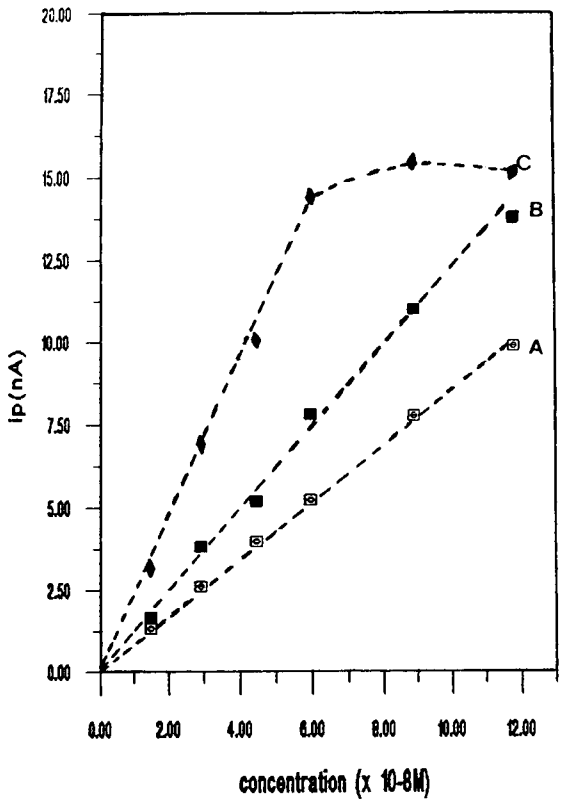

Fig. 12. Calibration graphs obtained for the determination of tipredane using differential pulse cathodic stripping voltammograms in B–R buffer, pH 4.5. $E_{acc} = 0.0$ V. Accumulation time, 120 s (curve A); 180 s (curve B) and 420 s (curve C).

Calibration graphs were linear from 1.0×10^{-8} to 10×10^{-8} M tipredane for t_{acc} of 2 and 3 min, as shown in Fig. 12. The linear range can be extended to 1.0×10^{-7}–5×10^{-7} M by preconcentrating for 2 min, ($y = 0.601 + 10.2 \times 10^{-7}x$; $r = 0.997$; $y =$ peak current (nA) and $x =$ concentration (M)). The detection limit under the optimum instrumental conditions was estimated as 5×10^{-10} M with 3 min accumulation (based on a signal-to-noise ratio of 3). The relative standard deviation, calculated from seven determinations at 1×10^{-7} M was 1.28%.

Certain urine components, such as uric acid (15 μg ml^{-1}) and albumin (12.5 μg ml^{-1}) were found to decrease the voltammetric response by 60%. Thus, the addition of 0.5 ml of urine to the cell containing 20 ml of 1×10^{-7} M tipredane in buffer was enough to suppress the signal completely. This indicates that components of the urine compete very effectively with the drug for a place on the electrode surface to the point of inhibiting its adsorption [21]. Thus, separation of the drug from the urine would be essential, and such methods would need to be developed. The use of solid phase extraction cartridges prior to using cathodic stripping voltammetry, for this purpose, is being used increasingly [22–24]. It should be noted, however, that Lan et al. [3] reported that tipredane is extensively biotransformed by liver homogenates, and they identified 14 of the 17 metabolites by mass spectrometry. Three major transformation pathways were identified.

Acknowledgements

The authors thank Dr. Steven C. Nicholls of Fisons Pharmaceuticals plc for providing samples of tipredane and for his interest in this work. MVBZ thanks FAPESP (Brazil) for financial support and the Instituto de Quimica (UNESP) Araraquara (Brazil) for leave of absence.

References

[1] R.J. Wynar, R.K. Varma, C.A. Free, R.C. Millonig and B.N. Lutsky, Arzeim. Forsch. Drug. Res., 36 (1986) 1782, 1787.
[2] R.G. Devlin, A.V. Dean, A.A. Sugerman, K.J. Kripalani and R.J. Taylor, J. Toxicol. Cutaneous Ocul. Toxicol., 5 (1986) 35.
[3] S.J. Lan, L.M. Scanlan, R.K. Varma, S.H. Weistein, B.M. Wanack, S.E. Unger, M.A. Porubcan and B.H. Migdalof, Drug Metab. Disp., 17 (1989) 532.
[4] M.R. Euerby, R.J. Lewis and S.C. Nicholls, Anal. Proc., 28 (1991) 287.
[5] M.R. Euerby, C.M. Johnson and S.C. Nicholls, Anal. Proc., 30 (1993) 46.
[6] P. Kabasakalian and J. McGlotten, J. Am. Chem. Soc., 78 (1956) 5032.
[7] E. Jacobsen and B. Korvald, Anal. Chim. Acta, 99 (1978) 255.
[8] H.S. de Boer, J. den Hatigh, H.H.J.L. Ploegmakers and W.J. Van Oort, Anal. Chim. Acta, 102 (1978) 141.
[9] H.S. de Boer and W.J. Van Oort, Anal. Chim. Acta, 120 (1980) 31.
[10] H.S. de Boer, W.J. Van Oort and P. Zuman, Anal. Chim. Acta, 130 (1981) 111.
[11] A.M. Bond, Modern Polarographic Methods in Analytical Chemistry, Marcel Dekker, New York, 1980.

[12] L.M. Rodriguez-Monge, E. Munoz, J.L. Avila and L. Camacho, Anal. Chem., 60 (1988) 2269.
[13] E. Munoz, J.L. Avila and L. Camacho, Anal. Chem., 63 (1991) 1574.
[14] M.H. Kim and R.L. Birke, Anal. Chem., 55 (1983) 522, 1735.
[15] M. de Juan, A.M. Heras, L. Camacho and J.L. Avila, J. Electroanal. Chem., 191 (1985) 303.
[16] E. Laviron, J. Electroanal. Chem., 52 (1974) 355.
[17] A.J. Bard and L.R. Faulkner, Electrochemical Methods. Fundamentals and Applications, Wiley, New York, 1980, Chap. 12, p. 525.
[18] E. Laviron, Bull. Soc. Chim. Fr., (1970) 1637.
[19] E. Laviron and B. Riollet, Bull. Soc. Chim. Fr., (1968) 5077.
[20] A.J. Fry, Synthetic Organic Electrochemistry, Harper & Row, 1992, Chap. 7, p. 245.
[21] A. Zapardiel, J.A. Perez-Lopez, E. Bermejo, L. Hernandez and A.G. Espartero, Anal. Lett., 24 (1991) 233.
[22] L. Hernandez, A. Zapardiel, J.A.P. Lopes and E. Bermejo, Talanta, 35 (1988) 287.
[23] M.O. Telting-Diaz, A.J. Miranda Ordieres, A. Costa Garcia, P. Tuñón Blanco, D. Diamond and M.R. Smyth, Analyst, 115 (1990) 1215.
[24] M.V.B. Zanoni, J.C. Moreira and A.G. Fogg, Analyst, in press.

ELSEVIER

Analytica Chimica Acta 298 (1994) 245–251

ANALYTICA CHIMICA ACTA

Silver selective electrodes based on thioether functionalized calix[4]arenes as ionophores

Elżbieta Malinowska [a], Zbigniew Brzózka [a], Krzysztof Kasiura [a], Richard J.M. Egberink [b], David N. Reinhoudt [b,*]

[a] *Department of Analytical Chemistry, Technical University of Warsaw, Noakowskiego 3, PL-00664 Warsaw, Poland*

[b] *Department of Organic Chemistry, University of Twente, P.O. Box 217, 7500 AE Enschede, Netherlands*

Received 10 February 1994; revised manuscript received 31 May 1994

Abstract

Silver selective electrodes based on thioether functionalized calix[4]arenes **1** and **2** as ionophores were investigated. For both ionophores the selectivity coefficients ($\log k_{Ag,M}$) were lower than -2.2 for Hg(II) and lower than -4.6 for other cations tested. The best results were obtained with membranes containing dithioether functionalized calix[4]arene (ionophore **2**), potassium tetrakis(4-chlorophenyl)borate (KTpClPB) and bis(1-butylpentyl)adipate (BBPA) as a plasticizer. The Ag(I)-response functions exhibited almost theoretical Nernstian slopes in the activity range 10^{-6}–10^{-1} M of silver ions.

Keywords: Ion selective electrodes; Calix[4]arenes; Silver selective electrodes; Thioether functionalized calix[4]arenes

1. Introduction

The commercially available solid-state silver electrode based on Ag_2S is one of the oldest solid-state electrodes known in the literature [1–5]. This electrode exhibits an excellent selectivity towards alkali, alkaline earth, and most heavy metal ions. However, the strong mercury interference ($\log k_{Ag,Hg} > 0$) [6] is a weakness of this electrode. Due to the appropriate exchange mechanisms at the silver sulfide surface, a response to Hg^{2+} ions is always observed. Morf et al. [7] claimed on the basis of the defect theory for silver selective membranes that the response of silver halide or sulfide sensors to Hg^{2+} ions is neither Nernstian nor linear. Consequently the evaluation of the real Ag^+/Hg^{2+} selectivity is a serious problem. This is the reason why a search for new silver selective sensors has been continued for the past few years. Improved mercury interference was obtained for a solid Araldite based silver selective electrode ($\log k_{Ag,Hg} = -4$), although the interferences of other heavy metal ions (e.g., copper and cadmium; $\log k_{Ag,M} = -2.5$) were increased [8]. The ion-selective electrode based on chalcogenide glasses described by Vlasov [9] seems to be by far the best. Selectivity coefficients with $\log k_{Ag,M} < -5.5$ were obtained for alkali, alkaline earth and heavy metal ions. The interference of mercury was low ($\log k_{Ag,M} = -3.2$). Pei et al. [10] presented a carbon paste electrode (carbon graphite with Nujol) as a potentiometric silver selective electrode. In this case the interferences of alkali and alkaline earth metal ions were negligible, for other cations the following values of $\log k_{Ag,M}$ were obtained: zinc(II), cobalt(II) and

* Corresponding author.

SSDI 0003-2670(94)00267-P

nickel(II), −3.2; lead(II), −2.3; copper, −2.1; and mercury(II) −0.7.

Neutral carrier based silver selective electrodes are characterized by lower selectivities as compared with the above described solid-state electrodes [1–9]. In most cases crown ethers derivatives have been used as an ionophores [11–23]. It was found that enhanced selectivity for silver ions is achieved, compared with crown ethers, when one or more oxygen donor atoms are replaced by sulfur. Lai and Shih [15] used 1,4-dithia-15-crown-5 (PVC/dibutyl phthalate) in an electrode for silver detection. This thiacrown ether showed the best sensitivity (40 mV dec.$^{-1}$) of all crown ethers tested. The selectivity coefficients (log $k_{Ag,M}$) towards interfering alkali, alkaline earth and transition metal ions were higher than −3.5 (for sodium, potassium and magnesium). The strongest interferent was mercury (+0.8). Better results were obtained by Oue et al. [16–18]. Both ion selective electrodes with mono- and dithiacrown ethers in a PVC/dioctyl phthalate (DOP) matrix were highly silver selective. The selectivity coefficients for silver with respect to the heavy and transition metal ions are < -3 and with respect to alkali and alkaline earth metal ions < -4. The mercury ions interfered most seriously (log $k_{Ag,M} = -2.2$ to -1.5). The selectivities of the silver electrodes with different thiacrown ethers were quite similar in spite of different sulfur atoms in the thiacrown ethers. However, these parameters influence the sensitivity of the electrode (DOP plasticized membranes) especially at high silver activities. Oue et al. [18] observed also that the sensitivity of the electrode with *o*-nitrophenyl octyl ether (*o*-NPOE) as a plasticizer was lower at high silver activities in comparison with the sensitivity of the electrode with bis(2-ethylhexyl) sebacate (DOS) or DOP. Casabo et al. [19–21] have described the performance of several thiabenzocrown ethers as ionophores for ion-selective electrodes (PVC/DOP). For all the ligands tested a Nernstian sensitivity towards silver was found. Mercury was the strongest interferent (log $k_{Ag,Hg}$ −2 to −2.6) while for other cations log $k_{Ag,M} < -4$. Also in this case it was found that despite the different geometry and number of sulfur donor atoms in the crown ethers, the selectivity coefficients of the corresponding electrodes were similar.

The possibility for a good coordination geometry for Ag^+ seems to be more important than the perfect ring size, explaining why lipophilic podand-like ionophores display respectable chelating effects. Recently O'Connor et al. [22] have described calixarene derivatives with four sulfur and/or nitrogen donors atoms as ionophores for silver selective electrodes (PVC/*o*-NPOE). All exhibited acceptable silver responses with the best (calix[4]arene substituted with four $-CH_2CO_2C_2H_4SCH_3$ groups) giving a response of 50 mV dec.$^{-1}$ in the Ag(I) ion activity range of 10^{-4} to 10^{-1} M. Selectivity coefficients (log $k_{Ag,M}$) were higher than −3.3 for copper(II), nickel(II), cobalt(II), cadmium(II) and higher than −2.0 for potassium, lead(II) and sodium ions. Mercury interfered the most (log $k_{Ag,M} = +2.0$).

In this paper we report on the use of two novel calix[4]arene derivatives functionalized with two or four thioether ($-C_2H_4SCH_3$) groups as silver selective electrodes, and electrode characteristics as response time and pH-dependence are presented. In addition, some results of potentiometric titrations of halides, by using these electrodes in comparison with commercial silver electrodes, are reported.

2. Experimental

2.1. Chemicals

All salts employed were of analytical grade and were purchased from POCH (Gliwice, Poland). The standard stock solutions (0.1 M) of metal nitrates were prepared in redistilled water; working solutions were obtained by dilution of the stock solution with redistilled water. The pH was adjusted by the addition of nitric acid or sodium hydroxide solutions.

2.2. Ionophores and membrane materials

The synthesis of ligands has been described previously [23]. High molecular weight poly(vinyl chloride) (PVC), potassium tetrakis(4-chlorophenyl) borate (KTpClPB), *o*-nitrophenyl octyl ether (*o*-NPOE) and bis(butylpentyl)adipate (BBPA) were obtained from Fluka. As a solvent for the membrane components freshly distilled tetrahydrofuran (THF) p.a. (POCh Gliwice) was used.

2.3. Membrane and electrode preparation

The membranes contained 1 wt.% ionophore, 75 mol% KTpClPB (relative to the ionophore), 65–66 wt.% plasticizer, and 33 wt.% poly(vinyl chloride) (PVC). The membrane components (200 mg in total) were dissolved in 2 ml of freshly distilled tetrahydrofuran (THF). This solution was placed in glass ring of 24 mm i.d. resting on a glass plate. After solvent evaporation overnight, the resulting membrane was peeled off from the glass mould and discs of 7 mm i.d. were cut out. Membrane discs were mounted in electrode bodies (Type IS 561; Philips, Eindhoven, Netherlands) for electromotive force (EMF) measurements. As internal filling solution, a 0.005 M solution of $AgNO_3$ and HNO_3 (pH 2) was used. The electrodes were than conditioned overnight in a solution of 0.01 M KNO_3 and 0.001 M $AgNO_3$. For each membrane composition two electrodes were prepared.

2.4. EMF measurements

All measurements were carried out at 20°C with cells of the following type: Ag; AgCl; KCl (0.1 M)/0.1 M KNO_3/sample solution//sensor membrane//internal filling solution; AgCl; Ag.

The EMF values were measured using a custom made 16-channel electrode monitor. Details of this equipment are described elsewhere [24]. Potentiometric selectivity coefficients ($k_{Ag,M}$) were determined by the fixed interference method [25,26] by increasing the activity of primary ion in the solution in steps of 0.5 log a_{Ag}, or for strong interfering ions by the separate solution method using 0.01 M solutions of metal nitrates at a constant pH 4 (for mercury pH 2). In these cases the experimentally obtained slope was used for the calculations. The activities of metal ions in aqueous solutions were calculated according to the Debye-Hückel approximation [27]. The performance of the electrodes was examined by measuring of EMFs of the primary ion solutions with the concentration range 10^{-8}–10^{-1} M in solutions stirred with a magnetic stirrer.

The response time ($t_{95\%}$) of the electrode was tested by measuring the time required to achieve a 95% steady potential for a 0.01 M solution, when the Ag(I) ion concentration was rapidly increased by one decade from 0.0001 to 0.01 M.

3. Results and discussion

Ionophores (**1** or **2**) (Fig. 1) with a small amount of potassium tetrakis(4-chlorophenyl)borate (as lipophilic anionic sites) were incorporated in a plasticized PVC membrane. Two plasticizers, a polar o-NPOE and a non-polar BBPA were investigated. Also membranes without the ionophores present were examined.

Fig. 2 shows the Ag^+ responses of electrode based on BBPA plasticized PVC containing ionophore **2** and KTpClPB in the presence of some interfering cations.

All tested membranes showed a response towards silver ions but the calibration graphs obtained for membranes containing an ionophore were different for these "blank membranes". The results are demonstrated in Fig. 3a for the electrodes with the *o*-NPOE plasticized membranes and in Fig. 3b for the BBPA plasticized membranes. The "blank membranes" showed a linear response at the high concentrations of silver ($>10^{-3}$ M). In both cases the slope was less than Nernstian (ca. 41 mV dec.$^{-1}$ for *o*-NPOE and 43 mV dec.$^{-1}$ for BBPA). The detection limit for membranes with an ionophore incorporated was lower by 2 units but the response resembled an S-curve (except for the membrane with **2** and BBPA). This deviation from Nernstian response might be explained by the "sample anion effect" or by the formation of extremely stable complexes of ligands with cations [28]. According to the model calculations described by Cobben [29], this S-curve type of response can be caused by the outer boundary potential (membrane–sample solution). The association constant (β_1) of complex formed between

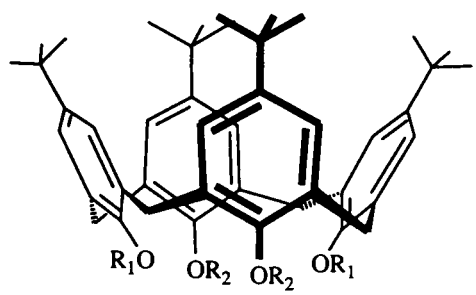

1 $R_1 = R_2 = CH_2CH_2SCH_3$

2 $R_1 = H$, $R_2 = CH_2CH_2SCH_3$

Fig. 1. Structures of ionophores.

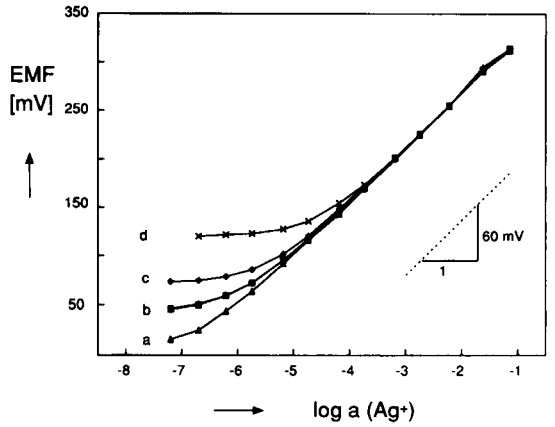

Fig. 2. Ag responses of electrodes based on ionophore **2** and BBPA as a plasticizer (with addition of KTpClPB) in the presence of 0.1 M of interfering cations. (a) K^+; (b) Mg^{2+} or Cu^{2+}; (c) Pb^{2+}; (d) $K^+ + 10^{-4}$ M Hg^{2+}.

the primary cation and the ionophore should be extremely high ($\beta_1 = 10^{13}$ mol l^{-1}) to cause such an effect. As is shown in Fig. 3a the electrodes based on **1** with *o*-NPOE as a plasticizer exhibited Ag-response in a very narrow range of silver ion concentrations ($10^{-5.5}$–$10^{-3.5}$ M) with the slope only 38 mV/decade. In this case the deviation from Nernstian response was the largest. For this electrode the influence of the concentration of the anionic site (0–90 mol% relatively to the ionophore) was studied. We found that the variation in the ratio KTpClPB to the ionophore did not substantially influence the response. With ionophore **2** and o-NPOE the slope of the linear response was close to the theoretical value (53.8 mV/decade) and in a wider range of Ag^+ concentrations.

It is known that in sensors for monovalent cations the use of relatively nonpolar membrane materials can improve the cation response [28,29]. This has been confirmed experimentally for ionophores **1** and **2**. With BBPA as the plasticizer the linear response range for both ionophores (**1** and **2**) becomes larger although for ionophore **1** a deviation from linearity at higher silver concentrations was observed.

Three compositions of a PVC membrane with KTpClPB: (**1**–BBPA), (**2**–BBPA) and (**2**–*o*-NPOE) have been studied in greater detail. The selectivity, response to the silver(I) ions concentration (slope and detection limit), pH dependence, and response time were measured. The results are given in Table 1. The logarithmic values of the selectivity coefficients (expressed as log $k_{Ag,M}$) are presented in Fig. 4. The preference for silver over other monovalent cations was more significant for membranes plasticized with *o*-NPOE than BBPA. It seems that without ionophore the selectivity is related to the hydration energy [30]. The incorporation of the ligand **1** or **2** into the membrane phase substantially affected the selectivity of the membranes as compared with the "blank membranes". For both ligands, and both plasticizers, the selectivity coefficients (log $k_{Ag,M}$) were lower than -4.6 for all cations tested, except mercury. The interference of mercury was more severe but still a selective response was found for *o*-NPOE plasticized membranes containing ligand **1** or **2**. The selectivity of the substituted bis[2-(meth-

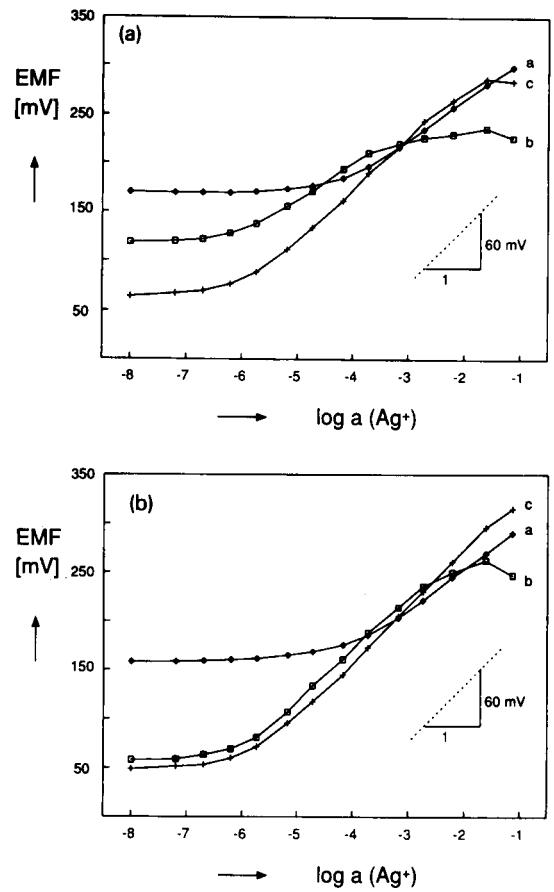

Fig. 3. (a) Ag responses of electrodes based on ionophores **1** or **2** and *o*-NPOE as a plasticizer (with KTpClPB) in the presence of 0.1 M $Mg(NO_3)_2$. (a) Without ionophore; (b) ionophore **1**; (c) ionophore **2**. (b) Ag responses of electrodes based on ionophores **1** or **2** and BBPA as a plasticizer (with KTpClPB) in the presence of 0.1 M $Mg(NO_3)_2$. (a) Without ionophore; (b) ionophore **1**; (c) ionophore **2**.

Table 1
Properties of Ag^+ selective membrane electrodes based on tetrakisthioether calix[4]arene **1** and bisthioether calix[4]arene **2** (PVC, *o*-NPOE or BBPA, 75 mol% KTpClPB)

	1		**2**	
	o-NPOE	BBPA	*o*-NPOE	BBPA
Slope (mV/dec.)	38.3	54.7	53.7	56.7
Response time, $t_{95\%}$ (s)		<15	<10	<10
Linear range (log *a*)	< −3.5	< −3.0	< −2.5	< −1.0
Detection limit	−5.5	−5.5	−6.0	−5.4
pH range		>3	>2.5	>2.5
Drift[a] (mV/day)	−2.6	−0.02	−1.0	−0.36

[a] Drift of measured potential for 0.01 M $AgNO_3$ solutions.

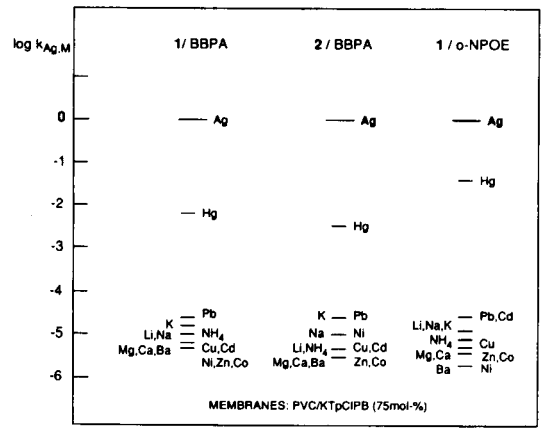

Fig. 4. Selectivity coefficients, log $k_{Ag,M}$, for PVC membranes containing ionophore **1** or **2**, anionic sites KTpClPB and *o*-NPOE or BBPA as plasticizer [0.1 M solutions of nitrates, pH 4, internal electrolyte: 0.05 M $AgNO_3 + HNO_3$, pH 2].

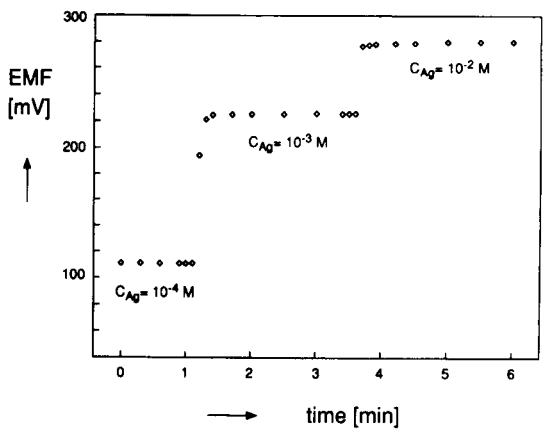

Fig. 5. Response time of electrodes based on ionophore **2** and BBPA as a plasticizer (with addition of KTpClPB) in the presence of 0.1 M KNO_3.

ylthio)ethoxy]calix[4]arene (**2**) was slightly better (−2.5) than of the tetra[2-(methylthio)ethoxy]-calix[4]arene (**1**) (−2.2). This leads to the conclusion that the number of sulfur donor atoms in the receptor molecule does not influence significantly the selective complexation of silver(I) ions. *o*-NPOE gave an increased selectivity coefficient of about 1 unit.

The response time ($t_{95\%}$) of the electrodes was tested by measuring the time required to achieve a 95% steady potential for a 10^{-2} M solution, when the silver ion concentration was rapidly increased one decade from 10^{-4} to 10^{-3} M and from 10^{-3} to 10^{-2} M. The response time was slightly longer for **1** (<15 s) than for **2** based membranes (<10 s). The results obtained for the electrode based on ligand **2**, BBPA as a plasticizer, and KTpClPB are presented in Fig. 5.

The pH dependence of the electrode response was examined using 10^{-4}, 10^{-3} and 10^{-2} M silver solutions. The electrodes are not pH sensitive in the range of pH 2.5–6. The upper pH limit is due to silver hydroxide formation. Fig. 6 shows the effect of pH on the response of **2**–BBPA electrode. Similar profiles were observed for other electrodes. These electrodes have been tested for 60 days. Properties of the electrodes are summarized in Table 1.

All electrodes were used in potentiometric titrations of halide ions (I^-, Br^-, Cl^-) with silver nitrate and their performance was compared with commercial silver selective electrodes (metallic and solid state). The results presented in Fig. 7a and b show that:

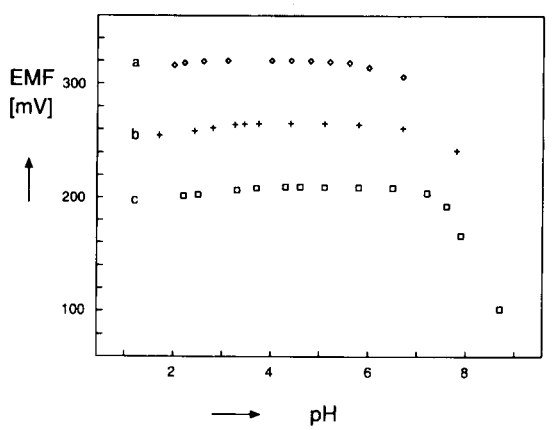

Fig. 6. pH response of Ag selective electrodes based on ionophore **2** and BBPA as a plasticizer (with addition of KTpClPB) in the presence of 0.1 M KNO_3. $C_{Ag(I)}$: (a) 10^{-2} M; (b) 10^{-3} M; (c) 10^{-4} M.

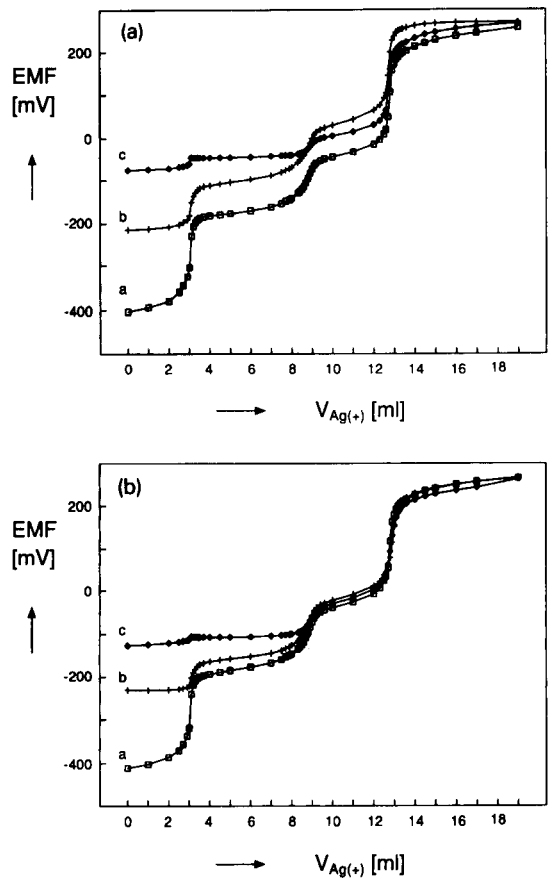

Fig. 7. (a) Potentiometric titration curves of a mixture of 4 ml KI, 6 ml KBr and 4 ml KCl (all 0.1 M) with 0.1 M $AgNO_3$ with: (a) metallic silver electrode; (b) Ag ISE based on ionophore **1** and *o*-NPOE; (c) Ag ISE based on ionophore **1** and BBPA. (b) Potentiometric titration curves of a mixture of 4 ml KI, 6 ml KBr and 4 ml KCl (all 0.1 M) with 0.1 M $AgNO_3$ with: (a) solid-state silver electrode; (b) Ag ISE based on ionophore **2** and *o*-NPOE; (c) Ag ISE based on ionophore **2** and BBPA.

(i) Using electrodes with *o*-NPOE plasticized membranes containing ligand **1** as well as **2** three end-points of this titration could be defined. However, the potential changes at the end-point, which corresponds with the determination of I^- ions, are significantly lower for these electrodes as compared with both metallic and solid-state ion-selective electrodes while for Br^- and Cl^- ions potential changes are similar.

(ii) For both electrodes with BBPA the end-point for I^- ions is imperceptible. Even for Br^- ions the end point is lower as compared with **1**–*o*-NPOE and **2**–*o*-NPOE as well as two commercial silver electrodes.

(iii) It seems that the true detection limit of the electrodes tested is lower than that obtained for solutions which were not metal buffer solutions for silver.

4. Conclusions

The present results suggest that calix[4]arenes derivatives containing thioether groups show high selectivity and, when the BBPA is used as a plasticizer, sensitivity towards silver ions. The best results were obtained for membranes containing dithioether functionalized calix[4]arene (ionophore **2**), KTpClPB and BBPA as a plasticizer. The determination of silver is possible over a wide range of concentrations in the presence of alkali, alkaline, and heavy metals ions. For mercury(II) ions the log $k_{Ag,M}$ values are -2.5 and comparable to the best ISE known so far.

Acknowledgements

This work was supported by the Polish State Committee for Scientific Research; Project No. 2 0775 91 01 sponsored in 1991–1994.

References

[1] T.S. Light and J.L. Swartz, Anal. Lett., 1 (1968) 825.
[2] M. Mascini and A. Liberti, Anal. Chim. Acta, 51 (1970) 231.
[3] E. Schmidt and E. Pungor, Anal. Lett., 4 (1971) 641.
[4] J. Vesely, O.J. Jensen and B. Nicolasen, Anal. Chim. Acta, 62 (1972) 1.
[5] C. Litenau, I.C. Popescu and V. Ciovirnache, Talanta, 19 (1972) 985.
[6] Y. Umezawa (Ed.), Handbook of Ion-Selective Electrodes: Selectivity Coefficients, CRC Press, Boca Raton, FL, 1990.
[7] W.E. Morf, G. Kahr and W. Simon, Anal. Chem., 46 (1974) 1538.
[8] A.K. Jain, R.P. Singht and S. Agrawal, Anal. Chem., 51 (1979) 1093.
[9] Yu.G. Vlasov, Fresenius' Z. Anal. Chem., 335 (1989) 92.
[10] J. Pei, Q. Yin and J. Zhong, Talanta, 38 (1991) 1185.
[11] B.P. Bubnis, J.L. Steger, Y.P. Wu, L.A. Meyers and G.E. Pacey, Anal. Chim. Acta, 139 (1982) 307.
[12] K. Kimura, H. Yano, S. Kitazawa and T. Shono, J. Chem. Soc., Perkin Trans. II, (1986) 1945.
[13] K. Kimura. H. Oishi, T. Miura and T. Shono, Anal. Chem., 59 (1987) 2331.
[14] C.J. Pedersen, J. Org. Chem., 36 (1971) 254.

[15] M.T. Lai and J.S. Shih, Analyst, 111 (1986) 891.
[16] M. Oue, K. Kimura, K. Akama, M. Tanaka and T. Shono, Chem. Lett., (1988) 409.
[17] M. Oue, K. Akama, K. Kimura, M. Tanaka and T. Shono, J. Chem. Soc., Perkin Trans. I, (1989) 1675.
[18] M. Oue, K. Akama, K. Kimura, M. Tanaka and T. Shono, J. Anal. Sci., 5 (1989) 165.
[19] J. Casabo, C. Perez-Jimenez, L. Escriche, S. Alegret, E. Martinez-Fabregas and F. Teixidor, Chem. Lett., (1990) 1107.
[20] J. Casabo, L. Escriche, S. Alegret, C. Jaime, L. Mestres, F. Teixidor, C. Perez-Jimenez, J. Rius, E., Molins and C. Miravitlles, Inorg. Chem., 30 (1991) 1893.
[21] J. Casabo, L. Mestres, L. Escriche, F. Teixidor and C. Perez-Jimenez, J. Chem. Soc., Dalton Trans., (1991) 1969.
[22] K.M. O'Connor, G. Svehla, S.J. Harris and M.A. McKervey, Talanta, 39 (1992) 1549.
[23] P.L.H.M. Cobben, R.J.M. Egberink, J.G. Bomer, P. Bergveld, W. Verboom and D.N. Reinhoudt, J. Am. Chem. Soc., 114 (1992) 10573.
[24] Z. Brzózka, Pomiary, Automatyka, Kontrola, 5 (1988) 422.
[25] G.G. Guilbault, R.A. Durst, M.S. Frant, H. Freiser, E.H. Hansen, T.S. Light, E. Pungor and J.D.R. Thomas, Pure Appl. Chem., 48 (1976) 127.
[26] A. Lewenstam and A. Hulanicki, Selective Electrode Rev., 12 (1990) 161.
[27] P.C. Meier, Anal. Chim. Acta, 136 (1982) 363.
[28] D. Ammann, W.E. Morf. P.C. Meier, E. Pretsch and W. Simon, Ion-selective Electrode Rev., 5 (1983) 16.
[29] P.L.H.M. Cobben, Ph.D. Thesis, University of Twente, Enschede, 1992.
[30] Y. Marcus, in Ion solvation, Wiley, New York, 1985, pp. 107–109.

ELSEVIER

Analytica Chimica Acta 298 (1994) 253–258

ANALYTICA CHIMICA ACTA

Lead selective electrodes based on thioamide functionalized calix[4]arenes as ionophores

Elzbieta Malinowska [a], Zbigniew Brzózka [a], Krzysztof Kasiura [a], Richard J.M. Egberink [b], David N. Reinhoudt [b,*]

[a] *Department of Analytical Chemistry, Technical University of Warsaw, Noakowskiego 3, PL-00664 Warsaw, Poland*

[b] *Department of Organic Chemistry, University of Twente, P.O. Box 217, 7500 AE Enschede, Netherlands*

Received 28 April 1994; revised manuscript received 31 May 1994

Abstract

Lead selective electrodes based on a di- and tetrathioamide functionalized calix[4]arene as ionophores were investigated. The Pb(II)-response functions exhibited almost theoretical Nernstian slopes in the activity range 10^{-6}–10^{-2} M of lead ions. For both ionophores a preference for lead over other cations was observed. The best results were obtained for membranes containing the tetrathioamide derivative (ionophore **1**), potassium tetrakis(4-chlorophenyl)borate and *o*-nitrophenyl octyl ether as a plasticizer. This electrode showed greatly improved selectivity over copper, zinc and cadmium ions as compared with commercial solid-state lead selective electrodes.

Keywords: Calix[4]arenes; Lead selective electrodes; Thioamide

1. Introduction

There is an increasing interest in the development of lead(II) ion-selective electrodes. Many compounds, either organic or inorganic, have been used as electroactive materials. The sulfide, oxide, selenide, and other salts of lead together with silver sulfide provide the active phase of solid-state electrodes [1–9]. For these electrodes other cations which form insoluble salts, e.g., cadmium, copper, mercury and silver interfere strongly with the electrode response towards lead(II), the influence of alkali and alkaline earth cations is negligible. Also, a chalcogenide glass electrode reported by Vlasow [10] exhibits the interference of copper and silver ions but the selectivity towards lead versus cadmium is improved.

The use of complexing agents offers the possibility of designing ligands with a wide range of functional groups, and consequently different abilities to complex cations. Several neutral compounds with oxygen, nitrogen and sulphur donor atoms have been examined as ionophores for lead selective electrodes [11–13]. The selectivity of dibenzo-18-crown-6 and its derivatives for lead in the presence of transition, alkali and alkaline earth metal ions has been investigated and values of log $k_{Pb,M}$ as high as -2.8 were found. Silver, potassium and copper showed the highest interference. Electrodes based on acyclic oxamides [14,15] have shown good selectivity for lead(II) ions in the presence of some transition, alkali and alkaline earth metal ions (log $k_{Pb,M} < -3$). It has been also described [16] that the incorporation in a membrane of macrocyclic oxamides induces a pronounced preference for lead over some

* Corresponding author.

SSDI 0003-2670(94)00266-O

transition and alkaline earth metal ions. However, the selectivity against monovalent ions was lower than that observed for the acyclic oxamides, and is depended on the number, the distribution of oxygen donor atoms and the ring size. Podands with antipyrylaminomethine groups as ionophores have been reported by Pyatova et al. [17]. The logarithmic selectivity coefficients were more negative than −3 except for potassium (−2.2), copper (−1.5) and silver (−0.3). Poly(hydroxamic acid) in silicone rubber as supporting material has been proposed for lead selective electrode [18]. Nickel, mercury and copper ions interfere strongly but for other cations values log $k_{Pb,M} > -1.6$ were reported. Kamata and Onoyama [19,20] have reported several acyclic dithiocarbamate ionophores. In all cases copper ions interfered strongly (log $k_{Pb,M} > 0$). Also the interference of sodium and potassium ions was significant.

Recently we have synthesized acyclic oxamides [21] and oxamide and thioamide derivatives of calix[4]arene which show good selectivities towards lead over other ions tested in CHEMFETs measurements [22].

In this paper we report on lead selective electrodes based on lipophilic thioamide functionalized calix[4]arenes **1** and **2** as receptor molecules.

2. Experimental

2.1. Chemicals

All salts employed were of analytical grade and were purchased from POCH (Gliwice, Poland). The standard stock solutions (0.1 M) of metal nitrates were prepared in redistilled water; working solutions were obtained by dilution of the stock solution with redistilled water. The pH was adjusted by the addition of nitric acid, sodium hydroxide or ammonia solution.

2.2. Ionophores and membrane materials

The synthesis of ligands used has been described previously [22]. High molecular weight poly(vinyl chloride) (PVC), potassium tetrakis(*p*-chlorophenyl) borate (KTpClPB), *o*-nitrophenyl octyl ether (*o*-NPOE) and bis(butylpentyl) adipate (BBPA) were obtained from Fluka (Buchs, Switzerland). As a solvent for membrane components, freshly distilled tetra hydrofuran (THF) p.a. (POCH) was used.

2.3. Membrane and electrode preparation

The membrane contained 1 wt% ionophore, 75 mol% KTpClPB (relative to the ionophore), 65–66 wt% plasticizer, and 33 wt% PVC. The membrane components, 200 mg in total, were dissolved in 2 ml of freshly distilled THF. This solution was placed in a glass ring of 24 mm i.d. resting on a glass plate. After overnight solvent evaporation, the resulting membrane was peeled off from the glass mould and discs of 7 mm i.d. were cut out. Membrane discs were mounted in electrode bodies (Type IS 561; Philips, Eindhoven, Netherlands) for electromotive force (EMF) measurements. As internal filling solution, a 0.005 M solution of $PbCl_2$ was used. The electrodes were subsequently conditioned overnight in a solution of 0.01 M $Pb(NO_3)_2$. For each membrane composition two electrodes were prepared.

2.4. EMF measurements

All measurements were carried out at 20°C with cells of the following type: Ag; AgCl; KCl (0.1 M)/0.1 M KNO_3/sample solution//sensor membrane//internal filling solution; AgCl; Ag.

The EMF values were measured using a custom made 16-channel electrode monitor. Details of this equipment are described in [23]. Potentiometric selectivity coefficients, $k_{Pb,M}$ were determined by the fixed interference method [24,25] with increasing the activity of primary ion in the solution in steps of 0.5 log a_{Pb} and/or, for hard interfering ions, by the separate solution method using 0.01 M solutions of metal nitrates at a constant pH of 4 (for mercury pH 2). In this case for calculations the experimentally obtained slope was used. The activities of metal ions in aqueous solutions were calculated according to the Debye-Hückel approximation [26]. The performance of the electrodes was examined by measuring EMFs of the primary ion solutions in the 10^{-7}–10^{-1} M concentration range in solutions stirred with a magnetic stirrer.

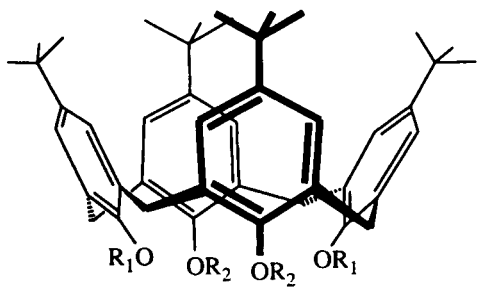

1 $R_1 = R_2 = CH_2C(S)N(CH_3)_2$

2 R_1 = n-propyl, $R_2 = CH_2C(S)N(CH_3)_2$

Fig. 1. Structures of ionophores.

3. Results and discussion

Structures of the examined ligands **1** and **2** are presented in Fig. 1.

The Pb(II)-response functions of membranes with **1** and **2** exhibited a nearly theoretical Nernstian slope for divalent cations and were linear to at least 10^{-6} (**1**) or 10^{-5} m (**2**) $Pb(NO_3)_2$. The calibration graphs in the presence of some interfering cations for **1** based electrodes are displayed in Fig. 2a and b.

The logarithmic values of the selectivity coefficients (expressed as log $k_{Pb,M}$) are presented in Fig. 3a. For both ionophores a preference for lead over the other cations tested was observed. The Pb selectivity is higher for the tetrathioamide (ionophore **1**) than for

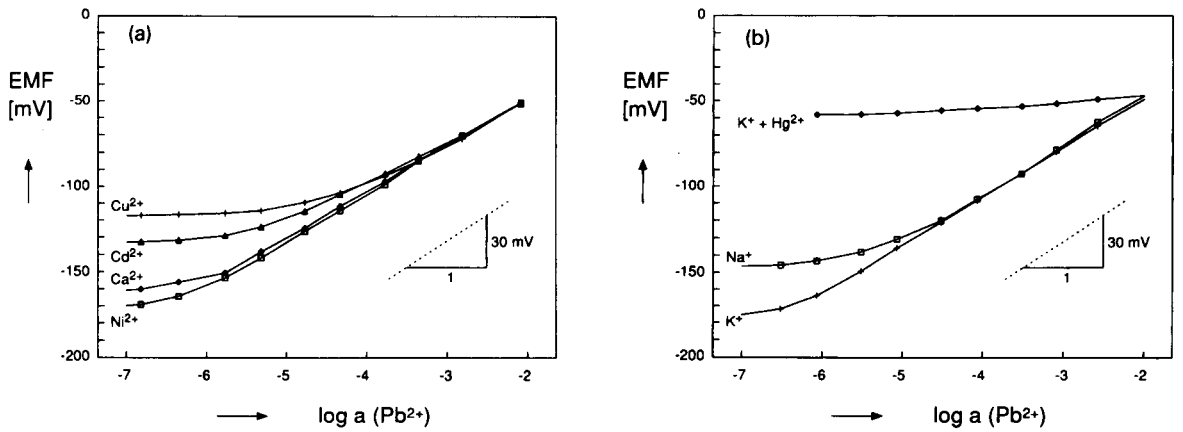

Fig. 2. Selectivity coefficients, log $k_{Pb,M}$, for PVC membranes with *o*-nitrophenyl octyl ether or bis(1-butylpentyl) adipate as plasticizer and with potassium tetrakis(4-chlorophenyl)borate (75 mol%). Membranes containing ionophore **1** or **2** (a) are compared with the "blank membranes" (b) [0.1 M solutions of nitrates, pH 4, internal electrolyte: 0.005 M $PbCl_2$].

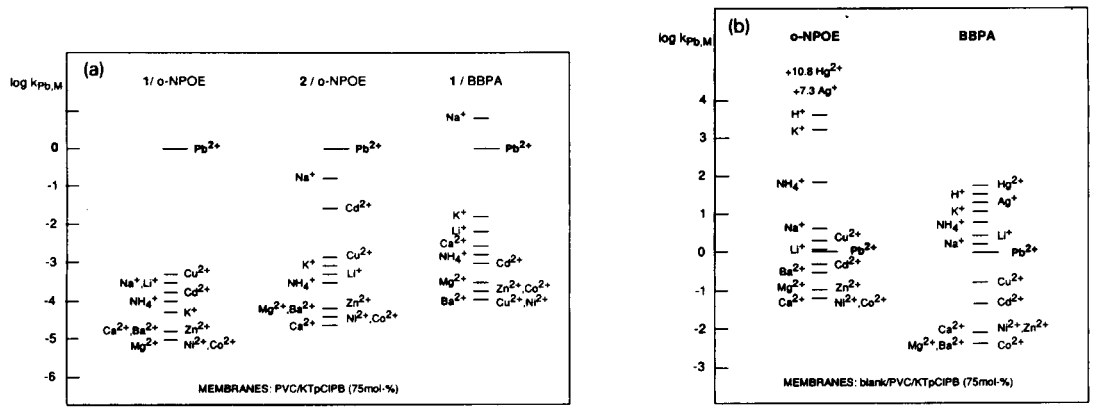

Fig. 3. Pb response of electrodes containing calix[4]arene ionophore **1** in the presence of 0.1 M of the chosen cations.

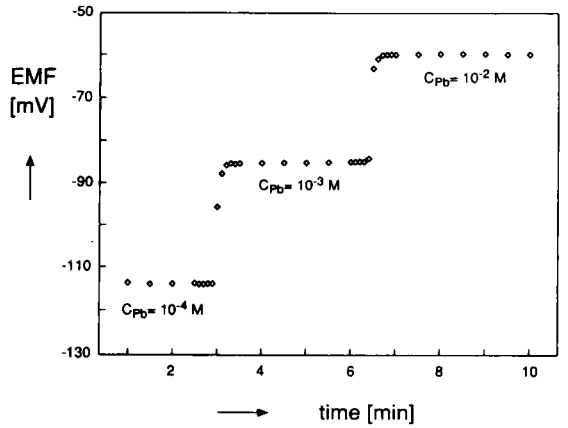

Fig. 4. Response time of electrodes containing calix[4]arene ionophore **1** in the presence of 0.1 M KNO_3.

the dithioamide (ionophore **2**) derivative of calix[4]arene. The smallest difference (<0.6 units) was found for calcium, barium, magnesium, zinc, copper, nickel, cobalt, lithium and ammonium ions while for cadmium, potassium and sodium ions this difference was even higher than 2 units. This leads to the conclusion that four thioamide groups are a prerequisite in a calix[4]arene based ionophore for selective complexation of lead(II) ions.

The incorporation of ligand **1** or **2** in *o*-NPOE plasticized membranes (in the presence of lipophilic anion sites) substantially affects the selectivity of the membranes as compared with the "blank membrane" (cf. Fig. 3a and Fig. 3b). Without ionophore only a slight selectivity towards divalent cations was observed (with the exception of copper and mercury). The examination of the influence of the KTpClPB concentration showed that membranes with ligands **1** and **2** but without KTpClPB do not induce selectivity towards lead ions. The observation that certain ligands behave as carriers only when lipophilic anionic sites are present in the membrane is well known [27]. An increased ratio of KTpClPB to ionophore improves the selectivity for lead(II) ions over monovalent cations and increases the linear range of electrode response in the higher concentration range of lead ions. We found that a ratio of ligand to KTpClPB of 1:0.75 is sufficient to exclude the sample anions influence and to obtain satisfactory selectivities for lead ions. With this composition further experiments were carried out.

It was found that for both electrodes, based on **1** and **2**, mercury ions did interfere. When the membrane with ionophore **2** came in contact with these ions the electrode was poisoned and did not show previous lead performance even after long conditioning in the lead nitrate solution. In the case of ionophore **1**, the electrode regained almost its lead response. The poisoning by mercury(II) ions has been mentioned by Kamata and Onoyama [19] for electrodes based on bis(diisobutyldithiocarbamate) neutral carrier with *o*-NPOE as a plasticizer.

The comparison of the selectivity data for "blank membranes" with *o*-NPOE and BBPA, suggests that the use BBPA as a plasticizer could reduce this effect. In the case of membranes based on BBPA plasticized PVC containing ionophore **1** the poisoning did not occur but the electrodes were affected by silver(I) and mercury(II) ions. The following selectivity coefficients, determined by a separate solution method for 10^{-2} M solutions of cations (pH 4 for lead and silver, and pH 2 for mercury), were obtained: log $k_{Pb,Hg} = +0.6$ and log $k_{Pb,Ag} = +1.5$. The selectivity coefficients versus other cations tested are shown in Fig. 3a. A change of the plasticizer for BBPA leads to a decrease of the selectivity towards lead ions over the cations tested, especially for alkali metal ions. The exception was copper(II). In this case log $k_{Pb,Cu}$ was lower (0.6) than for *o*-NPOE membranes plasticized.

The following properties of electrodes were tested: the selectivity, lead(II) response (slope, detection limit), pH dependence and response time. The electrode properties are summarized in Table 1.

The response time ($t_{95\%}$) of the electrodes was tested by measuring the time required to achieve a 95% value

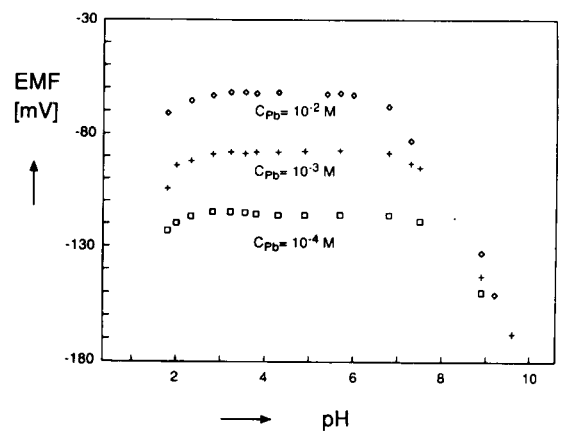

Fig. 5. pH response of electrodes containing calix[4]arene ionophore **1** in the presence of 0.1 M KNO_3.

Table 1
Properties of Pb-selective membrane electrodes based on tetra- and dithioamide calix[4]arenes **1** and **2** (PVC, *o*-NPOE, 75 mol%, KTpClPB)

Ionophore	Fresh membrane		After six weeks	
	1	**2**	**1**	**2**
Slope (mV/dec)	28.7	28.8	24.0	25.4
Response time t_{95}% (s)	<10	<8	<20	<10
Linear range (log *a*)	< −1.8	< −1.8	< −2.0	< −1.8
Detection limit	−6.5	−5.5	−6.0	−5.0
pH range	3–6	4–6		
Stability, 0.01 M Pb (mV/min), t = 25 min	< −0.01	−0.02	0.03	−0.04
Drift [a] (mV/day)			−1.5	−1.6

[a] Drift of measured potential for 0.01 M $Pb(NO_3)_2$ solutions.

of steady potential for a 10^{-2} M solution, when Pb(II) concentration was rapidly increased from 10^{-3} to 10^{-2} M and similarly for a change of Pb(II) concentration from 10^{-4} to 10^{-3} M. The results obtained for the electrode based on ligand **1** are presented in Fig. 4. In both cases (for **1** and **2**) the response time was less than 10 s.

The pH dependence of the electrode response was examined using 10^{-4}, 10^{-3} and 10^{-2} M $Pb(NO_3)_2$ solutions adjusted with nitric acid and ammonia. An electrode based on ionophore **1** showed an EMF plateau between pH 3 and 6 (Fig. 5), but based on **2** in a smaller pH range (4–6). The decrease of the potential in alkaline media can be explained by the formation of lead hydroxide in the solution, and at lower pH by the ionophore protonation.

4. Conclusions

The present results regarding the selectivity, electrode response, linear range, pH dependence and response time suggest that ligands tested can be used as ionophores for lead selective electrodes. The best results were obtained with membranes containing the tetrathioamide functionalized calix[4]arene (ionophore **1**), KTpClPB and *o*-NPOE as a plasticizer. For this membrane composition the slope is close to the theoretical for divalent ions in a wide range of lead(II) concentrations. The selectivity towards copper, zinc and cadmium ions is greatly improved as compared with commercial solid-state lead selective electrodes [28]. Moreover, for alkali metal ions the selectivity is higher than that of other lead selective liquid membrane electrodes [11–19].

Acknowledgement

This work was supported by the Polish State Committee for Scientific Research; Project No. 2 0775 91 01 sponsored in 1991–1994.

References

[1] J.W. Ross and M.S. Frant, Anal. Chem., 41 (1969) 967.
[2] H. Hirata and K. Higashlyama, Anal. Chim. Acta, 54 (1971) 415.
[3] H. Hirata and K. Higashlyama, Talanta, 19 (1972) 391.
[4] M. Mascini and A. Liberti, Anal. Chim. Acta, 60 (1972) 405.
[5] E.H. Hansen and J. Ruzicka, Anal. Chim. Acta, 72 (1974) 365.
[6] P. Kivalo, R. Virtanen, K. Wickstrom, M. Wilson, E. Pungor, G. Horvai and K. Toth, Anal. Chim. Acta, 87 (1976) 401.
[7] P. Gruendler, Anal. Lett. Part A, 14 (1981) 163.
[8] P.S. Thind, H. Singh, T.K. Bindal, Indian J. Chem., Sect. A, 21 (1982) 295.
[9] E. Pungor, K. Toth, G. Nagy, L. Polos, M.F. Ebel and I. Wernisch, Anal. Chim. Acta, 147 (1983) 23.
[10] Yu. G. Vlasov, Fresenius' Z. Anal. Chem., 335 (1986) 92.
[11] L.K. Shpigun, E.A. Novikov and Yu. Zolotov, Zh. Anal. Khim., 41 (1986) 617.
[12] E.A. Novikov, L.K. Shpigun and Yu. Zolotov, Zh. Anal. Khim., 42 (1987) 885.
[13] V.A. Popova, V.L. Volkov and I.V. Podgornaya, Zavod. Lab., 55 (1989) 25.
[14] E. Lindner, K. Toth, E. Pungor, F. Behm, P. Oggenfuss, D.H. Welti, D. Ammann, W.E. Morf, E. Pretsch and W. Simon, Anal. Chem., 56 (1984) 1127.
[15] E. Malinowska, Analyst, 115 (1990) 1085.
[16] E. Malinowska, T. Stankiewicz and J. Jurczak, Electroanalysis, 5 (1993) 489

[17] E.N. Pyatova, A.V. Kopytin, A. Yu. Tsivadze, E.G. Ilin, V.A. Popova, I.V. Podgornaya and Yu. A. Buslayev, Zh. Anal. Khim., 47 (1992) 535.
[18] K. Anuar and S. Hamdan, Talanta, 39 (1992) 1653.
[19] S. Kamata and K. Onoyama, Anal. Chem., 63 (1991) 1295.
[20] S. Kamata and K. Onoyama, Chem. Lett., (1991) 653.
[21] M. Battilotti, R. Mercuri, G. Mazzamurro, I. Giannini and M. Giongo, Sensors Actuators, Bl (1990) 438.
[22] P.L.H.M. Cobben, R.J.M. Egberink, J.G. Bomer, P. Bergveld, W. Verboom and D.N. Reinhoudt, J. Am. Chem. Soc., 114 (1992) 10573.
[23] Z. Brzozka, Pomiary, Automatyka, Kontrola, 5 (1988) 422.
[24] G.G. Guilbault, R.A. Durst, M.S. Frant, H. Freiser, E.H. Hansen, T.S. Light, E. Pungor and J.D.R. Thomas, Pure Appl. Chem., 48 (1976) 127.
[25] A. Lewenstam and A. Hulanicki, Selective Electrode Rev., 12 (1990) 161.
[26] P. C. Meier, Anal. Chim. Acta, 136 (1982) 363.
[27] F. Behm, D. Ammann and W. Simon, Helv. Chim. Acta, 68 (1985) 110.
[28] Y. Umezawa, Handbook of Ion-Selective Electrodes: Selectivity Coefficients, CRC Press, Boca Raton, FL, 1990.

ELSEVIER

Analytica Chimica Acta 298 (1994) 259–266

ANALYTICA CHIMICA ACTA

A microelectrode flow amperometric detector for water-soluble polymers

Victoria A. Vicente-Beckett [a,*], Min-Kuang Liu [b], J. Calvin Giddings [b], Stanley Pons [b], Marcus N. Myers [b]

[a] *Department of Applied Chemistry, Royal Melbourne Institute of Technology (City Campus), GPO Box 2476V, Melbourne 3001, Australia*
[b] *Department of Chemistry, University of Utah, Salt Lake City, UT 84112, USA*

Received 7 December 1993; revised manuscript received 2 June 1994

Abstract

A single electrode assembly, consisting of a platinum wire (20- or 25-μm diameter) microelectrode and a palladium coating (as auxiliary/pseudo-reference electrode) on the glass tubing housing the microelectrode, has been utilized as a flow amperometric sensor for water-soluble polymers. An ordinary 3-V dry cell was used as voltage source. Amounts of injected polymer were in the range 0.01–260 μg. The detector performance was superior to that of a differential refractive index detector in terms of limits of detection (sub-μg levels of polymer), baseline stability, and reproducibility of analytical signal.

Keywords: Amperometry; Flow system; Polymers; Water soluble polymers

1. Introduction

Polymer analyses and characterization, using methods such as field-flow fractionation (FFF) and size exclusion chromatography (SEC) have been limited by detection methods which have inadequate selectivity and sensitivity. Common detection methods include UV absorbance and differential refractive index. The former is limited to substances with chromophoric groups; the sensitivity is often inadequate at the polymer concentrations being analyzed and separation channels (in FFF) or columns (in SEC) tend to get overloaded in attempts to enhance analytical signals. Although the refractive index detection method is potentially more sensitive, it is extremely temperature-dependent and thus often suffers from drifting baseline signals, which may be overcome only by extended periods (several hours) of stabilization.

Electrochemical detection methods have had limited application in polymer detection because of the generally low solubility of polymers in aqueous media and the need to use a relatively high concentration of inert electrolyte in these techniques.

The last decade has seen the increase in application of microelectrodes, which have diameters much less than 100 μm. These electrodes have been shown to exhibit properties which could overcome some of the conventional requirements in electrochemical measurements, thus making them quite suitable for polymer detection [1–3]. In particular, the small electrode surface area requires very low charging current and steady-state currents are achieved practically instantaneously, making them ideal flow detectors. Since only very small currents are involved, the solution ohmic drop is

* Corresponding author.

SSDI 0003-2670(94)00268-Q

negligible and the electrode may be employed in solvents with low dielectric constant [4] or even in the absence of a supporting electrolyte, as demonstrated in this work. A two-electrode system may be used and a potentiostat is not necessary [5].

Knecht et al. [6] and White et al. [7,8] have successfully used a 9-μm carbon fibre voltammetric detector for open-tubular liquid chromatography. However, they employed the usual level of electrolyte (ca. 1 M) in the mobile phase.

This paper describes a low-volume microelectrode flow amperometric detector suitable for polymer analysis, following separation either by FFF or SEC. An ordinary alkaline dry cell was used as voltage source and ultra-pure water as the carrier solvent. The study was confined to the detection of water-soluble polymers in aqueous solutions.

2. Experimental

2.1. Electrode assembly

The two-electrode assembly (see Fig. 1(I)) consisted of a platinum microelectrode and a palladium film (which served as both auxiliary electrode and reference electrode) and was prepared according to a procedure described elsewhere [9]. A 20- or 25-μm diameter platinum wire was sealed with epoxy in a quartz tube (ca. 10 cm × 6 mm o.d., tapering to approximately 0.8 mm at the sensing tip). Electrical contact was made to the platinum through a fine copper wire attached to the platinum with silver-loaded epoxy. The outer surface of the quartz tube was painted with bright palladium (over a width of about two cm from the tip), and then fired in a tube furnace [9]. For electrical contact, a piece of insulated copper wire was soldered to the portion of the palladium film that remained outside the flow cell. The tip of the electrode was gently polished on 600-μm silicon carbide abrasive paper in a medium of water to expose the platinum wire. Routine polishing was performed on balsa wood in a medium of an aqueous slurry of alumina (progressing sequentially from 1.0-, 0.3-, to 0.05-μm size particles). During a day's use, the electrode surface showed no evidence of memory effects (i.e., the baseline signal was extremely reproducible) and thus repolishing the electrode or electrochemical pretreatment between runs was not necessary.

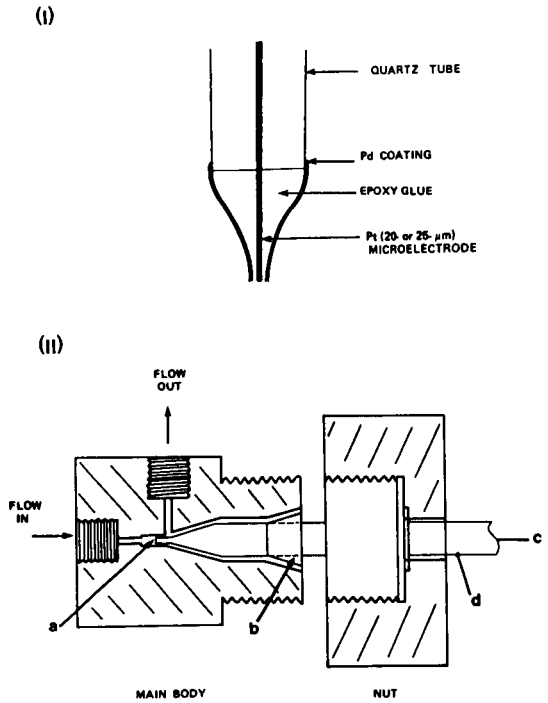

Fig. 1. (I) The electrode assembly; (II) cross-section of the flow cell. (a) Electrode sensing tip; (b) PTFE ferrule; (c,d) copper wire contact to Pt microelectrode and to Pd coating, respectively.

2.2. Flow cell

A diagram of the cross-section of the prototype flow cell, which was made of glass-reinforced teflon, is shown in Fig. 1(II). About two-thirds of the electrode body remained outside the cell. A tight seal within the flow cell was achieved using PTFE ferrules. The electrode assembly and the flow cell were contained in a 0.25-in thick aluminum Faraday cage ($6 \times 6 \times 6$ in^3) and shielded cables were used to minimize electrical noise.

The dead volume of this prototype cell was estimated using 6.9 mM potassium ferricyanide (in 0.5 M potassium chloride) as test solute, an applied potential of -0.5 V, and carrier flow rates between 0.070–0.27 ml/min. The extrapolated flow cell volume at zero flow rate was $98 + 10$ μl. This volume is much larger than the sensing volume because of the need to remove the

electrode assembly regularly for a daily routine of electrode surface mechanical reactivation.

2.3. Instrumentation

A 3-V Eveready alkaline power cell connected to a ten-turn 1-kΩ potentiometer was used as a voltage source. The microelectrode was kept as close to ground potential as possible: i.e., it was connected to the ammeter (Keithley 619 electrometer/multimeter; current range 0.1–10 nA) input and applied potentials were opposite to the actual potential of the electrode. The resulting current was recorded on Houston Omniscribe recorder. Where required, an home-built electronic device, which allowed signal scaling and subtraction, was used to offset the recorder baseline in order to enhance the current signal.

The performance of the electrochemical detector was compared to that of a Hewlett Packard 1037A differential refractive index detector (RI) operated at 30°C at its most sensitive measurement range [$(1/64) \times 10^{-6}\Delta$RI unit full range].

2.4. Flow-injection system

Flow-injection experiments were conducted to test the performance of the electrochemical detector. The flow-injection system included the solvent reservoir, the peristaltic pump (Gilson Minipuls 2), and a simple PTFE T-shaped injector port, which was kept as close as practicable to the flow cell (maximum distance was ca. 30 cm) using 0.58 i.d. PTFE tubing. Samples were introduced with either a 10- or a 50-μl Hamilton microsyringe.

2.5. Carrier solvent

Barnstead ultrapure water served as the carrier solvent and was continuously purged with helium to remove dissolved air. The baseline current varied with the applied potential but, provided that the potential was within ± 1.5 V, it was typically less than 0.3 nA. Towards these extreme values, the recorder baseline could be offset electronically to enhance the analytical signal.

2.6. Polymers

Several water-soluble polymers (listed in Table 2, together with their nominal average molecular weights, MW) were used to test the performance of the microelectrode detector. Polyvinylpyrrolidone (PVPD; MW 40,000 and 360,000), polyethylene oxide (PEO), and polyacrylic acid were obtained from Aldrich; PVPD (MW 10,000), dextran, and poly(acrylamide–acrylic acid) from Sigma; the polyacrylamides from American Cyanamid; and blue dextran from Pharmacia. In general, these polymers had limited solubilities in water, some dissolving only after standing overnight.

Injected polymer levels were between 0.01–259 μg.

3. Results and discussion

3.1. Electrochemical behavior of polymers

Preliminary experiments utilizing cyclic voltammetry in solutions of the polymer in 0.1 molar potassium nitrate were performed to determine the electrochemical behavior of the polymers. Only polyvinylpyrrolidone and polyacrylic acid exhibited steady-state currents at potentials < -0.7 V. In the case of the other polymers, any electroactivity was masked by the hydrogen or oxygen evolution reactions at the potential limits of the platinum electrode in water. The lack of electrochemical response in static solution conditions may be due to the slow diffusion of the large polymer molecules. Flowing conditions force these large species to impinge on the electrode surface, allowing electrochemical processes to occur.

However, it is possible to ascertain the current response as a function of applied potential for each polymer by recording a family of hydrodynamic amperograms (similar to those typified in Fig. 2) at different applied potentials. It may be noted from this figure that the peaks occurred approximately at the same position, demonstrating the constancy of the flow rate. These amperograms then allowed the selection of the optimum applied potential for detection of the test polymer based on the highest current response obtained relative to the baseline level.

Fig. 3 typifies a plot of the peak currents (or peak area) observed at different applied potentials using polyacrylamide as test polymer. It is seen that a limiting

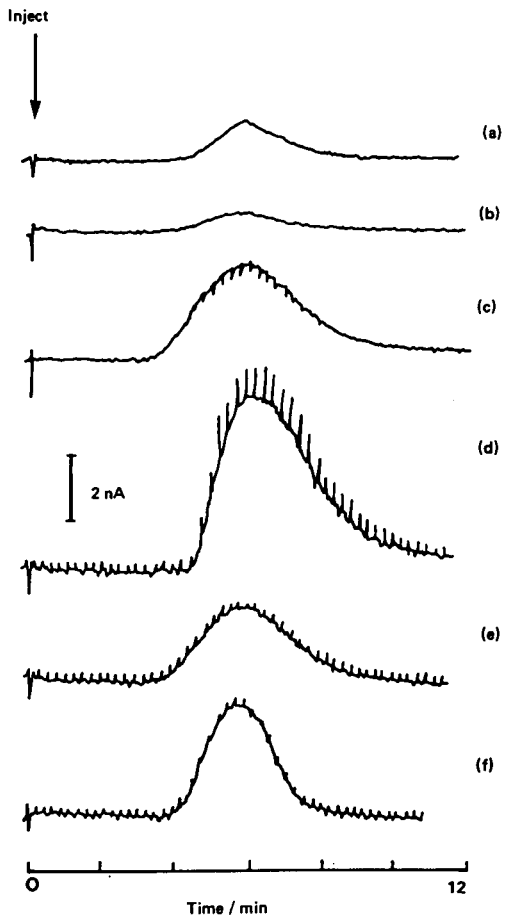

Fig. 2. Typical flow amperograms of some polymers, flow rate = 0.070 ml/min. Amount of polymer injected, applied potential: (a) 29 μg PVPD (MW 10,000), −0.9 V; (b) 29 μg PVPD (MW 40,000), −0.9 V; (c) 30 μg polyacrylic acid, −0.9 V; (d) 3.15 μg poly(acrylamide–acrylic acid), −1.1 V; (e) 29 μg PEO, −1.1 V; and (f) 29 μg dextran, −1.1 V.

current is not attained under the given carrier and flow conditions, confirming the static voltammetric behavior for most polymers.

It was found that generally all the polymers registered oxidative currents at applied potentials ≥ 0.7 V and reductive currents at applied potentials ≤ -0.7 V. This suggests that similar electroactive chemical moieties in the various polymers may be involved in these processes. From the range of polymers studied, the structural features present include unsaturation, alcoholic or phenolic, aldehydic, and carboxylic groups, which are all potentially electroactive (see for example [10]).

Some specificity of the polymer response may, however, be discerned from the flow amperograms in Fig. 2, wherein different peak shapes and analytical sensitivities (current per mass of polymer injected) were observed from approximately equal amounts of polymer (except in the case of the copolymer, curve d) at the same applied potential. This suggests that each polymer has a unique effect on the structure of the electrical double layer.

As indicated earlier, due to the electrochemical reaction of the carrier itself, the baseline currents at either end of the useful potential window were too high. Hence, applied potentials were limited to ± 1.5 V.

3.2. Flow-rate dependence

Table 1 shows the dependence of the peak current on the carrier flow rate, using 9.25 μg polyacrylic acid as test polymer and an applied potential of 1.3 V. Slower flow rates yielded better signal-to-noise ratios than faster ones. The faster flow rates allowed the polymers shorter residence time in the flow cell, leading to concentration polarization and thus giving lower peak currents.

It is noted that the baseline remained very stable at all flow rates, although the noise levels (caused by the pumping action) increased with flow rate. In general, however, low flow rates (i.e., less than 1.0 ml/min) are employed to effect good polymer separation of polymer fractions [11] and noise levels would therefore be acceptable.

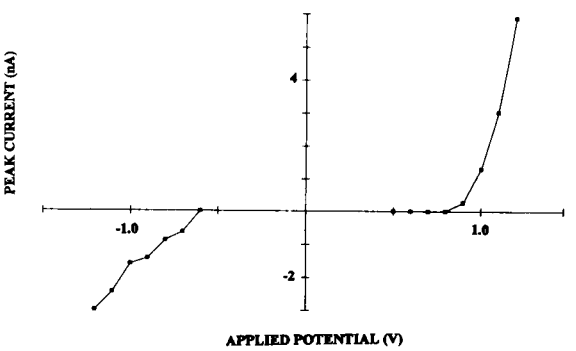

Fig. 3. Peak current as a function of applied potential, 34 μg polyacrylamide (MW 1,000,000), flow rate = 0.070 ml/min.

Table 1
Variation of current response with carrier flow rate

Flow rate (ml/min)	Peak current (nA)	Noise level (peak-to-peak) (nA)	Signal/noise ratio
0.041	6.1	0.34	18.0
0.068	5.5	0.42	13.0
0.102	5.1	0.48	11.0
0.124	5.0	0.66	7.6
0.167	4.8	0.72	6.7
0.196	4.8	0.93	5.2
0.270	4.6	1.42	3.3
0.348	4.5	1.50	3.0

3.3. *Microelectrode detector analytical performance*

The reproducibility of the analytical signals was excellent, with the precision of the peak current varying between 0.1–7.0%, while day-to-day reproducibility was better than 10%.

The peak current increased linearly with the amount of polymer injected. The linear range, correlation coefficient, and sensitivity (defined here as the slope of the plot of the current response against amount of injected polymer) are summarized in Table 2. The table shows that the highest sensitivities were given by blue dextran, polyacrylic acid, and poly(acrylamide–acrylic acid) copolymer.

The noise level was estimated from the oscillations in the amperograms of each polymer (cf. Fig. 2), and typically ranged between 10–100 pA. The limit of detection (LOD) was calculated by taking three times the noise level and dividing by the analytical sensitivity of the polymer injected. The lowest level detectable

Table 2
Analytical performance of the microelectrode and RI detectors [a]

Polymer (average MW)	applied E (V vs. Pd)	Linear range (μg)	Corr. coeff. (r)	Slope [b]	LOD (μg)
Dextran (20,800)	1.3	1.2–51.8	0.943	0.179	1.2
		3.9–259	0.999	0.0191	3.9
Blue Dextran (2,000,000) [c]	1.3	0.13–2.45	0.995	1.09	0.13
		–	–	–	–
Polyacrylamide (524,000)	−1.3	4.8–48.5	0.938	0.0333	0.72
		6.8–48.5	0.970	0.174	6.8
Polyacrylamide (1,140,000)	1.3	8.1–24.5	0.963	0.0310	8.1
		2.4–24.5	0.995	0.145	1.4
Polyacrylic acid (2,000,000)	1.3	0.56–18.5	0.986	0.902	0.20
		1.4–37.0	0.999	0.150	0.82
Polyvinylpyrrolidone (10,000)	1.3	2.9–43.3	0.962	0.306	0.46
		3.3–173	0.999	0.315	3.3
Polyvinylpyrrolidone (40,000)	1.3	3.9–48.8	0.997	0.0332	3.9
		2.4–48.8	0.999	0.145	0.22
Poly(acrylamide–acrylic acid) (200,000)	−1.3	0.32–9.45	0.944	0.752	0.24
		4.4–31.5	0.998	0.285	4.4
Polyethylene oxide (200,000)	−1.3	2.9–57.8	0.990	0.0965	2.1
		2.9–173	0.992	0.0614	2.4

[a] The first entry for each polymer refers to microelectrode measurements, while the second refers to ΔRI measurements at 30°C; flow rate = 0.070 ml/min.

[b] Current response (nA) or differential RI response in $\Delta RI \times (64 \times 10^6)$ units per μg of injected polymer.

[c] Microelectrode measurements with electronically offset recorder baseline. –, means no RI signals were obtained (due to continuously drifting baseline) after 2-h equilibration.

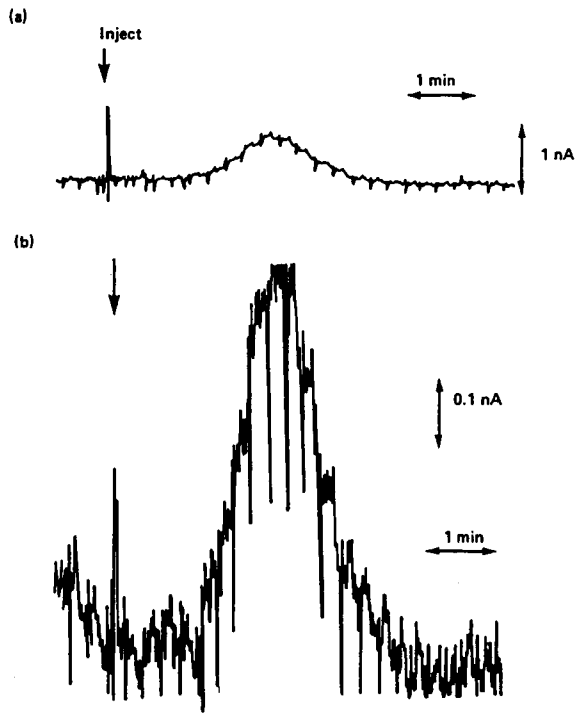

Fig. 4. Current signals of blue dextran, flow rate = 0.070 ml/min, 1.3 V: (a) 2.45 μg; (b) 0.245 μg, with recorder electronic offset.

was 0.13 μg blue dextran, while polyacrylamide (MW 1,140,000) gave the least sensitivity with LOD = 8.1 μg. The current signal may be enhanced at least 10-fold by electronically offsetting the recorder baseline (Fig. 4). Although the noise level was also magnified, the signal/noise ratio of about four was still satisfactory.

One approach to minimize the noise level is to incorporate a pulse dampener. Another alternative, which was used in this study, was to use a gravity pump. Gravity-fed carrier (where the solvent reservoir was elevated by at least 1 m from the workbench) gave a baseline which was free of the oscillations characteristic of the peristaltic pump (see Fig. 5b and d), thus dramatically improving the signal-to-noise ratio and the precision of the signals. For example, in the case of polyacrylic acid (MW 2,000,000), and an applied potential of 1.5 V, using a gravity pump resulted in a 14-fold increase in sensitivity (13 nA/μg polymer; linear range = 0.025–0.25 μg; $r = 0.997$), and LOD = 20 ng. However, due to limited time, no further studies were performed with the gravity pump.

3.4. Comparison with the refractive index detector

The second row of data for each polymer entry in Table 2 corresponds to the analytical measurements with a differential RI detector operated at its most sensitive setting. The linear range with the RI detector is seen to be wider for some polymers, notably dextran, PVPD (MW 10,000), and polyethylene oxide. This suggests that either electrode polarization or surface saturation effects may have limited the linear range observed at the microelectrode detector at the higher polymer levels.

Fig. 5 compares the analytical signals obtainable from the two detectors. As noted earlier, the microelectrode detector baseline hardly drifted under all conditions (curve a,b). In contrast, the RI detector baseline drifted continuously (curve c), even after a 2-h equilibration period; only after an overnight equilibration could a relatively stable baseline be realized (curve d). This long time was a huge drawback and generally only 2-h equilibration periods were observed.

The precision of the peak heights (or peak areas) and the retention times obtained with the RI detector (and 2-h equilibration periods) varied between 2–18%, the poorest reproducibility occurring at the lowest concentrations due to enormous baseline drift. Day-to-day reproducibility was 20–30% or better. The LOD in Table 2 was calculated by taking three times the standard deviation of the measured signals for the lowest level of polymer injected and dividing by the measured sensitivity for the polymer. It is seen from the LOD values in Table 2 that the RI detector was generally less sensitive than the microelectrode detector, except in two cases (polyacrylamide, MW 1,140,000 and PVPD, MW 40,000).

4. Conclusions

The microelectrode flow amperometric detector described in this work offers a relatively inexpensive and a highly sensitive method for detecting water-soluble polymers, and may be employed with only ultrapure water as the carrier. The electrode assembly and flow cell may be easily fabricated. Although the electrochemical processes involved may not yet be clearly understood, the electrochemical detector response was demonstrated to be very reliable and reproducible, and

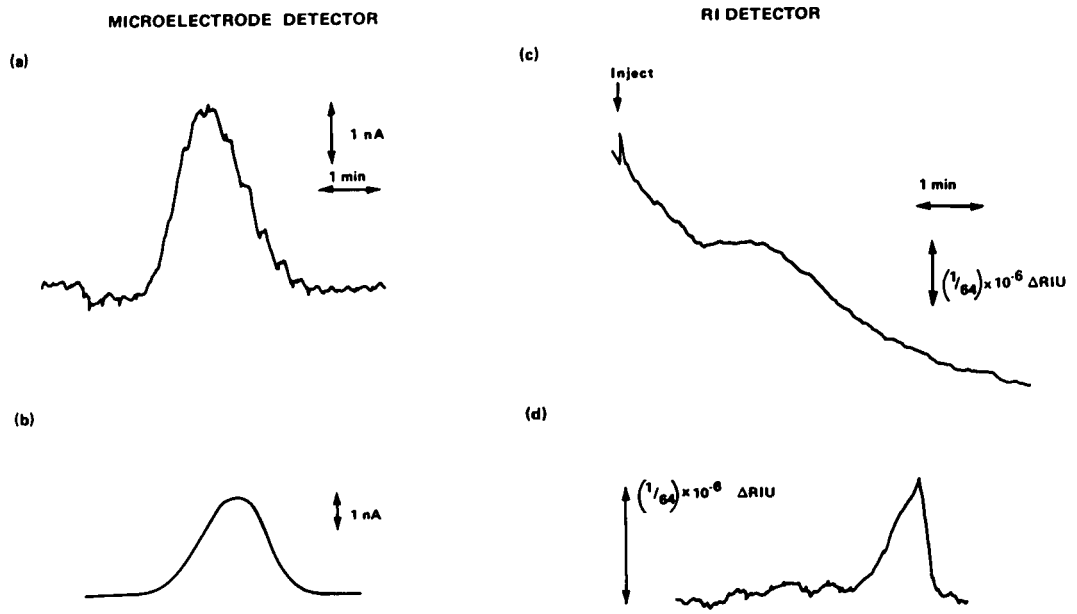

Fig. 5. Comparison of microelectrode (a,b) and RI (c,d) detector responses. (a) 2.45 μg blue dextran, flow rate = 0.070 ml/min; (b) 13.9 ng dextran (MW 20,000), gravity pump flow rate = 0.065 ml/min; (c) as in (a), but with 2-h equilibration prior to polymer injection; and (d) 1.02 μg dextran (MW 20,000), gravity pump flow rate = 0.236 ml/min, overnight equilibration.

the current signals exhibited excellent baseline stability. Improved sensitivity may be achieved using a gravity or low-pulse pump. The detector was largely superior to the differential RI detector at very low polymer concentrations, which is the region of interest in polymer separations.

Additional attractive features may be incorporated to enhance microelectrode detector performance and obtain further qualitative information. For example, rapid scan cyclic voltammetry [7,12] or Fourier transform electrochemistry [13] could provide more insight about the electrochemical processes involved during detection. Other carrier systems, particularly nonaqueous solvents, would also provide a much wider potential window for investigations [2,4,10,14], which may lead to further electrochemical differentiation and applications. This is the subject of current work.

Acknowledgements

The authors thank Mr. Joseph Pons for constructing the microelectrode assembly and Dr. Karin Caldwell for providing some of the test polymers. VV-B thanks the Department of Chemistry of the University of Utah for the use of its facilities, and the Institute of Chemistry of the University of the Philippines (her previous employer) for a sabbatical leave to undertake this work.

References

[1] B.S. Pons and M. Fleischmann, Anal. Chem., 59 (1987) 1391A.
[2] R.M. Wightman and D.O. Wipf, in A.J. Bard (Ed.), Electroanalytical Chemistry, Vol. 15, Marcel Dekker, New York, 1988, p. 267.
[3] M. Fleischmann, S. Pons, D. Rolison and P. Schmidt, Ultramicroelectrodes, Datatech, Morgantown, 1987, p. 1.
[4] A.M. Bond, M. Fleischmann and J. Robinson, J. Electroanal. Chem., 168 (1984) 299.
[5] J.W. Bixler and A.M. Bond, Anal. Chem., 58 (1986) 2859.
[6] K.A. Knecht, E.J. Guthrie and J.W. Jorgenson, Anal. Chem., 56 (1984) 479.
[7] J.G. White, R.L. St. Claire III and J.W. Jorgenson, Anal. Chem., 58 (1986) 293.
[8] J.G. White and J.W. Jorgenson, Anal. Chem., 58 (1986) 2992.
[9] J. Ghoroghchian, F. Sarfarazi, T. Dibble, J. Cassidy, J.J. Smith, A. Russell, G. Dunmore, M. Fleischmann and S. Pons, Anal. Chem., 58 (1986) 2278.
[10] A.J. Bard (Ed.), Encyclopedia of Electrochemistry of the Elements, Organic Section, Vols. 11 and 12, Marcel Dekker, New York, 1978.

[11] J.J. Gunderson and J.C. Giddings, in C. Booth and C. Price (Eds.), Comprehensive Polymer Science, Vol. 1: Polymer Characterization and Properties, Pergamon, Oxford, 1989, p. 279.
[12] J.O. Howell and R.M. Wightman, Anal. Chem., 56 (1984) 524.
[13] J. Hazi, A. Bond, A. Czerwinski and D. Elton, Proc. 12th Australian Symposium on Analytical Chemistry, Perth, Australia, 1993, p. 98.
[14] J. Cassidy, S.B. Khoo, S. Pons and M. Fleischmann, J. Phys. Chem., 89 (1985) 3933.

ELSEVIER

Analytica Chimica Acta 298 (1994) 267–270

ANALYTICA CHIMICA ACTA

Low blank determination of boron in geochemical materials

Susan Evans *, Thomas Meisel

Institut für anorganische, analytische und physikalische Chemie, Universität Bern, 3000 Bern 9, Switzerland

Received 1 March 1994; revised manuscript received 27 May 1994

Abstract

A new method for the determination of boron in material with high silica and low boron content is described. Low boron blank values (0.10 μg) could be achieved by using an acid digestion technique. Boron was separated from all interfering elements by eluting through a boron specific resin. Measurements were performed with inductively coupled plasma atomic emission spectrometry and spectrophotometry using azomethine-H. The method was tested on geochemical reference materials. It is demonstrated that this method is elegant as well as precise and accurate and applicable on small amounts of sample. It can be recommended for routine analysis in geochemical material.

Keywords: Atomic emission spectrometry; Inductively coupled plasma spectrometry; Ion exchange; Acid digestion; Azomethine-H; Boron; Geochemical materials

1. Introduction

Boron in geological material is often used as a tracer in surface geochemical processes, e.g., paleosalinity, erosion and rock alteration [1–4]. The most common digestion method using fusion with Na_2CO_3 involves a high boron blank value through impurities of the chemical (up to 15 $\mu g\ g^{-1}$ boron) [5]. Acids have a low boron blank value, but using HF–HNO_3 as digestion reagents causes losses of boron through volatilisation as BF_3. Applying spectroscopic methods the interference of iron has to be overcome [6–8], since geochemical materials often show high Fe/B ratios.

We therefore tried to develop a method which could reduce blank problems and avoid any spectral interferences from iron to lower the detection limit. Li-qiang and Zhu [9] suggest a digestion using a mixture of HNO_3–$HClO_4$–HF in the presence of H_3PO_4 which is acting as a complexing agent to prevent the loss of boron. This method was adapted, whereas the use of $HClO_4$ was avoided to lower the blank introduction. Boron can be separated from the matrix by solid phase extraction with a boron specific Amberlite resin as described by Smith et al. [10] and Kiss [11]. Our aim was to test the method by applying the combination of the two steps on geochemical reference materials.

2. Experimental

2.1. Material and reagents

Plastic ware was used throughout to avoid boron contamination from glass containers. The only indispensable contact to glass occurred by setting the pH using a glass electrode. All chemicals were of analytical grade, HF and HNO_3 were subboiled. Deionised bidistilled water was used throughout the procedure. Amber-

* Corresponding author.

SSDI 0003-2670(94)00269-R

lite IRA 743 (20–50 mesh) used as a boron specific resin was obtained from Fluka. Exchange columns (10 ml) from Bio-Rad were applied. A standard solution of 1000 $\mu g\ g^{-1}$ B as boric acid was obtained from Merck. The reference materials used were: RGM-1 (rhyolite) and GXR-6 (soil) from the United States Geological Survey (USGS) and JG-1 (granodiorite) and JB-1 (basalt) from the Geological Survey of Japan (GSJ).

2.2. Acid digestion step

Depending on the assumed boron content 30–100 mg of sample was weighed directly into 8-ml perfluoroalkoxy (PFA) vials with a screw top and flat bottom. After the addition of 2.5 ml HNO_3 (conc.) and 1.0 ml H_3PO_4 (85%) the suspension was thoroughly mixed. Thereafter 0.5 ml HF (40%) was added and after sealing the vial was mixed again. The vial was heated overnight on a hot plate not exceeding 120°C. To remove SiF_4, excess HF and most of the HNO_3, the lid was unscrewed and heating was continued until no condensation products remained (3–5 h). A clear solution of H_3PO_4 is the result after evaporating the volatile components. If the digestion was not complete, HNO_3 and HF were added again and the heating step was repeated. Only the soil sample retained a visible residue which did not affect the determination of the boron concentration. The solution was transferred quantitatively with water into a pre-weighted 50-ml polypropylene centrifugation tube. The pH was set between 8.0 and 8.5 with 10 M NaOH. The net weight was adjusted with water to 20 g, the suspension thoroughly mixed and the precipitate which contains various hydroxides was separated by centrifugation for 5 min.

2.3. Column extraction

The column was filled with 0.5 g of resin in water and covered with a thin layer of quartz wool. All elutions were performed at a flow rate of ca. 1 ml min^{-1}. The resin was conditioned by eluting 5 ml 3 M NH_4OH, 20 ml water, 10 ml 1 M HCl, 5 ml water and 5 ml 1 M HNO_3. After leaving the resin over night in this acid environment, it was activated by eluting 5 ml 1 M HNO_3 and 20 ml water. The supernatant after the centrifugation was loaded onto the column in portions. The column was washed with 2×5 ml water and the boron was eluted with 5×2 ml 1 M HNO_3 (in case of the spectrophotometric determination with 0.2 M HNO_3) into a pre-weighted plastic container. After washing the columns in the same manner as described above, they could be used for the extraction of the next set of samples.

2.4. Determination by ICP-AES or azomethine-H

The measurements were performed on a Philips PU 7000 ICP-AES apparatus with a grid nebuliser. The instrument was operated at 1.0 kW with a plasma gas flow rate of 12 l min^{-1}, nebuliser gas pressure of 36 p.s.i. (2.4 atm), no auxiliary gas flow and a sample uptake of 1.2 ml min^{-1}. The B spectral lines at 249.773 and 249.678 nm were measured by integrating 3×10 s per line. To control the quantitative removal of the iron, additional measurements were made on the Fe line at 259.940 nm by integrating 3×3 s.

The spectrophotometric determination with azomethine-H was previously described [6]. The absorption was measured at a wavelength of 430 nm.

2.5. Determination of blanks, recovery and reference material

To test the accuracy three separate digestions were performed on JB-1, JG-1 and GXR-6, four on RGM-1. Six digestions and elutions were made without adding any geochemical material acting as blank solutions. In addition four solutions containing known amounts of boron standard (between 0.8 and 1.7 μg B) were also treated in the same manner to check possible loss of boron during the digestion and the column extraction.

Only RGM-1 was analysed to test the spectrophotometric determination. Four separate digestions were made and three blank solutions were taken through the entire procedure.

3. Results and discussion

The average value of the six boron blanks measured by ICP-AES is 0.10 μg with a range between 0.05 and 0.16 μg. The limits of detection ($3s$) and determination ($10s$) were calculated from the standard deviation and were found to be 0.13 μg and 0.4 μg, respectively. Therefore, we suggest to weigh more than 50 mg of

Table 1
Boron contents ($\mu g\ g^{-1}$) of geochemical reference material found by ICP-AES determination

Material	This work (mean of two B lines)				$\bar{x} \pm$ S.D.	C.V. (%)	Lit.	Ref.
RGM-1	25.70	25.50	25.00	25.21	25.4 ± 0.31	1.2	28 ± 3	[12]
GXR-6	10.68	11.24	10.53		10.8 ± 0.35	3.5	9.8 ± 0.9	[13]
JB-1	9.65	10.23	10.24		10.0 ± 0.33	3.3	12.4	[14]
							10.2	[15]
JG-1	6.46	6.99	7.43		7.0 ± 0.49	7.0	6	[14]
							6.7	[15]

sample if the concentration is below 10 $\mu g\ g^{-1}$. The average of the blank was subtracted from all determinations. We suspect the ion exchange resin to be the largest contributor to the blank.

The recoveries found range between 97 and 101%. No significant loss of boron is evident throughout all steps.

In the samples with a high Fe/B ratio (GXR-6, 5700; and JB-1, 5000, ratios by weight) a significant Fe/B ratio up to 150 remained even after the column separation. In these cases the iron interference caused an enhancement of the emission up to 15% on the B line at 249.773 nm. This interference was subtracted as described in [6]. In all cases the interference on the B line at 249.678 nm is less than 5% and can be neglected.

The values for each determination of the reference materials as well as the known literature values are given in Table 1. The determinations of the two boron lines do not deviate more than 6%, and therefore only the mean value of both lines is given. The average determined for RGM-1 and GXR-6 is within the 1s limit of the recommended literature values [12,13]. The GSJ rock samples JB-1 and JG-1 deviate from the consensus values evaluated by Ando et al. [14]. In more recent literature [15] however values were found which are within the 1s limit of our determinations.

With the azomethine-H method a comparable value was found for RGM-1 ($27.6 \pm 2.6\ \mu g\ g^{-1}$). Limits of detection and determination of 0.4 μg and 1.2 μg, respectively, resulted. If no ICP-AES instrumentation is available, samples with a boron content of more than 12 $\mu g\ g^{-1}$ can be analysed using the spectrophotometric method.

It was not tested if subboiling of the HNO_3 and the HF is essential. An addition of $HClO_4$ might be necessary for more problematic materials (e.g., samples with a high tourmaline content), but this was not tested. In all the samples digested in the course of this work the boron was brought into solutions without any problem.

4. Conclusions

We have demonstrated that high precision and accuracy of boron determination is possible by applying this new technique to geochemical materials. The elimination of a major part of interfering iron and a very low blank results in lower detection limits thus allowing small sample quantities. When inserting 100 mg of sample and measuring by ICP-AES, boron concentrations down to 4 $\mu g\ g^{-1}$ can be determined. Applying the azomethine-H method, determinations down to 12 $\mu g\ g^{-1}$ are possible. In both cases fast and accurate routine analysis of boron in geochemical samples can be achieved.

Acknowledgements

ICP-AES measurements were carried out at the Gewässer- und Bodenschutzlabor des Kantons Bern. We thank U. Krähenbühl for constructive discussions and general support. Financial support was provided by the Swiss Federal Office of Public Health (FE 316-90-300) and the Swiss National Science Foundation.

References

[1] V.M. Goldschmidt and C. Peters, Nachr. Ges. Wiss. Göttingen. Math. Physik. Kl., III (1932) 402
[2] M.J. Furst, Geochim. Cosmochim. Acta, 45 (1981) 1
[3] W.E. Seyfried, D.R. Janecky and M.L. Mottl, Geochim. Cosmochim. Acta, 48 (1984) 557

[4] E. Bonatti, J.R. Lawrence and N. Morandi, Earth Planet. Sci. Lett., 70 (1984) 88
[5] J.W. Owens, E.S. Gladney and D. Knab, Anal. Chim. Acta, 135 (1982) 169
[6] S. Evans and U. Krähenbühl, Fresenius' J. Anal. Chem., 349 (1994) 454
[7] H.K.L. Gupta and D.F. Boltz, Microchim. Acta [Wien], (1974) 415
[8] U. de la Chevallerie-Haaf, A. Meyer and G. Henze, Fresenius' J. Anal. Chem., 323 (1986) 266
[9] X. Li-qiang and R. Zhu, Fresenius' J. Anal. Chem., 325 (1986) 534
[10] F.G. Smith, D.R. Wiederin, R.S. Houk, C.B. Egan and R.E. Serfass, Anal. Chim. Acta, 248 (1991) 229
[11] E. Kiss, Anal. Chim. Acta, 211 (1988) 243
[12] E.S. Gladney and I. Roelandts, Geost. Newsl., 14 (1990) 21
[13] E.S. Gladney and I. Roelandts, Geost. Newsl., 12 (1988) 253
[14] A. Ando, N. Mita and S. Terashima, Geost. Newsl., 11 (1987) 159
[15] H. Koshima and H. Onishi, Fresenius' J. Anal. Chem., 343 (1992) 287

ELSEVIER

Analytica Chimica Acta 298 (1994) 271–277

ANALYTICA CHIMICA ACTA

Development of an optrode membrane for the determination of picric acid based on fluorescence energy transfer

Hui-Hui Zeng, Ke-Min Wang, Ru-Qin Yu *

Department of Chemistry and Chemical Engineering, Hunan University, 410082 Changsha, China

Received 8 February 1994; revised manuscript received 17 May 1994

Abstract

An optrode membrane for the determination of picric acid based on fluorescence energy transfer between fluoranthene (donor) and fluorescein octadecyl ester (acceptor) was developed. When fluoranthene is excited at 362.2 nm, it emits light in a spectral region that overlaps significantly with the fluorescence excitation spectrum of fluorescein octadecyl ester. Consequently, non-radiative energy transfer occurs from fluoranthene (donor) to fluorescein octadecyl ester (acceptor). The fluorescence of fluoranthene is strongly quenched by picric acid, but that of fluorescein octadecyl ester is not. When the optrode membrane containing these two fluorophores contacts a solution of picric acid, the extent of fluorescence quenching is increased with a threefold increase in the Stern–Volmer quenching constant compared with the quenching of fluoranthene. This phenomenon is mainly due to the fluorescence quenching of the donor–acceptor pair by picric acid. Under the optimum conditions, the linear measuring range of picric acid is from 5.0×10^{-7} to 8.0×10^{-4} M. The described optrode membrane offer a more sensitive method for the determination of picric acid than the existing picric acid optrode membrane.

Keywords: Fluorimetry; Sensors; Fluorescence energy transfer; Optrode membrane; Picric acid

1. Introduction

The development of new optical sensors with higher sensitivity is of great interest in analytical chemistry. Recently, several fluorescent sensors based on the phenomenon of energy transfer have been constructed [1,2]. This kind of sensor is characterized by a higher sensitivity and large Stokes' shifts (which facilities the separation of the analytical signal from the excitation radiation). Therefore, research work in this area is becoming increasingly active.

Picric acid is an important organic acid and some picric acid optrode membranes have been developed based on the fluorescence quenching of polyaromatic hydrocarbons [3,4]. Also, a lipophilized fluorescein derivative was synthesized to determine the concentration of carboxylic acids by incorporating it in a plasticized PVC membrane [5]. From these experiments, it was found that the fluorescence emission spectrum of the polycyclic aromatic hydrocarbon fluoranthene overlapped seriously with the fluorescence excitation spectrum of fluorescein alkyl es-

* Corresponding author.

SSDI 0003-2670(94)00245-H

ter. If the PVC membrane containing fluoranthene and fluorescein octadecyl ester is excited at 362.2 nm (the excitation wavelength of fluoranthene), the fluorescence of fluorescein octadecyl ester will be observed. This process is called fluorescence energy transfer.

The theory of fluorescence energy transfer has been developed by Förster [6]. Two conditions are required for energy transfer to occur: an overlap between the emission spectrum of one fluorophore (donor) and the excitation spectrum of the second fluorophore (acceptor), and closeness of the two fluorescent molecules. In the above-mentioned PVC membrane, the first requirement is satisfied by the use of fluoranthene and fluorescein octadecyl ester as the donor and the acceptor fluorescent molecules, respectively, and the second condition is satisfied as a result of intermixing the two fluorescent molecules in the same PVC membrane. However, the fluorescence of fluoranthene is quenched by picric acid whereas that of fluorescein octadecyl ester is not. When this membrane contacts a solution of picric acid, strong fluorescence quenching of fluorescein octadecyl ester occurs. These results were used to develop a fluorescence-based optrode membrane with high sensitivity for the determination of picric acid.

2. Experimental

2.1. Reagents

Fluorescein octadecyl ester (FODE) was synthesized according to the literature [7]. Fluoranthene (C.P; Shanghai Chemical Reagents), poly(vinyl chloride) (high molecular weight) (Fluka Selectophore), bis(2-ethylhexyl) phthalate (C.P; Shanghai Chemical Reagents) and tetrahydrofuran (THF) (AR; Shanghai Chemical Reagents) were used for membrane preparation. A 0.01 M stock standard solution of picric acid was prepared by dissolving 11.45 g of picric acid (recrystallized twice) in 500 ml of distilled water. The actual concentration of picric acid was determined by titration with sodium hydroxide standard solution. Picric acid solutions of other concentrations were obtained by dilution of the stock standard solution with 1.8 M H_2SO_4.

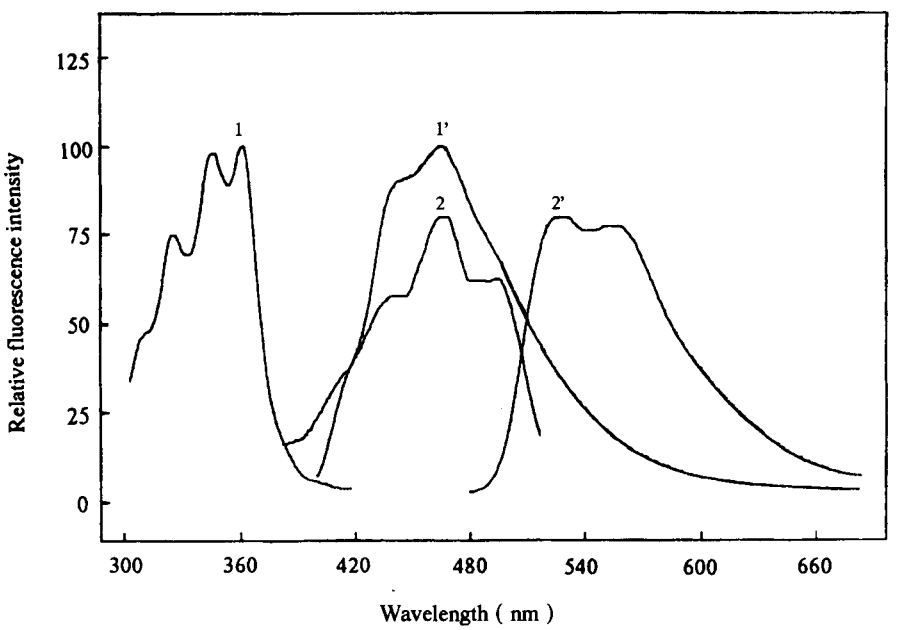

Fig. 1. Fluorescence spectra of fluoranthene and FODE: (1) excitation spectrum of fluoranthene; (1') emission spectrum of fluoranthene; (2) excitation spectrum of FODE; (2') emission spectrum of FODE.

2.2. Apparatus

Fluorescence was measured using a Hitachi M-850 spectrofluorimeter with a specially designed flow-through measuring cell similar to the device described elsewhere [8] (see below). Data processing was carried out on a Macintosh II computer.

2.3. Preparation of the optrode membrane

The optrode membranes were prepared from a mixture of 2.3 mg of fluoranthene, 5.8 mg of FODE, 50 mg of PVC and 100 mg of bis(2-ethylhexyl) phathalate. The membrane components were dissolved in 2 ml of freshly distilled THF. A circular 35 mm diameter quartz plate was mounted on the end of an aluminium alloy rod which was rotating at a high constant speed. From a syringe 0.2 ml of the THF solution was injected onto the central point of the plate. After a spinning time of only about 4 s (rotation frequency 600 rpm) two membranes of thickness ca. 4 μm were cast on to two 35 mm diameter quartz plates [9].

2.4. Procedure

Two identical membranes on their respective plates were mounted in the special flow-through measuring cell. The volume capacity of the cell was ca. 3.4 ml. The cell was introduced into the spectrofluorimeter at an appropriate position [10] to guarantee the detection of the intensity of fluorescence emission without interference from the excitation source. About 3 ml of sample solution were introduced and the fluorescence intensity F was measured. The membrane was washed with blank solution not containing picric acid until the fluorescence intensity (F_0) was stabilized.

3. Results and discussion

3.1. Choice of donor and acceptor

Fig. 1 shows the fluorescence excitation spectra and emission spectra of fluoranthene and

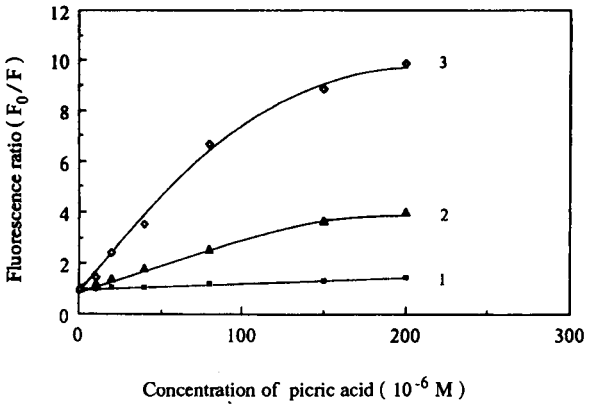

Fig. 2. Stern–Volmer plots for the quenching by picric acid of (1) FODE excited at 464.1 nm, monitored at 525.8 nm, (2) fluoranthene excited at 362.2 nm, monitored at 464.7 nm and (3) FODE and fluoranthene excited at 362.2 nm, monitored at 525.8 nm.

FODE. It can be seen that the emission spectrum of fluoranthene overlaps seriously with the excitation spectra of fluorescein octadecyl ester; the maximum excitation and emission wavelenghts of fluoranthene are 362.2 and 464.7 nm, respectively, and those of FODE are 464.1 and 525.8 nm, respectively. This satisfies the first of the above two conditions resulting in fluorescence energy transfer. Therefore, fluoranthene was chosen as the fluorescence donor and fluorescein octadecyl ester as the acceptor.

3.2. Fluorescence quenching effect of the donor and acceptor by picric acid

The fluorescence quenching of fluoranthene and FODE by picric acid was investigated in the PVC membrane. Curves 1 and 2 in Fig. 2 are the Stern–Volmer plots obtained in the quantitative study of fluoranthene and FODE. It illustrates that the extent of quenching of fluoranthene is much stronger than that of FODE. The Stern–Volmer quenching constants are 15 500 l mol^{-1} for fluoranthene and 2300 l mol^{-1} for FODE.

3.3. Effect of the amount of fluoranthene and FODE in the PVC membrane

By fixing the concentration of fluoranthene in the PVC membrane at 6.5×10^{-5} mol g^{-1} and

changing the concentration of FODE in the membrane, the fluorescence emission spectra of fluoranthene and FODE were observed using an excitation wavelength of 362.2 nm, the maximum in the fluorescence excitation spectrum of fluoranthene. When the relative concentration of FODE in the membrane increases, the peak intensity of fluoranthene at its maximum in the emission spectrum (464.7 nm) gradually weakens and at the same time the peak intensity of FODE at 525.8 nm (maximum in the emission spectrum of FODE) increases. It should be noted that in the absence of fluoranthene the emission spectrum of FODE would not appear as the excitation wavelength of fluoranthene was used. When the concentration of FODE is the same as that of fluoranthene, one would observe only the emission spectrum of FODE, as the energy of the excited electron state of fluoranthene molecules would be completely transferred to the FODE molecules. For this reason, the concentration ratio of fluoranthene to FODE is fixed at 1:1 in the PVC membrane, and the actual concentrations used are optimized experimentally.

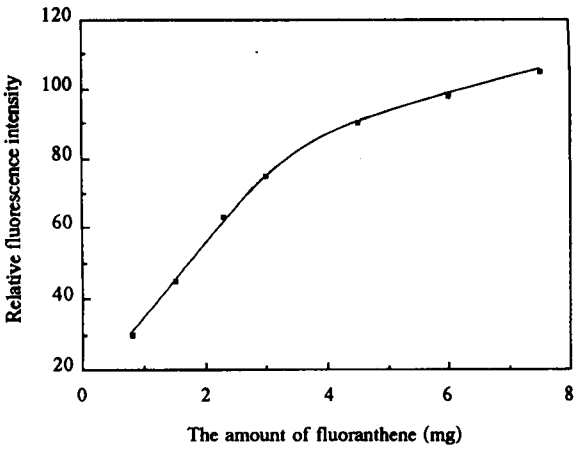

Fig. 3. Effect of the amount of fluoranthene and FODE in the PVC membrane.

Fig. 3 shows that the amounts of fluoranthene and FODE in the PVC membrane should be less than 3.0 and 7.6 mg, respectively (approximately the same molar concentration), otherwise an inner filter effect would be expected. However, the concentrations of fluoranthene and FODE in the

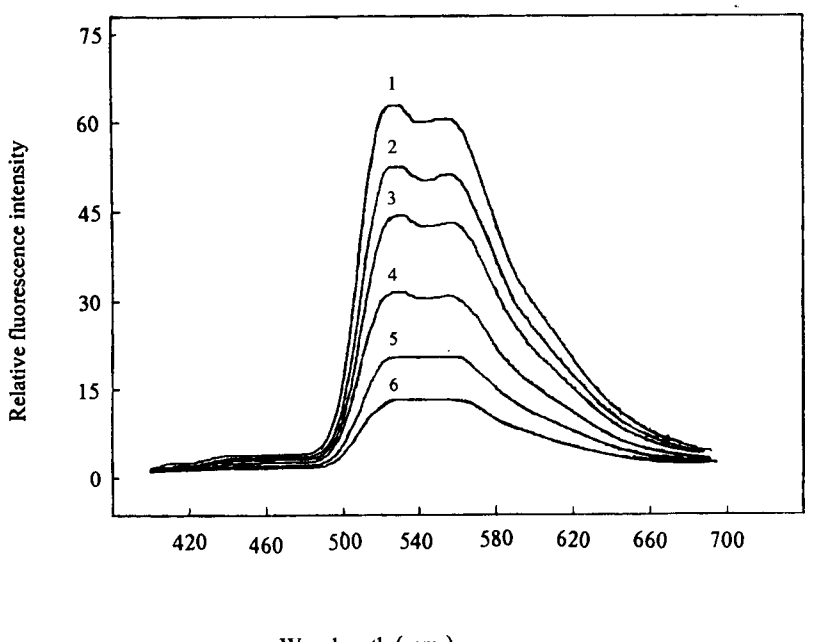

Fig. 4. Fluorescence emission spectra of optrode membrane in contact with different concentrations of picric acid: (1) blank solution; (2) 4×10^{-6}; (3) 1×10^{-5}; (4) 2×10^{-5}; (5) 4×10^{-5}; (6) 8×10^{-5} M.

PVC membrane should not be too low, otherwise the blank fluorescence intensity of the membrane would be too low and the sensitivity of the measurement would decrease. The amounts of fluoranthene and FODE in the PVC membrane were fixed at 2.3 and 5.8 mg, respectively, in the proposed procedure.

3.4. Energy-transfer process of the two-fluorophore system

When the optrode membrane containing fluoranthene and FODE was excited at 362.2 nm (maximum excitation wavelength of fluoranthene), only the fluorescence of FODE could be observed (see the curve 1 in Fig. 4). This is due to the dipole–dipole interactions between fluoranthene (donor) and FODE (acceptor), which results in the transfer of the excited-state energy from fluoranthene to FODE. The process could be described as follows [11]:

$D + h\nu \rightarrow D^*$ (excitation of donor)

$D^* + A \rightarrow (DA)^*$

(formation of donor–acceptor pair)

$(DA)^* \rightarrow D + A^*$

(formation of A* from donor–acceptor pair)

$A^* \rightarrow A + h\nu'$ (fluorescence of acceptor)

where D, A and DA represent fluoranthene, FODE and the fluoranthene–FODE pair, respectively.

3.5. Response to picric acid

When this optrode membrane contacted a solution of picric acid, its fluorescence was strongly quenched. Fig. 4 shows the fluorescence emission spectra of this optrode membrane in contact with a series of picric acid solutions. The extent of fluorescence quenching increased with increase in the concentration of picric acid solution. Curve 3 in Fig. 2 is the Stern–Volmer plot of the quenching of this optrode membrane. The Stern–Volmer constant for the quenching of this two-fluorophore system by picric acid is 46 200 l mol^{-1}, which is a threefold increase compared with the quenching of fluoranthene. The photophysical process involved in this optrode membrane can be described as follows:

$D + h\nu \rightarrow D^*$ (excitation of donor)

$D^* + Q \rightarrow D$ (quenching of donor)

$D^* + A \rightarrow (DA)^*$

(formation of donor–acceptor pair)

$(DA)^* + Q \rightarrow DA + Q$

(quenching of donor–acceptor pair)

$(DA)^* \rightarrow D + A^*$

(formation of A* from donor–acceptor pair)

$A^* + Q \rightarrow A + Q$ (quenching of acceptor)

$A^* \rightarrow A + h\nu'$ (fluorescence of acceptor)

where Q represents picric acid. According to the above equations, the overall quenching effect of this optical optrode membrane is caused not only by the quenching of the donor and acceptor, but also by the quenching of the donor–acceptor pair. The increase in the quenching constant in this kind of energy–transfer system may be mainly due to the quenching of the donor–acceptor pair.

Curve 3 in Fig. 2 can also be used as the calibration graph for the determination of picric acid. The equation of the calibration graph is

$$F_0/F = 1 + 46200C$$

where C is the molar concentration of picric acid. The linear measuring range of picric acid is from 5.0×10^{-7} to 8.0×10^{-4} M with a detection limit of 2.0×10^{-7} M.

3.6. Effect of acidity

Fig. 5 shows the effect of acidity on the optrode membrane for the determination of picric acid. The fluorescence intensity measurements were made on 4×10^{-5} M picric acid in H_2SO_4 solutions of different concentrations. The results show that the optimum concentration range of H_2SO_4 giving better responses is 1.4–2.4 M; in subsequent work, 1.8 M H_2SO_4 was used.

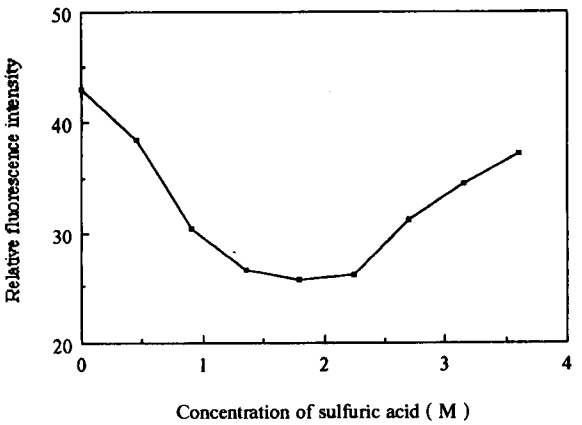

Fig. 5. Effect of acidity.

3.7. Reproducibility and response time

Fig. 6 shows the fluorescence intensity response versus time recordings for the optrode membrane when it was exposed to repeated concentration step changes between 1×10^{-5} and 1×10^{-4} M picric acid in 1.8 M H_2SO_4. The results show a remarkably high reproducibility of the optical signals. The mean fluorescence intensity values with standard deviations were found to be 43.7 ± 0.6 ($n = 5$, 1×10^{-5} M picric acid) and 12.7 ± 0.6 ($n = 5$, 1×10^{-4} M picric acid). From Fig. 6 it can also be seen that the response times of the optrode membrane are less than 20 s.

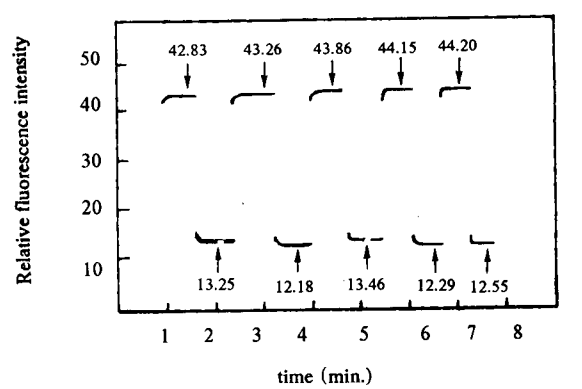

Fig. 6. Relative fluorescence intensity response versus time at 362.2 and 525.8 nm after several repeated concentration step changes.

3.8. Lifetime

The fluorescence signal at wavelengths of 362.2 and 525.8 nm for the optrode membrane in contact with 1×10^{-5} M picric acid in 1.8 M H_2SO_4 was recorded over a period of 8 h. From fluorescence intensity values taken every 30 min ($n = 16$), a mean value of 43.2 and a standard deviation of 0.8 were obtained. This shows that the optrode membrane has good short-term stability. The fluorescence signal of the optrode membrane at 362.2 and 525.8 nm dropped by 5% during the measurement of sample solutions over 1 week.

3.9. Selectivity

With the concentration of picric acid fixed at 3.6×10^{-4} M, there is no influence on the fluorescence signal of the optrode membrane when less than 0.05 M potassium perchlorate and sodium thiocyanate are present. This shows that the proposed optrode membrane has better selectivity over hydrophobic anions compared with picric ion-selective electrodes whose selectivity patterns are governed by the lipophilicity of anions. Nitrophenols with structures similar to those of picric acid quench the fluorescence signal to some extent. The selectivity sequence is picric acid > 2,4-dinitrophenol > *p*-nitrophenol > *o*-nitrophenol > *m*-nitrophenol. When the dissolved oxygen in sample solutions was expelled by bubbling nitrogen into the sample, an 18% increase in the fluorescence intensity for the optrode membrane was observed. Therefore, whenever possible, it is recommended to expel the dissolved oxygen from sample solutions before fluorescence measurements.

3.10. Application

As picric acid can react quantitatively with some drugs such as cinchonine and quinine to form insoluble prepicitates, the optrode membrane can be applied to the indirect determination of these drugs. The determination of cinchonine in a drug sample, for example, was carried out by the following procedure. About 4 g of sample were dissolved in 0.014 M sulfuric acid to make 500 ml of solution. To this solution 100 ml

of 4.27×10^{-2} M picric acid were added with stirring. The solution was filtered and the filtrate was diluted to an appropriate concentration with 1.8 M H_2SO_4. The picric acid content in the filtrate was determined by using the described optrode membrane. The measured mean concentration was 2.17×10^{-2} M, which was in good agreement with the result obtained with the standard spectrophotometric method [12] [$(2.14 \pm 0.01) \times 10^{-2}$ M]. Eight repeated measurements on different aliquots from the sample solution gave a standard deviation of 3×10^{-4} M. A similar procedure was applied for the determination of quinine. The measured concentration was $(1.09 \pm 0.03) \times 10^{-2}$ M (eight measurements), in close agreement with the result of the pharmacopoeial procedure [13] [$(1.08 \pm 0.01) \times 10^{-2}$ M].

Acknowledgements

The work described in this paper was supported by the National Science Foundation of China and the Chinese National Educational Committee Science Foundation for Excellent Young Teachers.

References

[1] D.M. Jordan, D.R. Walt and F.P. Milanovich, Anal. Chem., 59 (1987) 437.
[2] A. Sharma and O.S. Wolfbeis, Anal. Chim. Acta, 212 (1988) 261.
[3] H.H. Zeng, K.M. Wang, C.L. Liu and R.Q. Yu, Talanta, 40 (1993) 1569.
[4] H.H. Zeng, K.M. Wang, C.L. Liu and R.Q. Yu, Acta Chim. Sin., 52 (1994) 177.
[5] H.H. Zeng, K.M. Wang, X.H. Yang and R.Q. Yu, Anal. Chim. Acta, 287 (1994) 267.
[6] T. Förster, Ann. Phys. (Leipzig) 2 (1948) 55.
[7] S.S.S. Tan, P.C. Hauser, K.M. Wang, K. Fluri, K. Seiler, B. Rusterholz, G. Suter, M. Krüttli, U.E. Spichiger and W. Simon, Anal. Chim. Acta, 255 (1991) 35.
[8] K.M. Wang, K. Seiler, B. Rusterholz and W. Simon, Analyst, 117 (1992) 57.
[9] K. Seiler and W. Simon, Anal. Chim. Acta, 266 (1992) 73.
[10] H.H. Zeng, K.M. Wang, Z. Qin and R.Q. Yu, Chem. J. Chin. Univ. 14 (1993) 180.
[11] J.R. Lakowicz, Principles of Fluorescence Spectroscopy, Plenum Press, New York, 1983, p. 305.
[12] K.-Y. Shen, X.-M. Wang and Y.-P. Han, Handbook of Practical Separation and Identifieation Methods for Pharmaceutical Substances, People's Military Medical Publishing House, Beijing, 1986, p. 355.
[13] Pharmacopoeia of the People's Republic of China, Part II, Chemical Engineering Publ. House, Beijing, 1985, p. 545.

ELSEVIER

Analytica Chimica Acta 298 (1994) 279–284

ANALYTICA CHIMICA ACTA

Catalytic effect of cetyltrimethylammonium bromide on the horseradish peroxidase-catalysed fluorogenic reaction between hydrogen peroxide and *p*-hydroxyphenylpropionic acid

Q.G. Li *, J.G. Xu, X.Z. Huang, G.Z. Chen

Department of chemistry, Xiamen University, Xiamen 361005, China

Received 4 January 1994; revised manuscript received 25 April 1994

Abstract

A mechanistic study was made on the catalytic effect of cetyltrimethylammonium bromide (CTAB) on the horseradish peroxidase-catalysed fluorogenic reaction between *para*-substituted phenols and H_2O_2 with *p*-hydroxyphenylpropionic acid as a model compound. The effect of CTAB was due to the interactions between the reaction products and the surfactant molecules. Novel behaviour of sodium chloride in the reaction was also observed.

Keywords: Enzymatic methods; Fluorimetry; Horseradish peroxidase; Hydroxyphenylpropionic acid

1. Introduction

There are a great variety of analytical methods involving micellar media [1]. Most are equilibrium methods based on molecular absorption or emission spectroscopy [2]. Micelles increase the absorption or the relative fluorescence quantum yield of the analyte. Some also accelerate the reaction rate and even facilitate solubilization of the analytical system. There is an increasing tendency for the adoption of micelles in fluorimetric analysis [3–5].

Horseradish peroxidase (HRP)-catalysed fluorogenic reactions have found wide applications in the determination of both HRP and H_2O_2. HRP is the most widely used enzyme label in immunoassays [6]. H_2O_2 plays an important role in the atmospheric environment [7] and redox reactions in the ocean [8]. Also, H_2O_2 is the product of many oxidase-mediated reactions [9]. The exploration of the sensitive determination of both HRP and H_2O_2 has attracted many researchers for many years [10–15].

Among several applied fluorogenic hydrogen donors, *p*-hydroxylphenylpropionic acid (HPPA) is regarded as the best choice owing to its sensitivity, stability and low cost [14]. Few methods have been reported to improve the detection sensitivity involving HPPA. Matsumoto et al. [16] observed that the addition of concentrated NaOH to the equilibrium solution significantly increased the fluorescence of the product. In a previous

* Corresponding author.

Elsevier Science B.V.
SSDI 0003-2670(94)00203-X

study [17], it was found that two surfactants, cetyltrimethylammonium bromide and chloride (CTAB and CTAC) had catalytic effects on the fluorogenic reaction, and this was used to develop a sensitive flow-injection determination of HRP. The objective of the work reported here was to elucidate the novel catalytic effects of CTAB micelles.

2. Experimental

2.1. Chemicals

HRP (EC 1.11.1.7, R.Z = 3.0, 250 IU mg^{-1}) was purchased from SABC Beijing and HPPA from Tokyo Kasai. CTAB, 2,2′-dihydroxydiphenyl (2,2′-DHDP), 4,4′-dihydroxydiphenyl (4,4′-DHDP) and *p*-hydroxydiphenyl (HDP) were all laboratory reagents from Shanghai Chemical. Other reagents were of analytical-reagent grade. Water was deionized twice and then distilled in a sub-boiling quartz vessel.

2.2. Procedure

To a 1-cm quartz cell (with cap), 2.60 ml of 0.1 mol l^{-1} Tris–HCl (pH 8.0) [when CTAB was used, the solution was a mixture of 2.30 ml of 0.1 mol l^{-1} Tris–HCl (pH 7.5) and 300 μl of 1.0×10^{-3} mol l^{-1} CTAB], 100 μl of 0.725 IU ml^{-1} HRP (stored in a water–ice bath), 200 μl of 7.5 mmol l^{-1} HPPA (stored in a water–ice bath) and 100 μl of 0.003% H_2O_2 (stored in a water–ice bath) were sequentially added and mixed. The fluorescence kinetic curve was immediately recorded. For product increase, λ(ex), λ(em) = 325.6, 406.0 nm and 330.0, 417.0 nm were adopted in the absence and presence of CTAB, respectively. For reactant decrease, λ(ex), λ(em) = 290.6, 310.0 nm was adopted whether CTAB was used or not.

All measurements were made on a Shimadzu RF-5000 spectrofluorimeter at 31 ± 0.5°C. The bandpass was set at "EX/EM" = 1.0/5.0 nm, the sensitivity was "HIGH" and the scan speeds for both wavelength and time were "FAST". The spectra were not corrected.

3. Results and discussion

3.1. Catalytic effect of CTAB on the fluorogenic reaction

Fig. 1a shows that the addition of CTAB increases the reaction rate and the maximum rate is reached near the critical micelle concentration (CMC = 9.2×10^{-4} mol l^{-1}). It was noted previously [17] that the fluorescent properties of HPPA were not affected by CTAB in the concentration range used, hence the extent of the reaction can be estimated by recording the kinetic curve of HPPA with a decreasing rate. Fig. 1b shows that the extent of reaction is increased with the addition of CTAB. The greatest conversion rate of

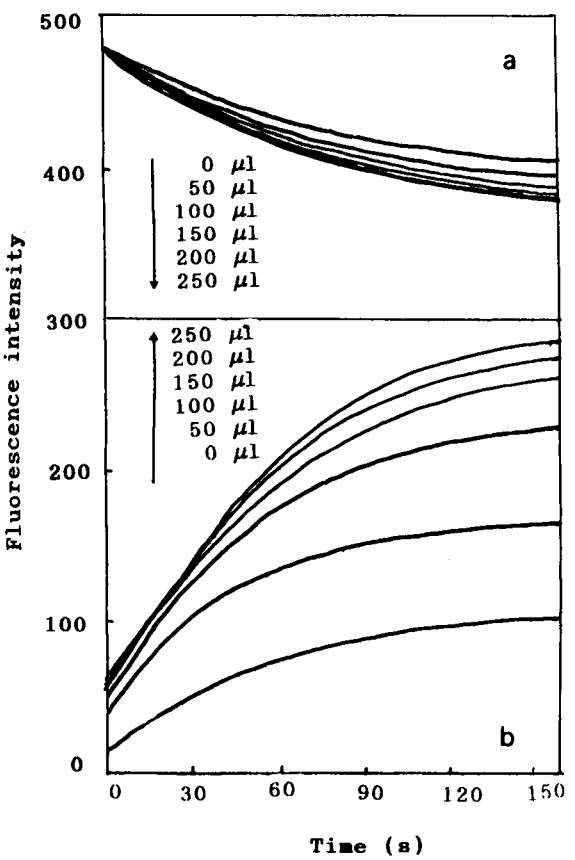

Fig. 1. Kinetic curves of (a) the product increase and (b) the reactant decrease (with the addition of CTAB (1.0×10^{-3} mol l^{-1}). The total volume was 3.0 ml with variation of CTAB.

HPPA was obtained near the CMC. The above results show that CTAB has an obvious catalytic effect on the reaction.

3.2. Mechanism of the CTAB catalytic effect

The HRP–HPPA–H_2O_2 reaction is as follows [12]:

$$HPPA + H_2O_2 \rightarrow DHPPA + 2H_2O \quad (1)$$

In the reactant solution, an acid–base equilibrium exists [17]:

$$DHPPA \rightleftharpoons DHPPA^{4-} + 4H^+ \quad (2)$$

I II

We assume that II interacts with CTAB as follows:

$$mDHPPA^{4-} + nC_{16}H_{32}(CH_3)_3N^+Br^- \rightleftharpoons \left[(C_{16}H_{32}(CH_3)_3N^+)_n(DHPPA^{4-})_m\right]^{n-4m} + nBr^- \quad (3)$$

where m is not determined and n is the aggregate number (ca. 78).

Under the experimental conditions, the concentration of CTAB was greater than that of DHPPA. When CTAB was near the CMC, micelles formed which had many negative charges on their surface, and III was in a more organized state. A further increase in CTAB would lead to no further increases in these states and cause no obvious fluorescence intensity changes.

The most important property of micelles is their ability to solubilize within their distinct structured regions compounds that are insoluble or sparingly soluble in water, allowing their location into or at the surface of the aggregate [1]. Moreover, ionic micelles can provide charged structures, where attractive or repulsive interactions with ionic solute may be present.

The mechanism of the catalytic effects of CTAB micelles can be interpreted as follows: reaction 3 promotes reactions 2 and 1, and thus increases the conversion rate of HPPA; concurrently, the fluorescence intensity (I) is: $I_{III} > I_{II} > I_I$, and this makes the product fluorescence increase.

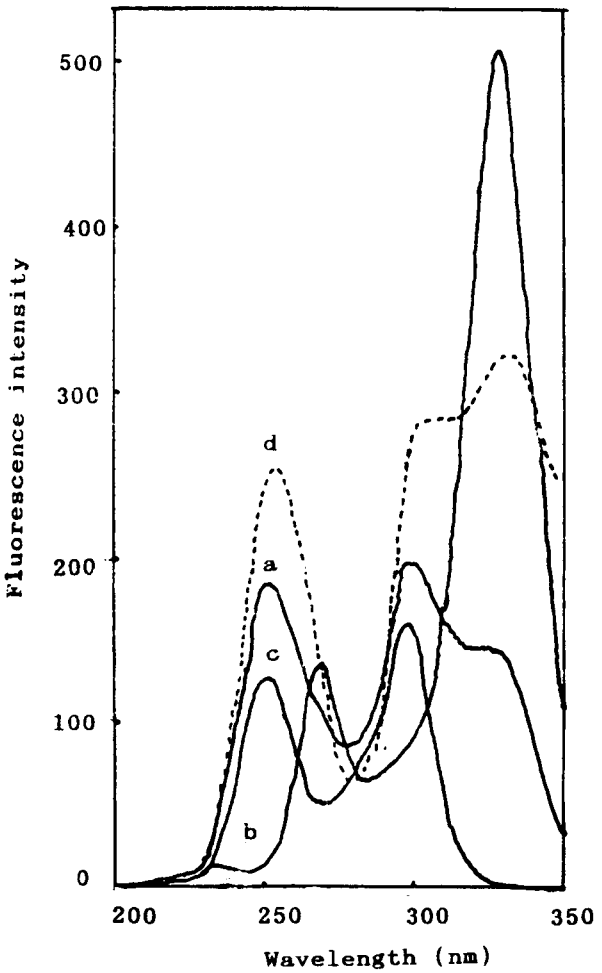

Fig. 2. Excitation spectra of the equilibrium solution. The equilibrium was obtained according to the Procedure. (a) Equilibrium solution at pH 7.5 [λ(em) = 406.0 nm]; (b) with the addition of 300 μl of NaOH (1.0 mol l^{-1}) [λ(em) = 406.0 nm]; (c) with the addition of 100 μl of HCl (1.0 mol l^{-1}) [λ(em) = 406.0 nm]; (d) with the addition of 300 μl of CTAB (1.0×10^{-3} mol l^{-1}) [λ(em) = 417.0 nm].

This mechanism assumed was supported by the following facts.

$I_{II} > I_I$. In a neutral medium (pH 7.5), the excitation spectrum of the product is as shown in Fig. 2a. The addition of concentrated NaOH (300 μl of 1.0 mol l^{-1} NaOH) greatly increased the 325-nm peak and decreased the 299-nm peak (Fig. 2b). The addition of concentrated HCl (109 μl of 1.0 mol l^{-1} HCl), on the other hand,

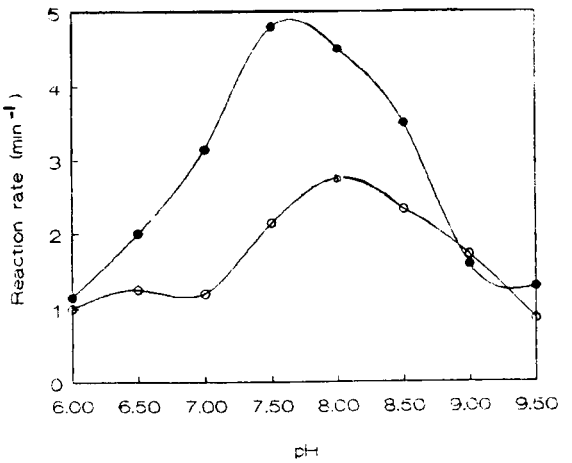

Fig. 3. pH dependence of the reaction rate, (●) with and (○) without CTAB micelle. The conditions were in accordance with the Procedure except that a different pH of 0.1 mol l^{-1} Tris–HCl was used.

decreased the 325-nm peak greatly and the 299-nm peak slightly (Fig. 2c). These results indicate that the 325-nm peak corresponds to the base and the 299-nm peak to the acid; the base was more fluorescent, i.e., $I_{II} > I_I$.

$I_{III} > I_{II}$. The addition of 300 μl of 1.0×10^{-3} mol l^{-1} CTAB (the final concentration of CTAB in the solution was near the CMC) to the neutral equilibrium solution gave the spectrum in Fig. 2d. The 325-nm peak shifted to 330 nm, and the fluorescence intensity increased. These results confirmed the formation of **III**, which was more fluorescent than **II**, i.e., $I_{III} > I_{II}$.

The enhancing effects of CTAB on the product fluorescence have advantages over that of concentrated NaOH. HRP is more active in neutral media. Increasing the pH, although it increases the product fluorescence, partially deactivated HRP and made the reaction become slower. Fig. 3 shows the dependence of the reaction rates on pH in the presence and absence of CTAB. The optimum pH values for the reaction were 7.5 and 8.0, respectively. This indicated that CTAB micelles partially overcome the problem of pH mismatch of the original reaction [18]. Further experiments showed that the fluorescence enhancement effect occurred over the entire range of pH. These observations suggested the potential to increase further the fluorescence intensity besides the addition of concentrated NaOH, and to develop a more sensitive method for the determination of HRP and H_2O_2.

3.3. Existence of reaction 3

According to reaction 3, the presence of a salt, e.g., NaCl or NaBr, would promote it to move to the left and cause a decrease in the reaction rate and fluorescence intensity. The results in Fig. 4a and b agree with this. With increase in NaCl concentration, both the reaction rate and fluorescence intensity decreased in the presence of CTAB, but increased in the absence of CTAB.

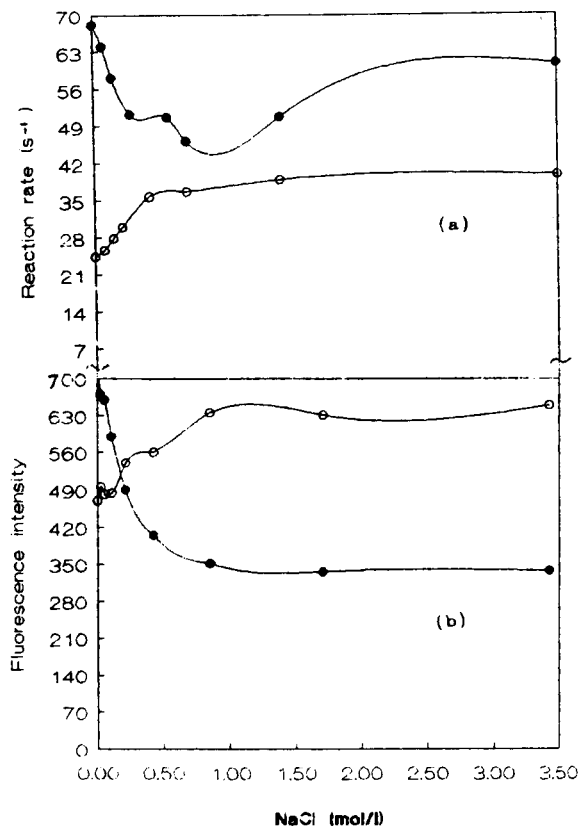

Fig. 4. Effect of NaCl on (a) the reaction rate and (b) the product fluorescence intensity in (○) the absence and (●) the presence of CTAB micelles. The conditions were in accordance with the Procedure except that the buffer contained various concentrations of NaCl.

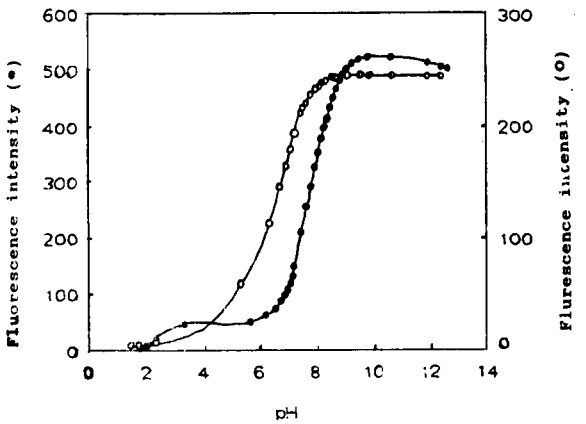

Fig. 5. Fluorimetric titration curves of $DHPPA^{4-}$ in the (○) presence and (●) absence of CTAB micelle. The equilibrium was obtained according to the Procedure. Different pH values were obtained with the addition of 1.0 mol l^{-1} NaOH and 1.0 mol l^{-1} HCl.

The effects of NaCl are of interest. Fig. 4 shows that NaCl has an enhancing effect on the reaction in the absence of CTAB. Even if in the presence of CTAB, when the concentration of NaCl was high enough, an increasing tendency was observed. Although the ionic strength was greater in the presence of a large amount of NaCl, the resulting pH change was not so significant (an increase in pH of 0.05 was observed when the NaCl concentration changed from zero to saturation). The enhancing effect on the fluorescence therefore cannot be attributed to the pH increase. Salt effects on fluorescence, to our knowledge, have seldom been reported, and remain to be further studied.

3.4. Reaction 3 promoting reaction 2

There is an acid–base equilibrium in the product, as stated above. The promotion of reaction 2 will lead to further acid dissociation of **I** and thus lower its pK_a value. Fig. 5 shows the titration curves of $DHPPA^{4-}$ in the absence and presence of CTAB. An obvious pK_a decrease was observed according to the inflection points (corresponding to the pK_a) of the two curves.

Micelles have a marked influence on acid–base equilibria involving compound in different ionization states [1]. The pK_a shift observed between water and micelle solution may be interpreted as either a pH change at the micellar surface or a change in the pK_a of molecules solubilized in the micelles. Incorporation in ionic micelles may induce, for the guest molecule, a pK_a shift of up to 2–3 units owing to electrostatic reaction in the Stern layer and ion exchange between the ionic micelles and the bulk [1].

3.5. Interaction between DHPPA and its analogues with CTAB

In order to obtain direct proof of the interaction between the product molecules and the micelle, the fluorescence behaviours of DHPPA and several analogous were studied. The structural formulae of DHPPA and its three analogues selected are as follows:

	R_2	R'_2	R_4	R'_4	R_5	R'_5
DHPPA:	–OH	–OH	–H	–H	$-(CH_2)_2CO_2H$	$-(CH_2)_2CO_2H$
2,2′-DHDP:	–OH	–OH	–H	–H	–H	–H
4,4′-DHDP:	–H	–H	–OH	–OH	–H	–H
PHDP:	–H	–H	–OH	–H	–H	–H

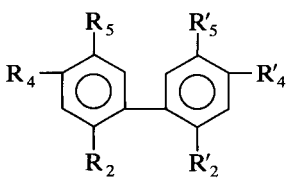

Fig. 6 shows their fluorescence intensities versus CTAB concentration. DHPPA, 2,2′-DHDP and PHDP behaved similarly. Their fluorescence was most enhanced near the CMC. The fluorescence decrease that occurred at some concentration of CTAB indicated the formation of insoluble chelates between the solute and the CTAB molecules (a cloudy solution was observed with 2,2′-DHDP). A further increase of CTAB concentration led to the formation of micelles, and made the chelates dissolve in the micelles and cause the fluorescence enhancement. The lack of fluorescent enhancement with 4,4′-DHDP may be attributed to its molecular structure. It has two OH groups on two opposite sides, which make it interact with CTAB in a different way to its analogues, which either have two OH groups on

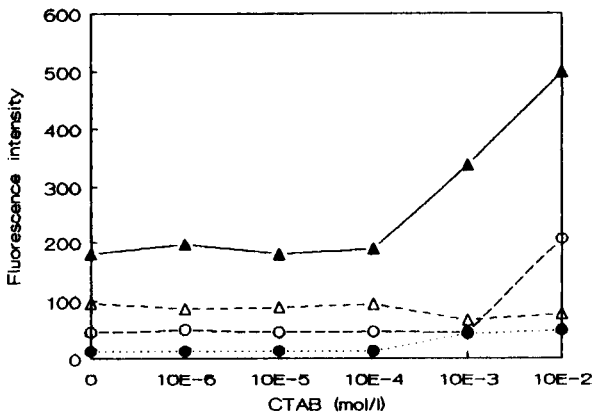

Fig. 6. Fluorescence intensity of DHPPA and its analogues in solutions of different CTAB concentration. A 200-μl volume of product (DHPPA) solution or 100 μl of analogue solution (saturated) was added to 2.0 ml of CTAB solution with different concentrations. λ(ex) and λ(em) were selected for each determination. ▲ = 2,2′-DHDP; △ = 4,4′-DHDP; ○ = *p*-HDP; ● = DHPPA. Other conditions were in accordance with the Procedure.

one side or one OH group in the molecule.

The fluorescence behaviours of these analogues were further studied in the presence of NaCl and NaCl plus CTAB micelles. With the exception of 4,4′-DHDP, the fluorescence decreased with the addition of NaCl in the presence of CTAB. However, NaCl itself made the fluorescence increase to some extent. This further confirmed the existence of reaction 3. The enhancing effect of CTAB also offers a practical means to improve the sensitivity of determination of these hydroxydiphenyl compounds [19].

From the point of the interactions between CTAB and the product, the catalytic effect of CTAB has been explained. The experimental results showed that the suggested mechanism is reasonable. The effect of NaCl and the influence of CTAB on the enzyme remain to be investigated.

References

[1] E. Pramauro and E. Pelizzetti, Trends Anal. Chem., 7 (1988) 260.
[2] D. Pérez-Bendito and S. Rubio, Trends Anal. Chem., 12 (1993) 9.
[3] L.J. Cline Love and G.J. Habarta, Anal. Chem., 56 (1984) 1132A.
[4] H. Hoshino and W.L. Hinze, Anal. Chem., 59 (1987) 496.
[5] J. Georges, Spectrochim. Acta Rev., 13 (1990) 27.
[6] R. Tijssen, Practice and Theory of the Enzyme Immunoassay, Elsevier, Amsterdam, 1985.
[7] D.W. Gunz and M.R. Holfmann, Atmos. Environ., 24 (1990) 1602.
[8] D. Price, P.J. Worsfold and R.F.C. Mantoura, Trends Anal. Chem., 11 (1992) 379.
[9] G.G. Guilbault, Enzymatic Methods of Analysis, Pergamon, Oxford, 1970, p. 77.
[10] A.S. Keston and R. Brandt, Anal. Biochem., 11 (1965) 1.
[11] W.A. Andreae, Nature, 175 (1955) 859.
[12] G.G. Guilbault, P. Brignac, Jr., and M. Zimmer, Anal. Chem., 40 (1968) 190.
[13] G.G. Guilbault, P. Brignac, Jr., and M. Juneau, Anal. Chem., 40 (1968) 1256.
[14] K. Zaitsu and Y. Ohkura, Anal. Biochem., 109 (1980) 109.
[15] V.M. Mekler and S.M. Bystryak, Anal. Chim. Acta, 264 (1993) 359.
[16] T. Matsumoto, T. Furuta, Y. Nimura and O. Suzuki, Anal. Biochem., 138 (1984) 133.
[17] Q.G. Li, J.G. Xu, X.Z. Huang and G.Z. Chen, Talanta, in press.
[18] G. Zhang, P.K. Dasgupta, W.S. Edgemond and J.N. Marx, Anal. Chim. Acta, 243 (1991) 207.
[19] Y.Q. Li and D.D. Ge, J. Yunnan Univ. (Nat. Sci.), 15 (1994) 88.

Announcement of meeting

EUROANALYSIS IX, BOLOGNA, ITALY, SEPTEMBER 1–7, 1996

THE ninth edition of EUROANALYSIS, the European Conference on Analytical Chemistry, will be held in Bologna, Italy, from September 1 to 7, 1996. The conference is organised jointly by the Working Party on Analytical Chemistry of the Federation of European Chemical Societies, the Italian Chemical Society and its Analytical Chemistry Division. Traditionally, this triennial conference provides a highly qualified forum for the international scientific community to meet and exchange ideas on the most recent developments in all branches of analytical chemistry.

Scientific Program
Following the EUROANALYSIS tradition, the ninth edition will aim to cover all branches of analytical chemistry, with emphasis on the problem-solving role of the discipline. Sessions on special topics are planned: *Education*, where the complete scheme of the "Eurocurriculum" in analytical chemistry will be discussed; *Validation in Analytical Chemistry; Reference Materials, Calibration and Traceability*; etc.

Every effort will be made to make the conference appealing to the whole community of analytical chemists. The scientific program will consist of invited lectures and contributed papers (oral and posters). In order to ensure high scientific quality, all contributed papers will be refereed by an international panel.

Submission of Papers
Participants wishing to present contributions in the oral or poster sessions should request an application form.

Language
The official language of the conference is English. No simultaneous translation service will be provided.

Exhibition
In the conference area a large exhibition of instrumentation as well as scientific publications and chemical products will be organised.

For further information, please contact: Prof. Luigia Sabbatini, EUROANALYSIS IX, Dipartimento di Chimica, Università di Bari, Via Orabona, 4, 70126 Bari (Italy). Tel.: +39-80-5442020; Fax: +39-80-5442026.

Calendar of forthcoming meetings

★ *indicates new or amended entry*

★ ***December 5–7, 1994***
Rome, Italy
Analytical Quality Control and Reference Materials: Life Sciences. *Contact*: Dr. Roberto Morabito, Environmental Department, ENEA Casaccia, Via Anguillarese 301, 00060 Rome, Italy. Tel: +39 6 3048-4933; Fax: +39 6 3048-6571.

★ ***December 12–14, 1994***
Barcelona, Spain
Sample Handling of Pesticides in Water. *Contact*: Dr. Damia Barcelo, CID-CSIC, C/Jordi Girona 18–26, E-08034 Barcelona, Spain. Tel: +34 3 204 0600; Fax: +34 3 204 5904. IAEAC, Mrs M. Frei, Strengigässli 20, CH-4123 Allschwil, Switzerland. Tel: +41 61 481 2789; Fax: +41 61 4820805.

★ ***January 22–25, 1995***
Orlando, FL, USA
International Conference — H-TAS[SM]. Hyphenated Techniques in Analytical Separations[SM]. *Contact*: Infoscience, 3000 Dundee Rd., Suite 313, Northbrook, IL 60062, USA. Tel: +1 708-291-9161; Fax: +1 708-291-0097.

January 22–25, 1995
Yokohama, Japan
International Symposium on Chromatography. 35th Anniversay of Research Group on Liquid Chromatography in Japan. *Contact*: Dr. Toshihiko Hanai, International Institute Technol. Analysis, 3-492 Marsumi, Eclairer 2-913, Kanagawaku, Yokohama 221, Japan. Fax: +81 45-402-6361.

★ ***January 29–February 2, 1995***
Würtzburg, Germany
HPCE '95. 7th International Symposium on High Performance Capillary Electrophoresis. *Contact*: Shirley E. Schlessinger, Symposium Manager, 400 East Randolph St., Suite 1015, Chicago, IL 60601, USA. Tel: +1 312-527-2011.

February 7–10, 1995
Montreux, Switzerland
4th International Conference on Automation, Robotics and Artificial Intelligence applied to Analytical Chemistry and Laboratory Medicine. *Contact:* International Conference on Automation and Robotics, c/o SCITEC, Av. de Provence 20, CH-100 Lausanne 20, Switzerland. Tel.: +41 21 624 15 33; Fax: +41 21 625 15 46. *USA*: Tel.: +1 (804) 924 5691; Fax: +1 (904) 924 5718.

★ ***February 15, 1995***
London, UK
One-day Symposium: Alternatives to Chemical Solvents Restricted by the Montreal Protocol: *Contact*: Ms. Paula Elliott, Secretary, Analytical Division, The Royal Society of Chemistry, Burlington House, Piccadilly, London W1V 0BN, UK. Tel: +44 (0)71-437-8656; Fax: +44 (0)71 734 1227.

★ ***February 19–23, 1995***
Nice, France
7th European Congress on Biotechnology and 6th Exhibition of Biotechnology Applied to Research, Industry and Agriculture. *Contact*: Société de Chimie Industrielles, 28 Rue Saint-Dominque, 75007 Paris, France. Tel: +33 1 4555-6946; Fax: +33 1 4555-4033.

★ ***February 22–24, 1995***
Las Vegas, NV, USA
IVth International Symposium on Field Screening Methods for Hazardous Wastes and Toxic Chemicals. *Contact*: Dr. Eric Koglin, U.S. EPA, EMSL-LV, P.O. Box 93478, Las Vegas, NV 89193-3478, USA. Tel: +1 702 798-2432; Fax: +1 702 798-3146.

★ ***March 1–2, 1995***
Tokyo, Japan
CHEMSPEC ASIA 95. *Contact:* Jane Malcolm-Coe, CHEMSPEC ASIA, Speciality Chemicals, Queensway House, 2 Queensway, Redhill, Surrey RH1 1QS, UK. Tel.: +44 737 768611; Fax: +44 737 761685.

March 6–10, 1995
New Orleans, LA, USA
PITTCON '95. Pittsburgh Conference on Analytical Chemistry and Applied Spectroscopy. *Contact:* Pittsburgh Conference, Suite 332, 300 Penn Center Blvd., Pittsburgh, PA 15235-9962, USA.

March 13–15, 1995
Durham, NC, USA
Low- and No-VOC Coating Technologies. 2nd Biennial International Conference. *Contact:* Ms. Coleen M. Northeim, Research Triangle Institute, P.O. Box 12194, Research Triangle Park, NC 27709-2194. Tel.: +1 (919) 541-5816; Fax: +1 (919) 541-7155.

★ ***March 20–24, 1995***
Düsseldorf, Germany
International Symposium on Instrumentalized Analytical Chemistry and Computer Technology. *Contact*: InCom Symposium and Exposition, Werner Günther, Sentaweg 16, 40468 Düsseldorf, Germany. Tel: +49 211 450-854; Fax: +49 211 454-2424.

★ ***April 3–6, 1995***
Madrid, Spain
7as Jornadas de Analisis Instrumental (JAI). The 7th edition of Instrumental Analysis Seminars. *Contact*: 7as Jornadas de Analisis Instrumental (JAI), Expoanalitica + Biociencia, Avda. Reina Mª Cristina – Palacio no. 1, 08004 Barcelona, Spain.

★ ***April 4–6, 1995***
Barcelona, Spain
14th Pharmaceutical Technology Conference. *Contact*: Prof. Mike Rubinstein, 14th Pharmaceutical Technology Conference, 24 Menlove Gardens North, Liverpool L18 2EJ, UK. Tel.: +44 (0)51 737 1993; Fax@ +44 (0)51 737 1070.

★ ***April 4–7, 1995***
Madrid, Spain
Expoanalitica + Biociencia. *Contact*: Expoanalitica + Biociencia, Avda. Reina Mª Cristina – Palacio no. 1, 08004 Barcelona, Spain.

April 4–7, 1995
Rome, Italy
Short Course on Chiral Resolution. *Contact*: Dr. Salvatore Fanali or Dr. Massimo Sinibaldi, CNR, Istituto di Cromatografia, C.P. 10, 00016 Monterotondo Scalo (Roma), Italy. Tel.: +39 6-90625328/90625836; Fax: +39 6 90625849; Telex: 624809 CNR MLI.

★ ***April 23–26, 1995***
St. Louis, MO, USA
6th International Symposium on Pharmaceutical and Biomedical Analysis (PBA '95). *Contact*: Shirley E. E. Schlessinger, Symposium Manager, 400 East Randolph St., Suite 1015, Chicago, IL 60601, USA. Tel: +1 312-527-2011.

★ ***April 26–28, 1995***
St. Louis, MO, USA
Sixth International Symposium on Chiral Discrimination. *Contact*: Shirley E. E. Schlessinger, Symposium Manager, 400 East Randolph St., Suite 1015, Chicago, IL 60601, USA. Tel: +1 312-527-2011.

May 7–10, 1995
Lund, Sweden
7th Symposium on Handling of Environmental and Biological Samples in Chromatography. *Contact:* IAEAC Secretariat, M. Frei-Häusler, Postfach 46, CH-4123 Allschwil 2, Switzerland. Tel.: +41 61-4812789; Fax: +41 61-4820805.

May 9–12, 1995
Jülich, Germany
6th International Hans Wolfgang Nürnberg Memorial Symposium on Metal Compounds in Environment and Life, 6: Analysis, Speciation and Specimen Banking. *Contact:* Dr. H.W. Dürbeck, Institute of Applied Physical Chemistry, Research Center, Jülich (KFA), D-52425 Jülich, Germany.

★ ***May 14–18, 1995***
St. Malo, France
EMAS '95. 4th European Workshop on Modern Developments and Applications in Microbeam Analysis. *Contact*: EMAS Secretariat, Universityof Antwerp (UIA), Department of Chemistry, Universiteitsplein 1, B-2610 Antwerp-Wilrijk, Belgium.

★ ***May 21, 1995***
Sanibel Island, FL, USA
Short Course: Techniques for Polymer Analysis and Characterization. *Contact*: Dr. Petr Munk (ISPAC-8 Chairman), Department of Chemistry, University of Texas at Austin, Austin, TX 78712, USA. Tel.: +1 512 471-4179; Fax: +1 512 471-8696.

★ ***May 22–24, 1995***
Sanibel Island, FL, USA
8th International Symposium on Polymer Analysis and Characterization. *Contact*: Dr. Petr Munk (ISPAC-8 Chairman), Department of Chemistry, University of Texas at Austin, Austin, TX 78712, USA. Tel.: +1 512 471-4179; Fax: +1 512 471-8696.

★ ***May 23, 1995***
Ghent, Belgium
Miniaturisation in Liquid Chromatography versus Capillary Electrophoresis. One-day Symposium. *Contact*: Prof.Dr. W.R.G. Baeyens, Symposium Chairman, University of Ghent, Dept. of Pharmaceutical Analysis, Lab. of Drug Quality Control, Harelbekestraat 72, B-9000 Ghent, Belgium. Tel.: +32 9 221 8951; Fax: +32 9 221 4175.

★ ***May 28–June 2, 1995***
Innsbruck, Austria
19th International Symposium on Column Liquid Chromatography (HPLC '95). *Contact*: HPLC'95 Secretariat, Tyrol Congress, Marktgraben 2, A-6020 Innsbruck, Austria. Tel.: +43 512 575-600; Fax: +43 512 575-607.

★ ***June 4–9, 1995***
Zaragoza, Spain
9th International Conference on Partitioning in Aqueous Two-Phase Systems: Advances in the Uses of Polymers in Cell Biology, Biotechnology and Environmental Sciences. *Contact*: Prof. M.J. Lopez-Pérez, Bioquimica y biologia Molecular, Facultad de Veterinaria, Avenida Miguel Servet 177, 50013 Zaragoza, Spain. Tel.: +34 76 492794; Fax: +34 76 591994; *or* Dr. Cristina Delgado, Molecular Cell Pathology, Royal Free Hospital Medical School, Rowland Hill Street, London NW3 2PF, UK. Tel.L +44 (0)71 794 0500 (ext. 5387); Fax: +44 (0)71 431 7594.

June 5–8, 1995
Singapore
Fifth Symposium on Our Environment and First Asia-Pacific Workshop on Pesticides. *Contact:* The Secretariat, 5th Symposium on Our Environment, c/o Department of Chemistry, National University of Singapore, Kent Ridge, Rep. Singapore 0511. Fax: +65 779-1691.

July 9–13, 1995
Barcelona, Spain
3rd International Symposium on Applied Mass Spectrometry in the Health Sciences and 3rd European Tandem Mass Spectrometry Conference. *Contact:* Prof. Emilio Gelpi, Palau de Congressos, Dept. Convencions, Av. Reina M. Cristina, s/n, 08004 Barcelona, Spain. Tel.: +34 3 4233101 ext. 8208-8213; Fax: +34 3 4262845.

July 9–14, 1995
Darwin, NT, Australia
13AC/4EC. 13th Australian Symposium on Analytical Chemistry: "Initiatives in Quality Solutions", in conjunction with 4th Environmental Chemistry Conference: "Chemistry in Tropical and Temperate Environments". *Contact:* Symposium Secretariat, 13AC/4EC, Convention Catalysts Int., GPO Box 2541, Darwin, NT 0801, Australia. Tel.: +61 89 811 875; Fax: +61 89 411 639.

July 9–15, 1995
Hull, UK
SAC 95. *Contact:* Analytical Division, The Royal Society of Chemistry, Burlington House, Piccadilly, London W1V 0BN, UK. Tel.: +44 71 437-8656; Fax: +44 71 734-1227.

★ ***June 11–14, 1995***
Washington, DC, USA
1995 International Symposium, Exhibit & Workshops on Preparative Chromatography. *Contact*: Janet Cunningham, c/o Barr Enterprises, 10120 Kelly Road-Box 279, Walkersville, MD 21793, USA. Tel.: +1 301 898-3772; Fax: +1 301 898-5596.

★ ***June 13–16, 1995***
Lyon, France
ESIS 95. European Seminar on Infrared Spectroscopy. *Contact:* G. Lachnal, Laboratoire des Materiaux Plastiques et Biomateriaux, Université Claude Bernard Lyon I, 43 Bd. du 11 Novembre, 69622 Villeurbanne Cedex, France. Tel.: +33 72431211; Fax: +33 72431249.

★ ***June 21–22, 1995***
Essen, Germany
CHEMSPEC EUROPE 95. *Contact:* Mike Tarrant, Exhibition Sales Director, CHEMSPEC EUROPE 95, FJM International Publications Ltd., Queensway House, 2 Queensway, Redhill, Surrey RH1 1QS, UK. Tel.: +44 737 768611; Fax: +44 737 761685.

★ ***June 25–29, 1995***
Padova, Italy
8th International Meeting on Tryptophan Research. *Contact*: Organizing Secretariat, Sistema Congressi, Via Jappelli 12, I-35121 Padova, Italy. Fax: +39 48-651320.

★ ***July 7–8, 1995***
Salt Lake City, UT, USA
Two-day Field-Flow Fractionation Workshop. *Contact*: Ms. Julie Westwood, FFF Research Center, Department of Chemistry, University of Utah, Salt Lake City, UT 84112, USA. Tel.: +1 801 581-5419; Fax: +1 801 581-4353.

★ ***July 10–12, 1995***
Park City, UT, USA
Fifth International Symposium on Field-Flow Fractionation (FFF '95). *Contact*: Ms. Julie Westwood, FFF Research Center, Department of Chemistry, University of Utah, Salt Lake City, UT 84112, USA. Tel.: +1 801 581-5419; Fax: +1 801 581-4353.

August 13–17, 1995
Seattle, WA, USA
ICFIA 95. Seventh International Conference on Flow Injection Analysis. *Contact:* ICFIA 95, c/o Gary D. Christian, Department of Chemistry BG-10, University of Washington, Seattle, WA 98195, USA. Tel.: +1 (206) 543-5340; Fax: +1 (206) 685-3478; E-mail: christia@chem.washington.edu

August 27–September 1, 1995
Leipzig, Germany
CSI XXIX. Colloquium Spectroscopicum Internationale XXIX. *Contact:* Gesellschaft Deutscher Chemiker, Abt. Tagungen, P.O. Box 90 04 40, D-60444 Frankfurt/ Main, Germany.

August 27–September 1, 1995
Budapest, Hungary
10th International Conference on Fourier Transform Spectroscopy. *Contact:* Mrs. Klára Láng/Mr. Attila Varga, Conference Office, Roland Eötvös Physical Society, P.O. Box 433, H-1371 Budapest, Hungary. Tel./Fax: +36 1 201-8682.

September 3–8, 1995
Villeneuve d'Ascq, France
6th European Conference on the Spectroscopy of Biological Molecules. *Contact*: Professor J.C. Merlin or Dr. S. Turrell, ECSBM'95, LASIR, Université des Sciences et Technologies de Lille, Bât. C5, 59655 Villeneuve d'Ascq Cedex, France. Tel.: +33 20436988 (JCM) or +33 20434920 (ST); Fax: +33 20436755; E-mail: ECSBM95@univ-lille1.fr.

September 4–5, 1995
Paris, France
Sample Handling of Pesticides in the Aquatic Environment. Short course preceding the 5th Workshop on Chemistry and Fate of Modern Pesticide. *Contact:* Prof. M.-C. Hennion, ESPCI, Lab. Chimi Analytique, 10 rue Vauquelin, 75005 Paris, France.

September 4–7, 1995
Potsdam, Germany
Design of Bioactive Compounds: Possibilities for Industrial Applications. *Contact:* SCI Conference Office, 14/15 Belgrave Square, London SW1X 8PS, UK.

September 6–8, 1995
Paris, France
5th Workshop on Chemistry and Fate of Modern Pesticides. *Contact:* Prof. M.-C. Hennion, ESPCI, Lab. Chimi Analytique, 10 rue Vauquelin, 75005 Paris, France.

September 12–15, 1995
Leuven, Belgium
5th International Symposium on Drug Analysis. *Contact:* Prof. J. Hoogmartens, Drug Analysis '95, Institute of Pharmaceutical Sciences, Van Evenstraat 4, B-3000 Leuven, Belgium. Tel.: +32 16 283440; Fax: +32 16 283448.

September 25–28, 1995
Moscow, Russia
5th Symposium on Kinetics in Analytical Chemistry (KAC '95). *Contact:* Prof. H.A. Mottola, Department of Chemistry, Physical Sciences 107, Oklahoma State University, Stillwater, OK 74078-0447, USA. Tel.: +1 (405) 744-5920; Fax: +1 (405) 744-6007.

★ ***October 6–7, 1995***
Vienna, Austria
3rd International Symposium on Philosophy, History and Education in Analytical Chemistry. *Contact:* Prof. Dr. M. Grasserbauer, Institut für Analytische Chemie, TU Wien, Getreidemarkt 9, A-1060 Wien, Austria. Fax: +43 1-567813.

★ ***October 6–7, 1995***
Vienna, Austria
3rd International Symposium on Philosophy, History and Education in Analytical Chemistry: "Analytical Chemistry in Search for the Truth". *Contact*: Prof. M. Grasserbauer, Institut für Analytische Chemie, TU Wien, Getreidemarkt 9, A-1060 Wien, Austria. Fax: +43 1-567813.

February 6–9, 1996
Bruges, Belgium
HTC 4. Fourth International Symposium on Hyphenated Techniques in Chromatography: Hyphenated Chromatographic Analyzers. *Contact*: Royal Flemish Chemical Society, Working Party on Chromatography, c/o Dr. R. Smits, BASF Antwerpen N.V., Central Laboratory, Haven 725, Scheldelaan 600, B-2040 Antwerp, Belgium. Tel.: +32 3-5612831; Telex: 31047 basant b; Fax: +32 3-5613250.

★ ***March 31–April 4, 1996***
Indianapolis, IN, USA
7th International Symposium on Supercritical Fluid Chromatography and Extraction. *Contact*: Janet Cunningham, c/o Barr Enterprises, 10120 Kelly Road-Box 279, Walkersville, MD 21793, USA. Tel.: +1 301 898-3772; Fax: +1 301 898-5596.

★ ***May 7–9, 1996***
Monte-Carlo, Monaco
VIIth International Symposium on Luminescence Spectrometry in Biomedical Analysis — Detection Techniques and Applications in Chromatography and Capillary Electrophoresis. *Contact:* Prof. Dr. Willy R.G. Baeyens, Symposium Chairman, University of Ghent, Pharmaceutical Institute, Dept. of Pharmaceutical Analysis, Lab. of Drug Quality Control, Harelbekestraat 72, B-9000 Ghent, Belgium. Tel.: +32 9 221.8951; Fax: (+32) 9 221-4175.

★ ***June 16–21, 1996***
San Francisco, CA, USA
HPLC '96 and Related Techniques: 20th International Symposium on High Performance Liquid Phase Separations. *Contact*: Janet Cunningham, c/o Barr Enterprises, 10120 Kelly Road-Box 279, Walkersville, MD 21793, USA. Tel.: +1 301 898-3772; Fax: +1 301 898-5596.

★ ***June 25–29, 1996***
Tarragona, Spain
VI Chemometrics in Analytical Chemistry. CAC 96 International Conference. *Contact:* Tel.: +34 77 559562; Fax: +34 77 559597; E-mail: rius@quimica.urv.es

★ ***September 1–7, 1996***
Bologna, Italy
EUROANALYSIS IX. European Conference on Analytical Chemistry. *Contact*: Prof. Luigia Sabbatini, Dipartimento di Chimica, Università di Bari, Via Orabona 4, 70126 Bari, Italy. Tel.: +39 80 5442020; Fax: +39 80 5442026 (*See "Meeting Announcement" for further details*).

Europt(r)ode 3:
The 3rd Eur. Conference on
Optical Chemical Sensors & Biosensors

Location Zürich, Switzerland
Date 31 March - 3 April 1996
Contact Dr. Ursula **Spichiger**; Center of Chemical Sensors, Biosensors, & Bioanalytical Chemistry; Department of Pharmacy; ETH Zürich - Technopark; Pfingstweidstrasse 30; CH-8005 Zürich; Switzerland; fax (*41) (1) 273-3450

The Data Analysis Handbook

By **I.E. Frank** and **R. Todeschini**

Data Handling in Science and Technology Volume 14

Analyzing observed or measured data is an important step in applied sciences. The recent increase in computer capacity has resulted in a revolution both in data collection and data analysis. An increasing number of scientists, researchers and students are venturing into statistical data analysis; hence the need for more guidance in this field, which was previously dominated mainly by statisticians.

This handbook fills the gap in the range of textbooks on data analysis. Written in a dictionary format, it will serve as a comprehensive reference book in a rapidly growing field. However, this book is more structured than an ordinary dictionary, where each entry is a separate, self-contained entity. The authors provide not only definitions and short descriptions, but also offer an overview of the different topics. Therefore, the handbook can also be used as a companion to textbooks for undergraduate or graduate courses.

Approximately 1700 entries are given in alphabetical order grouped into 20 topics and each topic is organized in a hierarchical fashion. Additional specific entries on a topic can be easily found by following the cross-references in a top-down manner. Several figures and tables are provided to enhance the comprehension of the topics and a list of acronyms helps to locate the full terminologies. The bibliography offers suggestions for further reading.

©1994 386 pages Hardbound
Price: Dfl. 325.00 (US$185.50)
ISBN 0-444-81659-3

ELSEVIER
An imprint of Elsevier Science

ORDER INFORMATION

ELSEVIER SCIENCE B.V.
P.O. Box 330
1000 AH Amsterdam
The Netherlands
Fax: +31 (20) 5862 845

For USA and Canada:
P.O. Box 945
New York, NY 10159-0945
Fax: +1 (212) 633 3680

US$ prices are valid only for the USA & Canada and are subject to exchange rate fluctuations; in all other countries the Dutch guilder price (Dfl.) is definitive. Customers in the European Union should add the appropriate VAT rate applicable in their country to the price(s). Books are sent postfree if prepaid.

Send your article on floppy disk!

All articles may now be submitted on computer disk, with the eventual aim of reducing production times and improving the reliability of proofs still further. Please follow the guidelines below.

With revision, your disk plus one final, printed and exactly matching version (as a printout) should be submitted together to the editor. **It is important that the file on disk to be processed and the printout are identical.** Both will then be forwarded by the editor to Elsevier.

The accepted article will be regarded as final and the files will be processed as such. Proofs are for checking typesetting/editing: only printer's errors may be corrected. No changes in, or additions to the edited manuscript will be accepted.

Illustrations should be provided in the usual manner and, if possible, on a **separate** floppy disk as well.

Please follow the general instructions on style/arrangement and, in particular, the reference style of this journal as given in the "Guide for Authors".

The preferred storage medium is a 5¼ or 3½ inch disk in MS-DOS or Macintosh format, although other systems are also welcome.

Please label the disk with your name, the software & hardware used and the name of the file to be processed.

For further information on the preparation of compuscripts please contact:

Elsevier Science B.V.
Analytica Chimica Acta
P.O. Box 330
1000 AH Amsterdam, The Netherlands
Phone: (+31-20) 5862 791 Fax: (+31-20) 5862459

ELSEVIER SCIENCE

PUBLICATION SCHEDULE FOR 1995

	O'94	N'94	D'94	J	F	M	A	M	J	J	A	S
Anal. Chim. Acta	296/2 296/3 297/1–2	297/3 298/1 298/2	298/3 299/1 299/2	299/3 300/1–3 301/1–3	302/1 302/2–3 303/3							
Vib. Spec.		8/1		8/2		8/3		9/1		9/2		9/3

INFORMATION FOR AUTHORS

Detailed "Instructions to Authors" for *Analytica Chimica Acta* was published in Volume 289, No. 3, pp. 381–384. Free reprints of the "Instructions to Authors" of *Analytica Chimica Acta* and *Vibrational Spectroscopy* are available from the Editors or from: Elsevier Science B.V., P.O. Box 330, 1000 AH Amsterdam, The Netherlands. Telefax: (+31-20) 5862 459.

Manuscripts. The language of the journal is English. English linguistic improvement is provided as part of the normal editorial processing. Authors should submit three copies of the manuscript in clear double-spaced typing on one side of the paper only. *Vibrational Spectroscopy* also accepts papers in English only.

Rapid publication letters. *Letters* are short papers that describe innovative research. Criteria for letters are novelty, quality, significance, urgency and brevity. Submission data: max. of 2 printed pages (incl. Figs., Tables, Abstr., Refs.); short abstract (e.g., 3 lines); *no* proofs will be sent to the authors; submission on floppy disc; *no* revision will be possible.

Abstract. All papers, reviews and letters begin with an Abstract (50–250 words) which should comprise a factual account of the contents of the paper, with emphasis on new information.

Figures. Figures should be suitable for direct reproduction and as rich in contrast as possible. One original (or sharp glossy print) and two photostat (or other) copies are required. Attention should be given to line thickness, lettering (which should be kept to a minimum) and spacing on axes of graphs, to ensure suitability for reduction in size on printing. Axes of a graph should be clearly labelled, along the axes, outside the graph itself.

All figures should be numbered with Arabic numerals, and require descriptive legends which should be typed on a separate sheet of paper. Simple straight-line graphs are not acceptable, because they can readily be described in the text by means of an equation or a sentence. Claims of linearity should be supported by regression data that include slope, intercept, standard deviations of the slope and intercept, standard error and the number of data points; correlation coefficients are optional.

Photographs should be glossy prints and be as rich in contrast as possible; colour photographs cannot be accepted. Line diagrams are generally preferred to photographs of equipment. Computer outputs for reproduction as figures must be good quality on blank paper, and should preferably be submitted as glossy prints.

Nomenclature, abbreviations and symbols. In general, the recommendations of IUPAC should be followed, and attention should be given to the recommendations of the Analytical Chemistry Division in the journal *Pure and Applied Chemistry* (see also *IUPAC Compendium of Analytical Nomenclature, Definitive Rules*, 1987).

References. The references should be collected at the end of the paper, numbered in the order of their appearance in the text (*not* alphabetically) and typed on a separate sheet.

Reprints. Fifty reprints will be supplied free of charge. Additional reprints (minimum 100) can be ordered. An order form containing price quotations will be sent to the authors together with the proofs of their article.

Papers dealing with vibrational spectroscopy should be sent to: Dr J.G. Grasselli, 150 Greentree Road, Chagrin Falls, OH 44022, U.S.A. Telefax: (+1-216) 2473360 (Americas, Canada, Australia and New Zealand) or Dr J.H. van der Maas, Department of Analytical Molecular Spectrometry, Faculty of Chemistry, University of Utrecht, P.O. Box 80083, 3508 TB Utrecht, The Netherlands. Telefax: (+31-30) 518219 (all other countries).

0003-2670/94/$07.00

PRINTED IN THE NETHERLANDS

THE NUCLEUS OF KNOWLEDGE

Available in April

ENCYCLOPEDIA OF ANALYTICAL SCIENCE

Editor-in-Chief

Alan Townshend
University of Hull, U.K.

Senior Editor

Paul Worsfold
University of Plymouth, U.K.

Editors

Stephen Haswell
University of Hull, U.K.

Ian Wilson
Zeneca Pharmaceuticals Macclesfield, U.K.

Robert Macrae
Formerly of University of Hull, U.K.

Helmut Werner
Technical University Vienna Austria

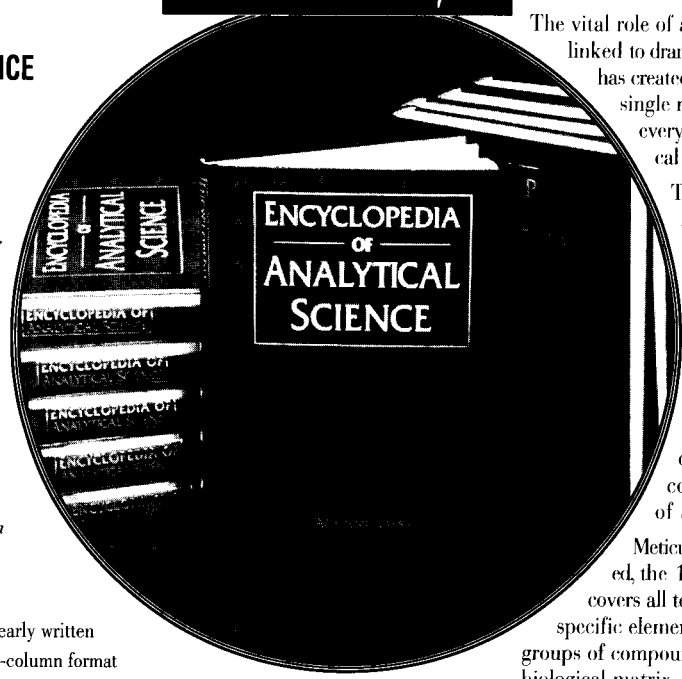

Key Features

- Meticulous organization, clearly written
- 6208 pages in large double-column format
- Authoritative and extensive coverage ensured by international editorial and advisory boards of 98 experts from 28 countries
- More than 800 authors from more than 40 countries
- 11,250 cross-references linking related articles
- 756 articles compiled under 301 subject entries, independently reviewed by 500 top specialists
- Expert organization of entries make research fast and easy for both specialist and non-specialist readers
- 9000 bibliographic entries and suggestions for further reading appear at each article's end to lead the reader straight to the primary literature
- 50,000 index entries, including synonyms and references, plus a full directory of authors and scientific referees listed in Volume 10
- 1330 tables and 2870 illustrations
- Color plate sections in each volume

Ten-Volume Set
Prepublication Price: $1595.00*
May 1995, c. 6208 pp./ISBN: 0-12-226700-1

*Prepublication price effective through final day of publication month.

The vital role of analysis, intrinsically linked to dramatic changes in technology, has created a pressing need for a single reference that encompasses every possible aspect of analytical science.

The **Encyclopedia of Analytical Science,** the first and only one of its kind, satisfies that need. An undertaking of unprecedented scope, the **Encyclopedia** harnesses the specialist knowledge of more than 800 international authors to provide detailed, comprehensive coverage of the practice of analytical science.

Meticulously organized and edited, the 10-volume **Encyclopedia** covers all techniques which determine specific elements, compounds, and groups of compounds in any physical or biological matrix.

The applications of analysis (within disciplines as varied as food science, medicine, geology, forensics, and environmental science) also receive extensive treatment, as do important characterization techniques such as microscopy and surface analysis.

The **Encyclopedia's** vast range of subjects are divided into discrete entries which reflect the expertise and dedication of its editorial and advisory boards. An extensive cross-referencing system also enables quick and easy research of all related information.

Although aimed at practicing analysts working in the scientific and industrial areas, the **Encyclopedia** has also been tailored to meet the needs of non-specialists, including undergraduate and postgraduate students.

As such, the **Encyclopedia of Analytical Science** serves as an essential and invaluable reference for libraries, research institutions, and industrial organizations throughout the world.